Field Monitoring of Curved Girder Bridges with Integral Abutments

BRIDGE ENGINEERING CENTER

Final Report
January 2014

IOWA STATE UNIVERSITY

Institute for Transportation

About the BEC

The mission of the Bridge Engineering Center is to conduct research on bridge technologies to help bridge designers/owners design, build, and maintain long-lasting bridges.

Disclaimer Notice

The contents of this report reflect the views of the authors, who are responsible for the facts and the accuracy of the information presented herein. The opinions, findings and conclusions expressed in this publication are those of the authors and not necessarily those of the sponsors.

The sponsors assume no liability for the contents or use of the information contained in this document. This report does not constitute a standard, specification, or regulation.

The sponsors do not endorse products or manufacturers. Trademarks or manufacturers' names appear in this report only because they are considered essential to the objective of the document.

Non-Discrimination Statement

Iowa State University does not discriminate on the basis of race, color, age, religion, national origin, sexual orientation, gender identity, genetic information, sex, marital status, disability, or status as a U.S. veteran. Inquiries can be directed to the Director of Equal Opportunity and Compliance, 3280 Beardshear Hall, (515) 294-7612.

Iowa Department of Transportation Statements

Federal and state laws prohibit employment and/or public accommodation discrimination on the basis of age, color, creed, disability, gender identity, national origin, pregnancy, race, religion, sex, sexual orientation or veteran's status. If you believe you have been discriminated against, please contact the Iowa Civil Rights Commission at 800-457-4416 or Iowa Department of Transportation's affirmative action officer. If you need accommodations because of a disability to access the Iowa Department of Transportation's services, contact the agency's affirmative action officer at 800-262-0003.

The preparation of this report was financed in part through funds provided by the Iowa Department of Transportation through its "Second Revised Agreement for the Management of Research Conducted by Iowa State University for the Iowa Department of Transportation" and its amendments.

The opinions, findings, and conclusions expressed in this publication are those of the authors and not necessarily those of the Iowa Department of Transportation or the U.S. Department of Transportation Federal Highway Administration.

Technical Report Documentation Page

1. Report No. InTrans Project 08-323	2. Government Accession No.	3. Recipient's Catalog No.	
4. Title and Subtitle Field Monitoring of Curved Girder Bridges with Integral Abutments		**5. Report Date** January 2014	
		6. Performing Organization Code	
7. Author(s) Lowell Greimann, Brent M. Phares, Yaohua Deng, Gus Shryack, and Jerad Hoffman		**8. Performing Organization Report No.** InTrans Project 08-323	
9. Performing Organization Name and Address Bridge Engineering Center Iowa State University 2711 South Loop Drive, Suite 4700 Ames, IA 50010-8664		**10. Work Unit No. (TRAIS)**	
		11. Contract or Grant No.	
12. Sponsoring Organization Name and Address Federal Highway Administration, U.S. Department of Transportation, 1200 New Jersey Avenue SE, Washington, DC 20590 TPF partners: Ohio DOT, Pennsylvania DOT, Wisconsin DOT, and Iowa DOT (lead state), 800 Lincoln Way, Ames, IA 50010		**13. Type of Report and Period Covered** Final Report	
		14. Sponsoring Agency Code TPF-5(169)	
15. Supplementary Notes Visit www.intrans.iastate.edu for color pdfs of this and other research reports.			

16. Abstract

Nationally, there are questions regarding the design, fabrication, and erection of horizontally curved steel girder bridges due to unpredicted girder displacements, fit-up, and locked-in stresses. One reason for the concerns is that up to one-quarter of steel girder bridges are being designed with horizontal curvature. There is also an urgent need to reduce bridge maintenance costs by eliminating or reducing deck joints, which can be achieved by expanding the use of integral abutments to include curved girder bridges. However, the behavior of horizontally curved bridges with integral abutments during thermal loading is not well known nor understood. The purpose of this study was to investigate the behavior of horizontal curved bridges with integral abutment and semi-integral abutment bridges with a specific interest in the response to changing temperatures.

The long-term objective of this effort is to establish guidelines for the use of integral abutments with curved girder bridges. The primary objective of this work was to monitor and evaluate the behavior of six in-service, horizontally curved, steel-girder bridges with integral and semi-integral abutments. In addition, the influence of bridge curvature, skew and pier bearing (expansion and fixed) were also part of the study.

Two monitoring systems were designed and applied to a set of four horizontally curved bridges and two straight bridges at the northeast corner of Des Moines, Iowa—one system for measuring strains and movement under long term thermal changes and one system for measuring the behavior under short term, controlled live loading. A finite element model was developed and validated against the measured strains. The model was then used to investigate the sensitivity of design calculations to curvature, skew and pier joint conditions. The general conclusions were as follows:

- There were no measureable differences in the behavior of the horizontally curved bridges and straight bridges studied in this work under thermal effects. For preliminary member sizing of curved bridges, thermal stresses and movements in a straight bridge of the same length are a reasonable first approximation.
- Thermal strains in integral abutment and semi-integral abutment bridges were not noticeably different. The choice between IAB and SIAB should be based on life – cycle costs (e.g., construction and maintenance).
- An expansion bearing pier reduces the thermal stresses in the girders of the straight bridge but does not appear to reduce the stresses in the girders of the curved bridge
- An analysis of the bridges predicted a substantial total stress (sum of the vertical bending stress, the lateral bending stress, and the axial stress) up to 3 ksi due to temperature effects.
- For the one curved integral abutment bridge studied at length, the stresses in the girders significantly vary with changes in skew and curvature. With a 10^0 skew and 0.06 radians arc span length to radius ratio, the curved and skew integral abutment bridges can be designed as a straight bridge if an error in estimation of the stresses of 10% is acceptable.

17. Key Words bridge thermal stresses—expansion pier bearings—fixed pier bearings—horizontally curved bridges—integral abutments—semi-integral abutments—steel-girder bridges		**18. Distribution Statement** No restrictions.	
19. Security Classification (of this report) Unclassified.	**20. Security Classification (of this page)** Unclassified.	**21. No. of Pages** 272	**22. Price** NA

FIELD MONITORING OF CURVED GIRDER BRIDGES WITH INTEGRAL ABUTMENTS

Final Report
January 2014

Principal Investigator
Brent M. Phares, Director
Bridge Engineering Center, Iowa State University

Research Assistants
Jerad Hoffman and Gus Shryack

Authors
Lowell Greimann, Brent M. Phares, Yaohua Deng, Gus Shryack, and Jerad Hoffman

A report from
Bridge Engineering Center
Iowa State University
2711 South Loop Drive, Suite 4700
Ames, IA 50010-8664
Phone: 515-294-8103 Fax: 515-294-0467
www.intrans.iastate.edu

TABLE OF CONTENTS

LIST OF FIGURES

LIST OF TABLES

LIST OF VARIABLES

A, B, and C	= gauge specific constants given by manufacturer
A_c	= the area of concrete
A_p	= cross-sectional area of the pile tips
A_s	= the area of the steel
$B_{abutment}$	= width of the abutment
B_e	= effective slab width,
D	= the depth of the web
DAF	= dynamic amplification factor
DC	= dead load for structural components
D_0	= initial reading
D_i	= reading at time i
$(EA)_{eff}$	= effective axial rigidity
$(EI_x)_{eff}$	= the effective flexural axial rigidity for X-axis bending
E_c	= the linear elastic modulus of concrete
E_s	= the linear elastic modulus of steel
G	= correction factor that converts digits to inches (provided by manufacturer)
I_f	= moment of inertia of a flange about its smaller principal axis
I_{ytb}	= moment of inertia of the bottom flange of the steel girder for Y-axis bending
I_{ytf}	= moment of inertia of the top flange of the steel girder for Y-axis bending
IM	= dynamic impact factor for live load
K	= a temperature correction coefficient given by the manufacturer (digits/°C)
K_p	= the coefficient of passive lateral earth pressure (psi/psi)
K_q	= end-bearing soil-spring resistance
K_v	= skin-friction soil-spring resistance
L	= length of bridge along curve
L	= length of the member
L_{eff}	= effective thermal length
L_{cable}	= the length of the cable
L_c	= the length of the concrete member
L_e	= equivalent cantilever length
L_g	= distance between equivalent M_g moments
L_{gauge}	= the distance from the top of the abutment to the pressure cells
L_{max}	= the total height of each abutment
L_p	= tributary pile length for each soil-skin-friction soil-spring
L_s	= the length of the steel member
LL	= vehicular live load
M	= resulting end moment
M and B	= constants for the model 1127 gauges given by the manufacturer
M_f	= lateral bending moment acting on the flanges
M_g	= resulting moment at location of strain gauges
M_{lat}	= the lateral flange moment in a girder at the brace point due to vertical loading
M_{lb}	= lateral bending moment in the bottom flange
M_{lt}	= lateral bending moment in the top flange

M_x	=	strong axis bending moment
MDF	=	moment distribution factors
N	=	a constant of either 10 or 12 (engineer's discretion)
P	=	applied load on composite section
P	=	the internal axial force
P_c	=	applied unit load on concrete
P_s	=	applied unit load on steel
P_{gauge}	=	the maximum stress measured at the location of pressure cells
P_{max}	=	the approximated maximum stress at the bottom of the abutment
P_{total}	=	the total approximate force applied to each abutment
R	=	the radius of the girder
Ri	=	the frequency reading produced by the gauge when the vibrating wire is plucked
TG	=	force effect due to temperature gradient
TU	=	force effect due to uniform temperature
Y(NA)	=	the distance to the neutral axis measured from the center of the bottom flange
Z	=	depth from top of soil to location of desired stress
Δ	=	applied lateral end displacement
b_{fb}	=	bottom flange width
b_{ft}	=	top flange width
d	=	centerline concrete slab to centerline bottom flange
f_{bw}	=	tension or compression stress due to warping of the cross-section
h_w	=	web height
t_{fb}	=	bottom flange thickness
t_{ft}	=	top flange thickness
t_s	=	slab thickness
t_w	=	web thickness
x	=	distance from center of flange to flange tip
x_i	=	distance from neutral axis to strain gauge i along the X-axis
y_i	=	distance from neutral axis to strain gauge i along the Y-axis
$\bar{y}$	=	distance from the center of the bottom flange to the neutral axis
α_c	=	the thermal expansion of concrete
α_{cable}	=	the coefficient of thermal expansion of the cable
α_{eff}	=	the effective thermal expansion coefficient of combined steel and concrete
α_s	=	the thermal expansion of steel
δ	=	displacement of composite section
δ_c	=	displacement of concrete
δ_s	=	displacement of steel
$\varepsilon_{current}$	=	the microstrain reading at its respective time
$\varepsilon_{reference}$	=	the microstrain reading on April 28, 2011 at 6 a.m.
ε_a	=	internal axial strain
ε_{ylt}	=	lateral bending strain in the top flange
ε_{ylb}	=	lateral bending strain in the bottom flange
ε_i	=	strain reading at gauge i
ε_x	=	strong axis bending strain
ε_t	=	internal torsional-warping strain

ε_s	= static strain
ε_d	= dynamic strain
ΔD_{cable}	= the correction
$\Delta D_{uncorrected}$	= the reading before a temperature correction
ΔL_{avg}	= the average bridge expansion computed via instrumentation data during the surveying time interval
ΔL_s	= the surveying expansion referenced to April 28, 2011 at 6 a.m.
$\Delta L_s'$	= the surveying expansion at the time of the survey on April 28, 2011
ΔT_{air}	= the ambient air temperature
ΔT_{eff}	= the effective bridge temperature
ΔT_c	= the change in temperature of the concrete member
ΔT_s	= the change in temperature of the steel member
Δd	= range of longitudinal movement of fixed pier or integral abutment
$\Delta \varepsilon$	= difference in microstrain
$\Delta \varepsilon_r$	= resistance axial strain
σ_x'	= total horizontal stress
σ_z'	= total vertical stress
σ_x	= strong axis bending stress
σ_{lb}	= lateral bending stress in the bottom flange
σ_a	= axial stress
ϕ'	= effective friction angle of the soil
γ'	= unit weight of soil
γ_p	= design load factor for permanent loads
γ_{TG}	= design load factor for temperature gradients
γ_{TU}	= design load factor for uniform temperature
ν_c	= Poisson's Ratio for concrete
ν_s	= Poisson's Ratio for steel

ACKNOWLEDGEMENTS

EXECUTIVE SUMMARY

The National Cooperative Highway Research Program (NCHRP) has shown concerns regarding the design, fabrication, and erection of horizontally curved steel girder bridges due to unpredicted girder displacements, fit-up, and locked-in stresses, including thermal stresses. Because curved steel girder bridges are used in up to one-quarter of the nation's steel girder bridges, having a better understanding of actual behavior – and therefore having better design methodologies – is of notable importance.

The primary objective of this work was to monitor and evaluate the behavior of six in-service, horizontally curved, steel-girder bridges with integral and semi-integral abutments and to provide design recommendations.

A national survey was conducted and a literature review was performed to capture the state-of-the-art regarding these types of structures. Also, a monitoring program was developed and deployed on six bridges located at the I-35, I-235, and I-80 interchange on the northeast side of Des Moines, Iowa to obtain strains and movements that result from long term temperature changes. An additional instrumentation system was installed to measure strains in the girders under short term loading with known truck weights and paths. The data gathered during the monitoring period of the project were post-processed to study important behavioral attributes. The sensitivity of long term thermal loading and short term live loading stresses to curvature, skew and pier bearing fixity was also studied.

The following general conclusions were made from the results of the study:

- There were no measureable differences in the behavior of the horizontally curved bridges and straight bridges studied in this work under thermal effects. For preliminary member sizing of curved bridges, thermal stresses and movements in a straight bridge of the same length are a reasonable first approximation.
- Thermal strains in integral abutment and semi-integral abutment bridges were not noticeably different. The choice between IAB and SIAB should be based on life – cycle costs (e.g., construction and maintenance).
- The measured internal strain in the abutment piles due to expansion and contraction of the bridge were generally below 50% of yield stress. The equivalent cantilever method of steel pile analysis fell short of accurately predicting weak axis bending strain.
- The soil pressures on the abutment backwalls were generally below the approximate passive soil pressures.
- Moment distribution factors for the short term live loading were influenced by the amount of curvature.
- An analysis of the bridges predicted a substantial total stress (sum of the vertical bending stress, the lateral bending stress, and the axial stress) up to 3 ksi due to temperature effects.
- For the one curved integral abutment bridge studied at length, the stresses in the girders significantly vary with changes in skew and curvature. An expansion bearing pier reduces the thermal stresses in the girders of the straight bridge but does not appear to reduce the stresses in the girders of the curved bridge.

- Since AASHTO requires a three-dimensional analytical model of the bridge and support conditions to calculate lateral bending stresses for the final design of all curved bridges, this model should also be used to calculate thermal stresses for final design of the curved bridge. (However, with a 10^0 skew and 0.06 radians arc span length to radius ratio (i.e., meeting the geometrical requirements to ignore curvature for strong axis bending), the curved and skew integral abutment bridges can be designed as a straight bridge if an error in the estimation of stress of 10% is acceptable.)

CHAPTER 1 INTRODUCTION

This chapter presents the background to the project and the problems it addresses, the objective and scope of the project, and the research plan undertaken during the project. The final section of this chapter summarizes the organization of this report.

1.1 Background

A report published by The National Cooperative Highway Research Program (NCHRP) raised concerns regarding the design, fabrication, and erection of horizontally curved steel girder bridges. These concerns are centered around difficult-to-predict girder displacements, fit-up issues, and unintended locked-in stresses. Because curved steel girder bridges are used in up to one-quarter of the nation's steel girder bridges, having a better understanding of actual behavior – and therefore having better design methodologies – is of notable importance. In order to have these concerns addressed, the NCHRP developed a research problem statement and gave it high priority for funding.

A major problem facing the nation today is the need to replace large numbers of bridges. Future engineers will need to utilize cost effective and durable designs in order to meet this challenge. Bridge joints permit relative movement between bridge deck spans and abutments; however, they must be continually maintained at a cost to the owner. Therefore, an urgent need exists to reduce bridge maintenance costs by eliminating or reducing deck joints. One way to achieve this is by expanding the use of integral abutments to include curved girder bridges.

1.2 Objective and Scope

The combined use of horizontally curved steel girder bridges and integral abutments looks to be a promising design; however, this combination is relatively new to the nation, and to Iowa. The purpose of the work summarized herein is to investigate the use of integral abutments on curved girder bridges through a monitoring and evaluation program of in-service bridges.

1.3 Research Plan

The objective of the research project was to gather information that will assist in the future design of integral-abutment, curved-girder bridges by monitoring and analyzing the behavior of curved steel girder bridges with integral abutments. There were three general task groups for this project, each of which consisted of several related tasks, as described below.

1.3.1 Task Group I: Information Collection

The use of integral abutments in curved girder bridges has either not been tried with great frequency or is not well documented in the technical literature. As such, the first project task group involved collection of information on the use of these combined structural systems. The following tasks were undertaken to fulfill this task group's objective:

Task A – Technical Advisory Committee

A technical advisory committee (TAC) was formed to assist the research team regarding issues related to curved girders, integral and semi-integral abutments, and fixed and expansion bearings at piers. The TAC also assisted in establishing performance metrics that could be used to evaluate the performance of curved-girder, integral-abutment bridges. The TAC was encouraged to provide other information they deemed useful to the research team.

Task B – Survey of Available Technologies

A survey, which was sent to all the nation's state DOTs, was conducted to determine if integral abutments have been used for horizontally curved bridges and, if so, what were the significant findings, conclusions, or recommendations regarding these types of bridges. The survey also requested that the state bridge engineers express concerns regarding potential behavioral issues and to provide any specific information related to instrumentation and monitoring of these types of bridges.

Task C – Review of Available Engineering Literature

Although a brief literature search and review had been performed before the project officially began, a more complete review was conducted to determine the past and present use of integral abutments for horizontally curved bridges and to uncover any concerns or problems associated with this type of bridge construction. Since significant information on curved-girder, integral-abutment bridges was not initially found in the literature, two general literature searches were conducted that individually addressed horizontally curved bridges and integral-abutment bridges separately in order to formulate potential behavioral issues and to develop a more refined project scope.

Task D – Inspect Existing Curved and Chorded Girder Bridges

The re-alignment of the intersection of Interstates I-35, I-80 and, I-235 (northeast mix-master) near Des Moines, Iowa included the demolition of the old bridges and the construction of six new bridges. Several bridge types were used in the reconstruction including curved girder bridges with integral or semi-integral abutments. For this task, two I-235 curved girder bridges were inspected to determine if there was any evidence of problems associated with the use of integral abutments.

1.3.2 Task Group II: Collect and Analyze Data on the Performance of Six Bridges

The reconstruction of the Northeast Mix-Master, started in 2008, provided the opportunity to monitor the behavior of curved and straight-steel girder bridges. The interchange design was planned so that semi-integral abutments were used in two curved-girder bridges, and integral abutments were used in two essentially identical curved bridges. There were six 26 ft wide

roadway bridges included in the research. Bridge characteristics are presented in Chapter 5 of this report. The following tasks highlight the steps taken by this task group:

Task E – Finalize an Instrumentation Plan

Working with the Iowa DOT Office of Bridges and Structures, the research team developed preliminary instrumentation schemes for five of the six Northeast Mix-Master bridges. These schemes are shown in Chapter 5, along with pertinent bridge information. The instrumentation layouts typically consist of strain gauges on girders and other elements, temperature sensors, sensors utilized to monitor the differential girder-to-substructure displacement at expansion piers and semi-integral abutments, and techniques for monitoring the global movement of the substructure elements. Along with the instrumentation placed on the bridges, each of the six bridges was outfitted with eight surveying-type reflectors for the purpose of performing monthly surveys of the bridges. These reflectors were placed on the exterior girders at both abutments and both piers. The survey procedure is discussed further in Chapter 5.

Task F – Monitor and Analyze the Behavior of the Selected Bridges

The bridges were monitored over a period of approximately 18 months for the long-term health assessment. During this period, the strains, temperatures, and displacements were recorded under a variety of loading conditions. In addition, the short-term health assessment was investigated by conducting a series of live load tests as described in Chapter 5.

Task G – Develop and Validate Simple Analytical Models for the Monitored Bridges

Using the collected data, simple analytical models were developed and validated. These models may be able to be extrapolated to other design conditions (e.g., geometry, soil conditions, etc.) that may provide information on other hypothetical situations.

1.3.3 Task Group III. Develop Project Conclusions and Recommendations

The focus of this task group was to summarize the entire project with a goal of developing recommendations that will assist bridge owners with decisions regarding the combined use of curved girders and integral abutments.

Task H – Establish a Meeting with the TAC

A final meeting with the TAC was held so that the research team could present the results of the project and some initial project conclusions. The TAC was then asked to provide detailed input.

Task I – Submit Final Report

The Final Report, presented herein, summarizing the results of the research was the final step for this task group.

1.4 Report Organization

Chapter 1 introduces the project including the project background, the objective and scope of the project, and the research plan. Chapter 2 presents the literature review, discusses the design of horizontally curved, steel-girder bridges, summarizes use of integral and semi-integral abutments, and presents circumstances in which both have been used. Chapter 3 summarizes a survey conducted of the nation's transportation departments in regard to their current design practices for horizontally curved, steel-girder bridges with integral and semi-integral abutments. Chapter 4 summarizes a bridge inspection conducted on two partially horizontally curved bridges with integral abutments. Chapter 5 presents the experimental procedure. Chapters 6 and 7 present the results from the testing described in Chapter 5. Chapter 8 presents an analytical investigation of design loading conditions. Chapter 9 presents a sensitivity study that was performed to investigate the influences of the curvature and skew on the stresses in girders of an integral abutment bridge. Finally, Chapter 10 presents conclusions, recommendations, and suggested future work with curved-girder, integral-abutment bridges.

CHAPTER 2 BACKGROUND/LITERATURE REVIEW

The design and analysis of straight, integral-abutment bridges (IABs) has a long and extensive history dating back as far as the 1930s. These bridges came about after the introduction of the Hardy Cross Method, and were considered a viable solution to the drawbacks of expansion joints and expansion bearings (Tennessee DOT 1996). Although there has been a tremendous amount of research on the response of straight IABs, less attention has been paid to their horizontally curved counterparts. Research on the use of integral abutments on horizontally curved bridges is scarce (Hassiotis 2006). This chapter attempts to summarize completed work on horizontally curved, integral-abutment bridges. This chapter also presents completed work on straight, integral-abutment bridges, and on horizontally curved, non-integral-abutment bridges.

2.1 Mechanics and Behavior of Horizontally Curved Girders

A single curved girder has three force components (vertical shear, radial shear, and axial load) and three moment components (strong axis bending (M_x), weak axis bending (M_y), and torsion (T)). For purposes of the following discussion, only the moment components are shown in Figure 2.1. The normal stresses induced in the upper and lower flanges of a wide flange shape by these three moments are illustrated in Figure 2.2. The stress due to the positive strong axis bending (M_x) causes tension in lower flange and an equal compression in the top flange and can be computed by the usual strength of materials approach by assuming plane sections remain plane (Figure 2.2a). Similarly, the stress due to the weak axis bending (M_y) causes tension on one side and compression on the other side of both the top and bottom flanges (Figure 2.2b). Stresses due to torsion (T) are typically divided into two categories: (1) pure torsion often called Saint-Venant's torsion and (2) warping torsion [steel text book reference]. The pure torsion stress is a shear stress induced into the flanges and, for thin walled open sections, usually neglected. The warping torsion is resisted by equal and opposite horizontal shears in the upper and lower flanges so that the upper flange is bent laterally in one direction and the lower flanges is bent laterally in the opposite direction. Hence, the cross section is warped and is no longer planar, as assumed in elementary beam theory. The moments that induce this bending are sometimes referred to as the bi-moments and result in normal stresses in the top and bottom flanges as illustrated in Figure 2.2c.

The total lateral moment in the flanges (M_{lt} and M_{lb} in the top and bottom flange, respectively) is the vector sum of the weak axis bending and the warping torsion bending as illustrated in Figure 2.3 and for one flange in Figure 2.4.

In NCHRP Report 424, Hall et al. (1999) describe that vertical bending is broken down into the first three components shown in Figure 2.5 all of which induce bending about the major axis, as in Figure 2.2. Component 1 represents the moment in each girder if all the girders deflected uniformly. Component 2 is the result of restoring forces in connecting members. Adjacent girder generally have different stiffnesses and different loads. Connecting members, such as the diaphragm and deck, shift load from the more flexible girders to the more stiff girders. The sum of components 1 and 2 are similar to the moments calculated for straight bridges determined by finding the moment at a bridge cross section from a line girder analysis and multiplying it by a distribution factor.

Component 3 moments occur because the girders have different radii. The outside girder is less stiff because of its larger radius (and, generally, longer span). If the cross sectional properties are about the same, the outside girder will develop a higher component 3 stress. According to Hall, component 4 stress is the lateral bending stress equal to the sum of the warping stress from the bi-normal moment (Figure 2.2c) and the radial bending stress (Figure 2.2b) as illustrated in Figure 2.3. Hall describes also describes an amplification effect similar to the P-delta effect in columns. It is usually a second order effect caused by the increased curvature of a curved girder due to lateral bending. The amplification effect is not included in first order linear analysis methods and can be included by considering large deflection theory. An approximation of lateral flange bending can be addressed through the V-load equation, discussed subsequently.
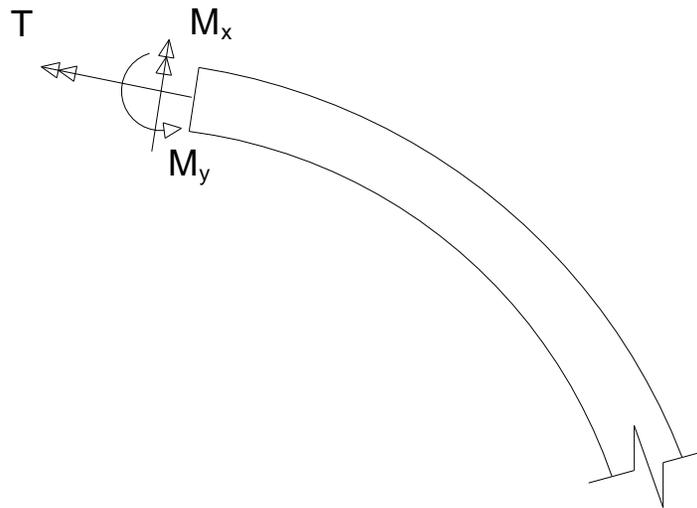
Figure 2.1. Three moment components in a single curved girder
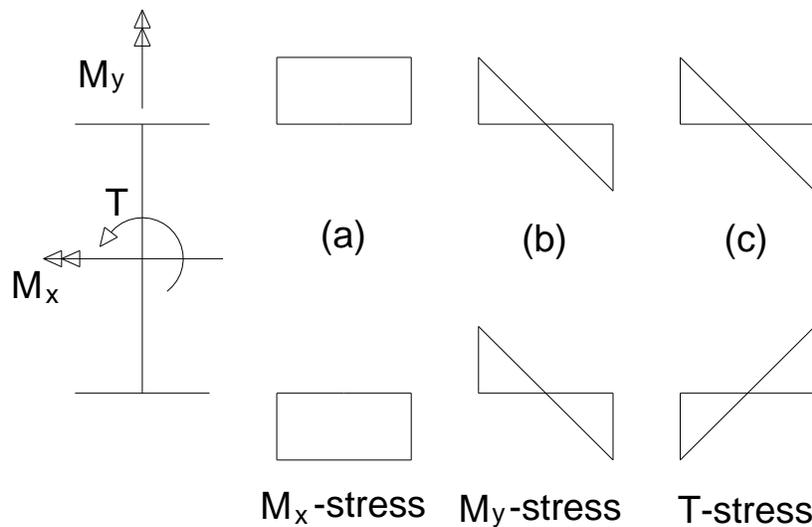
Figure 2.2. Normal stress in flanges due to three moment components
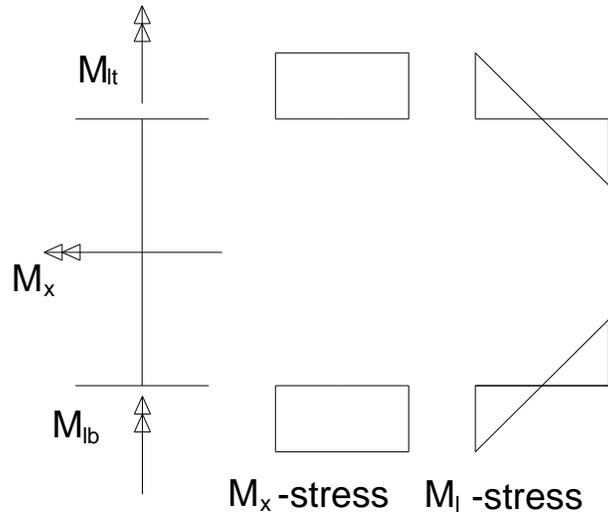
Figure 2.3. Normal stress in flanges due to major axis bending and lateral bending
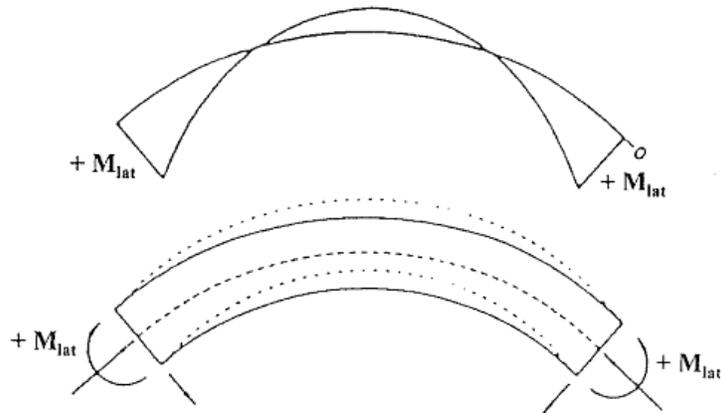
Figure 2.4. Lateral flange bending (from Figure A-1 Hall et al. 1999)
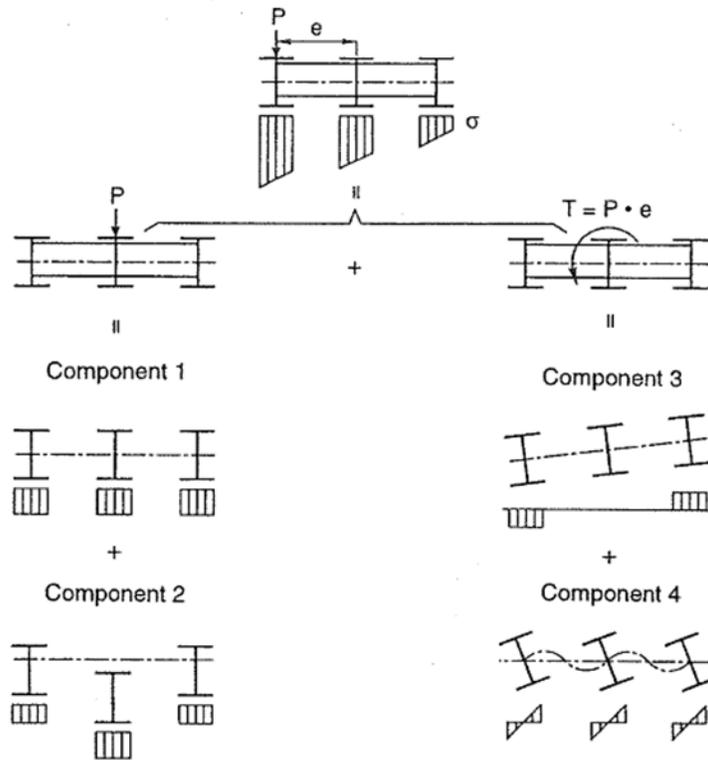
Figure 2.5. Four normal stress components (from Figure A-5 Hall et al. 1999)

Miller et al. (2009) state that curved beams create twisting effects, which result in warping out of plane similar to torsion. This phenomenon is referred to as a bimoment, a product of combined lateral flange bending and torsional shear. In addition, negligible second order effects, similar to P-Δ in columns, occur when the curved compression flange bows outwards, increasing the degree of curvature.

Lydzinski et al. (2008) further explain additional complications that arise when analyzing and designing I-girders in curved bridges. Complications range from the individual plates to the constructed girder as a whole. Compared to straight girders, horizontally curved I-girders are significantly different in the following ways:

- Flange local buckling may differ from the outer to the inner side of the web
- Local buckling is possible on the inner half of the tension flange
- S-shaped bending occurs in the web, causing an increase of stress at the web-flange connection
- Bending and torsion stresses are not decoupled, resulting in lateral bending behavior
- Twisting can occur under individual girder self-weight, causing construction issues in framing

Several levels of analysis can be used to determine girder responses. These include, but are not limited to, the line girder method, grid method, finite strip method, and finite element modeling

(FEM) analysis method. The simplest technique, line-girder method, assumes only vertical loads applied to a single girder. Engineers must determine the amount of load and location of load between girders. Component 1 is only considered during the line-girder analysis and Component 3 may be considered if the V-load method is also applied. The grid analysis considers Components 1, 2, and 3. Warping torsion is not recognized in the grid analysis, since only St. Venant torsion is used. Again, applying the V-load method indirectly accounts for lateral flange bending. Finite element analysis is capable of determining Components 1, 2, and 3. If large-deflection theory is used, then the effects of warping stress may also be accounted for (Hall et al. 1999).

2.2 Comparing Levels of Analysis for Horizontally Curved Bridges

Several levels of analysis can be used to determine girder responses [Hall reference]. These include, but are not limited to, the line girder method, grid method, finite strip method, and finite element modeling (FEM) analysis method. The simplest technique, line-girder method, assumes only vertical loads applied to a single girder. Only Component 1 stresses are determined in the line-girder analysis. Component 2 stresses are often determined by applying wheel load distribution factors to the line-girder method results. According to Hall, component 3 and 4 may be considered if the V-load method is also applied with the line-girder method. The grid analysis considers Components 1, 2, and 3. Warping torsion is not recognized in the grid analysis. Applying the V-load method indirectly accounts for lateral flange bending. Finite element analysis is capable of determining Components 1, 2, and 3. Component 4 can be included in the 3-D finite element analysis if the lateral flange bending degrees of freedom correspond to the moments in Fig. 2.X3 are incorporated into the model. If large-deflection theory is used, then the amplification effects may also be accounted for (Hall et al. 1999).

Very few studies have thoroughly compared different methods of analysis with respect to field test results in horizontally curved bridges. Nevling et al. (2006) attempt to evaluate the level of accuracy produced for various analysis methods through conducting research on a continuous three-span bridge. Table 2.1 details the three levels of analysis performed in the study. The bridge of interest is constructed of five, Grade 50, steel plate I-girders with the outside girder having a radius of 178.5 m (585.6 ft). The non-integral abutment skews range from 60^0 to 35^0.

An American Association of State Highway and Transportation Officials (AASHTO) HS20 design truck was applied as a live load to the bridge at various locations. The single instrumented radial cross-section focused on in this paper, includes the location of maximum positive moment at center span. At this location, strain gauges were placed on the four flanges on each of the five girders to analyze the superstructure's reaction to live loading.

Table 2.1. Levels of analysis (from Table 1 Nevling et al. 2006)

Level	Description	Analysis Tool
1	Manual	AASHTO Guide Specs
		V-load Method
2	2D Grillage	SAP2000
		MDX
		DESCUS
3	3D FEM	SAP2000
		BSDI

The study made conclusions comparing the three methods of analysis against one another, as well as the methods against field data. Compared to field results, Level 1 analyses predicted larger major axis bending moments for girders closer to the applied load and smaller major axis bending moments for girders furthest from the applied load. Correlations between Level 1 and 3 analyses to field results were inconclusive with respect to lateral bottom flange bending moments. Levels 2 and 3 predicted major axis bending moments similar to the field results. However, Level 2 predicted more accurate vertical bending moments compared to Level 1. The study concluded that Level 3 did not provide increased accuracy that was noticeable compared to Level 2 analyses. Thus, Level 2 analysis would be recommended based on the study findings.

Miller et al. (2009) also conducted a study comparing field testing to FEM. The study focused on a multi-girder, three-span, steel composite, horizontally curved I-girder bridge. Field testing consisted of attaching several strain gauges to the steel girders and diaphragms. Static and dynamic loading, similar to an HS20 truck, was applied and later replicated on a FEM. Results concluded that the FEM predicted a higher neutral axis location compared to the field results and composite section theory. The cause may be due to slippage of the shear studs in the haunches. Comparing the FEM to field results showed that larger diaphragm shear strains were found in the field than provided by FEM analysis. In addition, including pier flexibility most accurately compared to the field results. Lastly, the curved girder may require a refined mesh in the FEM to simulate ~~for~~ the complex strain distribution (Miller et al. 2009).

Another FEM study was performed by Lydzinski et al. (2008). The FEM replicated a continuous three-span horizontally curved I-girder bridge comparing dynamic and static loading responses. Dynamic loading concentrated on free vibrations. FEM found that plate elements adequately represented plate bending behavior and interactions in the cross framing. Refined meshing is more critical along the longitudinal direction of the bridge versus the transverse direction at a particular cross-section. Modeling the haunch with plate elements provided negligible differences compared to using rigid links. The authors further found that the piers can be modeled using beam elements rather than complicated 3D elements. Finally, the overall conclusion of the study indicated that including the pier model flexibility is significant in estimating the behavior of the entire bridge.

Barr et al. (2007) investigated the live-load response of a three span horizontally curved I-girder bridge. The study pertains to comparing field test data to a FEM analysis, as well as the V-load method. Conclusions of the study offer suggestions regarding FEM analysis results. These

suggestions explore differences between the FEMs and the V-load analysis methods. Their research focuses on a continuous three-span bridge constructed of five steel I-girders with a noncomposite deck. A field inspection of the bridge determined that the bearings were severely deteriorated and were not allowing the degrees of freedom to be released per design. Relevance of the frozen bearings was explored throughout the FEM.

The study concluded that the detailed FEM produced accurate strain readings under applied live loading. Replacing the frozen bearings with new bearings proved to be negligible because accounting for the amount of resistance provided by frozen bearings is challenging. Another conclusion found that using the V-load for positive moments was 6.8% unconservative for the exterior girders and 8.3% conservative for interior girders when compared to FEM. For negative moments, the V-load was 16.1% conservative for interior girders and 12% unconservative for exterior girders (Barr et al. 2007). These conclusions might indicate that the V-load method offers a relatively accurate preliminary method of analysis, while FEM analysis would be recommended for final design.

2.3 History of the Design Specifications for Horizontally Curved Bridges

Through the 1960s, curved steel bridges were increasingly designed and constructed as engineers realized their advantages. Because of this, a drive began towards developing the scarcely available specifications and guidelines. This led to the Consortium of University Research Teams (CURT) project managed by the Federal Highway Association (FHWA). The CURT project completed analytical and theoretical work, which eventually helped create a preliminary set of specifications for allowable stress design (ASD) which were later accepted by AASHTO in 1976. Through additional work by AASHTO committees and the American Iron and Steel Institute, LFD criteria were developed and transformed from the preliminary set of ASD specifications by CURT. The LFD criteria combined with the ASD criteria formed the 1980 AASHTO *Guide Specs*. After eight revisions, another edition was published in 1993.

The 1993 *Guide Specs* concepts were difficult to understand and could be easily misused by designers. The *2003 Guide Specs* offer more details for discussion of the specifications and include design examples. Design for the *2003 Guide Specs* includes general parameters, preliminary design, preliminary analysis, and refined design as four main categories. General parameters are broken down into two main divisions of design and construction. The design of the bridge is subdivided into general bridge geometry and limit states that incorporate: strength, fatigue, serviceability, and constructability. Criteria for preliminary design are outlined based on material strengths and girder geometries. Preliminary member sizes and framing can be calculated in accordance to Articles 5, 6, 9, and 12 of the specifications. As outlined in previous sections, preliminary analysis of a horizontally curved girder bridge can be much more sophisticated than a traditional straight girder bridge. A percentage of the applied load is often transmitted to the girder with the largest radius. Because of this, the entire structure must be analyzed as a whole, in contrast to only analyzing single girders with distribution factors. Often, small-deflection theory can be used for most bridges. Second-order analyses are usually recommended during construction phases and stability checks. If certain requirements are met, the effects of curvature may be neglected when considering vertical bending moments. Torsion

and lateral bending must account for curvature effects. The V-load method is recommended for simplified cases outlined in the specifications. Finite element theory is recommended for more refined analysis methods if the criteria for V-load are not met. Finally, design refinement is performed as an iterative process to ensure that all components meet design requirements such as strength, serviceability, fatigue, overload, detailing, and constructability.

Linzell et al. (2004) discusses the efforts leading up to the formation of the 2003 Guide Specifications for Horizontally Curved Highway Bridges by AASHTO, hereafter referred to as the Guide Specs. The 2003 Guide Specs encompasses load factor design (LFD) criteria, which has been eliminated by the development of the Load and Resistance Factor Design (LRFD) design provisions. In 2006, the AASHTO Bridge LRFD Design Specifications combined the specifications for straight bridges and curved bridges so that straight and horizontally curved bridges are in one manual.

2.4 Load Distributions for Horizontally Curved Bridges

Kim et al. (2007) studied live load radial moment distribution in horizontally curved girders. As previously stated, substantial normal stresses are present in horizontally curved girders due to warping torsion. Cross frames are designed to reduce these warping normal stresses. These primary members offer an additional load path for induced live loads, which has an effect on vertical bending of adjacent girders. Because of this, cross frames and diaphragms will have a significant influence on transferring load from one girder to the next. Transferring of load can be assessed by calculating girder distribution factors (GDF). The Kim et al. report focuses on developing GDF equations, which are primarily a function of cross framing details. The research employed both field studies and analytical models. Three increasing levels of complexity for modeling of the FEM were utilized and are shown in Figure 2.6. Based upon field measurements, results showed that Type I was conservative by up to 45%, Type II only differed by 10% and Type III provided slightly more accurate results than Type III. Due to the added increased effort for creating a Type III model, the slightly increased accuracy was deemed negligible. Radius, span length, and cross frames all were found to influence the live load distribution. On the other hand, the parapets and deck thickness were insignificant with respect to GDFs. Overall, the span length was found to be the most influential factor.
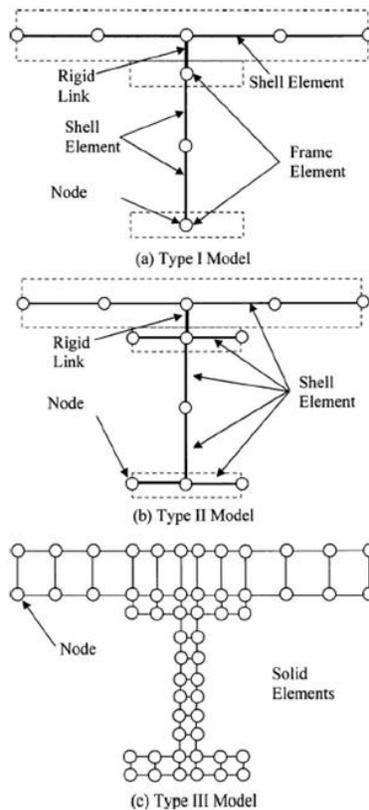
Figure 2.6. Levels of analysis (from Fig. 1 Kim et al. 2007)

A study by Miller et al. (2009), previously mentioned, made conclusions from calculated dynamic amplification factors (DAF). When comparing the FEM analysis to field data analysis, the study found that the FEM overestimated the stiffness of the diaphragm to girder connection as it predicted greater transfer of loads between adjacent girders as compared to field measurements. Consequently, load distribution was greater for the outermost girders. The field results indicated that DAF were within the limit of AASHTO recommendations.

In contrast to the research by Miller et al. (2009), Barr et al. (2007) determined that the FEM distribution factors differed by only 5% from the AASHTO (2003) standard distribution factors. This discrepancy could be due to varying degrees of complexity in each FEM.

2.5 Framing and Erection of Horizontally Curved Girders

Although steel I girders offer minimal torsional resistance, they are most commonly used in the construction of horizontally curved bridges. These members are only stable when connected via diaphragms or cross bracing, which leads to substantial interaction forces in those connecting members. Consequently, the analysis and design of the superstructure needs to accommodate these forces (Linzell et al. 2004).

In a dissertation from the University of Maryland, Thanasattayawibul addresses the two main types of curved girder framing, closed and open framing (Thanasattayawibul 2006). Closed framing resists torsion through the interactions of girders that are connected by diaphragms or floor beams along with lateral bracing at girder flange locations. In contrast, open bracing does not include the horizontal bracing of girder flanges. Combinations of closed and open framing can be used during construction of curved bridges. Cross frames and diaphragms act as secondary members in straight bridges; however, they act as load-carrying members in curved bridges. The report also notes that spacing of cross frames has a significant effect on warping stresses.

In a presentation, associated with HNTB, LaViolette further highlights the importance of erecting horizontally curved members (LaViolette 2009). He explained that lateral bending is primarily caused by warping normal stresses along with wind loads, skew, and overhangs of girders during construction. Throughout construction and erection phases, many calculations must be made to account for the several stages of construction. Stability of each individual girder and the multi-girder system as a whole must be met. Often, these calculations and checks are made by performing a 3D finite element analysis to investigate each sequence of construction. Structural engineers must account for load capacities and stabilities at all stages of construction. Notable loadings to be accounted for should include self-weights and attachments, wind loads, loads induced during lifting and tie downs, girders rolling due to unbalanced loadings, and several more. Additionally, issues during erection can be prevented by properly noting the alignment. Such preventions include detailing sufficient cross framing, using falsework, properly placing holding cranes, and thoroughly following procedures outlined for pinning, bolting and tightening. A detailed set of erection drawings are extremely important. LaViolette states that drawings should include work area plans, erection sequences, temporary supports, rigging details, etc. Neglecting to follow rigorous construction plans have proven to cause catastrophic failures resulting in injuries and death.

2.6 Integral Abutments and Horizontally Curved Girders

One key factor in general bridge design can be eliminating expansion joints and expansion bearings throughout a bridge structure. The installation and maintenance of bearing joints can be problematic due to leaky joints, which result in corrosion and buildup of debris at the bearings.. Eliminating these joints can potentially decrease maintenance costs and ultimately increase the structure life. In order to eliminate joints and seals, integral abutments were introduced. Integral abutment bridges are designed without joints in the bridge deck. They are designed to accommodate thermal movements typically by providing flexibility of the abutment piles.. These bridges are less expensive to construct, simple to detail in design, and require less maintenance (Mistry 2000).

However, incorporating integral abutments with horizontally curved girders can be more difficult to understand and analyze as compared to an equivalent straight girder bridge. Doust (2011) assessed the effect of introducing integral abutments to horizontally curved bridges. The study focused on the live-load response of a curved steel I-girder IAB. Abutment pile moments were found to be approximately 20% larger than an equivalent straight bridge. Direct relationships

between abutment pile moments and the bridge radius or length were not apparent, although, the orientation of the pile with respect to possible bridge skews may be significant and require further investigation beyond the original Doust study.

2.7 Past Work on Thermal Loading on Horizontally Curved IABs

The most recent study to investigate the thermal behavior of horizontally curved, steel-girder, integral-abutment bridges was completed by Doust at the University of Nebraska (Doust 2011). In this study, a detailed investigation was conducted into the behavior of horizontally- curved, steel-girder, integral-abutment bridges and horizontally curved, concrete slab, integral-abutment bridges using the finite-element-analysis program SAP 2000. Multiple bridges were modeled with varying horizontal curvatures and total bridge lengths. The study considered the effect of different loading conditions applied to the bridges, namely gravity loads, lateral loads (longitudinal and transverse), temperature effects, concrete shrinkage, and earth pressure. From the investigation, the author concluded that for bridges longer than a specific length, dependent mainly upon bridge curvature, the internal forces due to expansion are smaller in a horizontally curved bridge than in a straight bridge of similar length. Regarding bridge displacement, the author was able to develop an equation to predict the direction of end displacements of a horizontally curved, integral-abutment bridge. This was important because the author also concluded that the abutment piles should be oriented to produce strong-axis pile bending in the direction of this maximum displacement. Based on this study, orienting the piles in such a fashion will reduce the maximum bending stress in the piles.

Another study involving curved, integral-abutment bridges was presented in a dissertation by Thanasattayawibul at the University of Maryland (Thanasattayawibul 2006). This work was a parametric study performed using a three-dimensional finite-element model to investigate the effect that different parameters would have on the behavior of horizontally curved, steel-girder, integral-abutment bridges. Bridge length, temperature, soil profile type, span length, radius, and pile type were the defining parameters selected in this study. As a result of this study, conclusions and recommendations were made for the future research and for the design of horizontally curved, steel-girder, integral-abutment bridges.

2.8 Select Past Work on Thermal Loading on Straight IABs

ABAQUS/CAE 6.5-1 was used to conduct numerical simulations on the response of a three span, IAB to thermal loads (Shah 2007). The purpose of the study was to investigate the soil-structure interaction due to temperature changes on IABs with different types of soil behind the abutments and along the piles. Three different soil conditions, incorporating non-linear soil response and three different temperature changes, were imposed on a model of the Bermis Road Bridge: F-4-20, Fitchburg, Massachusetts. The non-linear response of the soil was modeled using linear springs and an iterative equivalent linear approach. The spring stiffness was determined based on recommendations by *Manuals for Design of Bridge Foundations* published by the NCHRP in 1991 (Barker et al. 1991). According to the study, the overall behavior of IABs is significantly affected by the type of soil surrounding the bridge abutments. As expected, an increase in soil compaction adjacent to the abutment results in smaller pile tip displacements and smaller pile

bending moments. Also, at lower soil compaction levels the abutment translation tends to be larger and the abutment rotation tends to be smaller; at higher compaction levels the abutment rotation tends to be larger and the abutment translation tends to be smaller. The author also noted that vertical thermal gradient in the abutment, although considered a rigid body, produced bending of the abutment.

Abendroth and Greimann (2005) conducted a thorough investigation into the thermal behavior of IABs. First, an extensive literature review was conducted on the following topics: performance of joint-less bridges, bridge field studies, pile tests (field tests and laboratory tests), analytical studies (thermal analysis and integral-bridge analytical studies), integral-abutment design models (bridge temperature, coefficient of thermal expansion and contraction for concrete, bridge displacement, pile design, and approach slabs), and flange local buckling of I-shaped beams.

The thermal load responses of two IABs were monitored by developing a bridge-monitoring program to obtain long-term air and concrete temperature; pile and girder strain; longitudinal and transverse abutment displacements; relative, longitudinal displacements between the bridge girders and their pier caps; pile-head rotation relative to the abutment pile cap; and abutment rotations in a vertical plane that is parallel to the length of the bridge (1-4).
Next, finite-element models of two integral-abutment bridges were developed. These models were then calibrated and refined using the experimental results. The measured and predicted results of abutment displacements and member strains were compared to verify the accuracy of the finite-element models. Lastly, the authors developed recommendations and design procedures. The recommendations and procedures covered integral-abutment backwalls, pile caps, abutment piles, and connections; design examples were provided. Conclusions the authors drew were as follows: a good correlation exists between longitudinal displacements of the integral abutments and the recorded changes in the average bridge temperatures, the extrapolated maximum bending strains at the flange tip of the HP abutment piles exceeded the minimum yield strain of the steel at one of the bridges and was equal to approximately 73% of the minimum yield strain of the steel at the other bridge, the measured longitudinal strains in the PC girders were within acceptable limits for both bridges, and the vertical rotations and longitudinal displacements of the abutments for both bridges were over estimated by the finite-element models when compared to the measured experimental results. The authors also made a number of design recommendations from the results of their study. Please refer to Chapter 10 of Abendroth and Greimann (2005) for more details on their conclusions.

In 2005, the Federal Highway Administration (FHWA), in conjunction with West Virginia University, hosted a conference on integral abutment and jointless bridges. The purpose of the conference was to establish the current practices with regard to design, maintenance and rehabilitation, and construction of integral abutment and jointless bridges and to present case studies regarding the use of IABs. Each of the topics had five to seven presentations reporting on studies completed across the United States. One example was a presentation by Frosch et al. (2005). In this study the authors, in conjunction with the Indiana DOT, instrumented four bridges in Indiana to observe the in-service behavior of straight, integral-abutment bridges. Some notable conclusions were drawn from the study. First, the movement of the abutment can be conservatively estimated using the theoretical thermal expansion and contraction of the superstructure by $\Delta L = \alpha(\Delta T)L$. Secondly, the primary thermal response of the abutment is to

translate longitudinally and that minor abutment rotations can be ignored for analysis. Lastly, piles integrally connected with the abutment experience double curvature bending but pinned connections can be detailed to eliminate the double curvature.

2.9 Past Work on Thermal Loading on Horizontally Curved Non-IABs

Hall et al. (1999) established design specifications for horizontally curved, steel-girder bridges. This report was published by NCHRP and was based upon over one hundred studies. Section 3.4 of this report addresses thermal loads in the bridge superstructure. It states:

According to the Recommended Specifications, curved bridges should be designed for the assumed uniform temperature change specified in AASHTO Article 3.16. The orientation of bearing guides and the freedom of bearing movement is extremely important in determining the magnitude and direction of thermal forces that can be generated. For example, sharply skewed supports and sharp curvature can cause very large lateral thermal forces at supports if tangential movements are permitted and radial movements are not permitted. Under a uniform temperature change, orienting the bearing guides toward a fixed point and allowing the bridge to move freely along rays emanating from the fixed point will theoretically result in zero thermal forces. Other load conditions, however, can dictate the bearing orientation. The bearing restraints and orientation, as well as the lateral stiffness of the substructure, must be considered in a thermal analysis (15).

Section 3.4 of the Hall et al. report discusses the need, in certain conditions, to consider deck temperature gradients as specified by the AASHTO LRFD Specifications. If the width of the deck is less than one-fifth of the longest span, the bridge is considered narrow and uplift can occur. Section 8.3 of this report addresses thermal induced movements in the bearings and states "Bearing devices should be designed to accommodate movements due to temperature changes in the superstructure and to accommodate rotations about the tangential and radial axes of the girder" (25).

Moorty and Roeder (1992) studied the effect various geometric parameters, orientation of the bearings, and the stiffness and resistance of the substructure had on the thermal response of curved bridges. Analytical models of a 600-ft long, three span, horizontally curved, steel-girder bridge had vertically varying temperature distributions applied to them. The location of the fixed point, the bearing orientation, the relative stiffness of the bearings, the stiffness of the piers, and the angle of curvature varied between models. The Sutton Creek Bridge was also used in a field study conducted by the authors to compare and validate the information provided by their models. The Sutton Creek Bridge is a 658-ft long, three-span, horizontally curved, steel-girder bridge in the Kootenai National Forest in Montana. For the field study, the bridge temperature, the ambient air temperature, and the bridge movements were measured over a three-day period and the wind speed and cloud cover were estimated from local newspapers and radio stations. From their work, Moorty and Roeder were able to draw a number of conclusions about the design of horizontally curved, steel-girder bridges. For example, the authors state that the method of predicting thermal movements recommended by AASHTO is reasonable for straight orthogonal bridges, but a more refined analysis may be required for skew and curved bridges.

Furthermore, an increase in the curvature of the bridge results in an increase in the radial movements and stresses in the bridge. The relative stiffness of the bridge, the girder bearings, and the substructure influence the tangential and radial movements in a horizontally curved bridge; and the transverse movements and stresses in bridges increase with an increase in the skew angle and the width of the bridge.

CHAPTER 3 SURVEY OF STATES

In March of 2010, a survey of state transportation agencies regarding their experience with horizontally curved bridges with integral abutments was conducted. This chapter covers the purpose of the survey, describes the survey, and reports the information obtained by the survey.

3.1 Purpose

The purpose of the survey was to synthesize the state-of-the-practice with regard to the design and construction of horizontally curved bridges with integral and semi-integral abutments and to gather available information on the behavior of these types of bridges.

3.2 Description of Survey

For this survey, an online questionnaire was utilized. This format helped with distribution of the survey and helped minimize response time. The DOTs were sent an email that asked for their participation in a short questionnaire along with a brief description of the questionnaire and why the survey as being conducted. The DOTs were also provided with a web page link and a password that allowed them access to the questionnaire. The survey consisted of ten questions formulated to assess the agencies experience with horizontally curved steel girder bridges with integral abutments. Following an initial evaluation of the responses, follow-up phone interviews were conducted with the states that were deemed to have the most experience. Of the 50 state agencies, a total of 27 participated, six of which were contacted for the follow-up phone interview. The survey questionnaire and responses can be found in the APPENDIX.

3.3 Information Gained

3.3.1 Reasons for Construction

Out of the responding agencies, those that construct horizontally curved, steel girder bridges with integral or semi-integral abutments indicated that they do so for corrosion protection and elimination of expansion joints/expansion bearings. Some agencies also indicated that they consider restrained girder ends as a benefit for both uplift and torque. Agencies that do not construct horizontally curved, steel girder bridges with integral or semi-integral abutments do so because of poor soil conditions, extreme temperature ranges, unfamiliarity with design, concerns with additional forces on the girders, and a general lack of need for integral abutment bridges. One state indicated that, "Integral abutments inhibit movements at bridge ends. This movement is necessary to dissipate energy during seismic events."

3.3.2 Published or Unpublished Reports

Agencies were asked if they were aware of any published or unpublished documents that addressed the design, monitoring, or performance of horizontally curved, integral or semi-integral abutment, bridges. Pennsylvania, who was the only state that indicated that they knew of

any published information, indicated that they had contracted with Penn State University to monitor four straight integral abutment bridges and to develop a design methodology based on the monitored behavior of the bridges.

Vermont was the only state that was aware of any current or contemplated research regarding horizontally curved, integral or semi-integral abutment bridges. In that work a single curved girder bridge is being monitored. The monitoring began in the early winter of 2009 and, at the time of this survey, had not yet resulted in published information.

3.3.3 Additional Limitations

For the most part, responding agencies do not have limitations on radius, total length, or material type for horizontally curved bridges with integral or semi-integral abutments beyond the limitations that are applicable to straight bridges with integral or semi-integral abutments. Several agencies place a limit on the skew angle and the span length, such as skew angle is limited to 30 to 45° and the span length is limited to anywhere between 250 ft to 450 ft.

3.3.4 Common Design Methods

The most commonly indicated analysis method used in the design of horizontally curved bridges with integral or semi-integral abutments was the grillage method (used by 46% of the respondents). The grillage method is an analysis technique where the physical deck is idealized into an equivalent "grid" of structural members (Hall 1999). The next most commonly indicated analysis method was the finite element method (used by 31% of the respondents). The finite element method is a numerical technique where the structure is idealized into a mesh of elements (Hall 1999). The V-load method was cited as the third most common analysis method (used by 27% of the respondents). The V-load method is an approximate solution that assumes a distribution of radial forces between the girders. The radial forces are a result of the need to balance axial forces acting on a horizontally curved girder. Diaphragm members are assumed to resist the radial force and, as a result, cause a moment on the inside and outside girders (Richardson 1976). Finally the M/R method, an approximate method used for box girder bridges (Hall 1999), was the least cited analysis method (used by 8% of the respondents). The M/R method is a technique that follows the logic that the difference in total bending moment between any two points is the area under the shear diagram except that it utilizes torsional moments. The total change in total torsional moment between any two points is equal to the change in area under the (M/R – t) diagram between those two points (Richardson 1976). The percentage of respondents that used each respective analysis method do not sum to 100% because several (31%) respondents use more than one analysis method.

3.3.5 Follow-up Interview

Personnel in six states (Missouri, Nebraska, Tennessee, Vermont, Washington, and Wyoming) were interviewed by telephone to get further clarification on their initial survey responses. Most of the agencies started using integral abutments in the 1970s. Some agencies started using semi-

integral abutments in the 1960s and integral abutments later. None of the agencies have any evidence of thermal expansion performance issues associated with horizontally curved steel girder bridges with integral abutments. None of the interviewed agencies use a specific erection scheme that differs from that for a horizontally curved bridge without integral abutments. All of the agencies believe that expansion and contraction of the bridge occurs with temperature changes; however, each agency has their own method to address this matter. Tennessee is the only state that attempts to fully quantify the thermal movements. All other agencies design structural components to accommodate the thermal movements. Each of the agencies uses approach slabs that are tied to horizontally curved integral abutment bridges. Typically, reinforcing bars are designed to work as a "pin" connection allowing relative rotation but not translation at the slab/bridge joint. Lastly, none of the interviewed agencies had any specific limits placed on the design of these bridges. Each state allows their designers to use their judgment in design of a bridge with suggestions to guide, not limit, their design.

CHAPTER 4 IN-SERVICE BRIDGE INSPECTIONS

On July 26, 2010 two members of the research team accompanied an Iowa DOT Bridge Inspection crew while they inspected two steel girder bridges that were built in 2005 in the Des Moines, Iowa area. These bridges are partially curved and have integral abutments. This chapter covers the purpose of the inspection, the location and geometry of the bridges, and the inspection findings. The purpose of the visit was to identify any evidence of problems associated with the use of horizontally curved, steel-girder bridges with integral abutments.

4.1 Bridge Location and Geometry

The first bridge inspected was Bridge No. 7707.50235, which carries West 19th Street over I-235 in Des Moines and has a horizontally curved off ramp on the northwest side of the bridge. The bridge cross section near the north abutment is comprised of ten steel girders with variable cross-sectional dimensions. The three most easterly girders are straight and the other seven girders are curved, with the degree of curvature increasing towards the western-most exterior girder. Due to the increasing degree of curvature, the spacing between the girders also increases as the girders approach the abutment. At the section near the north abutment the bridge deck is crowned over the fourth girder from the east side of the bridge. The deck slope varies to the west of the crown, is constant at 2.5% to the east over the straight girders, and is approximately zero at the sidewalk.

The second bridge inspected was Bridge No. 7708.20235. This bridge carries West 3rd Street over I-235 in Des Moines and has a horizontally curved off ramp on the northeast side of the bridge. The bridge cross section near the north abutment has nine steel girders with varying cross-sectional dimensions. North of the north pier all nine girders have horizontal curvature. The curvature of the girders increases from the west to the easternmost exterior girder. As with Bridge 7707.50235 the girder spacing increases from west to east. The bridge deck is horizontal at the sidewalk then varies while sloping to the east.

4.2 Inspection Findings

4.2.1 19th Street Bridge

While inspecting the 19th Street Bridge, the north abutment and girders were visually inspected for cracking and other signs of damage. Also, the bridge deck and guard rail were visually inspected. Figure 4.1 displays a typical hairline crack in the north abutment near its mid-width. This crack runs vertically along the abutment and extends roughly over about 80% of the visible height of the abutment. This cracking is typical of hairline cracking observed in the abutment. However, these cracks could not be specifically attributed to curvature of the bridge girders.

Figure 4.1. North abutment hairline crack

Figure 4.2 displays slight cracking near the interface between the steel girders and the north abutment at the bottom flange of the steel girders. These cracks typically are oriented downward at a 45° angle from the corners of the bottom flange. These cracks appeared at each of the girder-to-north abutment connections.

Figure 4.3 displays cracking in the off-ramp slab that runs perpendicular to the expansion joint. There were multiple cracks found similar to the one shown. It is interesting to note that these cracks do not follow the curve of the underlying girder.

Figure 4.4 displays transverse cracking in the deck slab. The crack shown is close to the mid-span of the bridge and runs the full width from side-to-side of the bridge. This crack was not the only transverse crack found in the slab, but was the longest.

Figure 4.5 displays transverse cracking in the guardrail that divides the roadway and pedestrian sidewalk. These cracks typically occur at five ft increments along the length of the barrier and occur on both sides of the bridge.

Figure 4.2. North abutment and bottom flange interface

Figure 4.3. Off-ramp slab cracking

Figure 4.4. Deck transverse cracking

Figure 4.5. Guardrail transverse cracking

Figure 4.6 shows the joint at the sidewalk between the approach slab and the bridge. Comparing Figure 4.6 to Figure 4.3 reveals that the joint at the sidewalk is open more than the expansion joints in the deck.

4.2.2 Third Street Bridge

While inspecting the 3rd Street Bridge, the north abutment and girders were checked for cracking and any signs of other types of damage. Despite the similarities in design, the West 3rd Street Bridge displayed less damage than that of the West 9th Street Bridge. However, there were some notable discoveries.

Figure 4.6. Approach slab/bridge joint

Figure 4.7 displays slight cracking at the joint between the steel girders and the north abutment at the bottom flange of the steel girders. These cracks run downward at a 45° angle from the corners of the bottom flange. These cracks appeared at each of the girder-to-north abutment connections. Most notably about this figure is the oxidation that has occurred around the cracks and below the girder.

Figure 4.7. North abutment and bottom flange interface

Figure 4.8 is another photograph of cracking occurring in the abutment. This figure shows evidence of salt water infiltration as indicated by the formation of calcium carbonate crystals around the cracks.

Figure 4.8. Calcium carbonate formation

While on inspection, a possible fatigue crack indication, shown in Figure 4.9, was found in the girder-to-diaphragm connection of one of the horizontally curved girders. Upon further testing conducted by the Iowa DOT, the defect identified on the weld toe adjacent to the top flange on the stiffener to the web weld was the result of a lack of fusion at the weld toe.

Figure 4.9. Girder-to-diaphragm welded connection

CHAPTER 5 EXPERIMENTAL PROCEDURE

One of the principal aspects of this project was to monitor the behavior of horizontally curved, steel girder, integral and semi-integral abutment bridges under changes in temperature and live load. As such, six bridges constructed by the Iowa DOT were instrumented with various sensors at various locations. Behaviors under live loads were evaluated using point-in-time testing and the behaviors under temperature variations were monitored for a period of approximately 18 months.

5. 1 Bridge Location and Geometry

5.1.1 Site Plan View

The intersection of Interstate 80, Interstate 35, and Interstate 235 on the northeast side of Des Moines, also known as the northeast mix-master (NEMM), was the location for the testing associated with this work. Overall, there were six 26 ft wide roadway bridges that were included in the research. The interchange layout was configured such that semi-integral abutments were used in two of the curved bridges and integral abutments were used in two of the curved bridges. In general the bridges had geometries that made them essentially mirror-images. Two other ramp bridges at the NEMM are straight with integral abutments and are generally in this work for comparison purposes. Figure 5.1 displays the location and site layout of the NEMM.

Map Data ©2011 Google
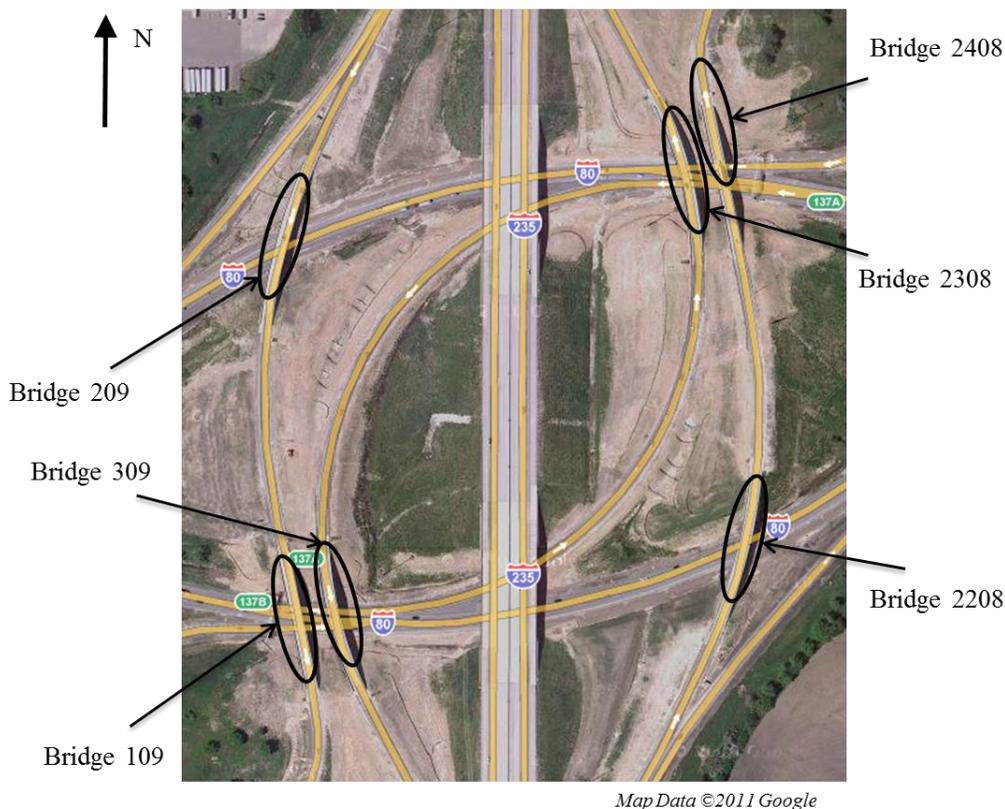
Figure 5.1. NEMM bridge locations and site layout

The six bridges labeled in Figure 5.1 are part of an on ramp or an off ramp at the NEMM interchange. The Iowa DOT assigned the bridge labels, identifying them as shown in the figure. The top left bridge, Bridge 109; and the bottom right bridge, Bridge 2408; are the straight, steel-girder bridges with integral abutments. The remaining four bridges are the horizontally curved, steel-girder bridges with integral and semi-integral abutments: Bridge 209, 309, 2208, and 2308. The center of curvature for each of the horizontally curved bridges is the same for all four girders of the same bridge and therefore the radii for the girders vary.

5.1.2 Bridge Configurations

Bridge 109 is a one lane, three-span bridge with a straight-alignment and spans of 80 ft, 144 ft, and 80 ft, as shown in Figure 5.2. The spans are measured between the centerline of the abutments and the piers. The baseline of the bridge, a line that is a base for measurement and for construction, is located 4 ft – 6 in. east from the west exterior girder and the abutments and piers are skewed 15°. The bridge abutments are integral abutments, the south pier is an expansion pier (EP), and the north pier is a fixed pier (FP).
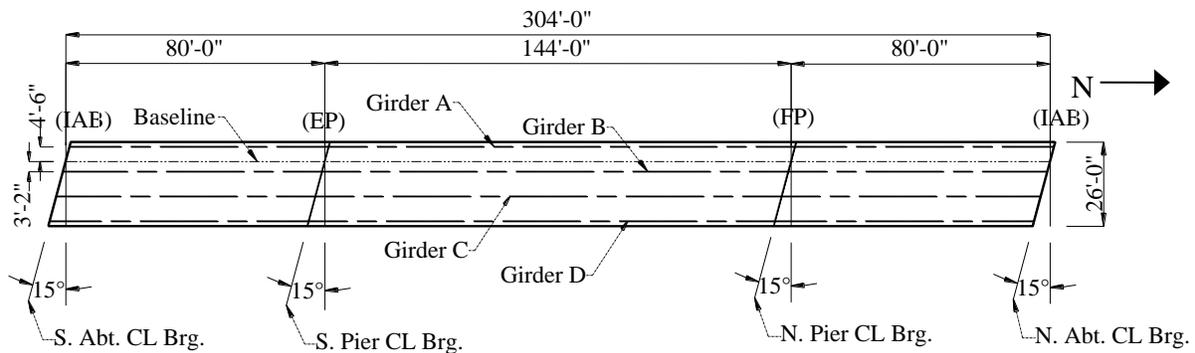
Figure 5.2. Bridge 109 plan view

Bridge 209 is a one lane, three-span, semi-integral abutment bridge with a 1,340 ft horizontal curvature radius, and spans of 90 ft, 152 ft, and 90 ft, as shown in Figure 5.3. The spans are measured along the bridge baseline between the centerline of the abutments and the piers. The baseline is located 4 ft - 6 in. east of the centerline of the west exterior girder (i.e., Girder A). The abutments and piers are skewed at a 35° right ahead. The radius of the baseline is 1,340 ft. The abutments are semi-integral abutments, the south pier is an expansion pier, and the north pier is a fixed pier.
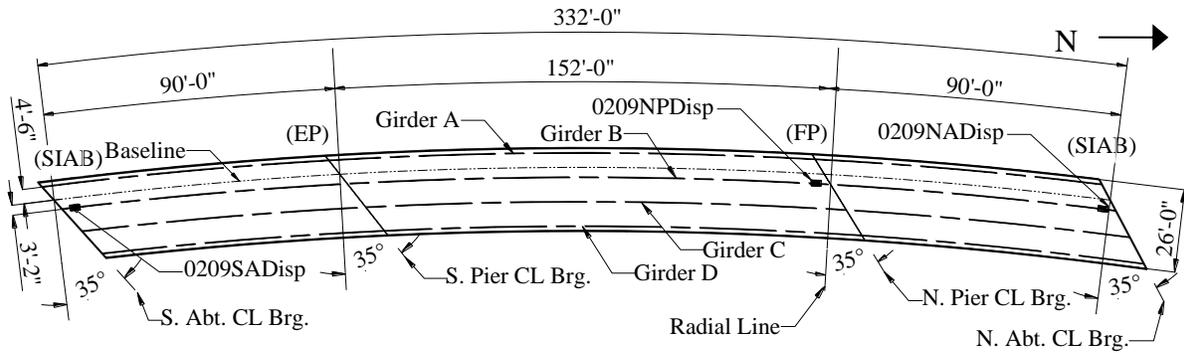
Figure 5.3. Bridge 209 plan view

Bridge 309 is a one lane, three span, integral abutment bridge with a 950 ft horizontal baseline curvature radius, and spans of 85 ft, 149 ft, and 85 ft, as shown in Figure 5.4. The baseline is located 2 ft – 6 in from the west exterior girder, measured perpendicular to the roadway. The abutments and piers are skewed at 15° left ahead. The south pier is a fixed pier and the north pier is a fixed pier.
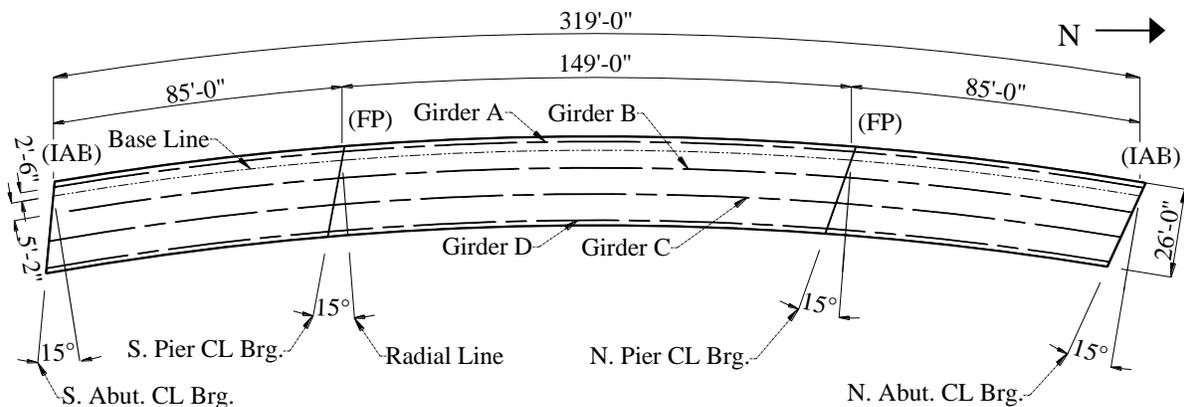
Figure 5.4. Bridge 309 plan view

Figure 5.5 shows the plan view for Bridge 2208. This bridge is a one lane, three span bridge with a horizontal radius of 1340 ft and spans of 90 ft, 150 ft and 90 ft. The baseline is located 4 ft – 6 in. west of the east exterior girder, and the abutments and piers are skewed at 35° right ahead. The abutments are integral abutments, the south pier is an expansion pier, and the north pier is a fixed pier.
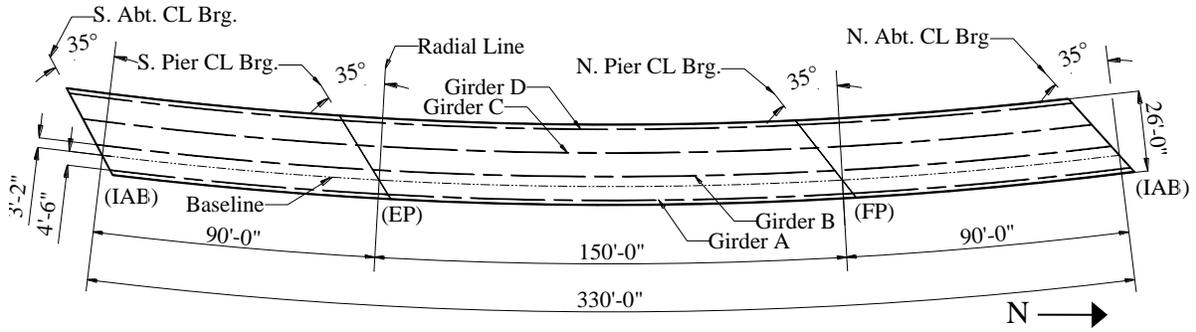
Figure 5.5. Bridge 2208 plan view

Bridge 2308 is a one lane, three span semi-integral abutment bridge with spans of 80 ft, 142 ft and 80 ft and a horizontal curvature of 950 ft, as shown in Figure 5.6. The baseline is located 2 ft − 6 in. from the east exterior girder, and the abutments and piers are skewed at 35° left ahead. The north and south piers are fixed piers.
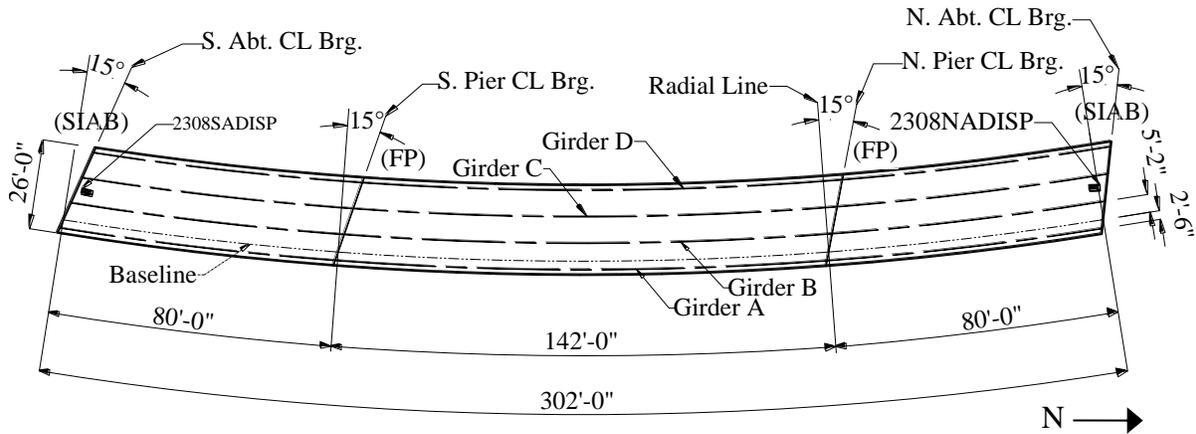
Figure 5.6. Bridge 2308 plan view

Bridge 2408 is a one lane, three span integral abutment bridge with spans of 80 ft, 144 ft and 80 ft, as shown in Figure 5.7. The abutments and piers are skewed at 15° left ahead. The south pier is a fixed pier and the north pier is an expansion pier.

Geometric similarities and differences for the six bridges become more apparent in a tabular presentation than with the separate plan views for these bridges that are shown in Figures 5.2 through 5.7. Table 5.1 lists the length, width, skew angle, curve, radius, spans, abutment type, and pier fixity for each bridge.
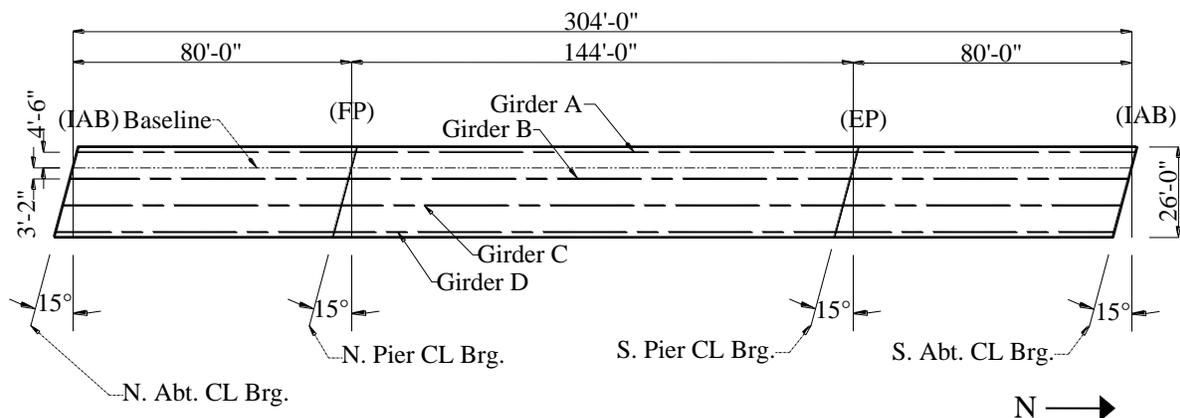
Figure 5.7. Bridge 2408 plan view

Table 5.1. NEMM bridge geometry

Design No.	109	209	309	2208	2308	2408
Length (ft)	304	332	319	330	302	304
Width (ft)	26	26	26	26	26	26
Skew (°)	15	35	15	35	15	15
Radius (ft)	N/A	1340	950	1340	950	N/A
Spans (ft)	80-144-80	90-152-90	85-149-85	90-150-90	80-142-80	80-144-80
Abut. Type	Integral	Semi-Integral	Integral	Integral	Semi-Integral	Integral
S. Pier Fixity	Expansion	Expansion	Fixed	Expansion	Fixed	Fixed
N. Pier Fixity	Fixed	Fixed	Fixed	Fixed	Fixed	Expansion

After an examination of Table 5.1, one will notice there are bridge pairings based on general geometry and restraint conditions. Additionally, all bridges are generally similar in terms of span lengths and total length. Bridges 109 and 2408 are both straight bridges with the same abutment type and the same skew angle. The only notable difference between these two bridges is the geographic location of their expansion and fixed piers. Bridges 209 and 2208 share similar span lengths, total length, radius of horizontal curvature, pier fixity, and skew angle. The only major difference between the two bridges is their abutment type. Bridges 309 and 2308 are almost identical to one another. The only major difference between Bridges 309 and 2308 is the abutment type.

5.1.3 Bridge Cross Section

Except for the girder dimensions and diaphragm configuration, the cross-sectional properties for all six bridges are similar. Each of the bridges has a roadway width of 26 ft and a total width of 29 ft-2 in. The horizontally curved bridges have non-composite bent plate diaphragms and the straight bridges have cross frames with WT horizontal members and angle diagonal members. The typical bridge cross section is shown in Figure 5.8. The left half of the figure shows the

diaphragm configuration for the horizontally curved bridges and the right side of the figure shows the cross frames of the straight bridges.
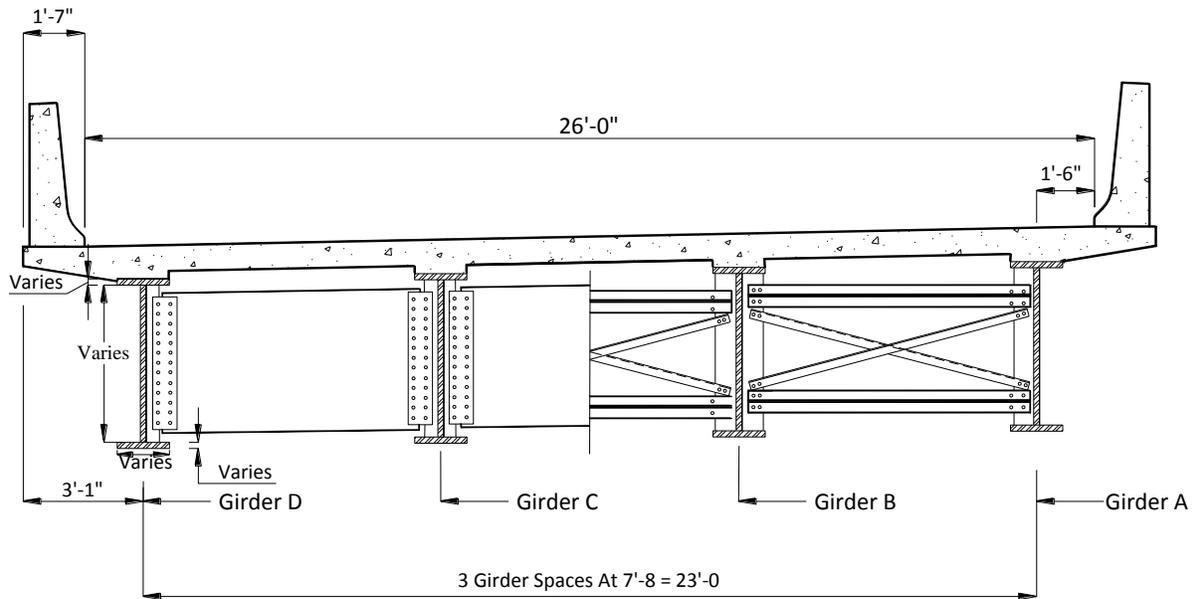
Figure 5.8. Typical bridge cross section

For the six bridges at the NEMM, the Iowa DOT labeled the west exterior girder as Girder A and the east exterior girder as Girder D. However, in this work, the exterior girder on the outside of the curve has been labeled Girder A and the exterior girder on the inside of the curve has been labeled Girder D. Therefore, for the four horizontally curved bridges, Girder A measures the longest total length. Similarly, Girder D measures the shortest total length.

5.1.4 Girder Cross Section

All six bridges were constructed with welded, I-shaped, plate girders. Along with the variation within a span and from span-to-span, field splices and slab haunches change the cross-sectional properties of the girders. In this work variations in slab haunches were ignored. Table 5.2 lists the girder dimension at the locations within each span that were monitored with strain gauges. The gauge locations are discussed in Section 5.2.2.

Table 5.2. Steel girder dimensions (all dimensions in inches)

Bridge	Span and Girder Location											
	North and South Span Girder A						Center Span Girder A					
	t_{ft}	b_{ft}	t_w	h_w	t_{fb}	b_{fb}	t_{ft}	b_{ft}	t_w	h_w	t_{fb}	b_{fb}
109	-	-	-	-	-	-	3/4	16	7/16	54	1 1/8	16
209	1	22	7/16	42	1	22	3/4	18	7/16	42	1 1/4	22
309	1	20	7/16	48	1	20	7/8	20	7/16	48	1 3/8	20
2208	1	22	7/16	42	1	22	3/4	18	7/16	42	1 1/4	22
2308	7/8	18	7/16	48	1	18	3/4	18	7/16	48	1 3/8	18
	North and South Span Girder D						Center Span Girder D					
	t_{ft}	b_{ft}	t_w	h_w	t_{fb}	b_{fb}	t_{ft}	b_{ft}	t_w	h_w	t_{fb}	b_{fb}
109	-	-	-	-	-	-	3/4	16	7/16	54	1 1/8	16
209	1	20	7/16	42	1	20	3/4	18	7/16	42	1 1/8	20
309	7/8	18	7/16	48	1	18	3/4	18	7/16	48	1 3/8	18
2208	1	20	7/16	42	1	20	3/4	18	7/16	42	1 1/8	20
2308	7/8	16	7/16	48	7/8	16	3/4	16	7/16	48	1 1/8	16

Note: "-" = location with no strain gauge; t_{ft} = top flange thickness; b_{ft} = top flange width; t_w = web thickness; h_w = web height; t_{fb} = bottom flange thickness; b_{fb} = bottom flange width.

To aid in data analysis, a local coordinate system was established for each girder as shown in Figure 5.9. In this coordinate system, while facing north, the positive X-axis direction is to the left and the positive Y-axis direction is downward.

In the positive moment regions the concrete deck was made composite with the steel girders with welded shear studs. In this work it was assumed that the effective cross-section of each composite girder was symmetric about their local Y-axis. The effective slab width is considered twice the distance from the centerline of the girder to the end of the deck overhang for each bridge. A constant slab thickness of 8 in. was also assumed.

The approximate cross sectional properties of Girder A and Girder D, at the location of strain gauges, are listed in Table 5.3 and Table 5.4 respectively. For each strain gauge location, Table 5.3 lists $(EA)_{eff}$, the effective axial rigidity; $(EI_x)_{eff}$, the effective flexural axial rigidity for X-axis bending; I_{ytf}(steel) and I_{ytb}(steel), the moment of inertia of the top and bottom flange for Y-axis bending, respectively; and Y(NA), the distance to the neutral axis (in the Y direction) measured from the center of the bottom flange. These properties were used to calculate internal forces and moments in the girders from the measured strains.
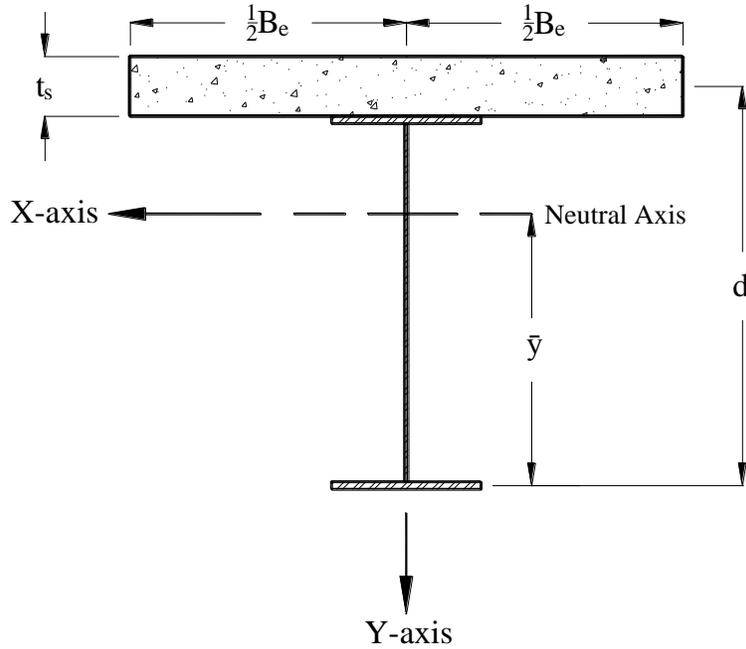
Figure 5.9. Local girder coordinate system

where,

B_e = effective slab width,

t_s = slab thickness

d = centerline concrete slab to centerline bottom flange, and

$\bar{y}$ = distance from the center of the bottom flange to the neutral axis.

Table 5.3. Girder A composite section properties at strain gauge locations

			North and South Span Girder A		
Bridge	**$(EA)_{eff}$ (k)**	**$(EI_x)_{eff}$ (k-in.^{2})**	**I_{ytf} (Steel) (in.^{4})**	**I_{ybf} (Steel) (in.^{4})**	**Y (NA) (in.)**
209	$4.1e^6$	$1.4e^9$	$8.9\,e^2$	$8.9e^2$	$3.6e^1$
309	$4.0e^6$	$1.7e^9$	$6.7e^2$	$6.7e^2$	$4.1e^1$
2208	$4.1e^6$	$1.4e^9$	$8.9e^2$	$8.9e^2$	$3.6e^1$
2308	$3.9e^6$	$1.5e^9$	$4.3e^2$	$4.9e^2$	$4.1e^1$
			Center Span Girder A		
Bridge	**$(EA)_{eff}$ (k)**	**$(EI_x)_{eff}$ (k-in.^{2})**	**I_{ytf} (Steel) (in.^{4})**	**I_{ybf} (Steel) (in.^{4})**	**Y (NA) (in.)**
109	$3.7e^6$	$1.7e^9$	$2.6e^2$	$3.0e^2$	$4.6e^1$
209	$4.0e^6$	$1.5e^9$	$3.6e^2$	$11.1e^2$	$3.4e^1$
309	$4.2e^6$	$2.0e^9$	$5.8e^2$	$9.2e^2$	$3.9e^1$
2208	$4.0e^6$	$1.5e^9$	$3.6e^2$	$11.1e^2$	$3.4e^1$
2308	$4.0e^6$	$1.8e^9$	$3.6e^2$	$6.7e^2$	$3.9e^1$

Table 5.4. Girder D composite section properties

Bridge	$(EA)_{eff}$ (k)	$(EI_x)_{eff}$ (k-in.^{2})	I_{ytf} (Steel) (in.^{4})	I_{ybf} (Steel) (in.^{4})	Y (NA) (in.)
	North and South Span Girder D				
209	$4.0e^6$	$1.3e^9$	$6.7e^2$	$6.7e^2$	$3.6e^1$
309	$3.9e^6$	$1.5e^9$	$4.3e^2$	$4.9e^2$	$4.1e^1$
2208	$4.0e^6$	$1.3e^9$	$6.7e^2$	$6.7e^2$	$3.6e^1$
2308	$3.7e^6$	$1.3e^9$	$3.0e^2$	$3.0e^2$	4.23^1
	Center Span Girder D				
109	$3.7e^6$	$1.7e^9$	$2.6e^2$	$3.0e^2$	$4.6e^1$
209	$3.8e^6$	$1.3e^9$	$3.6e^2$	$7.5e^2$	$3.5e^1$
309	$4.0e^6$	$1.8e^9$	$3.6e^2$	$6.7e^2$	$3.9e^1$
2208	$3.8e^6$	$1.3e^9$	$3.6e^2$	$7.5e^2$	$3.5e^1$
2308	$3.7e^6$	$1.5e^9$	$2.6e^2$	$3.8e^2$	$4.1e^1$

5.1.5 Pier Bearings

Two types of pier bearings were used for the NEMM bridges studied in this work. Figure 5.10 shows an expansion pier bearing. For this pier design a curved sole plate with a pintle is welded to the girder bottom flange. The curved sole plate sits on a pintel plate which rests on a neoprene pad, which is on top of the pier cap. An expansion pier is designed to allow rotation about an axis perpendicular to the longitudinal direction of the girder at the pier location. The pad allows some rotation about an axis parallel to the longitudinal direction. Translation in the longitudinal and transverse directions of the girder at the pier location is allowed.

Figure 5.11 shows a fixed pier bearing. For this pier design a curved sole plate with a pintle is welded to the girder bottom flange. The curved sole plate rests on a masonry plate, which is attached to the top of the pier cap. A fixed pier is designed to allow only rotation about an axis perpendicular to the longitudinal direction of the girder at the pier location. Translation in all directions of the girder is restrained at the pier location.

(a) On Location

Curved Sole Plate
Pintle
Neoprene Pad
Pier Cap
Pintle plate

(b) Schematic
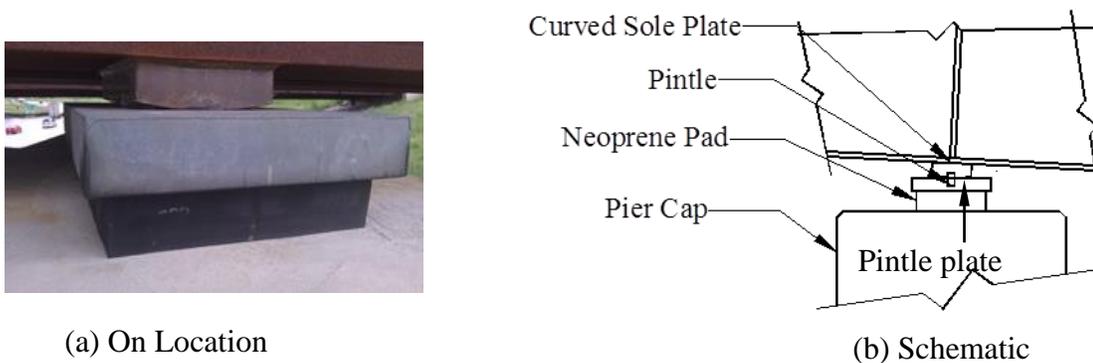
Figure 5.10. Expansion pier bearing

(a) On Location

(b) Schematic
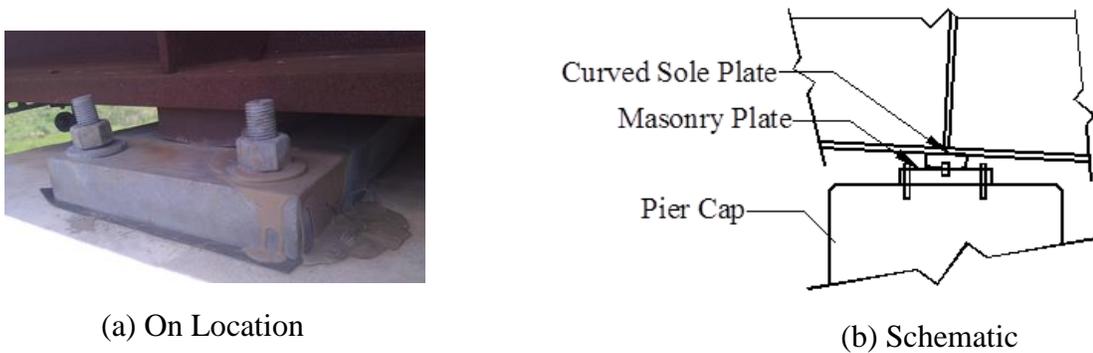
Figure 5.11. Fixed pier bearing

5.1.6 Substructure Description

The research presented in this report involved bridges with differing abutment and pier fixity conditions, as listed in Table 5.1. Each IAB at the NEMM was 29 ft – 2 in. wide in the radial direction, the width of each maskwall measured 1 ft – 7 in., and the height of each integral abutment varied from bridge to bridge. Figure 5.12 shows a typical front elevation of an IAB used at the NEMM.

Each girder bears on a short length of an S3x7.5, which bears on the abutment pile cap, as shown in Figure 5.13. The entire abutment is supported by vertical piles, with size and spacing varying from bridge to bridge. For clarity, the reinforcing steel in the reinforced concrete backwall, mask wall, and pile cap are not shown. Some of the vertical reinforcing bars extend from the pile cap into the abutment backwall and mask walls to form a composite section between the pile cap and the abutment walls.
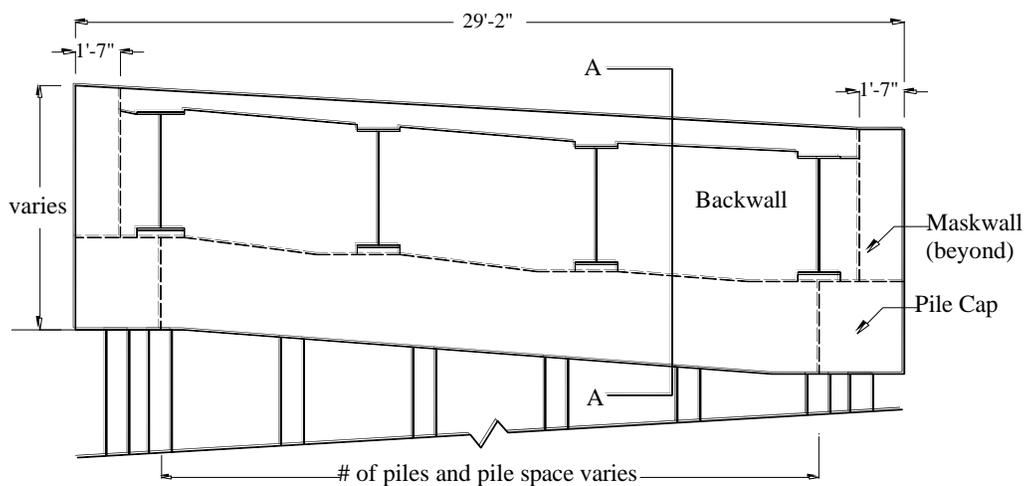
Figure 5.12. Integral abutment – front elevation
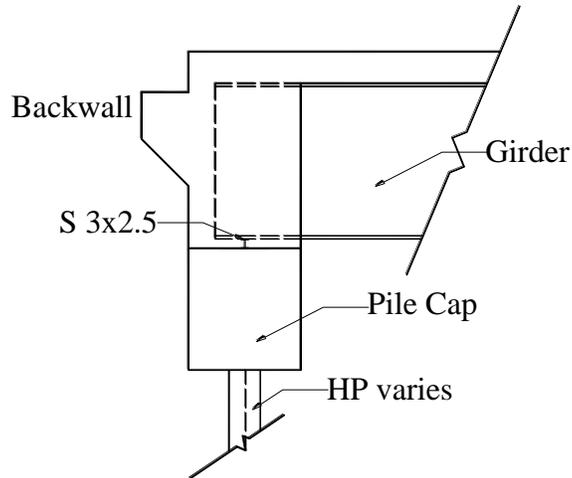
Figure 5.13. Integral abutment Section A-A

Figure 5.14 shows a typical front elevation of a SIAB used at the NEMM. Each girder bears on a curved sole plate with a pintle and a laminated neoprene pad, as shown in Figure 5.15.
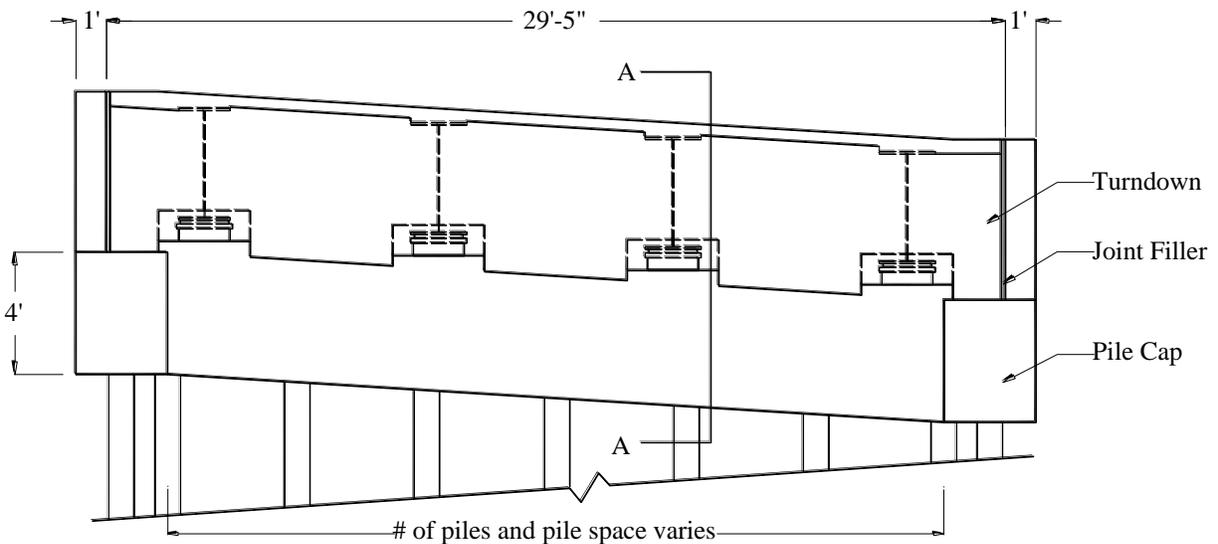
Figure 5.14. Semi-integral abutment – front elevation

Not shown in these figures are the reinforcing steel in the reinforced concrete backwall, mask wall, and pile cap. For the SIAB, no vertical reinforcing bars extend from the pile cap into the backwall. Semi-integral abutments eliminate expansion joints from the bridge deck and their design is intended to eliminate bending strains in the piles due to bridge expansion and contraction because horizontal displacement can occur along the interface between the abutment backwall and pile cap.

5.1.7 Pile Geometry

Both abutments of Bridge 309 (the only bridge to have instrumented substructure elements) had eight HP 10 x 57 piles set in predrilled holes filled with bentonite. Figure 5.16 shows the global coordinate system for the north and south abutment piles of Bridge 309. For these piles, the positive X-axis direction was chosen to be in the same direction as outward expansion of the bridge and the positive Y-axis direction follows the right-hand-rule for a Cartesian coordinate system. For convenience the coordinate system originates at the top of the pile. This coordinate system facilitates better comparisons between abutment pile bending strains and abutment displacements.
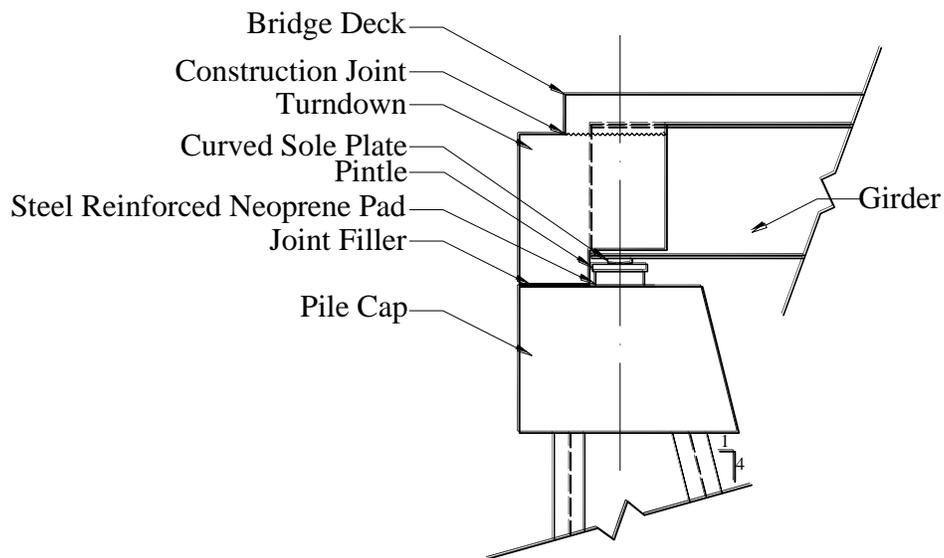
Figure 5.15. Semi-integral abutment Section A-A

(b) South Abutment-Plan View   (c) North Abutment-Plan View

(a) South Abutment–Elevation View   (d) North Abutment–Elevation View
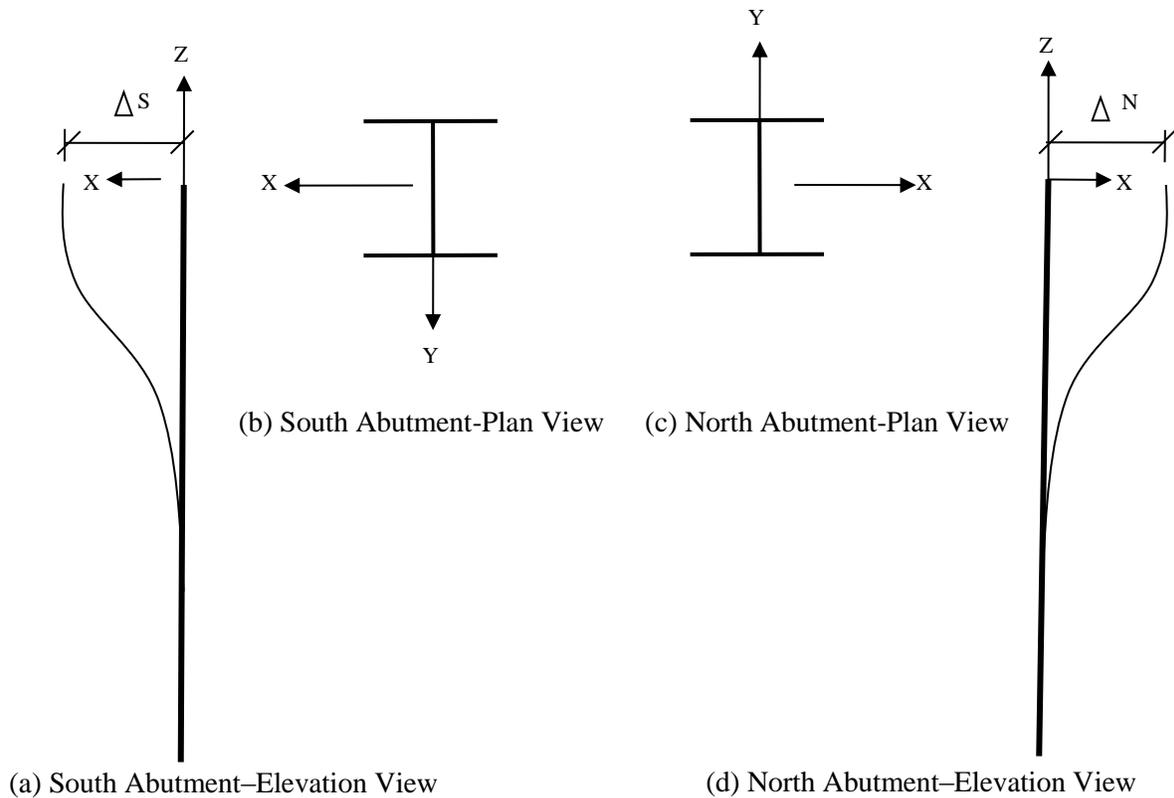
Figure 5.16. Integral Abutment pile coordinate system for Bridge 309

5.2 Long-Term Instrumentation and Data Collection Protocol

5.2.1 Electronic Gauge Instrumentation

Five of the six bridges described previously were instrumented with a variety of electronic devices for measuring changes in strains, displacements, and temperatures that occurred during the bridge monitoring period for the project. The most common instrument attached to the bridges was the Geokon Model 4150 vibrating-wire strain gauge. This gauge is designed to measure load-induced strain on structural steel members. Strains are measured using the vibrating-wire principle: as the tension in a wire changes, so does its vibration frequency. A change in the vibration frequency relates to a change in strain in the wire and, therefore, any element, to which the gauge is mounted. The tension is measured by plucking the wire and measuring the resonant frequency of vibration with an electromagnetic coil positioned next to the wire (Geokon 2009c). Figure 5.17 shows a vibrating strain gauge mounted to a piece of steel prior to the application of the protective coatings.

Figure 5.17. Vibrating-wire strain gauge

For this work, strain gauges measured strains at mid-span of select girders and spans. Only the exterior girders (Girder A and Girder D) were monitored. Horizontally curved bridges were monitored at each span and one straight bridge, Bridge 109, was monitored at mid-span of the center span.

At the locations monitored, four strain gauges were attached to the inside face of the top and bottom flanges. The gauges were placed 1 in. from the flange tips and oriented to measure the longitudinal strains. Four strain gauges were also attached to the inside faces of both flanges of six piles of Bridge 309. These gauges were placed at a distance of 1 in. from the flange tips. The gauges were located 9 in. below the abutment pile cap.

The next most common instrumentation attached to the bridges is the Geokon Model 4420 vibrating wire crack meter. This instrument is designed to measure movement across joints. In the case of this work, the gauge was used to measure the movement between the bridge girders and piers and/or the bridge girders and abutments, depending on the particular bridge being monitored. Herein, this gauge is referred to as an expansion meter. The instrument consists of a vibrating-wire sensing element in series with a spring, which is connected to the wire at one end and to a connecting rod at the other end. As the connecting rod is pulled out from the gauge body, the spring is stretched causing an increase in the tension. This increase in tension is sensed by the vibrating-wire element. Since the tension in the wire is directly proportional to the spring extension, the opening of the joint can be determined (Geokon 2008). Figure 5.18 shows an expansion meter attached to the bottom of a steel girder and to the top of a semi-integral abutment. A similar detail was used to attach an expansion meter at pier locations.

Figure 5.18. Expansion meter

An instrument that was used on only Bridge 309 is the Geokon Model 4427 vibrating-wire long-range displacement meter. This instrument is designed to measure displacements of up to 2 meters. The instrument consists of a spool on which is wound stainless-steel aircraft cable. As the bridge temperature increases, which will induce bridge expansion, the cable unwinds from the spool. When the bridge temperature decreases, which will cause the bridge contraction, the cable is rewound on the spool. The spool is connected to a lead-screw in such a way that the rotation of the spool is converted into a linear motion of the lead-screw. The lead-screw is connected to a Model 4450 vibrating-wire displacement transducer, which measures the linear motion between the two attached objects (Geokon 2009b). Figure 5.19 shows a vibrating-wire long-range displacement meter attached to the abutment backwall. To permit the measurement of relative displacements between two points that are far apart, a long steel aircraft cable was connected to the cable that extends from the reel of the transducer. Bridge 309 was instrumented with three of these sensors allowing relative movement between each of the substructure elements to be monitored.

Figure 5.19. Long-range displacement meter

Ambient air temperature was measured using the Geokon Model 4700 vibrating-wire temperature-gauge. Inside the temperature gauge is a tensioned steel wire. The body of the gauge is stainless steel, while the wire is normal grade steel. As the temperature changes the wire and the body expand and contract at differing rates, causing a change in tension in the wire. The change in tension results in a different vibrating frequency for the wire, which is converted into a temperature change (Geokon 2004). Figure 5.20 shows a gauge on the bottom of one of the bridge decks.
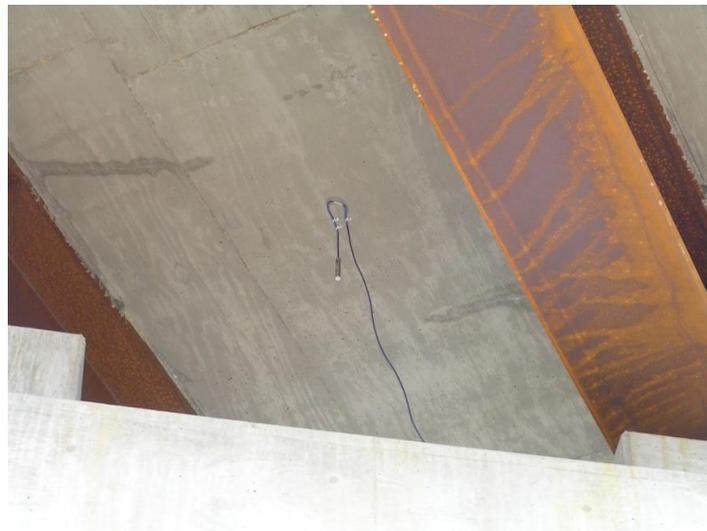
Figure 5.20. Temperature gauge

There were a few instrumentation devices that were attached to the bridges whose locations could not be photographed. Geokon thermistors, Model 3800, were placed at mid-depth of the bridge decks. These gauges are typically used to measure hydration and cooling temperatures in

mass concrete (Geokon 2009a). In this work the gauges measured the temperature of the deck concrete.

On the back side of each abutment pile caps for Bridge 309, two Geokon vibrating-wire pressure cells, Model 4800, were attached. These gauges measure the pressure of the soil induced on the abutment backwall. Earth pressure cells are constructed by welding together the periphery of two stainless-steel plates and leaving a narrow space between them. The hollow space created by the plates is completely filled with de-aired hydraulic oil. The oil pressure is converted to an electrical signal by a hydraulically connected pressure transducer. The electrical signal is transmitted through a signal cable to the readout location (Geokon 2010).

Each of the monitored bridges was instrumented in different ways depending upon individual configurations and the project goals. As shown in Figure 5.21, Bridge 109 had the least amount of instrumentation. Four strain gauges were attached at mid-span of the center span on Girder A and Girder D. Also, an expansion meter 109NPDisp was mounted to the north pier to measure relative movement between Girder B and the fixed pier to determine what relative movement occurred.
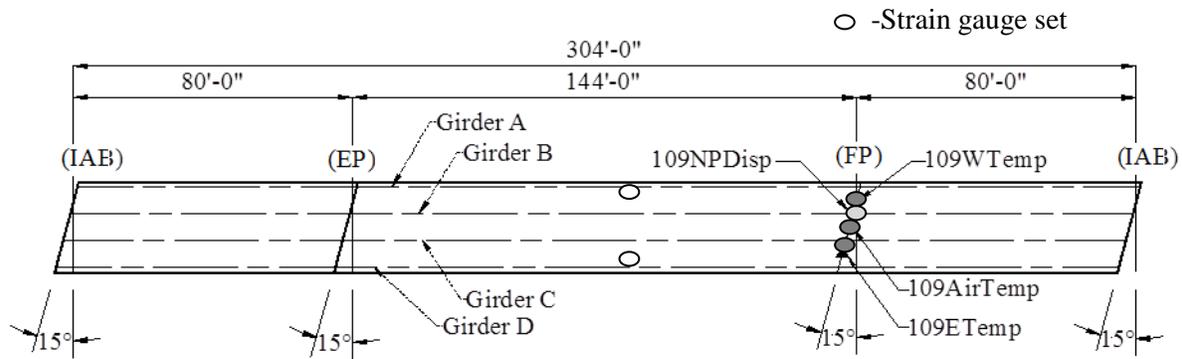
Figure 5.21. Bridge 109 instrumentation

Figure 5.22 shows the instrumentation that was installed on Bridge 209. Strain gauges were installed on the flanges of Girder A and Girder D at the mid-length of all three spans. Also, expansion meters 209SADisp, 209NPDisp, and 209NADisp were mounted to the south abutment, north pier, and north abutment, respectively. The expansion meters measured the relative movement in a direction tangential to the horizontal curve for Girder B. Relative movement was also measured between Girder B, near each end. Also relative movement between Girder B and the expansion pier was monitored.
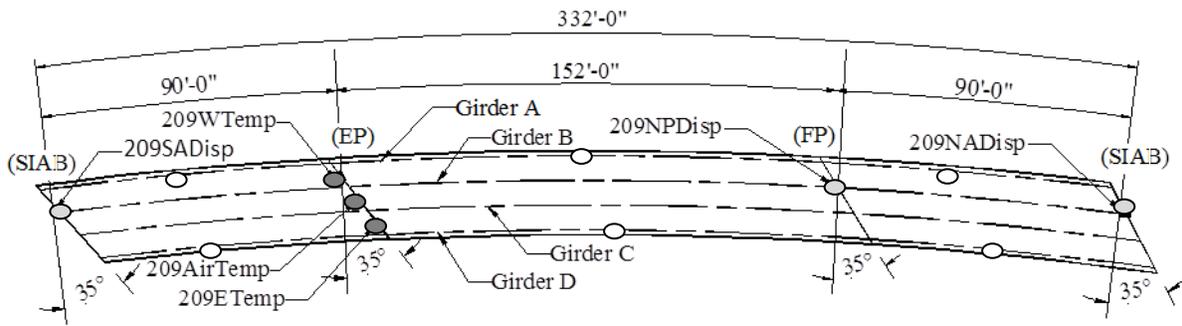
Figure 5.22. Bridge 209 instrumentation

Bridge 309 was the most heavily instrumented bridge. Figure 5.23 shows the location of these monitoring devices. Strain gauges were attached to Girder A and Girder D at mid-length of each span. Not shown on the figure are the strain gauges that were attached to the three piles at each abutment. Long-range displacement meters 309SAP1Disp, 309P1P2Disp, and 309NAP2Disp were mounted at the south abutment, south pier, and north abutment, respectively, to measure the change in the chord length of each span. Two pairs of pressure cells 309SAPrW and 309SAPrE, and 309NAPrW and 309NAPrE were mounted at the third points of each abutment width and at the mid-height of the pile cap to measure soil pressure behind the south and north abutments, respectively. Lastly, temperature gauges 309ETemp and 309WTemp were installed inside the deck on the east and west side of the north pier to measure the concrete temperature and temperature gauge 309AirTemp was hung below the deck at the middle of the north pier to measure ambient air temperature.
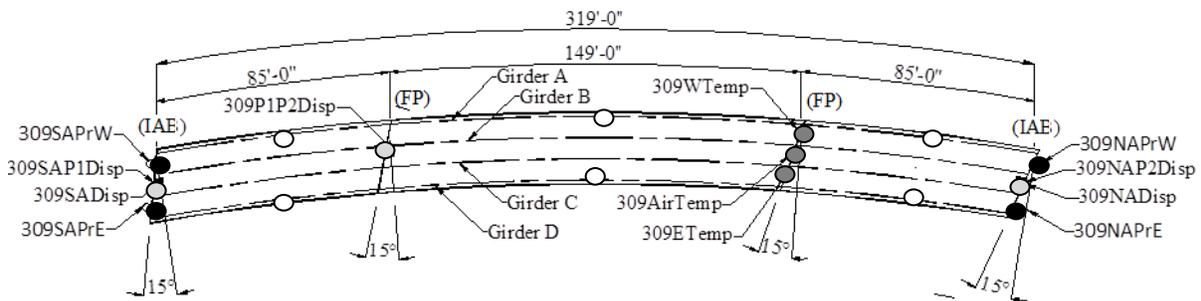
Figure 5.23. Bridge 309 instrumentation

As shown in Figure 5.24, the instrumentation for Bridge 2208 was similar to that used on Bridge 209, with the exception that expansion meters were not placed at the abutments. Expansion meter 2208NPDisp was mounted on the south pier to measure relative movement between Girder B and the pier, an expansion pier.
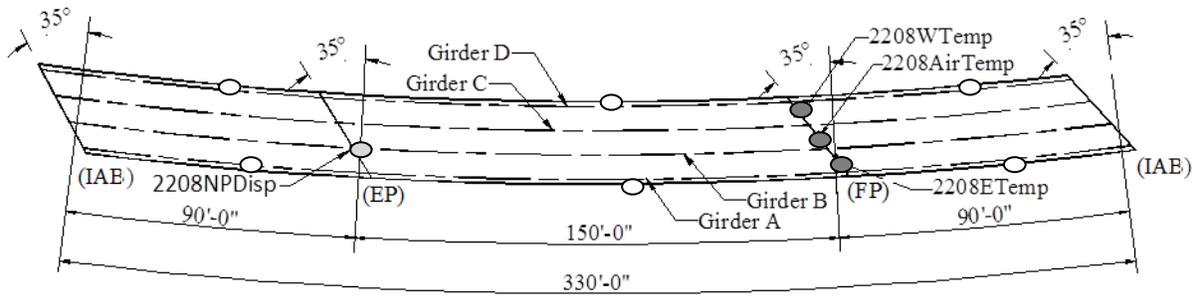
Figure 5.24. Bridge 2208 instrumentation

Figure 5.25 shows that the Instrumentation for Bridge 2308 was similar to that used on Bridge 209, with the exception that expansion meters were not placed at either pier. Expansion meters 2308SADisp and 2308NADisp were mounted on the south and north abutments, respectively, to measure relative movement between Girder B and the abutments. Also, temperature gauges 2308ETemp and 2308WTemp were cast inside the deck at mid-length of center span to measure the concrete temperature and temperature gauge 2308AirTemp was hung below the deck mid-length of center span to measure ambient air temperature surrounding that location of the bridge.
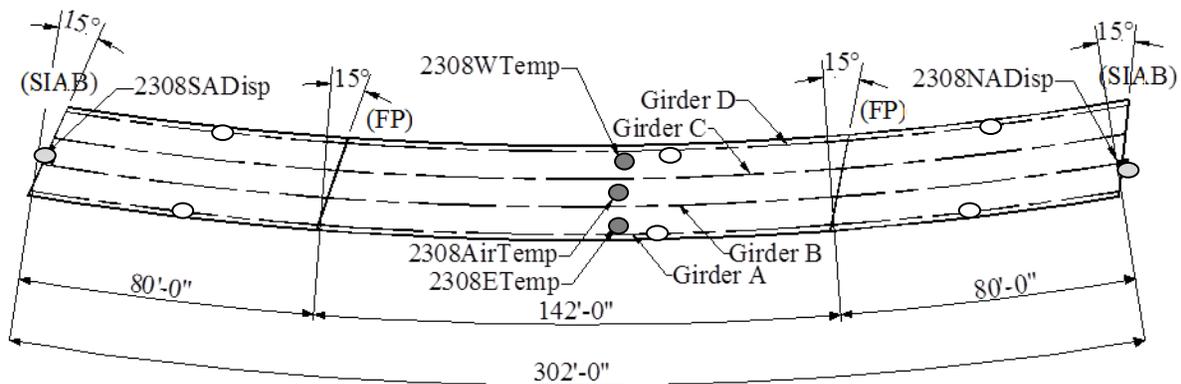
Figure 5.25. Bridge 2308 instrumentation

Along with all the gauges presented in this section, a data collection and storage system for each bridge was assembled, configured, and installed. The data acquisition system consisted of Campbell Scientific data loggers and associated components. The system featured solar power so that line power was not required. Data from each sensor was collected once an hour during the monitoring period.

5.2.2 Survey Instrumentation

Surveying techniques were used to monitor displacements of each of the previously described six bridges. Each bridge had prism reflectors that were mounted near the bearing points of Girder A and Girder D. These reflectors were used as survey targets for monthly surveys of each bridge during the monitoring period. In total, each bridge had eight reflectors that were located at the

abutments and piers. As shown in Figure 5.26, a reflector was bolted to the bottom flange of a metal channel track that was attached to the girder bottom flange. Each reflector was positioned directly below the girder web and was aligned for optimal viewing. These reflectors provided a consistent point to survey each bridge.

Figure 5.26. Reflector instrumentation

Twelve bench marks were installed near the six bridges to establish consistent survey coordinate systems. These benchmarks (which were assumed to not move) were then used to establish the X, Y, Z coordinates for each reflector location. The bench marks consisted of a 3 in. dia. by 10 ft long steel pipe that was embedded 42 in. into the ground. The bottom of the pipe was encased into a concrete footing that rested on undisturbed soil below the frost depth. Figure 5.27a shows a bench mark post during construction. A PVC pipe was sleeved over the steel pipe to shield the steel pipes from direct sunlight that could cause a temperature gradient in the steel pipe and to shield the post from wind that could cause the post to vibrate. A survey reflector was attached to the top of each steel pipe. To shield the reflector from direct sunlight and wind, a T-shaped PVC plumbing fixture was placed over the top of the vertical PVC pipe as shown in Figure 5.27b. The goal with placing these benchmarks was to establish a set of non-moving points in the vicinity of each bridge therefore allowing movements of the bridges to be assessed.

Figure 5.28 shows the relative locations of the reflectors (309P01 through 309P08) that were attached to the Bridge 309 girders, three reflectors (109BM1 though 109BM3) that were mounted to the top of bench mark posts, and the two relative positions where the surveying instrumentation was placed (309TS1 and 309TS2) for Bridge 309. Note that the locations shown in this figure for the total station and for the bench marks were not drawn to scale. Further, this configuration is representative of that utilized at all bridges. From each total station location, the

eight reflectors on the bridge girders and the three reflectors on the bench mark posts were clearly visible when viewed with the survey instrument.

(a) Construction   (b) Operational

Figure 5.27. Survey benchmark

The surveyor used a Topcon GPT-7501 Pulse Total Station to monitor the bridges during the monitoring period of the project. The GPT-7501 Total Station is accurate to 1 in. at 3000 meters and comes pre-loaded with Windows CE.NET.4.2 and TopSURV 7.2 surveying software (Topcon 2007).
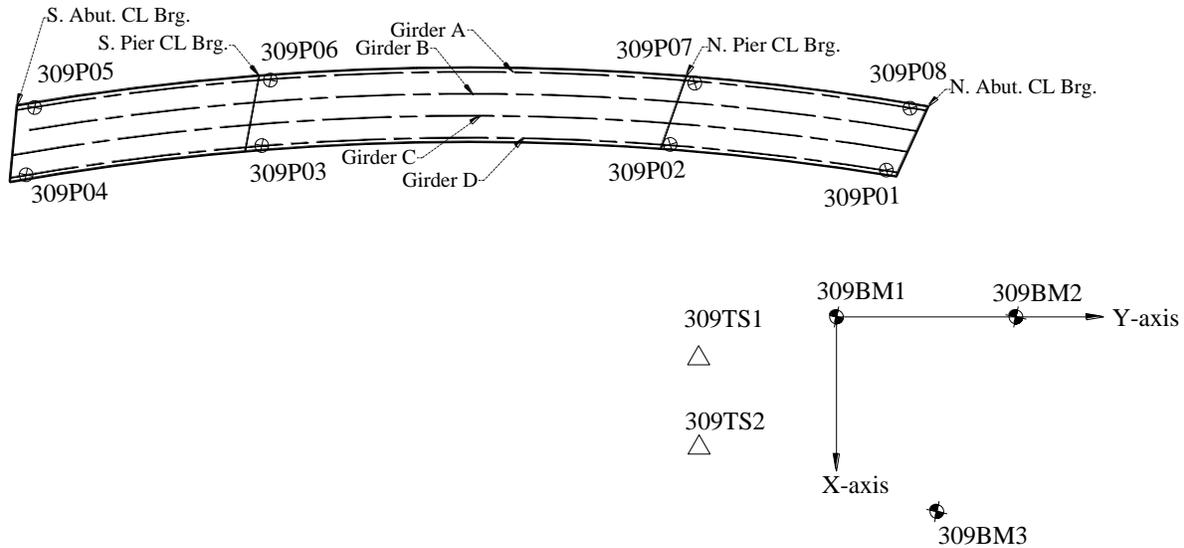
Figure 5.28. Bridge 309 reflector, TS, and BM locations

5.2.3 Data Collection

Once a month a team traveled to the NEMM. While there, the team retrieved the electronic data and surveyed the bridges in the following order: 309, 109, 2208, 2308, 2408, and 209. The survey process at each bridge took approximately one hour. Three survey cycles were completed in which the surveyor shot and recorded the relative location of the benchmark reflectors and the bridge reflectors. The data for each point were stored in the total station as slope distance, horizontal angle, and zenith angle. In all cycles the total station was rotated through 360° such that any closure error could be accounted for while post-processing the data. After the first three cycles, the surveyor moved and re-setup the total station and repeated the process used during the first three cycles. After all six bridges were surveyed the data were transferred from the total station to a permanent storage location.

The team post processed the data to transform the new survey data into a Cartesian coordinate system originating at BM1. With the Y-axis oriented from BM1 to BM2 and the X-axis 90° clockwise from the Y-axis, as shown in Figure 5.28.

5.3 Short-Term Instrumentation and Data Collection Protocol

5.3.1 Strain Transducer Information

Strain transducers were used to test live load, superstructure behavior of one straight bridge and four horizontally curved bridges. Bridge Diagnostics, Inc. (BDI) strain transducers were used throughout the testing. These temporarily placed transducers are designed to measure load-induced strain on structural members. In this testing, the structural members instrumented were limited to the steel girders of the superstructure of all five bridges. The BDI strain transducers

are 3 in. reusable gauges that mount directly to the surface of the structure using adhesive. An example photograph of a mounted transducer is shown in Figure 5.29.

Figure 5.29. Mounted strain transducer

The superstructure of each curved bridge was instrumented with 40 strain transducers. Each of the four I-girders was outfitted with four transducers at two separate radial cross-sections. In all cases the first cross-section, Section 1, is located at half the unbraced length between two diaphragms. Section 2 is located where diaphragms are present. Both sections are parallel to the radius of curvature and adjacent to one another. The instrumented sections of each bridge are illustrated in the plan views of Figure 5.30 through Figure 5.34.
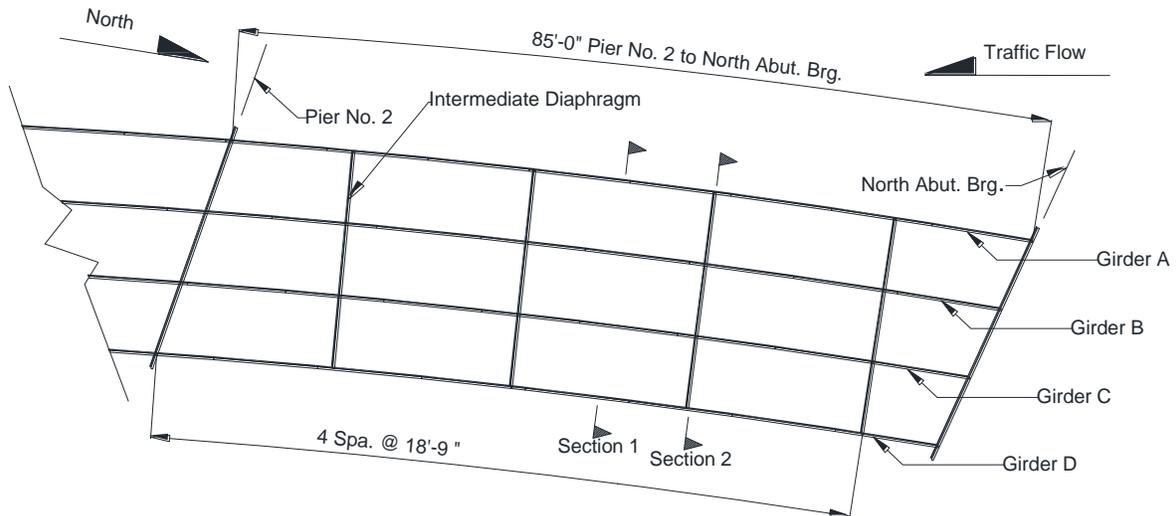
Figure 5.30. Bridge 309 plan view

Traffic Flow

90'-0" South Abut. Brg. to Pier No.1

North

Intermediate Diaphragm

Pier No. 1

South Abut. Brg.

Girder A

Girder B

Girder C

Section 2   Section 1

Girder D

4 Spa. @ 17'-2 $\frac{3}{8}$"
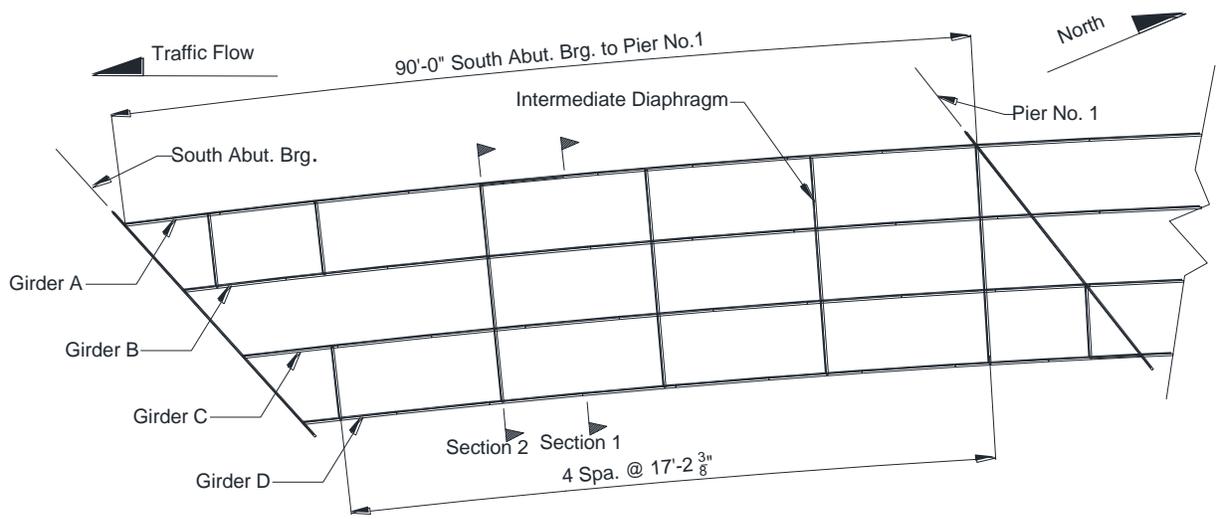
Figure 5.31. Bridge 209 plan view

North

Traffic Flow

South Abut. Brg.

4 Spa. @ 17'-2 $\frac{3}{8}$"

Intermediate Diaphragm

Pier No. 1

Girder D

Girder C

Girder B

Girder A

Section 2 Section 1

90'-0" North Abut. Brg. to Pier No. 1
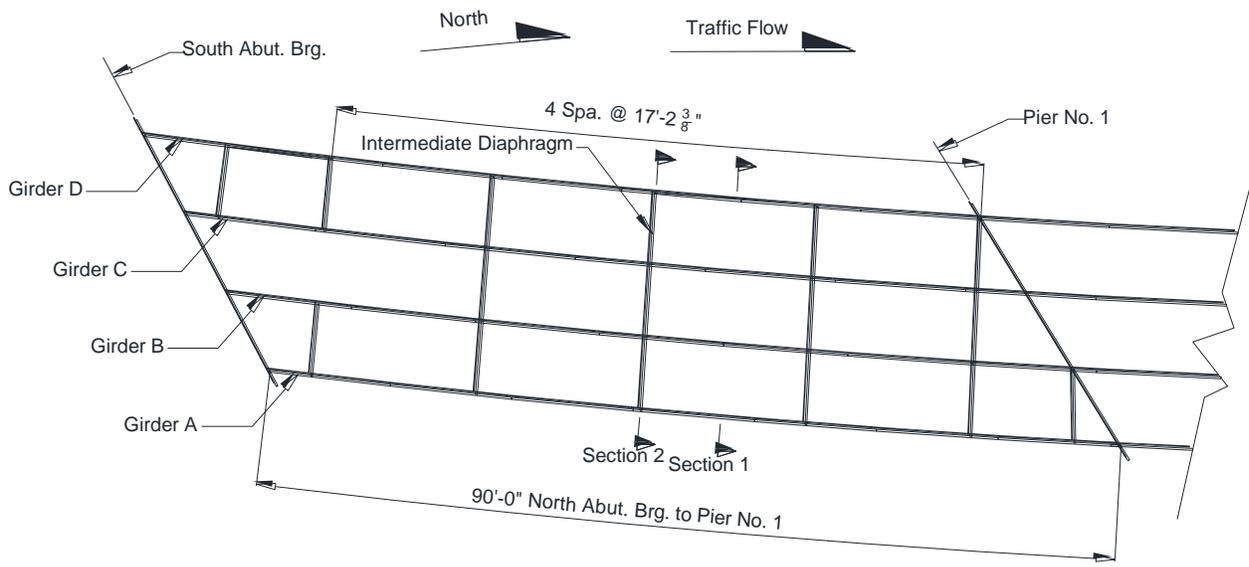
Figure 5.32. Bridge 2208 plan view
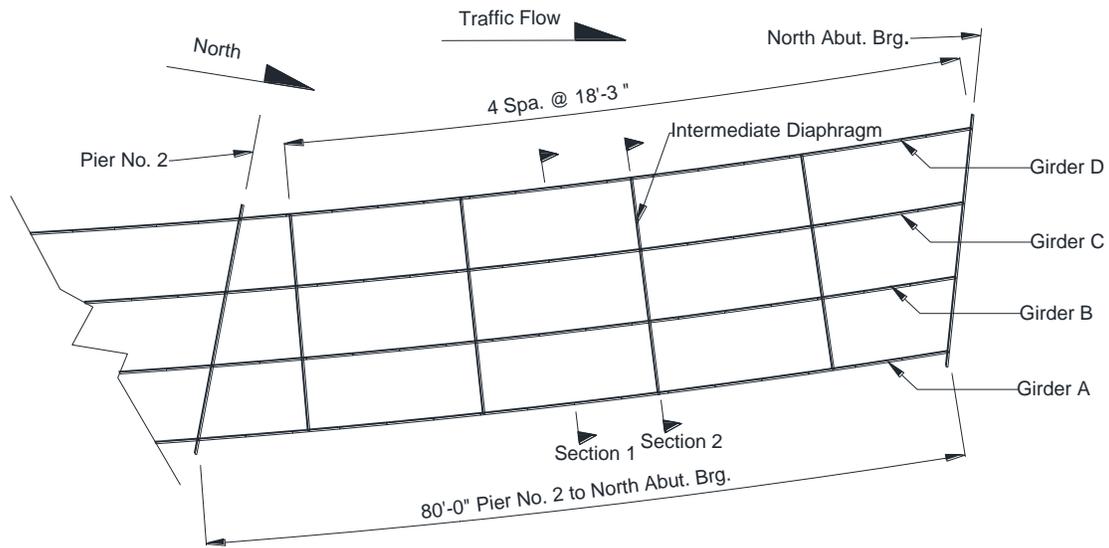
Figure 5.33 Bridge 2308 plan view
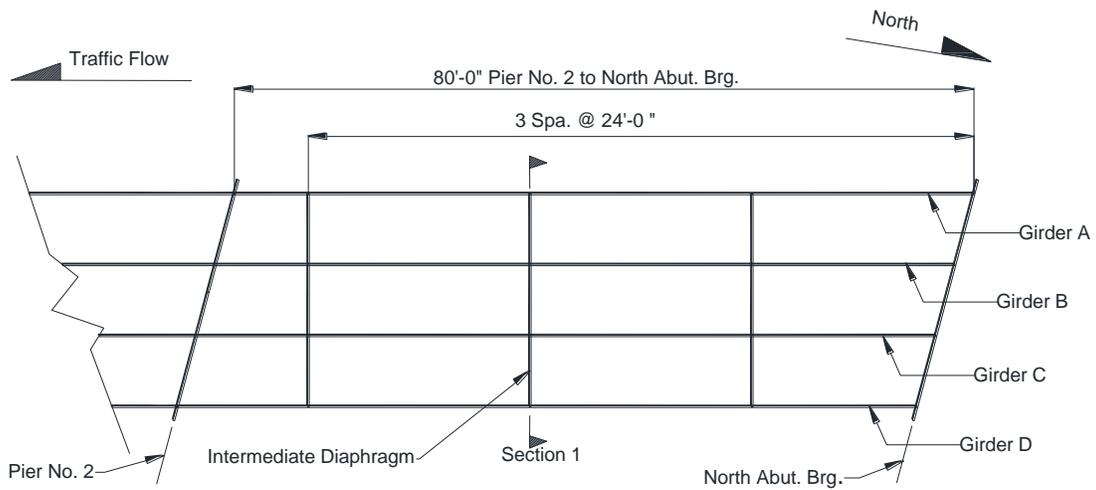
Figure 5.34. Bridge 109 plan view

Four strain transducers were placed on the upper and lower flanges of each girder at both sections shown in Figure 5.35 and Figure 5.36. In Section 2, the two diaphragms towards the inside of the curve were instrumented with transducers at mid-length. The diaphragm towards the outermost of the curve was instrumented with four transducers located at the one-third points as shown in Figure 5.36. Figure 5.37 displays the detailed placement of the transducers on both the girder and diaphragm flanges.

52

Only 16 transducers were placed on the only straight bridge tested, Bridge 109. These transducers were installed only at one section. This section is comparable to Section 1 in the curved bridges, where the transducers were placed at half the unbraced length between two cross frame sections as illustrated in Figure 5.34. No Bridge 109 diaphragms or cross frames were instrumented.
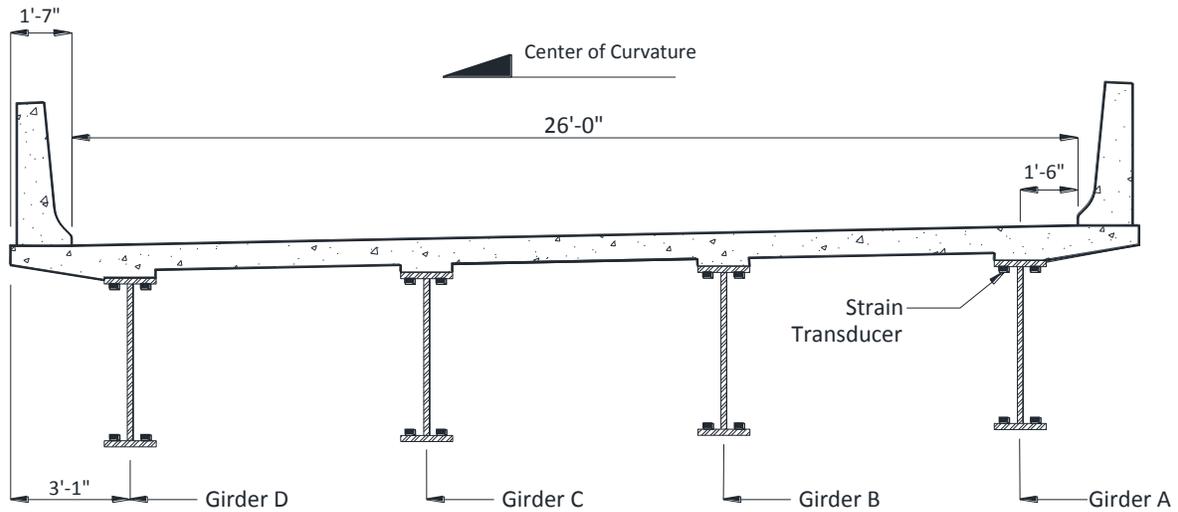
Figure 5.35. Section 1 strain transducer locations
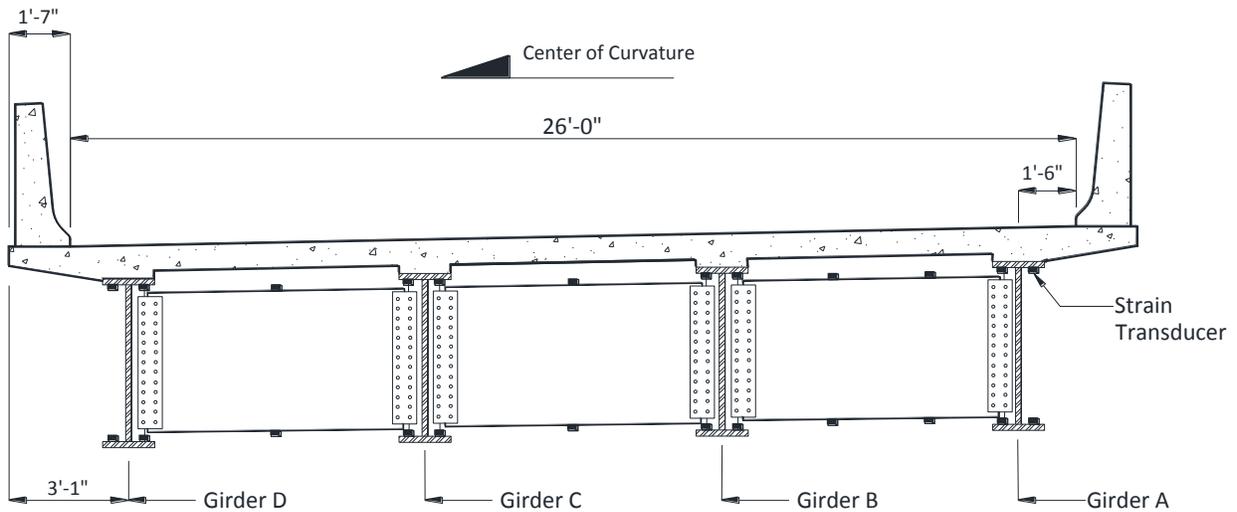
Figure 5.36. Section 2 strain transducer locations
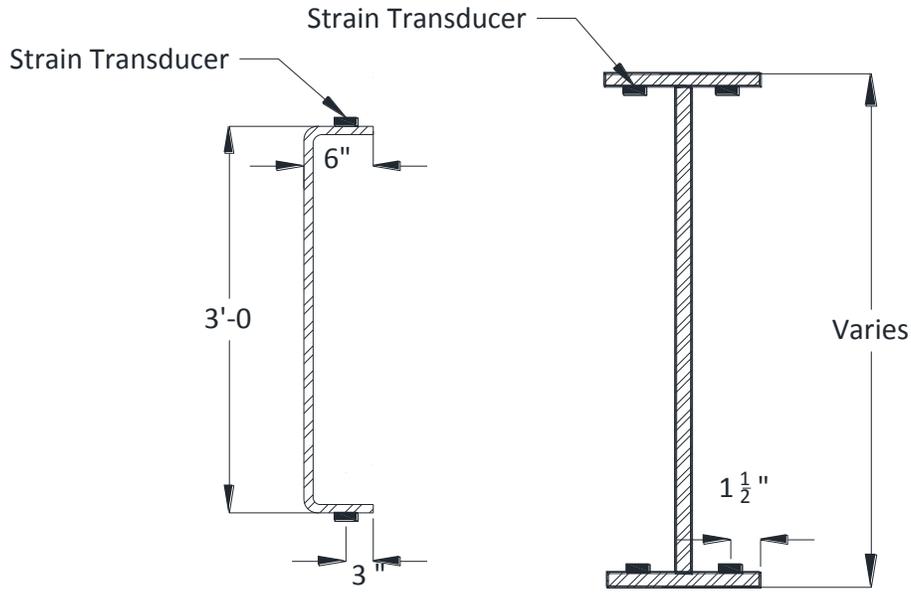
Figure 5.37. I-girder and diaphragm strain transducer detail

5.4 Live Load Testing

This section discusses three aspects of live load testing, the test vehicle, load paths, and static and dynamic test procedures.

5.4.1 Test Vehicle

A three-axle Iowa Department of Transportation dump truck was used for live load testing of all five bridges. The test vehicle consisted of three axles, one steer axle and two drive axles. Loaded with gravel, the gross vehicle weight of the truck was approximately 48,700 lb. Individual axle weights along with the gross vehicle weight were recorded at a Certified Automated Truck Scale located in Des Moines. Refer to Figure 5.38 for axle spacing and loading.
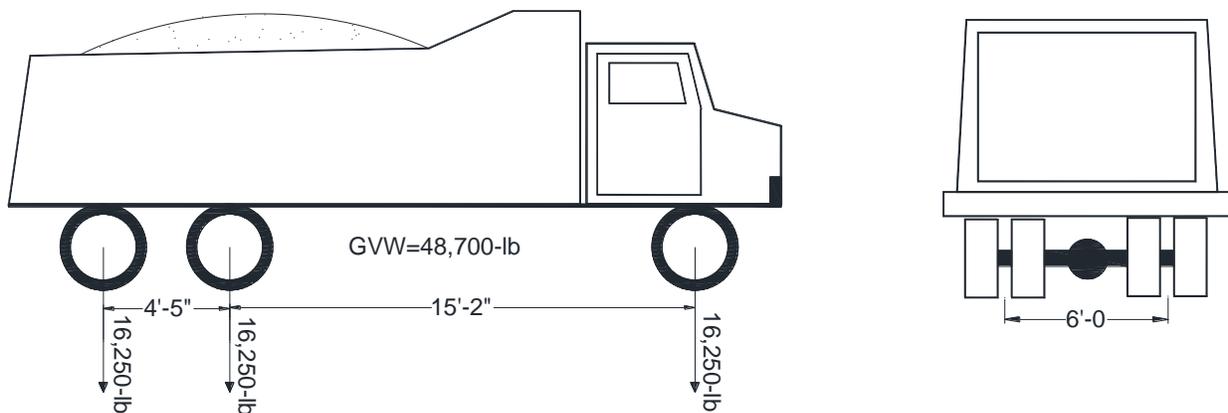
Figure 5.38 Truck configuration and loading

5.4.2 Load Paths

Three parallel load paths were pre-defined so as to induce extreme and typical truck positions. The driver-side wheels were placed 2 ft from the inner barrier rail on Load Path 1 (LP1). Load Path 2 (LP2) was centered on the bridge deck. The passenger-side wheels were placed 2 ft from the outer barrier rail on Load Path 3 (LP3). These three paths are outlined in Figure 5.39, which represents a general horizontally curved bridge.

(a)

(b)
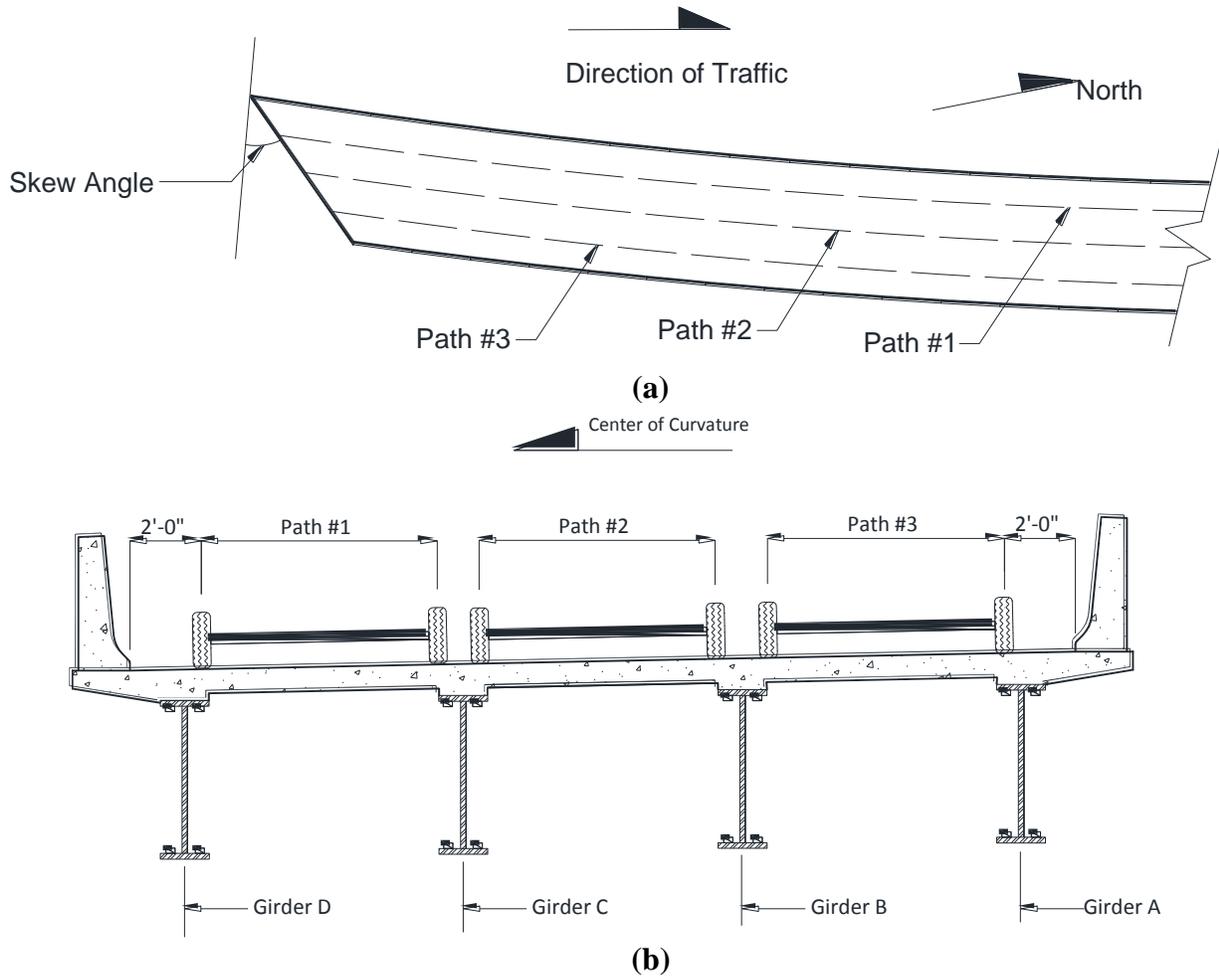
Figure 5.39. (a) Plan view and (b) cross section view of load path placement

5.4.3 Static Load Data Collection

Static load testing was conducted for all three load paths. For each trial, the truck travelled across the bridge along the individual load path at a crawl, or walking pace. Each load path consisted of two identical trials to ensure that consistent data were being collected. Hence, six total static load trials were logged.

Prior to collecting data on the acquisition software, each individual strain transducer was zeroed and the sample frequency was set to 20 Hz. Once the testing trials began, longitudinal tracking of the vehicle occurred at 20 ft intervals.

5.4.4 Dynamic Load

Only two trials were conducted for the dynamic load cases. For this testing, the speed of the truck was increased to approximately 35-45 mph. Again, two identical trials were performed to ensure consistent data collection. Load Path 2 was used for both trials. Due to the increased speed, the truck could not be safely placed at a constant 2 ft from the barrier rails; consequently, Load Paths 1 and 3 were not used. Data were collected at 100 Hz. Since the truck was moving at increased speeds, only start and end of bridge truck positions were recorded.

CHAPTER 6 LONG-TERM EXPERIMENTAL PROCEDURE AND RESULTS

6. 1 Pre-analysis

6.1.1 Thermal Strains due to Solar Radiation

During initial evaluation of data collected from the strain gauges mounted on the girders an unusual amount of outliers were noticed. It was found that the cover used to protect the strain gauges did not provide enough thermal protection when exposed to direct sunlight. The sunlight raised the temperature of the gauge significantly and resulted in what were determined to be erroneous readings. To remedy this, only girder strain gauge data collected between 9 p.m. to 6 a.m. were considered in the analysis.

6.1.2 Setting a Reference Date

Because the installed instrumentation measured changes over time a reference date is needed to be set. The reference date is the date where the sensors were essentially zeroed. The reference date was selected to be the reading at 6 a.m. April 28, 2011. April 28th was the first date that all the measured data were believed to be high quality. Prior to this date, the team had instrumentation issues that resulted in erroneous data.

No April 28th survey data were available at the 6 a.m. reference date since surveys were performed during the daylight. However, the survey from the April 28th survey was set as the reference date for the survey data.

All data in this report are presented with respect to the reference date. Therefore, all date reference data presented here is equal to the difference between the instrument reading at that date and the instrument readings at the reference date. For example, the difference between the strain reading at the reference date and the current strain reading would be calculated as:

$$\Delta\varepsilon = \varepsilon_{current} - \varepsilon_{reference} \tag{6.1}$$

where,
$\quad\quad \Delta\varepsilon \quad$ = difference in microstrain,
$\quad\quad \varepsilon_{current}$ = microstrain reading at its respective time, and
$\quad\quad \varepsilon_{reference}$ = microstrain reading on April 28, 2011 at 6 a.m.

Since there is a slight difference between the reference date for the instrumentation data and for the surveying data, to compare instrumentation data and surveying data, the difference between the reference positions of the two data sets had to be taken into account. Equation 6.3 presents the proper conversion. Effectively, equation 6.3 aligns the reference date of the survey data and the instrumentation data when they are displayed together.

$$\Delta L_s = \Delta L_s{}' + \Delta L_{avg} \tag{6.3}$$

where,

  ΔL_s = adjusted surveying total bridge expansion referenced to April 28, 2010 at 6 a.m.,
  $\Delta L_s'$ = surveying total bridge expansion at the time of the survey on April 28, 2011; and
  ΔL_{avg} = average bridge expansion computed via instrumentation data during the surveying
time interval.

6.1.3 Effective Temperature and Effective Alpha

Since concrete and steel expand and contract at differing rates, it was necessary to formulate an effective coefficient of thermal expansion, α_{eff}, to simulate the composite behavior of the bridge. In this section, the following variables will be utilized.

  α_{eff} = effective thermal expansion coefficient of combined steel and concrete,
  A_c = area of concrete,
  A_s = area of the steel,
  E_c = linear elastic modulus of concrete,
  E_s = linear elastic modulus of steel,
  α_c = thermal expansion coefficient of concrete,
  α_s = thermal expansion coefficient of steel,
  L_c = length of the concrete member, and
  ΔT_c = change in temperature of the concrete member,
  L_s = length of the steel member,
  ΔT_s = change in temperature of the steel member,
  ΔT_{eff} = effective bridge temperature,
  P_s = applied unit load on steel,
  P_c = applied unit load on concrete,
  P = applied load on composite section,
  δ_s = displacement of steel,
  δ_c = displacement of concrete, and
  δ = displacement of composite section.

Equation 6.4 has been used in previous studies and will be used herein to represent the effective thermal expansion (Abendroth 2005).

$$\alpha_{eff} = \frac{(A_c E_c \alpha_c + A_s E_s \alpha_s)}{(A_c E_c + A_s E_s)} \tag{6.4}$$

To describe the temperature of the entire bridge, an effective temperature, T_{eff}, was derived. Figure 6.1 displays a rectangular concrete member with an axial tension load, P_c, and the resulting displacement, δ_c.

58
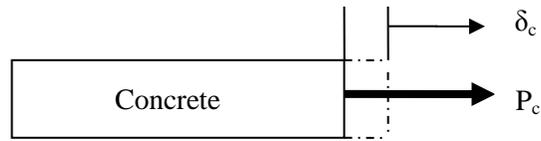
Figure 6.1. Concrete member

Equation 6.5 is the governing equation that combines the change in length due to the applied load and due to a change in temperature of the concrete member.

$$\delta_c = \frac{P_c L_c}{A_c E_c} + \alpha_c \Delta T_c L_c \tag{6.5}$$

Figure 6.2 displays a rectangular steel member with an axial tension load, P_s, and the resulting displacement, δ_s.
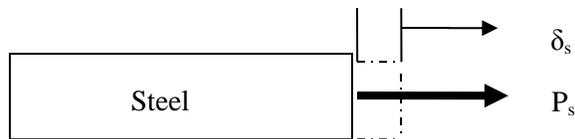
Figure 6.2. Steel member

Equation 6.6 is the governing equation that combines the change in length due to applied load and due to a change in temperature of the steel member.

$$\delta_s = \frac{P_s L_s}{A_s E_s} + \alpha_s \Delta T_s L_s \tag{6.6}$$

Next in a perfectly composite element, it is assumed that the change in length of the concrete member, δ_c, is equal to the change in length of the steel member, δ_s, and the length of both members, L_c and L_s, are also equal to L. Figure 6.3 displays a composite concrete and steel rectangular member with an axial tension, P, and a resulting change in length, δ.
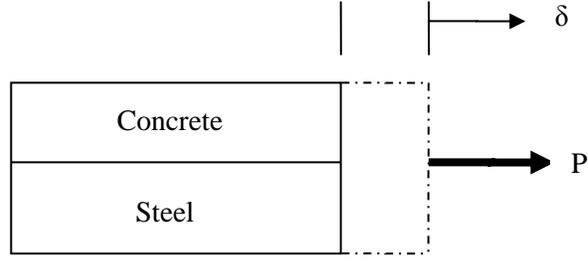
Figure 6.3. Composite concrete and steel member

Considering the assumptions stated in the previous paragraphs and Equations 6.5 and 6.6 and the equation for the effective thermal expansion coefficient for combined steel and concrete (Equation 6.4). An effective bridge temperature can be derived as follows:

1. Since $\delta = \delta_s = \delta_c$ and $L = L_s = L_c$
   a. Then $\delta = \left(\frac{P_s L}{A_s E_s}\right) + \alpha_s \Delta T_s L = \left(\frac{P_c L}{A_c E_c}\right) + \alpha_c \Delta T_c L$
2. If $P_c + P_s = P$ and $P = 0$ for free expansion
   a. Then $P_s = -P_c$
   b. And $\delta = \left(\frac{-P_c L}{A_s E_s}\right) + \alpha_s \Delta T_s L = \left(\frac{P_c L}{A_c E_c}\right) + \alpha_c \Delta T_c L$
   c. Re-arranging like terms $\alpha_s \Delta T_s - \alpha_c \Delta T_c = P_c \left(\frac{1}{A_c E_c} + \frac{1}{A_s E_s}\right)$
   d. Lastly $P_c = \left(\dfrac{\alpha_s \Delta T_s - \alpha_c \Delta T_c}{\frac{1}{A_c E_c} + \frac{1}{A_s E_s}}\right)$
3. Substitute equation from step 2d into eq. 6.5
   a. $\delta = \left(\dfrac{(\alpha_s \Delta T_s - \alpha_c \Delta T_c)L}{A_c E_c \left(\frac{1}{A_c E_c} + \frac{1}{A_s E_s}\right)}\right) + \alpha_c \Delta T_c L$
   b. $\delta = \left(\dfrac{(\alpha_s \Delta T_s - \alpha_c \Delta T_c)L}{\left(1 + \frac{A_c E_c}{A_s E_s}\right)}\right) + \alpha_c \Delta T_c L$
   c. $\delta = \left(\dfrac{\alpha_s \Delta T_s L - \alpha_c \Delta T_c L + \alpha_c \Delta T_c L\left(1 + \frac{A_c E_c}{A_s E_s}\right)}{\left(1 + \frac{A_c E_c}{A_s E_s}\right)}\right)$

By simplifying step 3c one last time equation 6.7 results. Equation 6.7 gives the free change in length of the combined concrete and steel member under a uniform temperature change.

$$\delta = \left(\frac{A_c E_c \alpha_c \Delta T_c L + A_s E_s \alpha_s \Delta T_s L}{A_c E_c + A_s E_s}\right) \tag{6.7}$$

In a similar manner:

$$\Delta T_{eff} = \left(\frac{\delta}{L}\right)\left(\frac{1}{\alpha_{eff}}\right) \tag{6.8}$$

60

Substituting equations 6.4 and 6.7 into equation 6.8 produces the final equation for the effective bridge temperature, $\Delta T_{eff.}$

$$\Delta T_{eff} = \frac{(A_c E_c \alpha_c \Delta T_c + A_s E_s \alpha_s \Delta T_s)}{(A_c E_c \alpha_c + A_s E_s \alpha_s)} \qquad (6.9)$$

Utilizing the temperatures measured from each of the strain gauges, and from the temperatures gauges embedded in the concrete, an effective temperature could be calculated when all measurements were taken.

6.1.4 Temperature Correction for Long-Range Distance Meters (LRDM)

Internal Correction

Temperature ranges greater than 50° Fahrenheit impact an LRDM displacement reading (Geokon 2009). Given the expected operational temperature ranges, it was necessary to apply a temperature correction to the results. Equation 6.10 is the controlling formula for making such corrections.

$$\Delta D_{corrected} = \Delta D_{uncorrected} + K(T_i - T_0)G \qquad (6.10)$$

where,
$\Delta D_{uncorrected} = $ reading, in inches, before a temperature correction,
$K = $ a temperature correction coefficient given by the manufacturer (digits/°C), and
$G = $ correction factor that converts digits to inches (provided by manufacturer).

$\Delta D_{uncorrected}$, and K are calculated by the following equations:

$$\Delta D_{uncorrected} = D_i - D_0 \qquad (6.11)$$
$$K = MR_i + B \qquad (6.12)$$

where,
$D_0 = $ initial reading,
$D_i = $ reading at time i,
M and $B = $ constants for the model 1127 gauges given by the manufacturer, and
$R_i = $ the frequency reading produced by the gauge when the vibrating wire is plucked.

To calculate R_i it is necessary to use equation 6.13. The quadratic formula is then solved to calculate the values of R_i.

$$D_i = AR_i^2 + BR_i + C \qquad (6.13)$$

where,
A, B, and $C = $ gauge specific constants given by manufacturer.

External Correction

An external temperature correction was applied to the cable connected to the LRDMs. Specifically, as the cable temperature rose above the initial temperature, the cable would naturally lengthen. As a result, the measured value would be smaller than actual. Similarly, as the cable temperature lowered below the initial temperature, the cable would naturally shorten. As a result, the measured displacement would be greater than actual displacement. Equation 6.14 shows the appropriate correction that is applied.

$$\Delta D_{cable} = \alpha_{cable} \Delta T_{air} L_{cable} \tag{6.14}$$

where,
ΔD_{cable} = the correction,
α_{cable} = the coefficient of thermal expansion of the cable,
ΔT_{air} = the ambient air temperature, and
L_{cable} = the length the cable.

6.2 Member Strains and Forces

As mentioned previously, five of the six bridges in the study were instrumented with strain gauges. The data collected from these strain gauges were used to calculate the internal strains and forces induced in each bridge due to ambient temperature changes. Member strains are induced as a result of restraining temperature induced expansion and contraction of a bridge.

6.2.1 Superstructure

Girder Resolved Strains and Forces

As discussed previously, a girder coordinate system was established and the important girder section properties calculated. Figure 6.4 depicts the forces considered in analysis of the composite section. The forces were chosen to align with the AASHTO codified approach for calculating lateral forces due to live loading (AASHTO 4-3).

Referencing Figure 6.4, the following describes each of the external forces induced on each composite section , measured by each strain sensor on the steel cross section, and then resolved using the subsequently described process: P represents the axial force induced on the composite cross-section; tension is positive. M_x represents strong axis bending of the composite cross-section, M_x is positive when the top flange is in compression. M_{lt} and M_{lb} represent lateral bending of the top and bottom steel flange, respectively. As is considered in AASHTO, tension in the flange tip on the outside of the curve is considered positive. The lateral moment in the concrete is represented as M_{lc} so that the total lateral moment would the sum of M_{lt}, M_{lb} and M_{lc}.

According to AASHTO: (1) flange lateral bending is the bending of a flange about an axis perpendicular to the flange plane due to lateral loads applied to the flange and/or non-uniform

torsion in the member (AASHTO 4-3), (2) flange lateral bending stress is the normal stress caused by flange lateral bending (AASHTO 4-3), and (3) lateral moments M_{lt} and M_{lb} are the moments about the Y-axis in the top and bottom flange, respectively, and replaces combined weak axis bending plus torsional warping. For reference Equation 6.15 can be found in the AASHTO Bridge Design Guidelines (Eq. C4.6.1.2.4b-1), and is used to calculate the lateral flange moment, M_{lat}, in a girder at the brace point due to vertical loading (Note: current AASHTO specifications contain no codified approach for calculating temperature induced loadings):

$$M_{lat} = \frac{M_x L^2}{NRD} \qquad (6.15)$$

where,

M_x = major axis bending,

L = length of the member,

N = a constant of either 10 or 12 (engineer's discretion),

R = the radius of the girder, and

D = the depth of the web.
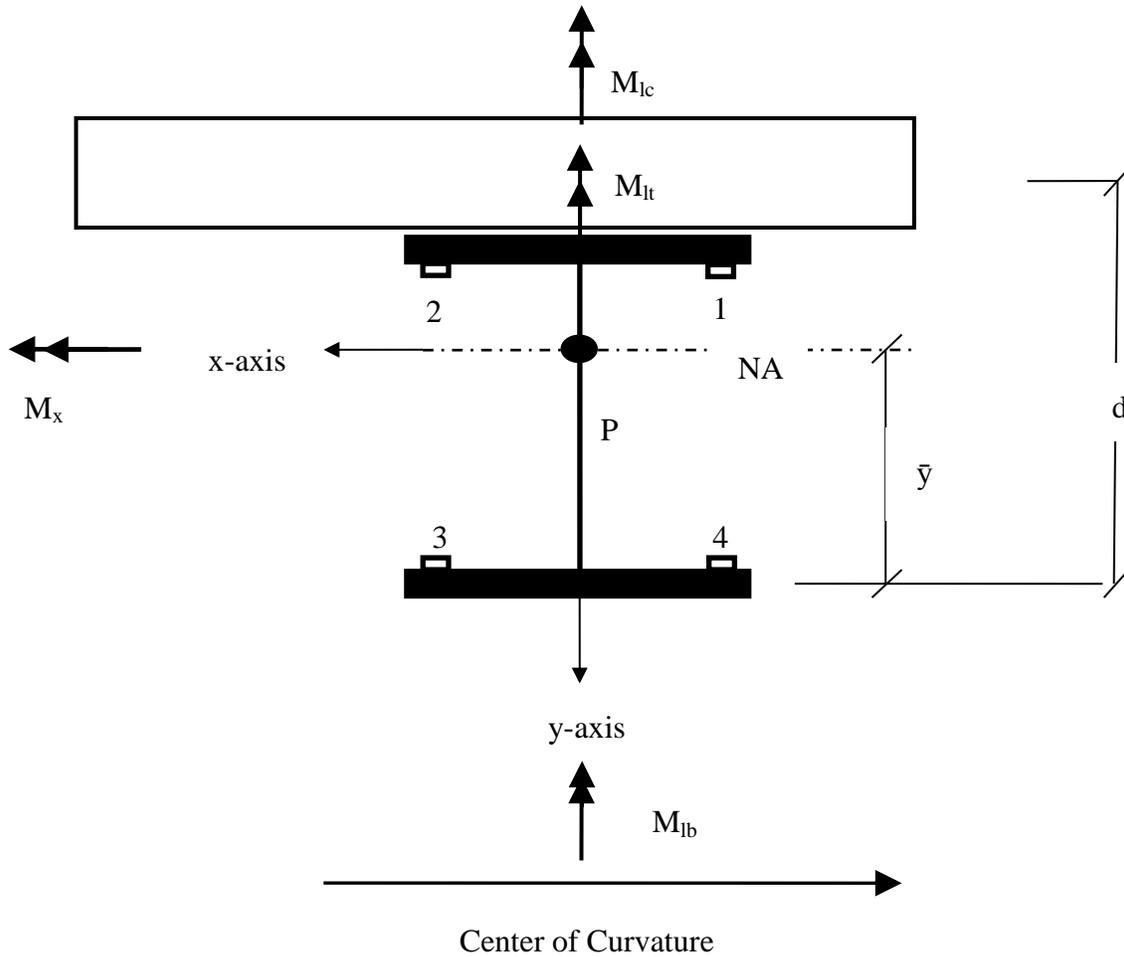
Figure 6.4. Resolved girder forces

Utilizing the four measured strains at each steel girder cross section and the specific girder cross sectional properties (Table 5.4), one is able to calculate the four resolved forces in the composite section described previously. Figure 6.5 displays a set of matrices that describe the relationship between the four known internal strains at the strain gauge locations and the four desired internal strains.

$$
\begin{Bmatrix} \varepsilon_1 \\ \varepsilon_2 \\ \varepsilon_3 \\ \varepsilon_4 \end{Bmatrix} = \begin{bmatrix} 1 & y_1 & x_1 & 0 \\ 1 & y_2 & x_2 & 0 \\ 1 & y_3 & 0 & x_3 \\ 1 & y_4 & 0 & x_4 \end{bmatrix} \begin{Bmatrix} \dfrac{P}{(AE)_{eff}} \\ \dfrac{M_x}{(EI_x)_{eff}} \\ \dfrac{M_{lt}}{E_s I_{yft}} \\ \dfrac{M_{lb}}{E_s I_{yfb}} \end{Bmatrix}
$$

Figure 6.5. Four equations and four unknowns

where,

ε_i = strain reading at gauge i,

x_i = distance from neutral axis to strain gauge i along the X-axis, and

y_i = distance from neutral axis to strain gauge i along the Y-axis.

The relationship between internal axial strain and internal axial force is described by equation 6.16. The relationship between major axis bending strain and major axis bending moment is described by equation 6.17. The relationship between lateral bending strain and lateral bending moment in the top and bottom flange in represented by equations 6.18 and 6.19.

$$
\varepsilon_a = \frac{P}{(AE)_{eff}} \tag{6.16}
$$

where,

ε_a = internal axial strain, and

P = the internal axial force.

$$
\varepsilon_x = \frac{M_x y_3}{(EI_x)_{eff}} \tag{6.17}
$$

where,

ε_x = strong axis bending strain, and

M_x = strong axis bending moment.

$$
\varepsilon_{ylt} = \frac{M_{lt} x_2}{E_s I_{yft}} \tag{6.18}
$$

where,

ε_{ylt} = lateral bending strain in the top flange, and

M_{lt} = lateral bending moment in the top flange.

$$\varepsilon_{ylb} = \frac{M_{lb}x_4}{E_s I_{yfb}}$$

(6.19)

where,

ε_{ylb} = lateral bending strain in the bottom flange, and
M_{lb} = lateral bending moment in the bottom flange.

Typical Girder Strain Data at Gauge versus Time

Figures 6.6 through 6.9 illustrate typical girder strain gauge data versus date. Each of the figures represents a specific girder flange location and the illustrations represent data from the center span of Girder D on Bridge 309. (The strains are the strains due to stress, sometimes called load strain. In this work, the loading is primarily thermal. Vibrating wire gauges measure slowly changing strain that would filter out most moving live load strains.) (As described in Section 6.1, all strains are in the time interval from 9 pm to 6 am and the reference (or zero) strain is at 6 am, April 28, 2011).
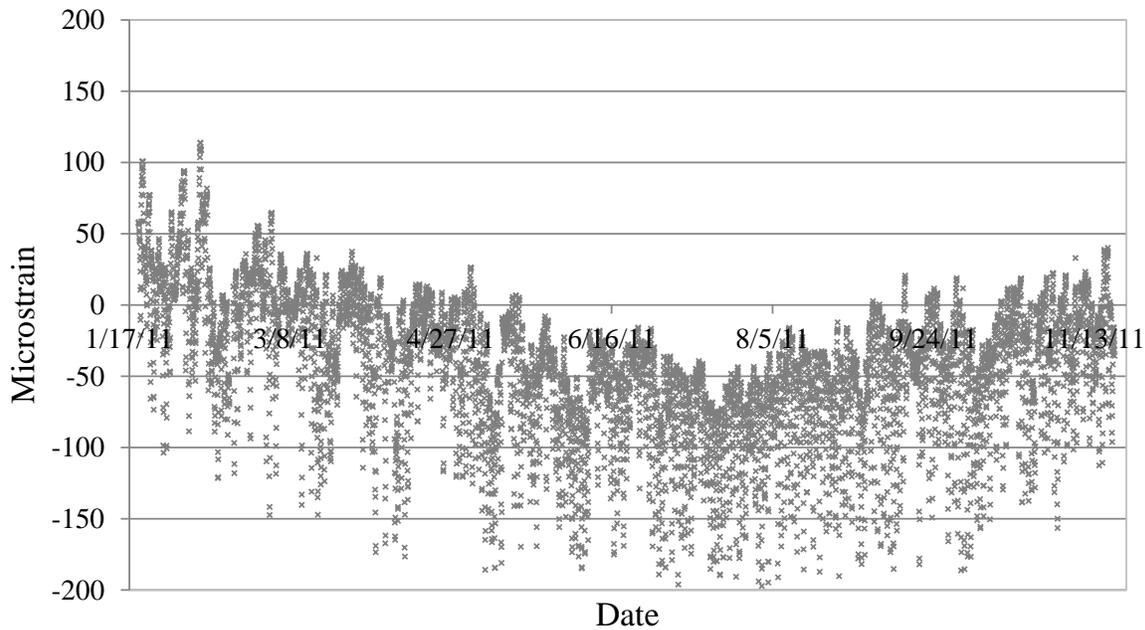
Figure 6.6. Bottom flange east strain gauge reading
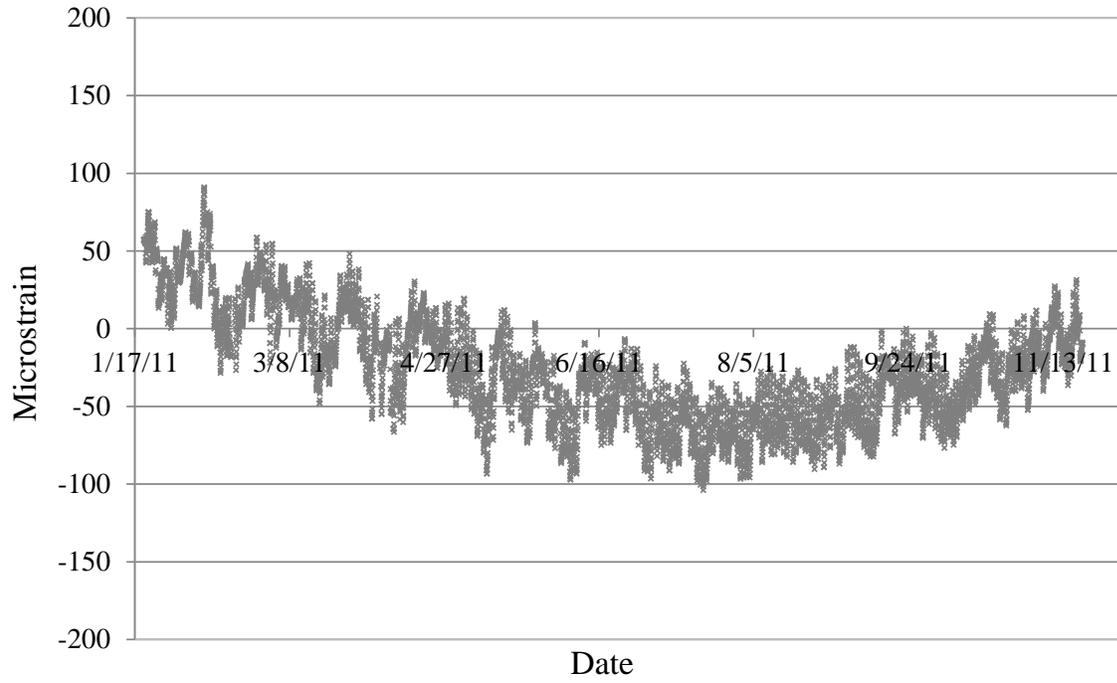
Figure 6.7. Top flange east strain gauge reading
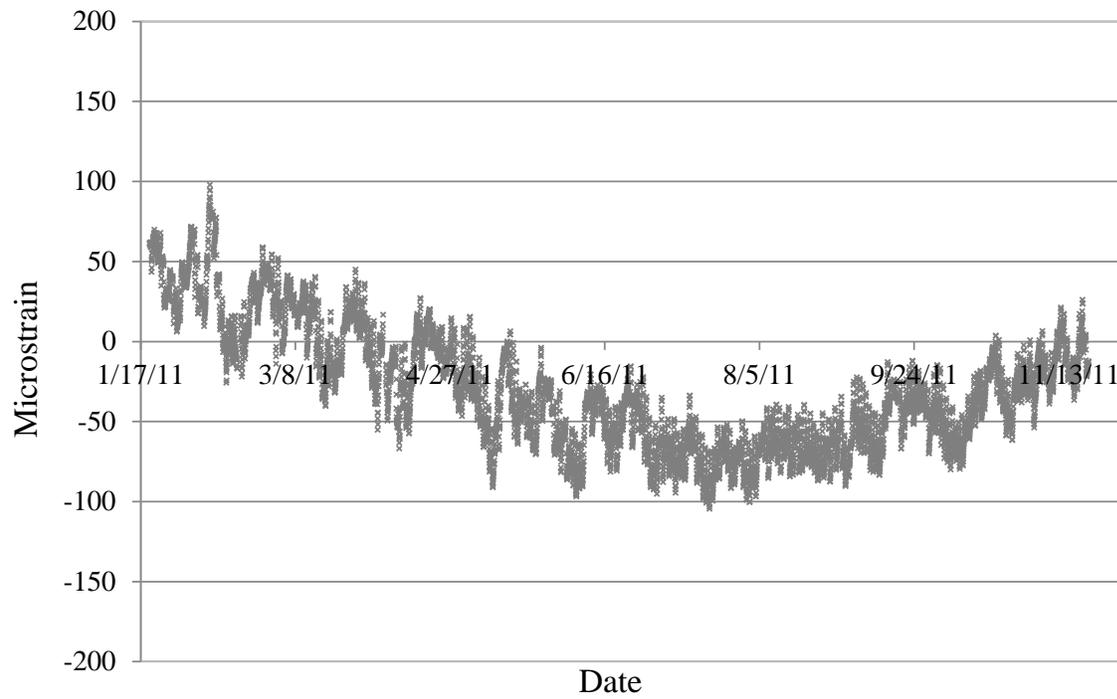
Figure 6.8. Top flange west strain gauge reading
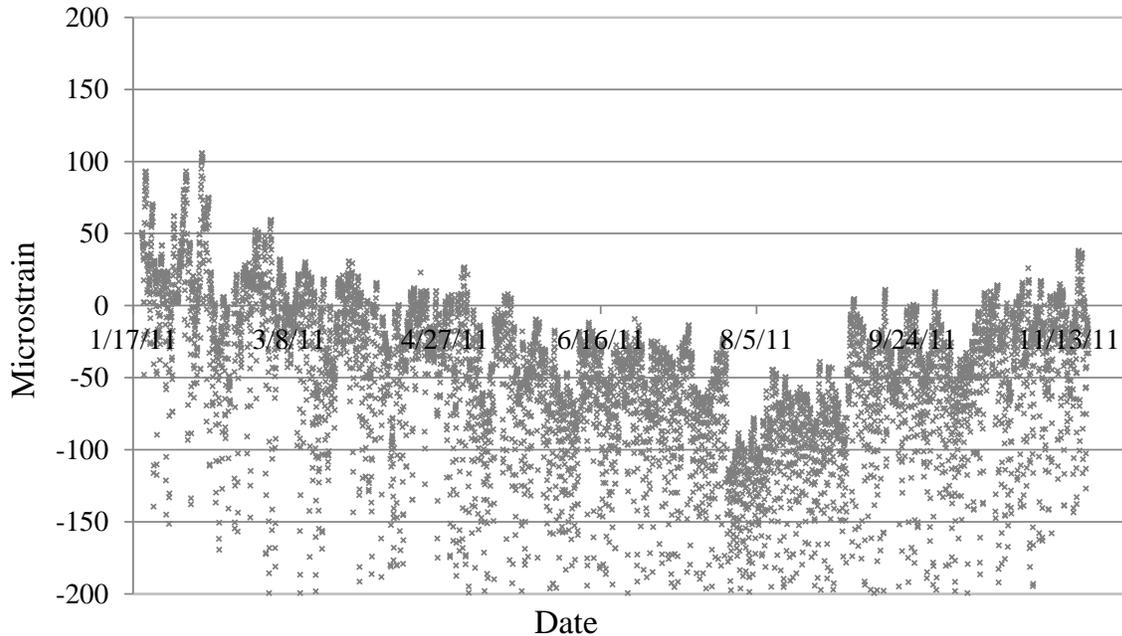
Figure 6.9. Bottom flange west strain gauge reading

Typical Girder Strains versus Time

Figure 6.10 though Figure 6.13 show the internal girder component strain measurements versus time for the four calculated strains at the center span of Girder D of Bridge 309 using Equations 6.16 through 6.19 and the measured strains at the four gauge locations. Figure 6.10 shows internal axial strain versus time, Figure 6.11 shows strong axis bending strain versus time, Figure 6.12 shows top flange lateral bending versus time, and Figure 6.13 shows bottom flange lateral bending versus time. In each figure, the light grey data shows the strain from the life of the project and the black data with white highlights shows the daily strain cycle from specific days of the project. The data denoted by squares represent a low temperature day, the data denoted by circles represent a moderate temperature day, and the data denoted by the triangles represent a high temperature day.

Figure 6.9 through 6.13 show a daily and annual cycle when compared with the date. The annual cycle range is larger than the daily cycle range for axial strain. In the case of major axis bending and lateral flange bending in both the top and bottom flanges the daily cycle range is comparable to the annual cycle range.
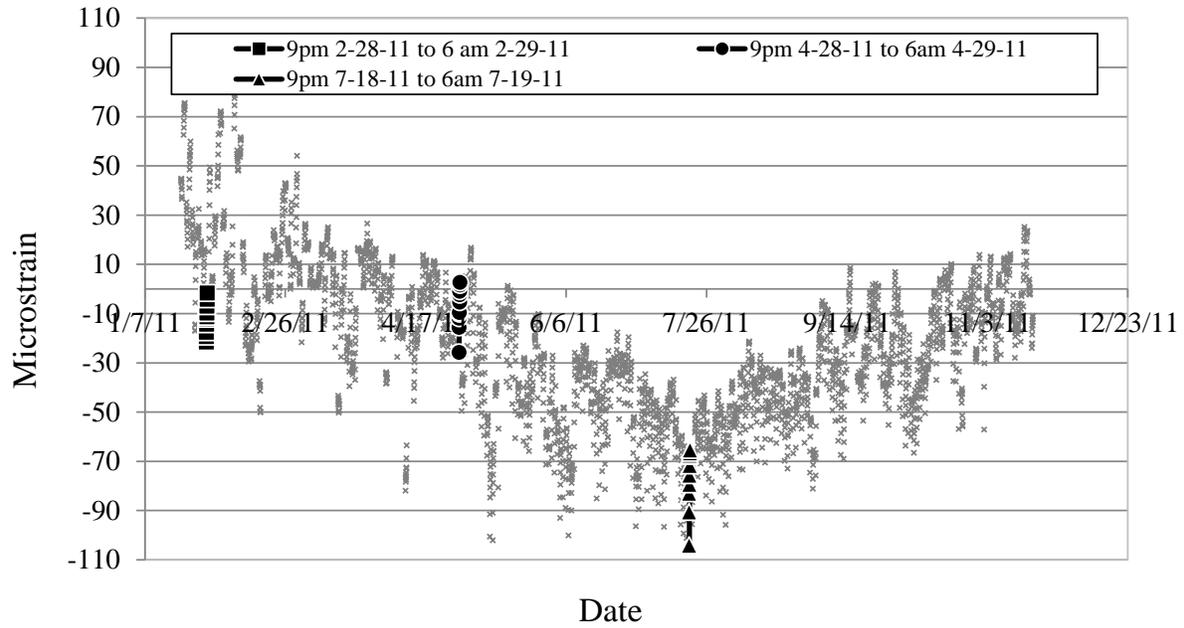
Figure 6.10. Axial strain versus time
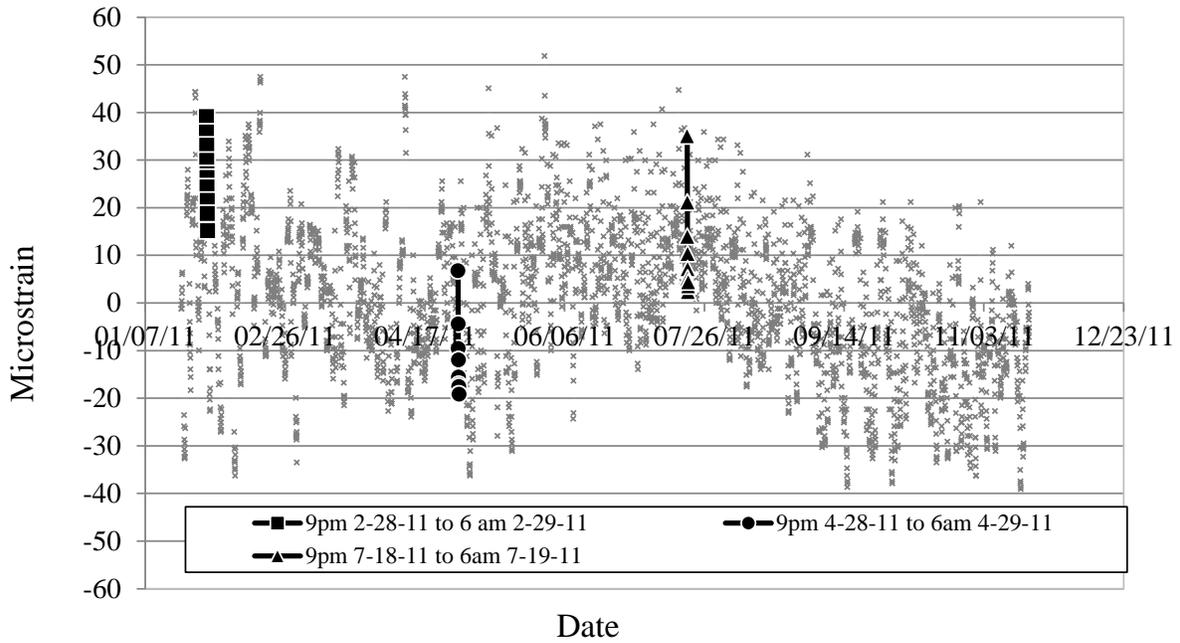
Figure 6.11. Major axis bending versus time
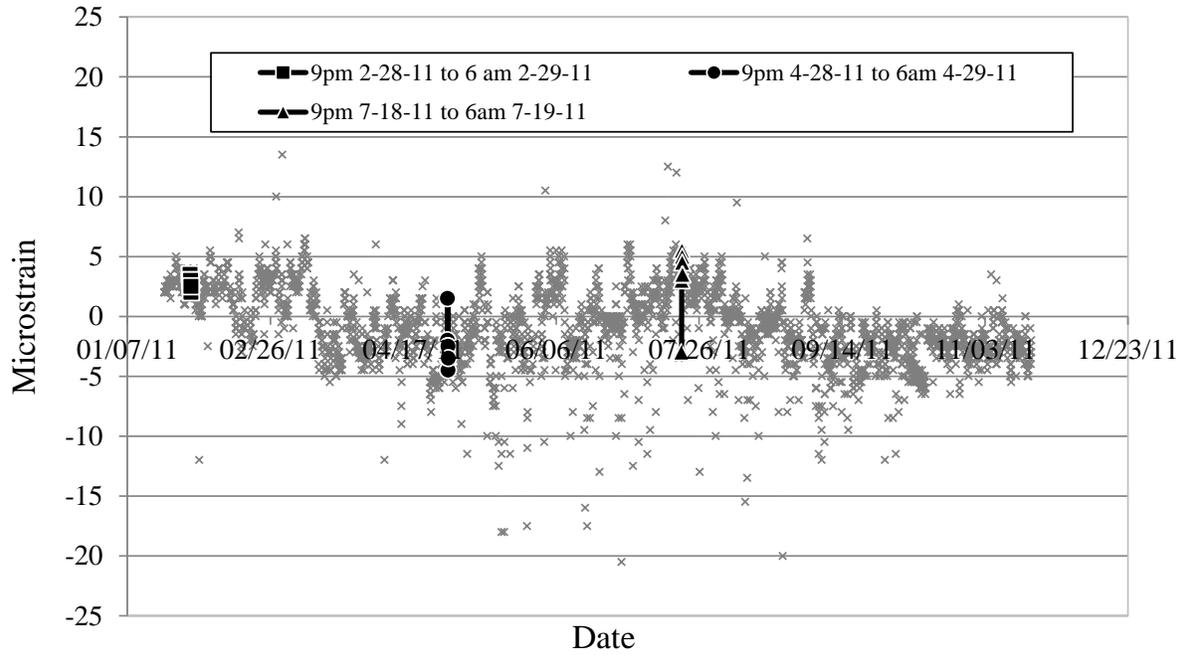
Figure 6.12. Top flange lateral bending versus time
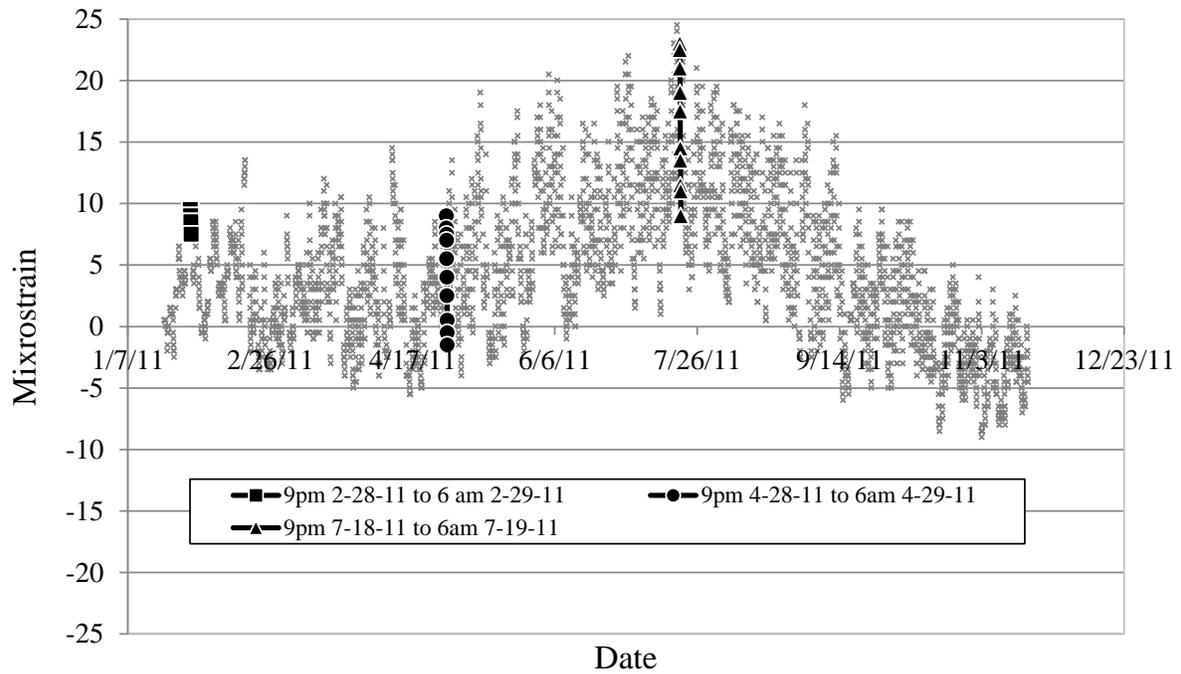
Figure 6.13. Bottom flange lateral bending versus time

Typical Girder Strains versus Teff

Figure 6.14 though Figure 6.17 show the internal girder strain measurements versus the effective bridge temperature for the four calculated strains at the center span of Girder D of Bridge 309. Figure 6.14 shows internal axial strain versus effective bridge temperature, Figure 6.15 shows strong axis bending strain versus effective bridge temperature, Figure 6.16 shows top flange lateral bending versus effective bridge temperature, and Figure 6.17 shows bottom flange lateral bending versus effective bridge temperature. In each figure, the light grey data shows the strain for the entire effective bridge temperature range, and the black data with white highlights shows the strain for an effective bridge temperature for single days. As with the previous figures, the data denoted by squares represent a low temperature day, the data denoted by circles represent a moderate temperature day, and the data denoted by the triangles represent a high temperature day.
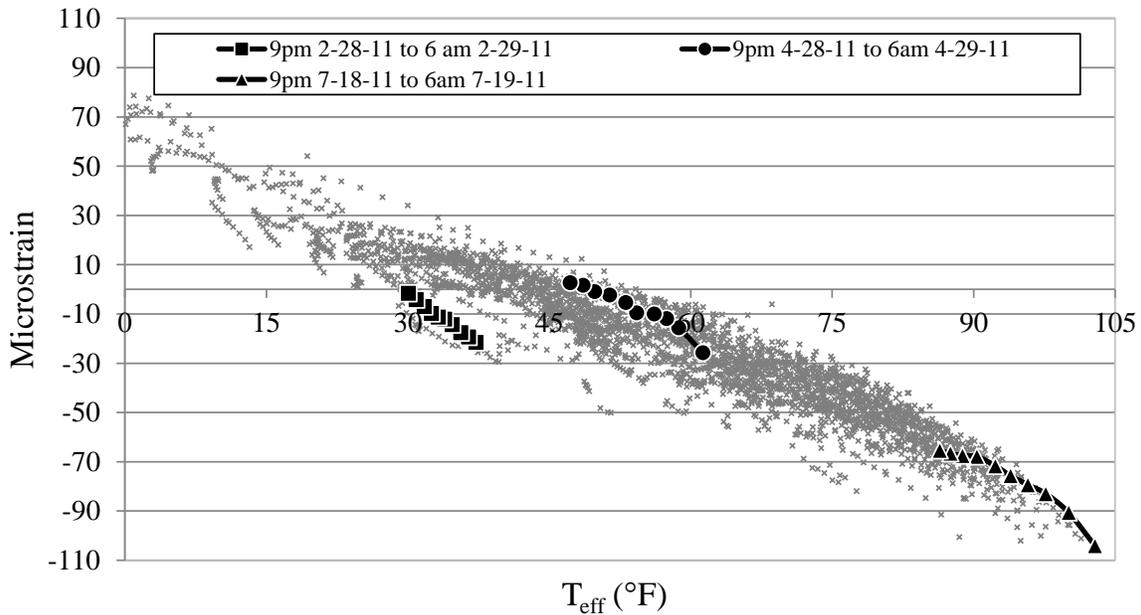
Figure 6.14. Axial strain versus T$_{eff}$

71
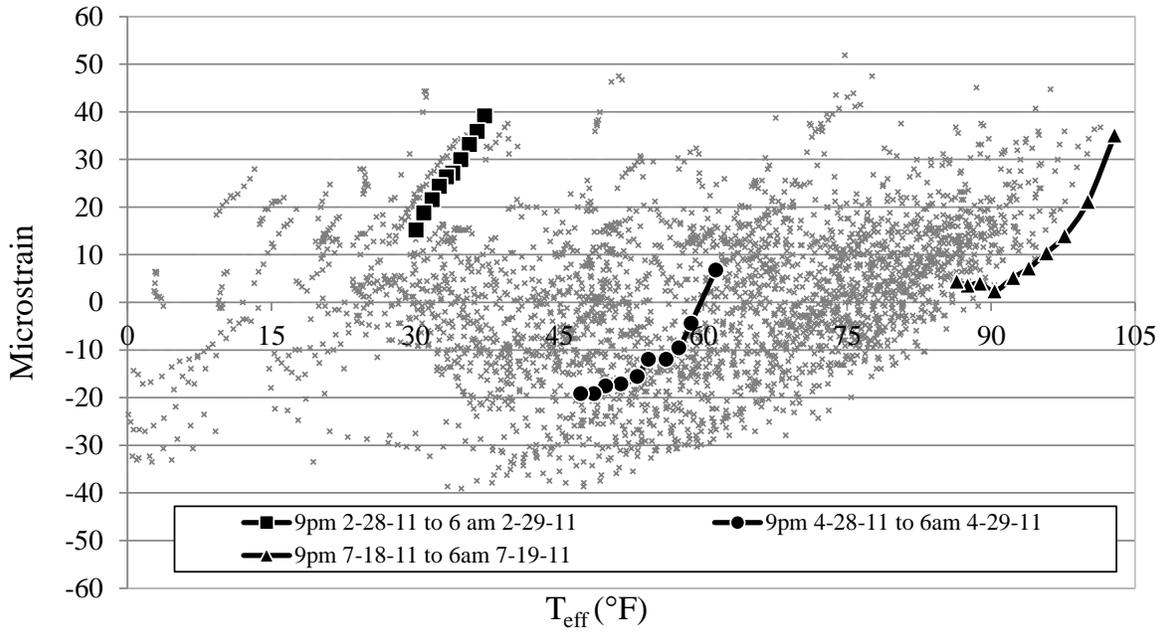
Figure 6.15. Major axis bending versus T$_{eff}$
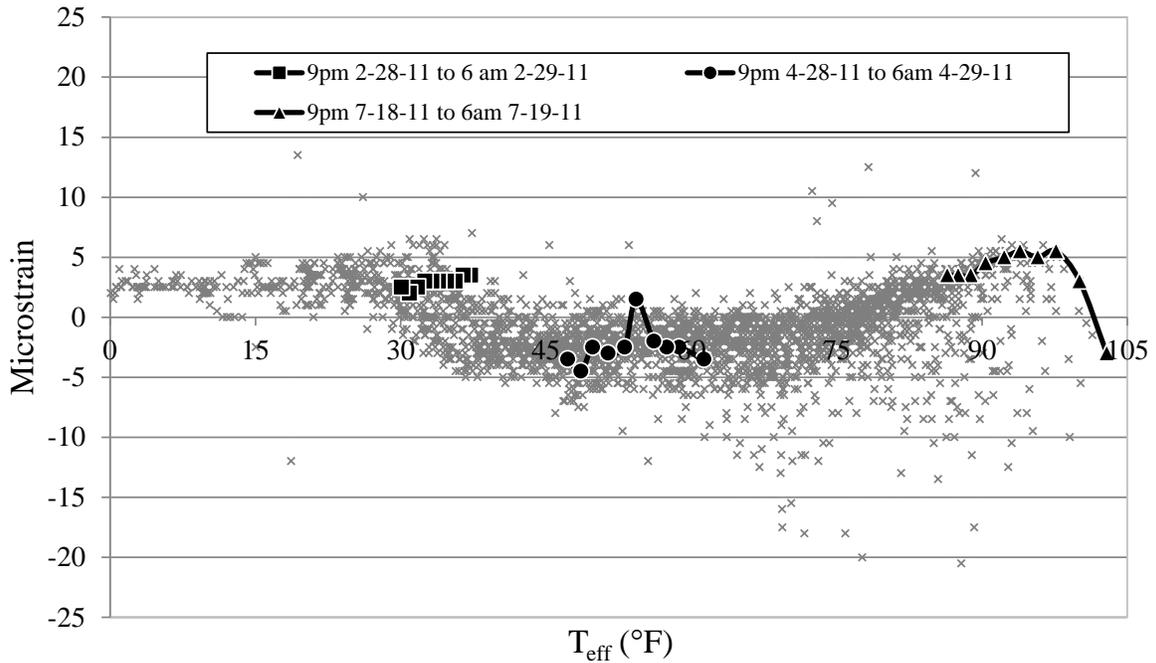
Figure 6.16. Top flange lateral bending versus T$_{eff}$
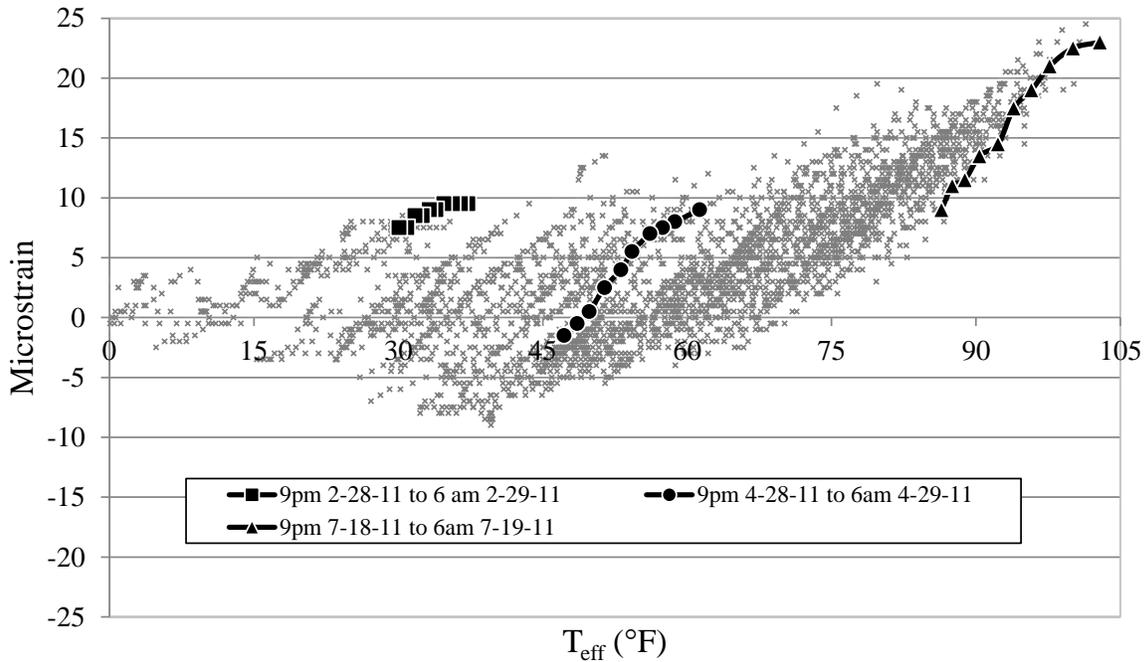
Figure 6.17. Bottom flange lateral bending versus T_{eff}

Each of the internal strains has different relationships with temperature. Axial strain exhibits a generally linear relationship with the daily and annual effective bridge temperature cycles, and the daily range for axial strain is small compared to the annual range for axial strain. The relationship between strong axis bending strain and the annual effective temperature cycle is very difficult to describe. However, the daily range for strong axis bending strain is comparable to the annual range and displays a consistent, non-linear, relationship. Top and bottom flange lateral bending strain display a smaller daily and annual strain range compared to axial and strong axis bending strains. Top flange lateral bending strain is consistently between 5 and -5 microstrain but with no obvious relationship with temperature. Bottom flange lateral bending strain shows a somewhat linear relationship with daily effective temperature cycles, the range of which is proportion to annual effective temperature cycles.

Girder Strain and Force Range

For further data analysis, the research team determined a strain range experienced at each location over an equivalent temperature change. Over the course of a year, each location experiences a change in T_{eff} of approximately 100 °F. For each strain type the range was determined similar to the results displayed in Figure 6.18. In this way, the dashed lines represent the strain range over an annual effective temperature cycle. Note that this process was completed with some level of judgment involved and in many cases the upper and lower bounds did not necessarily capture all data points.

Once the strain range for each internal strain was determined, the ranges were tabulated and summarized based on strain type, bridge, and span location. Table 6.1 shows the values collected

for outside girder, Girder A, for each bridge. Table 6.2 shows the values collected for the inside girder, Girder D, for each bridge. All values displayed are in microstrain.

Once the internal strain ranges were tabulated, the internal force ranges were calculated by substituting values from Table 6.1 and Table 6.2 and the composite section properties in Table 5.4 into equations 6.16–6.19. Table 6.3 and Table 6.4 display the calculated values based on force type, bridge, and span location, for their respective girder.

After the internal strain and force ranges were tabulated, the values were represented alongside their respective locations on representations of the bridges. For ease of interpretation Bridge 309 and Bridge 2308 were placed on the same graphic and Bridge 209 and Bridge 2208 were similarly compared due to their similar geometries. From the illustration, the research team made observations about the nature of the results with respect to bridge configuration.
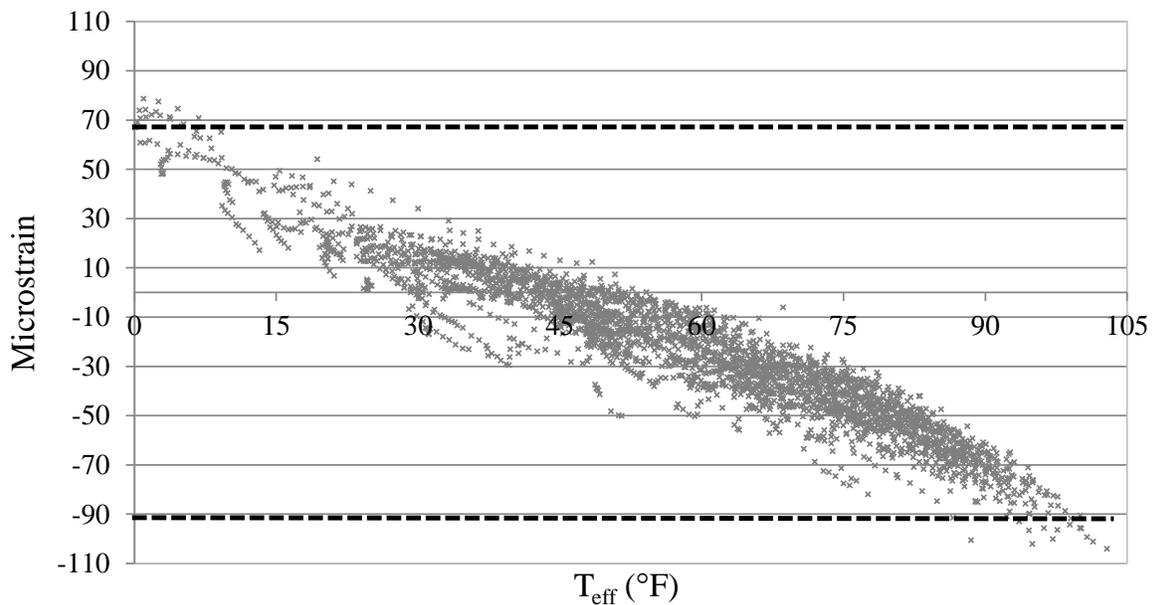
Figure 6.18. Strain range calculation – axial strain example

Table 6.1. Girder A strain range (in Microstrain)

	Bridge #	S span	C span	N span	Avg.
$\varepsilon_a = P/(AE)_{eff}$	109	NA	180	NA	180
	209	150	155	150	152
	309	170	160	170	167
	2208	70	85	120	92
	2308	130	150	80	120
$\varepsilon_x = M_x y_3/(EI_x)_{eff}$	109	NA	70	NA	70
	209	80	80	80	80
	309	50	40	50	47
	2208	110	80	100	97
	2308	60	60	100	73
$\varepsilon_{lt} = M_{lt} x_1/E_s I_{yt}$	109	NA	60	NA	60
	209	100	25	25	50
	309	20	15	15	17
	2208	10	40	NA	25
	2308	40	10	60	37
$\varepsilon_{lb} = M_{lb} x_3/E_s I_{yb}$	109	NA	NA	NA	NA
	209	NA	20	NA	20
	309	NA	NA	15	15
	2208	20	NA	20	20
	2308	30	10	NA	20

Table 6.2. Girder D strain range (in Microstrain)

	Bridge #	S span	C span	N span	Avg.
$\varepsilon_a = P/(AE)_{eff}$	109	NA	180	NA	180
	209	180	200	180	187
	309	130	180	180	163
	2208	140	120	80	113
	2308	190	220	140	183
$\varepsilon_x = M_x y_3/(EI_x)_{eff}$	109	NA	70	NA	70
	209	110	20	90	73
	309	80	70	80	77
	2208	90	70	80	80
	2308	60	100	35	65
$\varepsilon_{lt} = M_{lt} x_1/E_s I_{yt}$	109	NA	40	NA	40
	209	10	50	20	27
	309	30	10	40	27
	2208	15	10	20	15
	2308	15	20	70	35
$\varepsilon_{lb} = M_{lb} x_3/E_s I_{yb}$	109	NA	10	NA	10
	209	30	35	10	25
	309	15	30	25	23
	2208	120	NA	15	68
	2308	NA	90	60	75

Table 6.3. Girder A force range (in kip)

	Bridge #	S span	C span	N span	Average
$P = \varepsilon_a(AE)_{eff}$	**109**	NA	666	NA	666
	209	610	618	611	613
	309	685	668	686	680
	2208	285	339	489	371
	2308	500	598	308	469
$M_x = \varepsilon_x(EI_x)_{eff}/y_3$	**109**	NA	2580	NA	2580
	209	3070	3630	3070	3260
	309	2060	2100	2060	2070
	2208	4220	3630	3840	3900
	2308	2290	2750	3820	2950
$M_{lt} = \varepsilon_{lt}E_sI_{yt}/x_1$	**109**	NA	64	NA	64
	209	257	33	64	118
	309	43	28	32	34
	2208	26	53	NA	39
	2308	62	13	93	56
$M_{lb} = \varepsilon_{lb}E_sI_{yb}/x_3$	**109**	NA	NA	NA	NA
	209	NA	64	NA	64
	309	NA	NA	32	32
	2208	52	NA	52	51
	2308	53	24	NA	39

Table 6.4. Girder D force range (in kip-in.)

	Bridge #	S span	C span	N span	Average
$P = \varepsilon_a(AE)_{eff}$	109	NA	666	NA	666
	209	712	768	712	731
	309	501	717	693	637
	2208	554	461	317	444
	2308	700	823	516	680
$M_x = \varepsilon_x(EI_x)_{eff}/y_3$	109	NA	2580	NA	4030
	209	3930	776	3220	2640
	309	3050	3370	3050	3160
	2208	3220	2720	2860	2930
	2308	1930	3810	1130	2290
$M_{lt} = \varepsilon_{lt}E_sI_{yt}/x_1$	109	NA	42	NA	42
	209	22	66	43	44
	309	46	13	62	40
	2208	32	13	43	29
	2308	19	21	87	42
$M_{lb} = \varepsilon_{lb}E_sI_{yb}/x_2$	109	NA	12	NA	12
	209	64	85	22	57.
	309	26	73	44	48
	2208	258	NA	32	145
	2308	NA	143	74	109

Figures 6.19 through 6.30 display the internal strains for the four curved and the one straight bridge that has electronic instrumentation mounted to their girder flanges. In the figures, north is to the right with respect to Bridge 309 and Bridge 209. North is to the left with respect to Bridge 2308 and Bridge 2208. All values are in microstrain.

Figures 6.19 through 6.21 show the measured internal axial strains, ε_a, for each of the five bridges. The results for each of the measured locations are roughly the same (150 to 170 $\mu\varepsilon$). The strain values are somewhat larger for semi-integral abutments and the center span strain is somewhat greater when between two fixed piers.

Figures 6.22 through 6.24 show the measured internal strong axis bending strains, ε_x, for each of the five bridges. The results for most measured locations all fall in the range of 60 to 90 microstrain. The measured results at the center span of the horizontally curved bridges are typically very close to the measured results at the center span of the straight bridge.
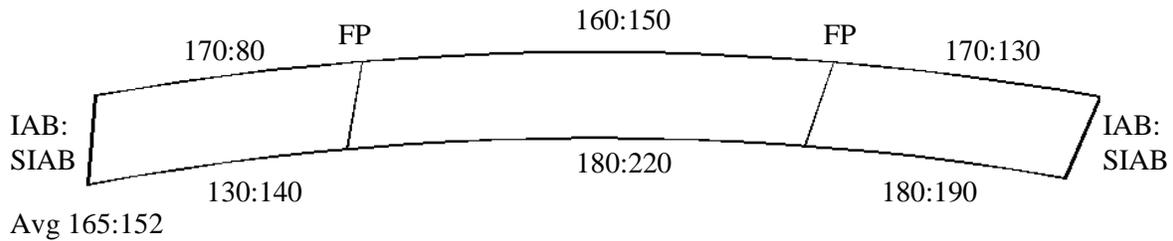
Figure 6.19. Bridge 309:2308 axial strain range
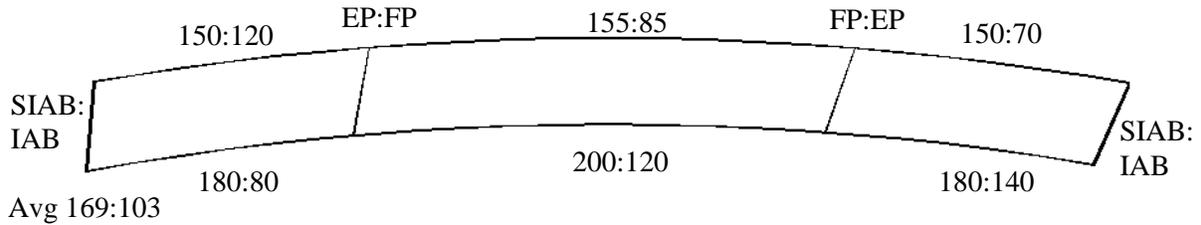
Figure 6.20. Bridge 209:2208 axial strain range
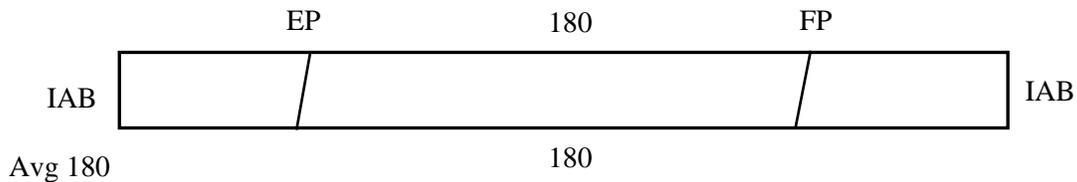
Figure 6.21. Bridge 109 axial strain range
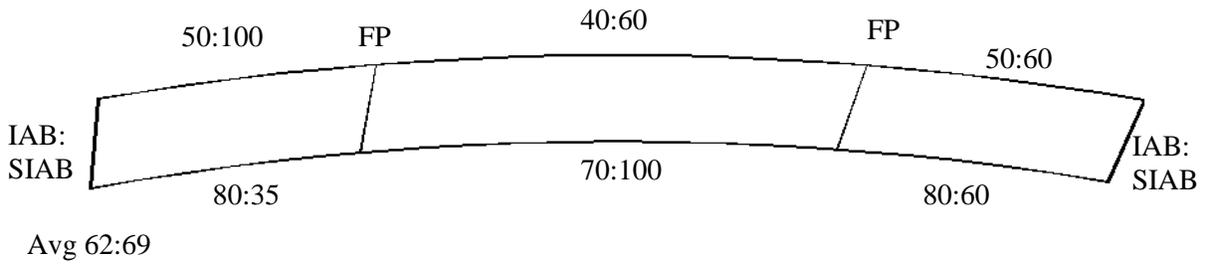
Figure 6.22. Bridge 309:2308 strong axis bending strain range
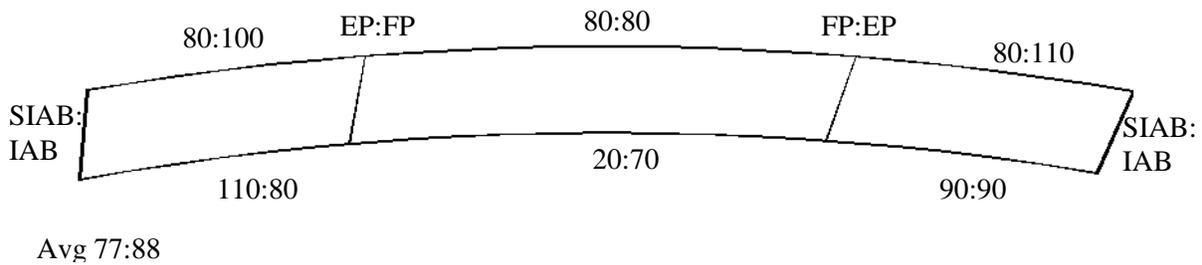
Figure 6.23. Bridge 209:2208 strong axis bending strain range
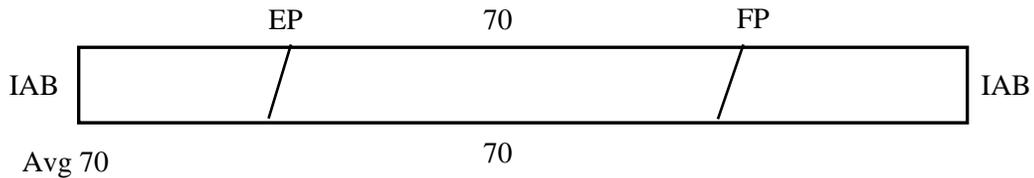
Figure 6.24. Bridge 109 strong axis bending strain range

Figures 6.25 through 6.27 show the measured internal top flange lateral bending strain, ε_{lt}, for each of the five bridges. The results from the measured values are all roughly equivalent (20—30 $\mu\varepsilon$), with some outliers. There are no notable differences with respect to bridge radius or skew, and the results from the straight bridge are only slightly higher than the results from the horizontally curved bridges.
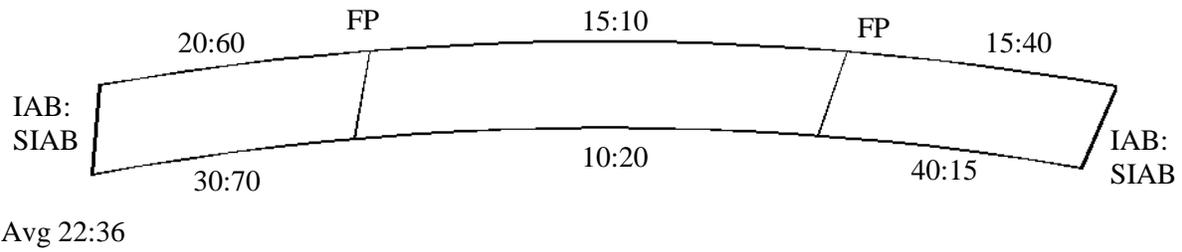
Figure 6.25. Bridge 309:2308 lateral bending strain top flange
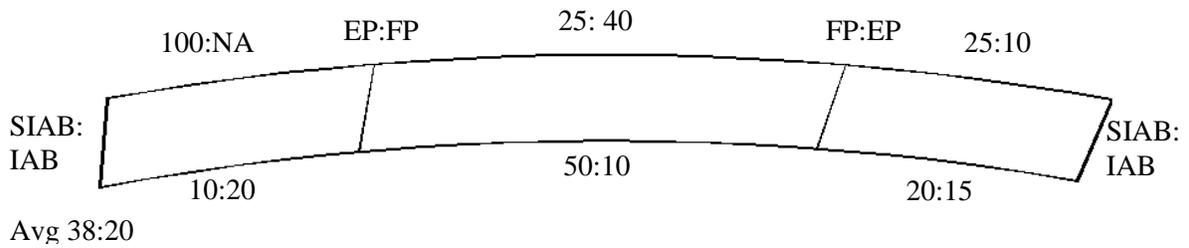
Figure 6.26. Bridge 209:2208 lateral bending strain top flange
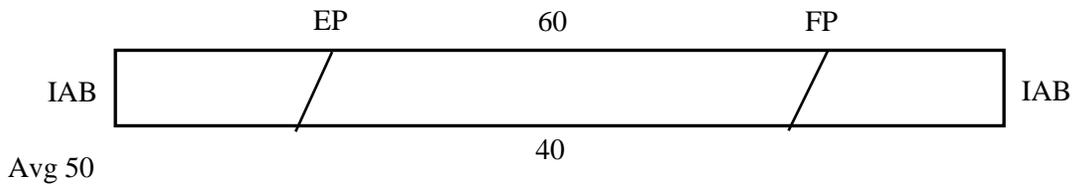
Figure 6.27. Bridge 109 lateral bending strain top flange

Figures 6.28 through 6.30 show the measured internal bottom flange lateral bending strain, ε_{lb}, for each of the five bridges. The results from the measured values are similar to the results of top flange lateral bending strain (typically about 20 to 30 $\mu\varepsilon$). As with top flange lateral bending, there are no notable differences between the straight and curved bridges and no notable difference with respect to bridge radius or skew.

NA:NA   FP   NA:10   FP   15:30

IAB:SIAB   15:60   30:90   25:NA   IAB:SIAB

Avg 19:48
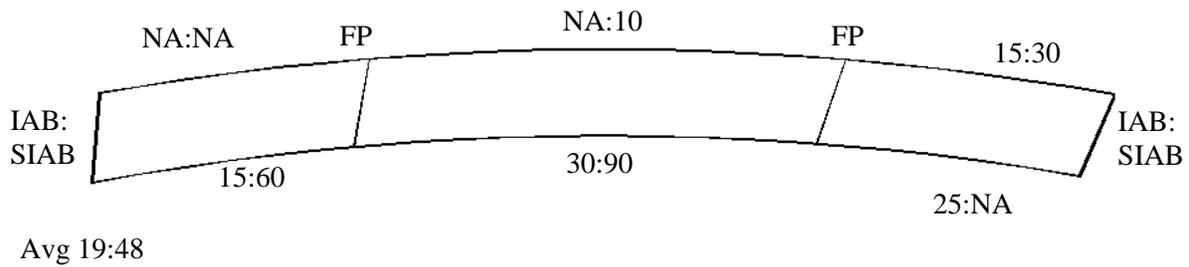
Figure 6.28. Bridge 309:2308 lateral bending strain bottom flange

NA:20   EP:FP   20:NA   FP:EP   NA:20

SIAB:IAB   30:15   35:NA   10:120   SIAB:IAB

Avg 23:44
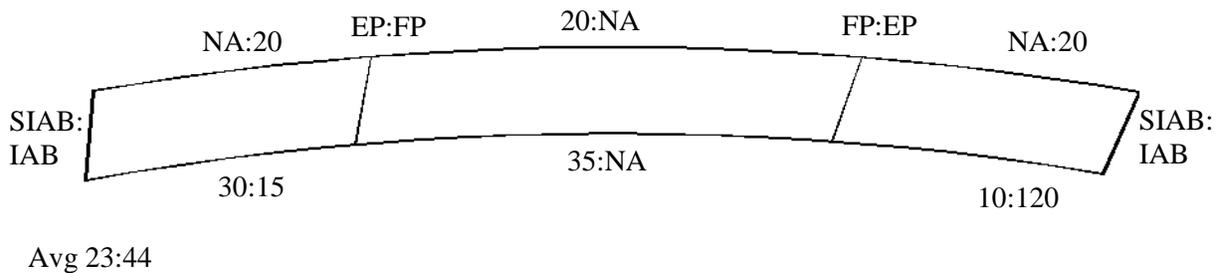
Figure 6.29. Bridge 209:2208 lateral bending strain bottom flange

EP   NA   FP

IAB   10   IAB

Avg 10
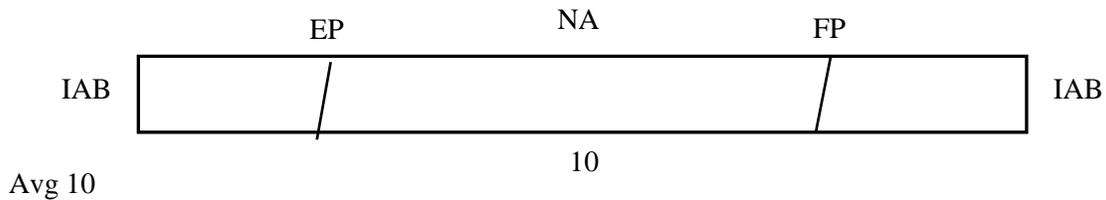
Figure 6.30. Bridge 109 lateral bending strain bottom flange

Figures 6.31 through 6.42 show the calculated internal forces for the four curved and the one straight bridge that had strain gauge instrumentation on their girders. As with the internal strain figures, north is to the right with respect to Bridge 309 and Bridge 209, and north is to the left with respect to Bridge 2308 and Bridge 2208.

Figures 6.31 through 6.33 show the internal axial force, *P*, for each of the five bridges. The results for the inside girder of bridge 109, the straight bridge, is lower than Bridge 309, 209 and 2308; and is higher than the results for the inside girder of Bridge 2208. The outside girder for Bridge 109 is close to Bridge 209, 309, and 2308; and is higher than the outside girder of Bridge 2208. All values in the figures are in kip.
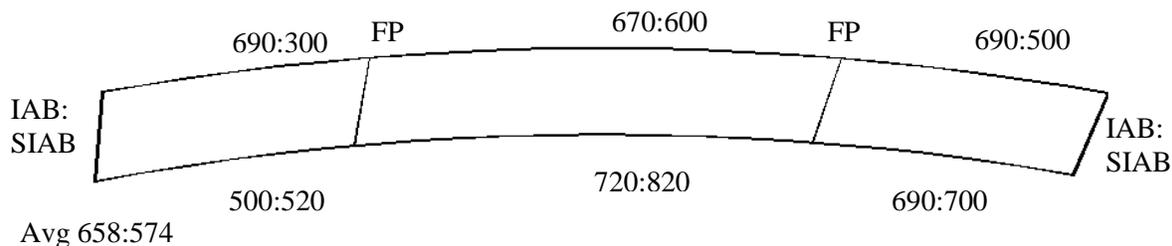
Figure 6.31. Bridge 309:2308 axial force range
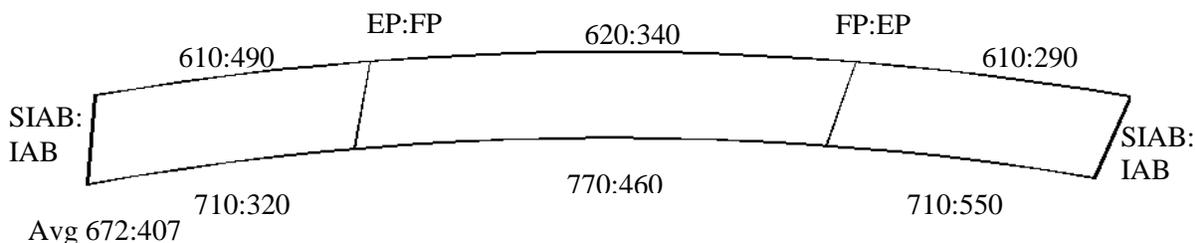
Figure 6.32. Bridge 209:2208 axial force range
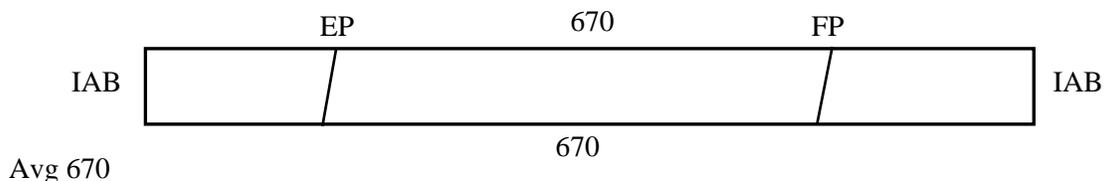
Figure 6.33. Bridge 109 axial force range

Figures 6.34 through 6.36 show the internal strong axis bending moment, M_x, for each of the five bridges. With the exception of one span, the values at the center span of Bridge 309 and Bridge 2308, between two fixed piers, are generally higher than the center span values of the other bridges. The inside girder results of Bridge 109 are lower than the inside girder results of Bridge 309 and Bridge 2308 and are similar to the results of the inside girder results of Bridge 209 and Bridge 2208. The outside girder results are lower than the outside girder results of Bridge 209 and Bridge 2208, and are similar to the outside girder results of Bridge 309 and Bridge 2308. All values in the figures are in kip-in.

Figures 6.37 through 6.42 shows the results of internal lateral flange bending moment in the top and bottom flanges. Since a number of gauges malfunctioned and their data had to be ignored, the results of lateral flange bending in both the top and bottom flanges were incomplete for all the bridges, which made it hard to draw any solid conclusion. However, typically the results were larger in the bottom flanges, and the lateral flange bending moment was smaller in Bridge

109, the straight bridge, than in any of the horizontally curved bridges. All values in the figures are in kip-in.

Figure 6.34. Bridge 309:2308 strong axis moment range

2060:3820   FP   2100:2750   FP   2060:2290

IAB:
SIAB

3050:1130   3370:3810   3050:1930

IAB:
SIAB

Avg 2616:2619

Figure 6.34. Bridge 309:2308 strong axis moment range

3070:3840   EP:FP   3630:3630   FP:EP   3070:4220

SIAB:
IAB

3930:2860   776:2720   3220:3220

SIAB:
IAB

Avg 2948:3413
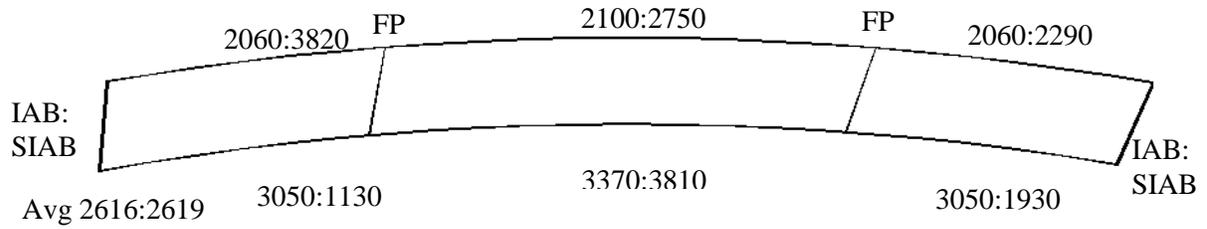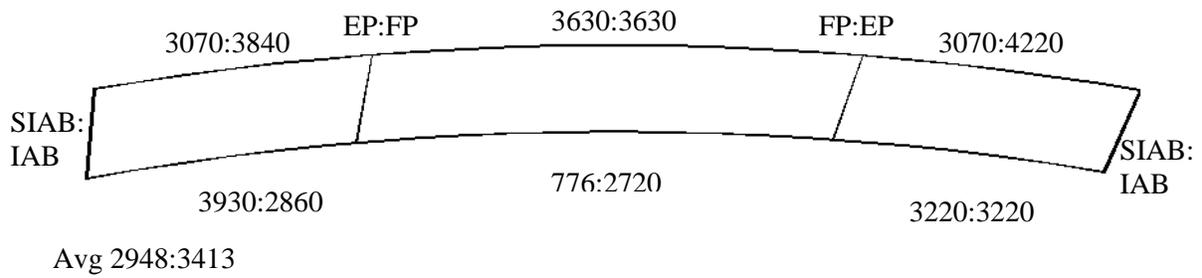
Figure 6.35. Bridge 209:2208 strong axis moment range

EP   2580   FP

IAB   IA

2580

Avg 2580
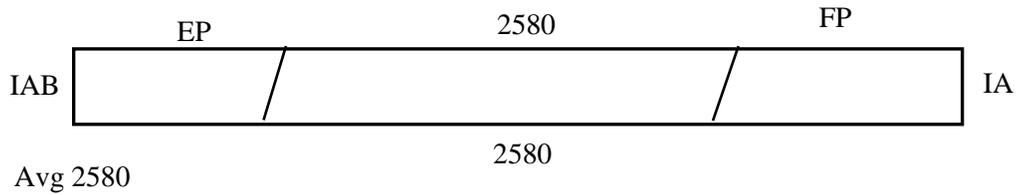
Figure 6.36. Bridge 109 strong axis bending moment range

82

FP   28:13   FP
43:93   32:62
IAB: IAB:
SIAB   SIAB
13:21
46:87   62:19

Avg 37:49
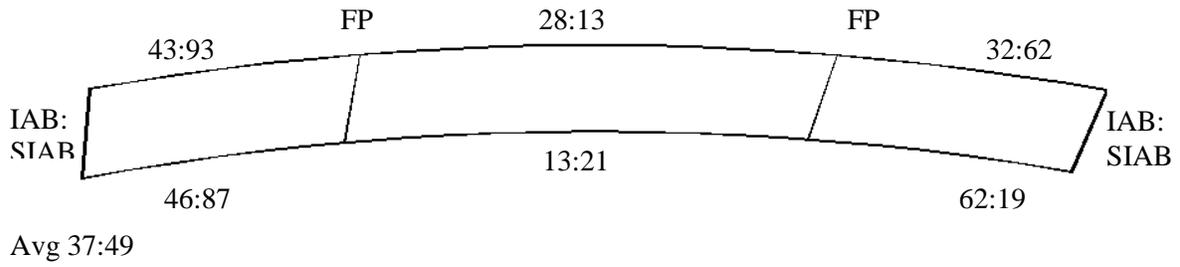
Figure 6.37. Bridge 309:2308 lateral bending moment top flange

EP:FP   33:53   FP:EP
260:NA   64:26
SIAB: SIAB:
IAB   IAB
22:43   66:13
43:32

Avg 91:34
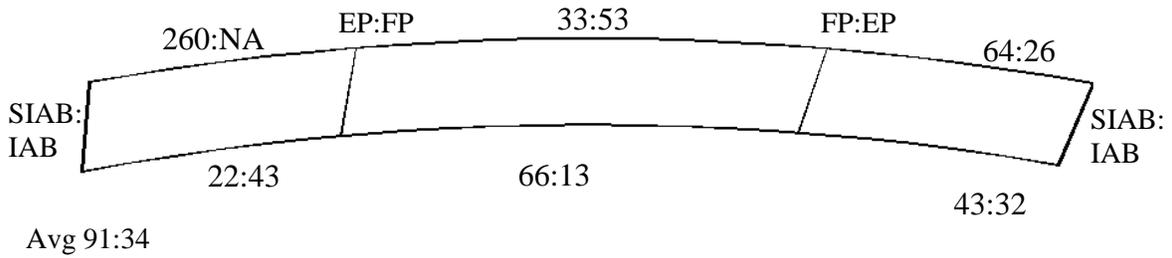
Figure 6.38. Bridge 209:2208 lateral bending moment top flange

EP   64   FP
IA   IAB

42
Avg 53
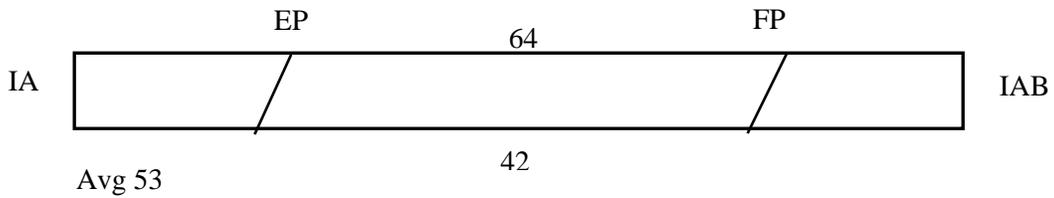
Figure 6.39. Bridge 109 lateral bending moment top flange

NA:NA   FP   NA:24   FP
32:53
IAB: IAB:
SIAB   SIAB
73:143
26:74   44:NA

Avg 40:74
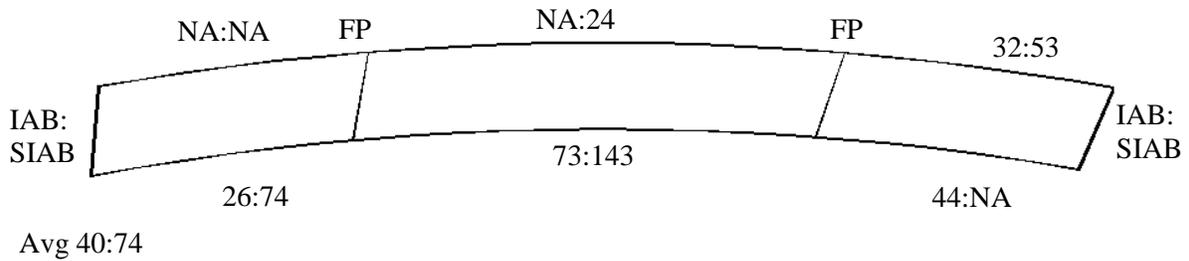
Figure 6.40. Bridge 309:2308 lateral bending strain bottom flange

83
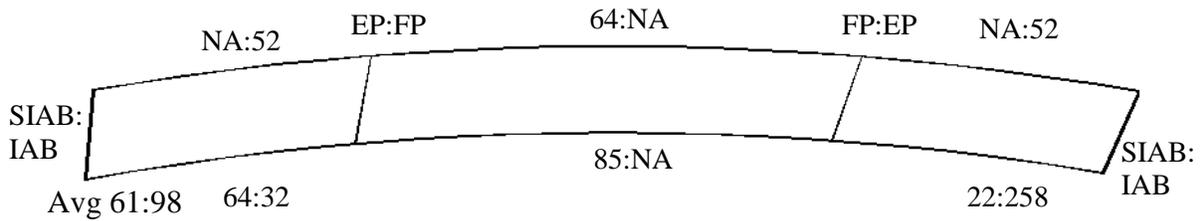
Figure 6.41. Bridge 209:2208 lateral bending strain bottom flange

Figure 6.42. Bridge 109 lateral bending strain bottom flange

6.2.2 Substructure

Pile Resolved Strains

There are six piles cast into each abutment pile cap of Bridge 309. At the north abutment, the west most pile, outside the curve, was labeled NAHP1, and the labeling continued east with the east most pile, inside the curve, labeled NAHP6. At the south abutment, the west most pile, outside the curve, was labeled SAHP1, and the labeling continued east with the east most pile, inside the curve, labeled SAHP6. At each abutment of Bridge 309 piles HP1, HP4, and HP6 were instrumented with strain gauges, the results of which are discussed in this section.

As discussed previously, the coordinate system for each set of piling was established so that the positive X-axis was in the direction of outward expansion and the positive Y-axis was 90 degrees counter-clockwise from the X-axis. In both the north and south abutment piles, positive minor axis bending caused tension in the outside flange. The positive direction of the other strains was different between each abutment and was controlled by the equations used to calculate the strains. Figure 6.43(a) shows the pile coordinate system and the resultant strains of the south abutment piles. Figure 6.43(b) shows the pile coordinate system and the resultant strains of the north abutment piles.

Using the sign conventions shown in Figure 6.43, the total internal strain at all four gage locations were used to calculate the four resultant strains in the south abutment instrumented piles. Equations 6.20 through 6.23 are the necessary equations to determine the resultant strains. Equation 6.22.1 was used to determine the weak axis bending strain in the south abutment piles

while Equation 6.22.2 was used to determine the weak axis bending strain in the north abutment piles. The rest of the equations are relevant for the piles at either abutment.

(a) South abutment   b) North abutment
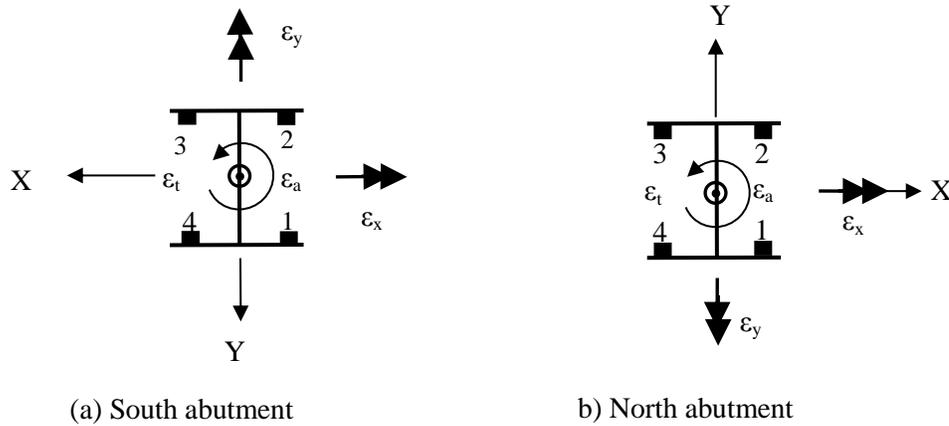
Figure 6.43. Abutment pile internal forces

$$\Delta\varepsilon_a = \frac{1}{4}(\varepsilon_1+\varepsilon_2+\varepsilon_3+\varepsilon_4) \tag{6.20}$$

$$\Delta\varepsilon_x = \frac{1}{4}(-\varepsilon_1+\varepsilon_2+\varepsilon_3-\varepsilon_4) \tag{6.21}$$

$$\Delta\varepsilon_y = \frac{1}{4}(\varepsilon_1+\varepsilon_2-\varepsilon_3-\varepsilon_4) \tag{6.22.1}$$

$$\Delta\varepsilon_y = \frac{1}{4}(-\varepsilon_1-\varepsilon_2+\varepsilon_3+\varepsilon_4) \tag{6.22.2}$$

$$\Delta\varepsilon_t = \frac{1}{4}(-\varepsilon_1+\varepsilon_2-\varepsilon_3+\varepsilon_4) \tag{6.23}$$

where,

ε_a = internal axial strain,
ε_x = internal strong axis bending strain,
ε_y = internal weak axis bending strain, and
ε_t = internal torsional-warping strain.

Figures 6.44 through 6.47 show the typical results of internal strains versus effective bridge temperature. These results are from HP1 of the north abutment. The gray, background data in the figures are the total data over the length of the monitoring period. Three separate days of data are also displayed in the figures, separate from the total data. January 28, 2011, a cold day, is represented by triangles; April 28, 2011, a moderate day, is represented by circles; and July 19, 2011, a hot day, is represented by squares.

Figure 6.44 shows the typical internal axial strain in the piles. A solid description of a relationship between axial strain and effective temperature is hard to produce. The range due to the annual effective temperature cycle is large compared to the strain range due to the daily effective temperature cycle. Internal axial strain is small compared to strong axis bending and weak axis bending strain but is large compared to torsional-warping strain.
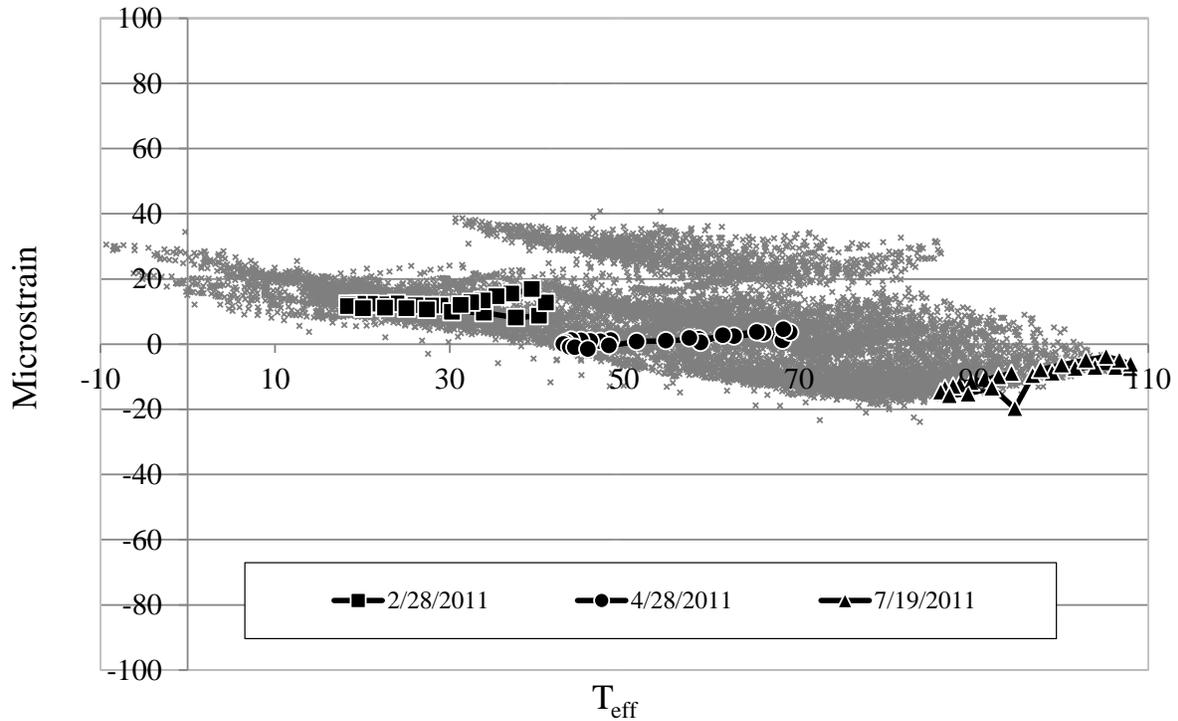
Figure 6.44. Typical internal axial strain

Figure 6.45 shows the typical internal strong axis bending strain in the piles. The results show a strong linear relationship with effective bridge temperature. The range due to the annual effective temperature cycle is larger compared to the strain range due to the daily effective temperature cycle. The resulting strong axis bending strain range is larger than the internal axial strain and torsional-warping strain range but is small compared to the minor axis bending strain.
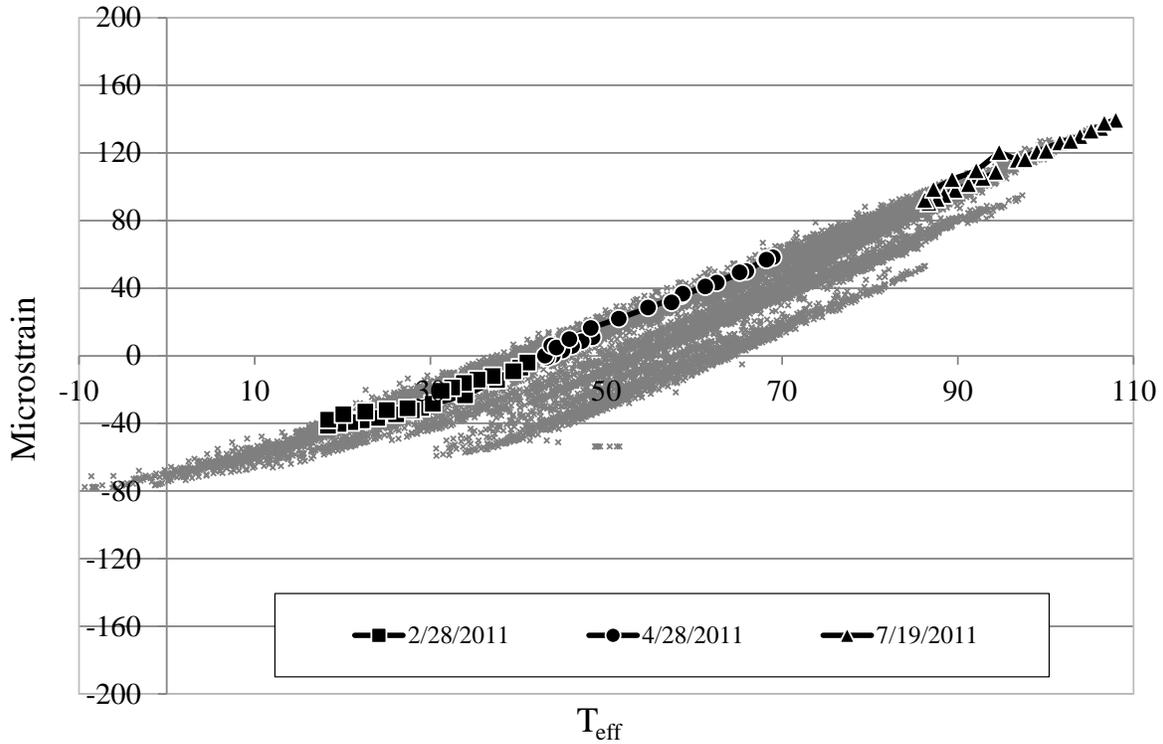
Figure 6.45. Typical internal major axis bending strain

Figure 6.46 shows the typical internal weak axis bending strain in the piles. As expected because the piles are oriented for weak axis bending, the weak axis bending strain range is much large than the range of any other measured internal strain. The results show a strong linear relationship with effective bridge temperature. The range due to the annual effective temperature cycle is large compared to the strain range due to the daily effective temperature cycle.

Figure 6.47 shows the typical internal torsional-warping strain in the piles. Typically the data tends to hover around a value of zero microstrain. There is no solid relationship between the strain and the effective bridge temperature, and the ranges due to the annual effective temperature cycle and the daily effective temperature cycle are both minimal.

As was done with the measured internal girder strain, the measured internal strain ranges at each instrumented pile location were found and tabulated for comparison. Table 6.5 shows the measured pile internal strain ranges.

Table 6.5. Measured pile internal strain ranges

Pile/Strain	NH1	NH4	NH6	SH1	SH4	SH6
$\varepsilon_a(\mu\varepsilon)$	60	90	60	120	90	80
$\varepsilon_x(\mu\varepsilon)$	220	240	240	140	160	190
$\varepsilon_y(\mu\varepsilon)$	900	800	590	810	710	700
$\varepsilon_t(\mu\varepsilon)$	45	60	30	NA	NA	20

The internal weak axis bending strain showed larger ranges than the other three strains in all six monitored piles with an average of 751 microstrain. The internal strong axis bending strain showed the next largest strain ranges in all six monitored piles with an average of 198 microstrain. The average internal axial strain range of all six piles was 83 microstrain. The smallest of all four strains was the torsional-warping strain with an average of 39 microstrain for the four piles with available results.
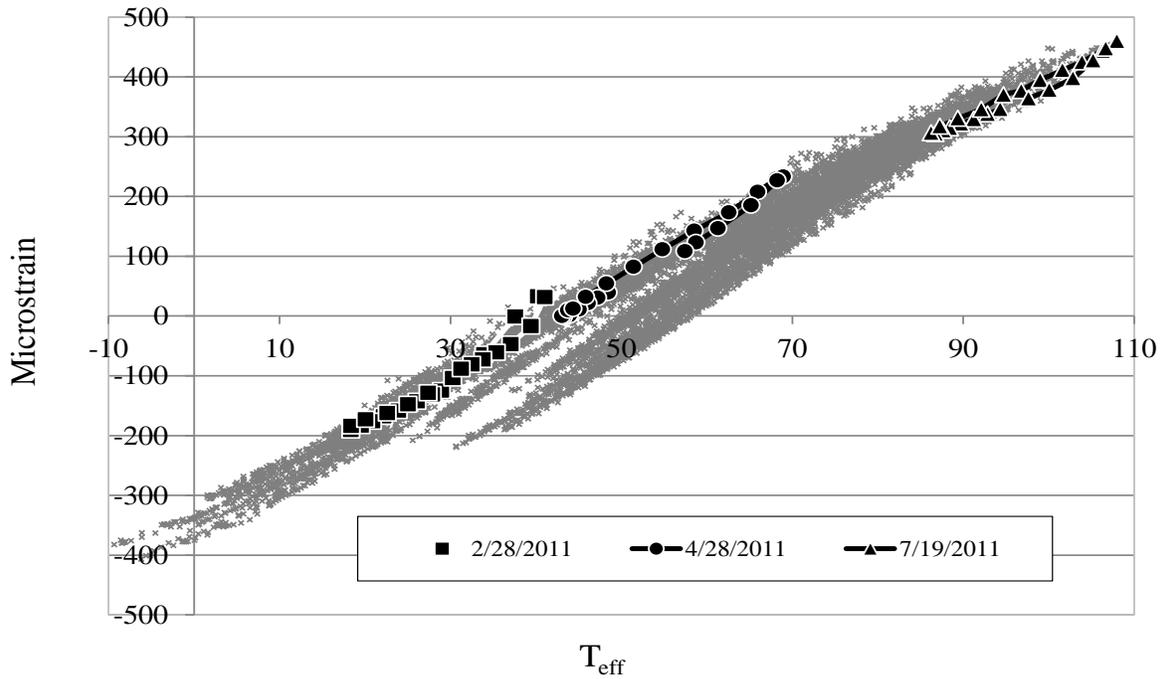
Figure 6.46. Typical internal minor axis bending strain
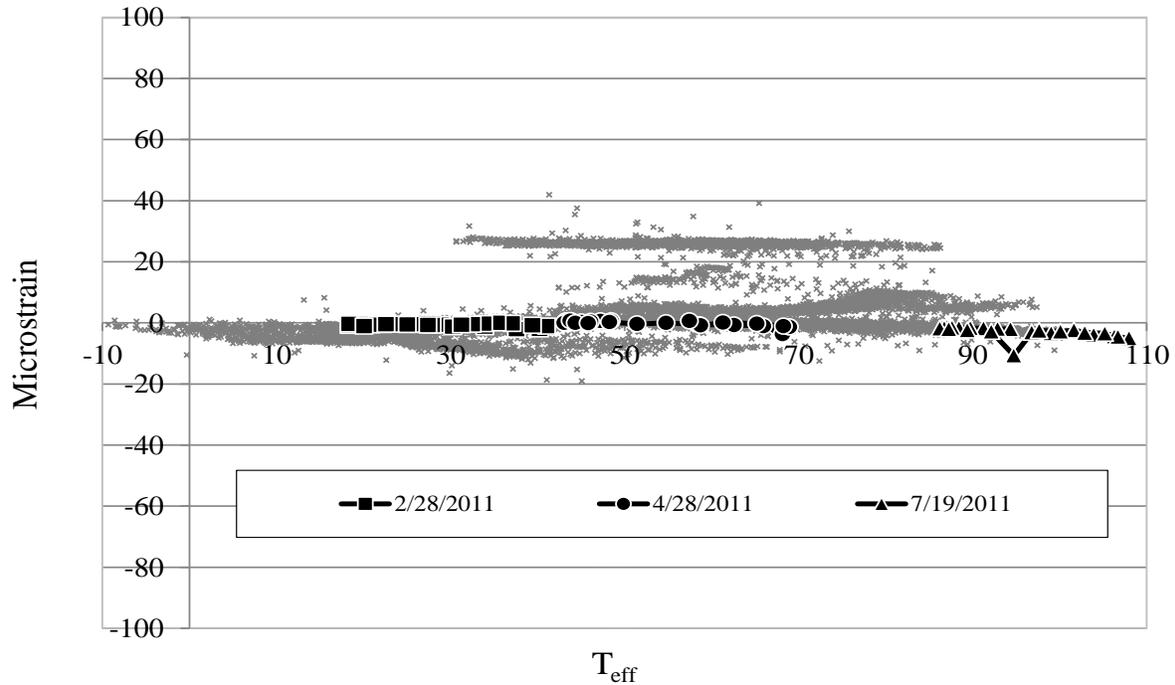
Figure 6.47. Typical internal torsional-warping strain

Using the cross-sectional properties of the HP 10x57 abutment piles and the measured pile internal strain range, the pile internal force ranges were calculated. Table 6.6 shows the calculated values. In the table axial load, P, strong axis bending, Mx, and weak axis bending, My, were calculated using familiar strength of materials equations. The lateral bending moment, Mf, is a lesser known quantity and was calculated using the following equation from Salmon, et al (2009):

$$\varepsilon_t = \frac{f_{bw}}{E_s} = \frac{M_f x}{I_f E_s}$$
(6.24)

where,

f_{bw}	= tension or compression stress due to warping of the cross-section
E_s	= modulus elasticity of the steel
M_f	= lateral bending moment acting on the flanges
x	= distance from center of flange to flange tip
I_f	= moment of inertia of a flange about its smaller principal axis

Table 6.6. Calculated pile internal force ranges

Pile/Force	NH1	NH4	NH6	SH1	SH4	SH6
P(kips)	290	440	290	590	440	390
M_x(kip-in.)	380	410	410	240	270	320
M_y(kip-in.)	520	460	340	470	410	400
M_f(kip-in.)	12	16	8	NA	NA	5

As shown in Table 6.6, axial load in the South abutment is typically higher than axial load in the North abutment, although both abutments show similar values. Generally minor axis bending is larger than major axis bending in all instrumented piles in both the North and South abutments, and lateral flange bending, where data are available, is very small compared to all other measured forces.

Abutment Backwall Pressure

The soil pressure on the abutment backwalls of Bridge 309 increases as the bridge expands into the backfill soil. This condition is called passive soil pressure (Coduto 2001) and was measured by the pressure cells mounted to the abutment backwalls. If the soil conditions in the abutment backfill are known, the maximum passive soil pressures can be approximated using the following equations:

$$K_p = \frac{\sigma_x'}{\sigma_z'}$$
(6.25)

$$K_p = tan^2(45° + \phi'/2)$$
(6.26)

$$\sigma_z' = \gamma'Z$$
(6.27)

where,
      K_p = the coefficient of passive lateral earth pressure (psi/psi),
      σ_x' = effective horizontal stress (psi),
      σ_z' = effective vertical stress (psi),
      ϕ' = effective friction angle of the soil (degree)
      γ' = buoyant unit weight of soil (lb/in.^{3}), and
      Z = depth from top of soil to location of desired stress (in.)

By making a few assumptions on the backfill soil properties the research team was able to approximate the range of passive soil stress on the north and south abutments of Bridge 309. The approximation was calculated at the depth of the pressure cells. According to the bridge plan set, the backfill soil consists of A-6 soil type, a clayey soil with >35% passing the 0.075mm sieve (ASTM D3283). Considering the soil classification, the following assumptions were made following recommendations by Coduto 2011:

    $\phi \approx 30°—40°$, and
    $\gamma \approx 110—135$ pcf

By substituting the assumptions for ϕ and γ into Equations 6.25 through 6.27 the research team was able to calculate an approximate range between 10 and 19 psi for passive stress on the abutment backwalls at the depth of the pressure cells for Bridge 309.

Figures 6.48 through 6.51 show the external stress on the north and south abutment pressure cells attached to Bridge 309, respectively. As expected, the stresses increase as the temperature increases and drops to zero at lower temperatures. According to the figure, over the life of the monitoring period of the project, the north abutment experienced higher stresses. Also shown in the figure are the upper-bound and lower-bound approximations of passive pressure, denoted by dashed horizontal lines.

Figure 6.48 shows the external stress on the north-west abutment pressure cell on Bridge 309 versus the effective temperature of the bridge. The north-west corner of the bridge is outside of the horizontal curve and is on the side of the bridge that is elongated due to skew.

Figure 6.49 shows the external stress on the north-east abutment pressure cell on Bridge 309 versus the effective temperature of the bridge. The north-east corner of the bridge is on the inside of the horizontal curve and is on the side of the bridge that is shortened due to skew. The measured passive stress range was the greatest at this location, compared to the other three locations.
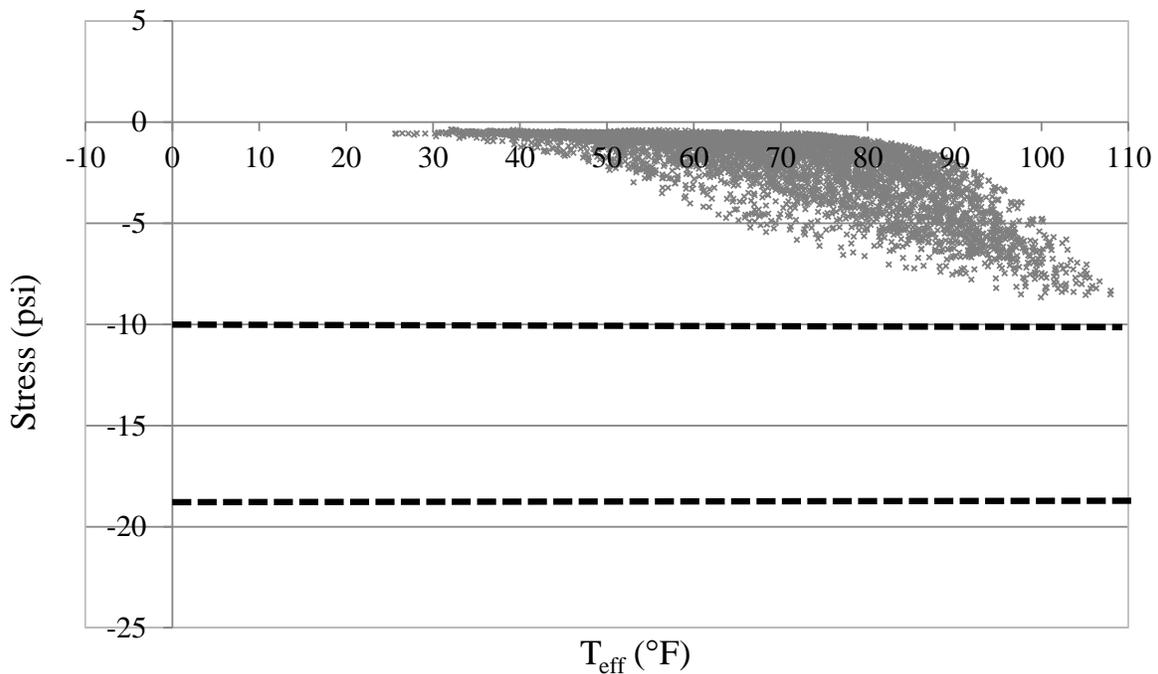
Figure 6.48. Northwest abutment backwall pressure versus effective temperature
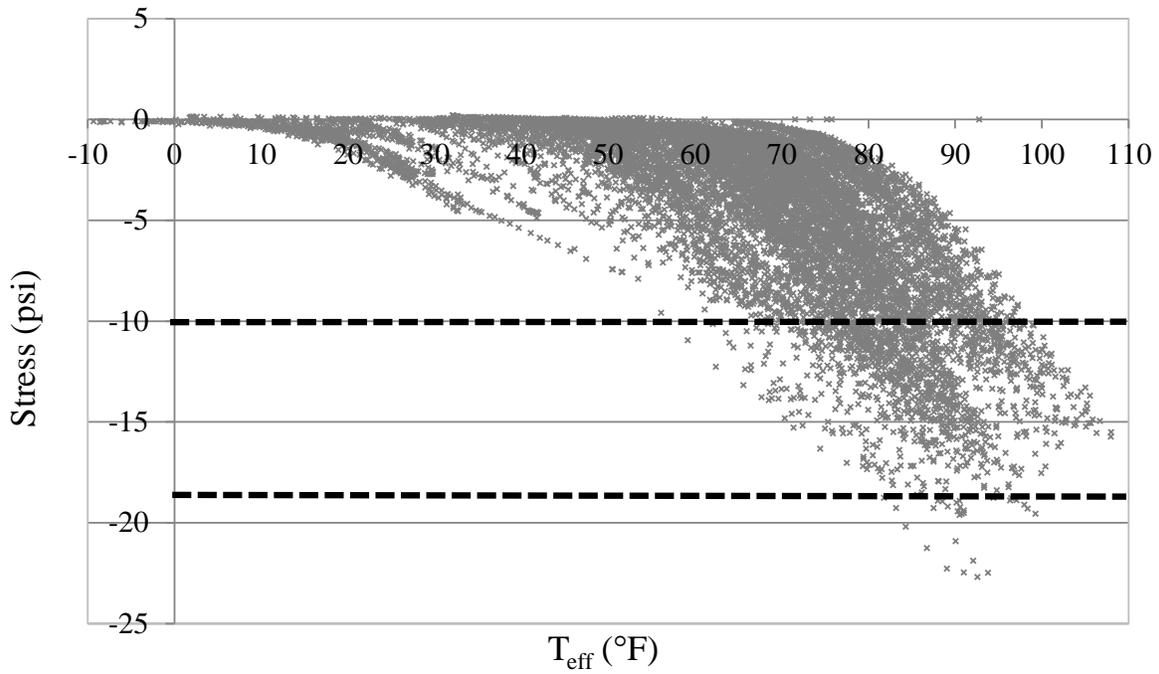
Figure 6.49. Northeast abutment backwall pressure versus effective temperature

Figure 6.50 shows the external stress on the south-west abutment pressure cell on Bridge 309 versus the effective temperature of the bridge. The south-west corner of the bridge is on the outside of the horizontal curve and is on the side of the bridge that is shortened due to the skew.
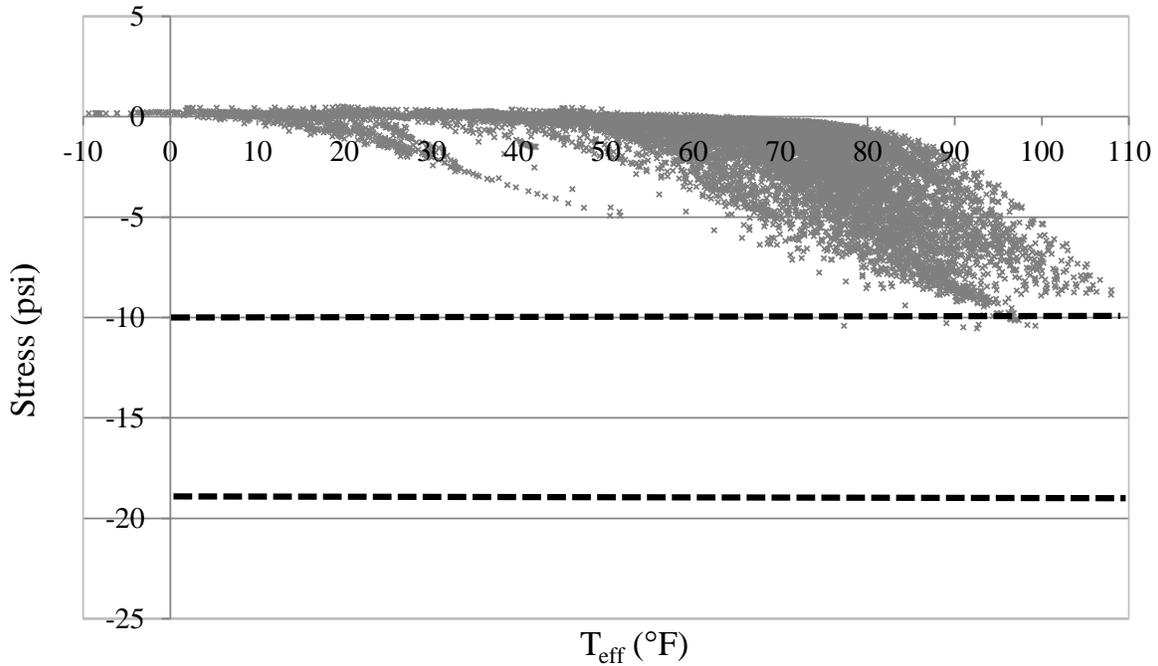
Figure 6.50. Southwest abutment backwall pressure versus effective temperature

Figure 6.51 shows the external stress on the south-east abutment pressure cell on Bridge 309 versus the effective temperature of the bridge. The south-east corner of the bridge is on the inside of the horizontal curve and is on the side of the bridge that is elongated due to the skew.

During the monitoring period of the project a critical hardware component had to be replaced. As a result, six months of data from the south end of Bridge 309 was considered untrustworthy and had to be disregarded. Losing this period of data could have influenced the stress ranges measured and could be a reason for higher stress ranges in the north abutment. Additionally, the soil compaction of the backfill may have varied between the north and south abutment.

From the pressure cell results, an estimation of the axial stresses in the girders due to soil pressure was calculated, with the purpose of checking the values obtained from the strain gauges. If the soil behind each abutment was assumed to be homogenous and the stress distribution increases linearly from zero at the surface downward as shown in Figure 6.52. Soil pressure ranges from the pressure cells, mounted 10 in. below the abutment corbel, were observed over a 100 °F range. The measured pressure range for the soil pressure at the bottom of the pile cap was then found by Equation 6.28.

$$p_{max} = \frac{p_{gauge}L_{max}}{L_{gauge}}$$
(6.28)

where,
    L_{max} = the total height of each abutment,
    L_{gauge} = the distance from the top of the abutment to the pressure cells,

P_{gauge} = the maximum stress measured at the location of pressure cells, and
P_{max} = the approximated maximum stress at the bottom of the abutment.
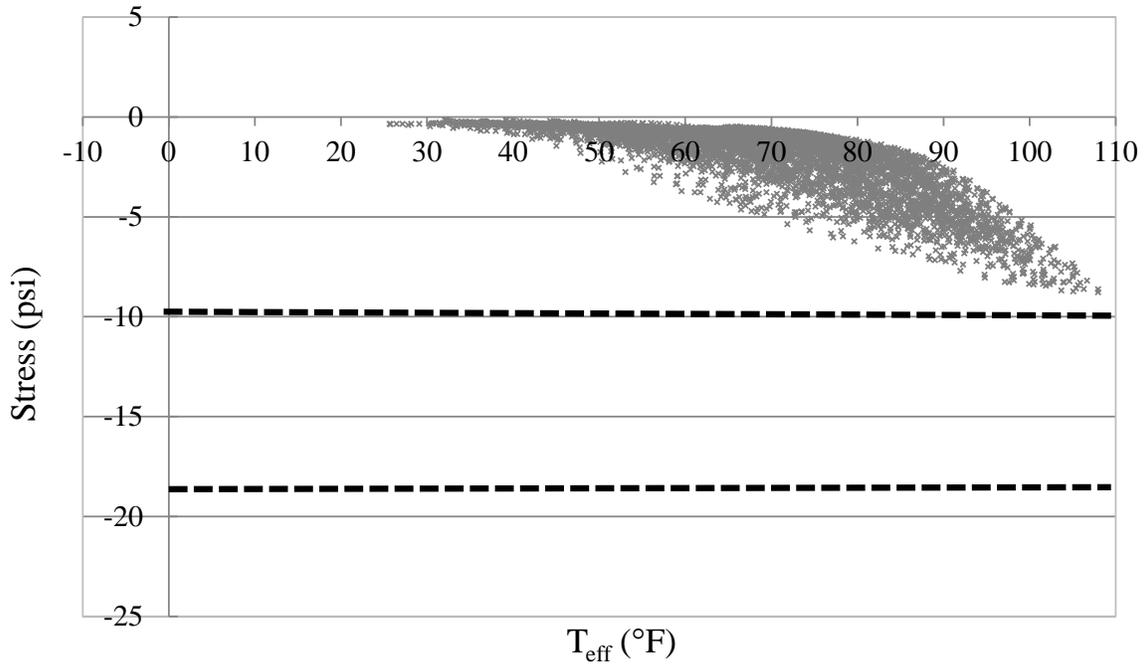
Figure 6.51. Southeast abutment backwall pressure versus effective temperature
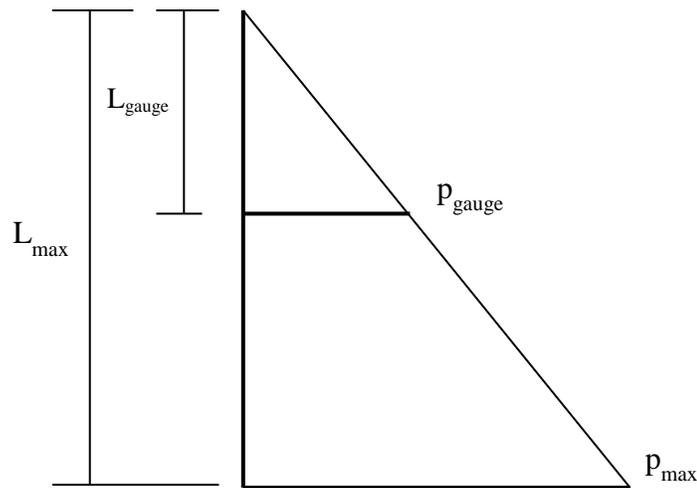
Figure 6.52. Assumed backfill passive stress distribution

Since the measured values of p_{gauge} were different for the east and west pressure cells of each abutment, the calculated values of p_{max} were inconsistent. Therefore, for each abutment an

94

average pressure, p_{avg}, was calculated from the two corresponding values of p_{max} and was assumed constant across the length of the abutment backwall. For each abutment a total passive force (kips) applied to the respective abutment backwall was calculated by

$$P_{total} = (1/2)L_{max}p_{avg}B_{abutment} \qquad (6.29)$$

where,

P_{total} = the total approximate force applied to each abutment, and

$B_{abutment}$ = width of the abutment

It was assumed the total force was distributed evenly among each of the four girders, from which a single girder force, $P_{pergirder}$, could be calculated. Table 6.7 shows the results of the approximation.

Table 6.7. Approximation of girder axial force from abutment backwall pressure

	NAPRW (GA)	NAPRE (GD)	SAPRW (GA)	SAPRE (GD)
$P_{approx.}$ (kip)	134		73	
$P_{measured}$(kip)*	690	690	690	500

The discrepancy between the measured and calculated axial forces can be explained by other restraining forces, such as forces from the piers, piles, and pavement.

6.3 Measured Displacements

6.3.1 Superstructure Displacement

Coordinate Systems and Coordinate Transformations

The raw survey data for each bridge were initially transformed into global bridge coordinates X and Y, as described previously. To make the raw data useful, the research team transformed the data into local coordinate systems. Figure 6.53 shows both of the local coordinate systems and the global coordinate system. Each abutment and pier has two Cartesian coordinate systems that originate at their respective interior reflector. The first of the two local coordinate systems is aligned with the skew of the abutments and piers. The x-axis of the first system is related to the abutment/pier geometry. The y-axis is 90 degrees counter-clockwise to the x-axis. Displacements for these systems are labeled u, x-axis displacement, and v, y-axis displacement.

The second of the two local coordinate systems is related to the bridge radius. The r-axis is aligned with the radial line passing through the same origin. The t-axis is 90 degrees counter-clockwise to the r-axis and runs tangent to the bridge's horizontal curve. Displacements for the radial system are labeled u′, r-axis displacement, and v′, t-axis displacement.
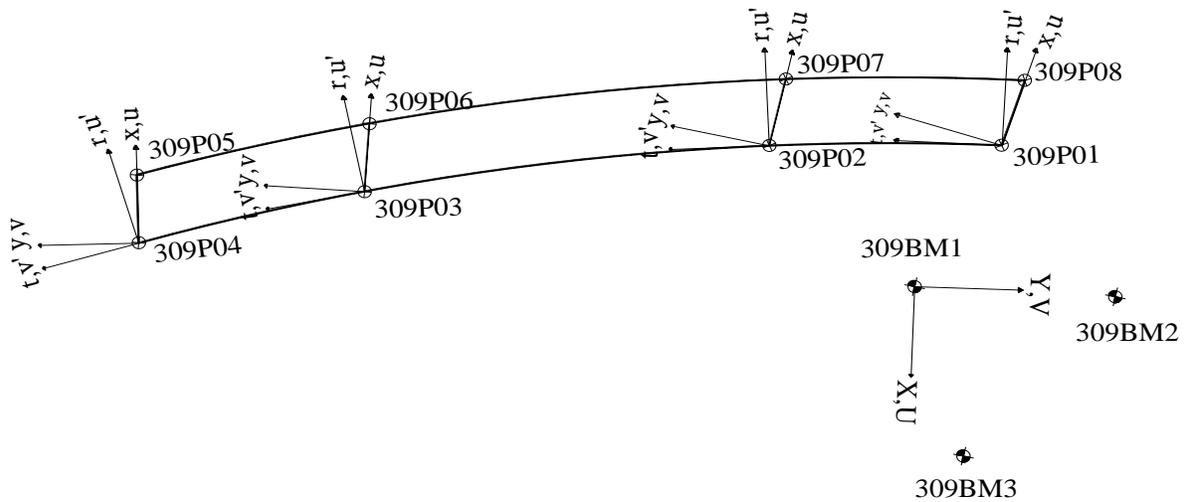
Figure 6.53. Local abutment and pier coordinate systems

Bridge 309 Benchmark Three Movements

The surveying results rely upon the assumption that the benchmarks remain stationary throughout the length of the project and their location can be measured accurately with a total station. Figure 6.54 shows the average location of benchmark three for Bridge 309, as measured by the monthly surveys, for each month a survey was conducted. Each month is represented by a circle and is labeled accordingly. The figure shows that there are errors in either the assumption that the benchmark remains stationary or that its location can be accurately measured during each survey. In general, most of the months are within roughly 0.3in. of each other. Two outliers, August 2011 and November 2011, are roughly 0.6 in apart.

Aug-11

Nov-10   Sept-11

Dec-10

                                    0.100 in.
Feb-11   Oct-11
Jan-11Aug-10July-11

July-10

Apr-11
Mar-11
May-11
June-11

Nov-11
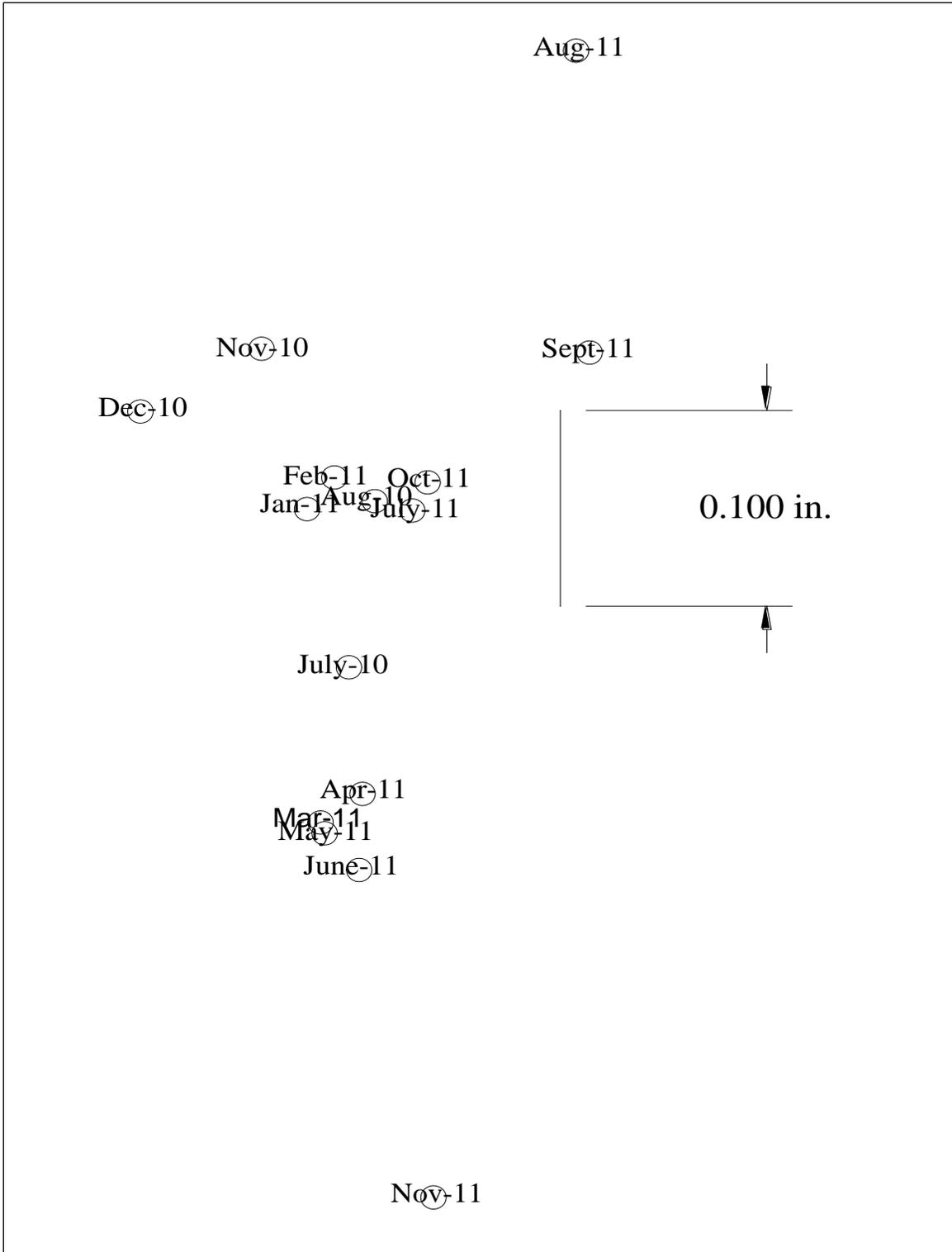
Figure 6.54. Bridge 309 benchmark three movements

Total Change in Length

Throughout the project each bridge at the NEMM was surveyed each month. From these data the research team was able to track the length changes of each bridge. The total change in length for each bridge was calculated from the displacements in the t-axis direction, v′, at both abutments. Figures 6.55 through 6.60 show the change in length of bridges 109, 209, 309, 2208, 2308, and 2408 versus effective bridge temperature. In each of the figures, each survey month is represented by a rectangle where the vertical sides of the rectangle represent the 95% confidence interval of the results and the horizontal sides of the rectangle represent the change in effective temperature during the time of the survey. The solid diagonal line represents the change in length based on free expansion and contraction of the bridge, and the dashed diagonal line represents the best fit line from the survey results.

Figure 6.55 shows the measured values of the change bridge length versus the effective temperature for Bridge 109, a straight integral abutment bridge with two fixed piers. The best fit line of the surveying results shows a linear relationship between the change in length and the effective temperature of the bridge that is similar to that of the theoretical free expansion line.

Figure 6.56 shows the total change in length of Bridge 209, a semi-integral abutment bridge with a fixed and expansion pier, as calculated by the surveying as well as by expansion meters mounted on each abutment. The movements measured by the expansion meters record a plateauing at both ends of the temperature spectrum, something the research team was unable to explain.

Figure 6.57 shows the total change in length measurements of Bridge 309 measured by the monthly survey as well as by long-range distance meters mounted at each abutment and pier. Bridge 309 is an integral abutment bridge with two fixed piers. For the most part, the measured results from the survey data and from the long-range distance meters correspond to one another and both show a linear relationship between the change in length of the bridge and the effective temperature of the bridge.

Figure 6.58 shows the total change in length versus effective bridge temperature for Bridge 2208, an integral abutment bridge with a fixed and expansion pier. The best fit of the survey line and the theoretical free expansion line produce very close results, suggesting less expansion restraint at this bridge.

Figure 6.59 displays the total change in length of Bridge 2308 by surveying and expansion meter measurements. As with bridge 209, the expansion meters plateau at high and low temperatures. Bridge 2308 is a semi-integral abutment bridge with two fixed piers.

Figure 6.60 shows the total change in length of Bridge 2408 versus the effective bridge temperature. As with Bridge 109, Bridge 2408 is a straight bridge with integral abutments and two fixed piers.
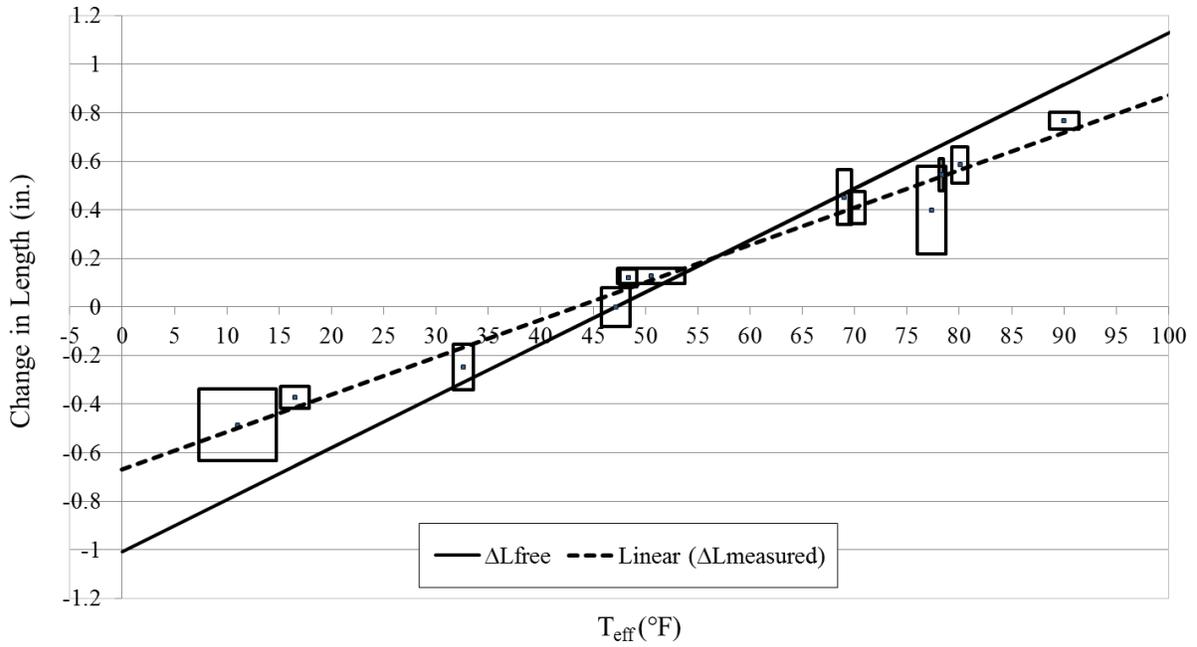
Figure 6.55. Bridge 109 total change in length
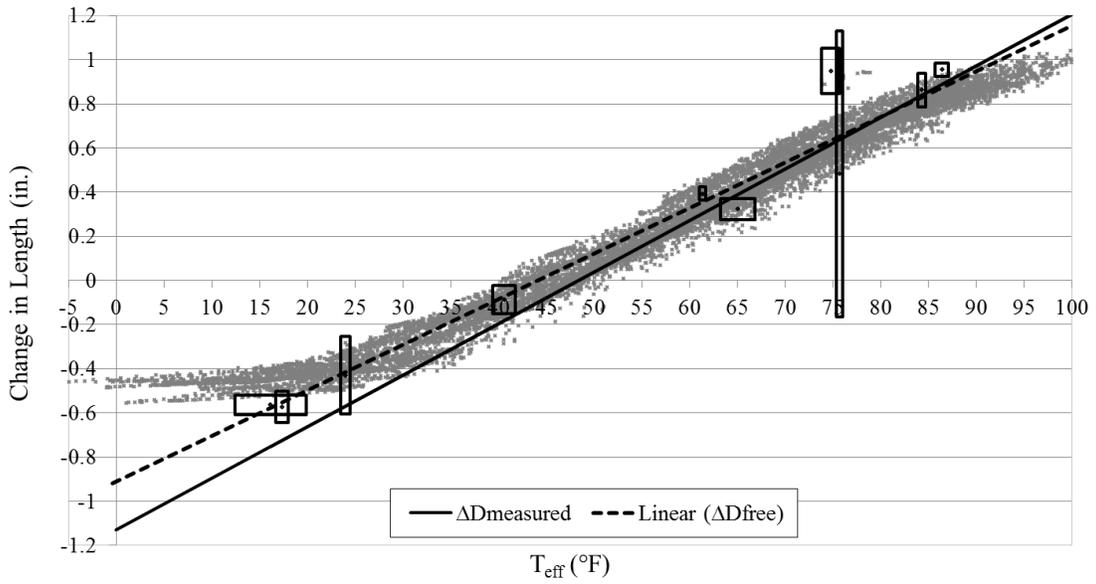
Figure 6.56. Bridge 209 total change in length
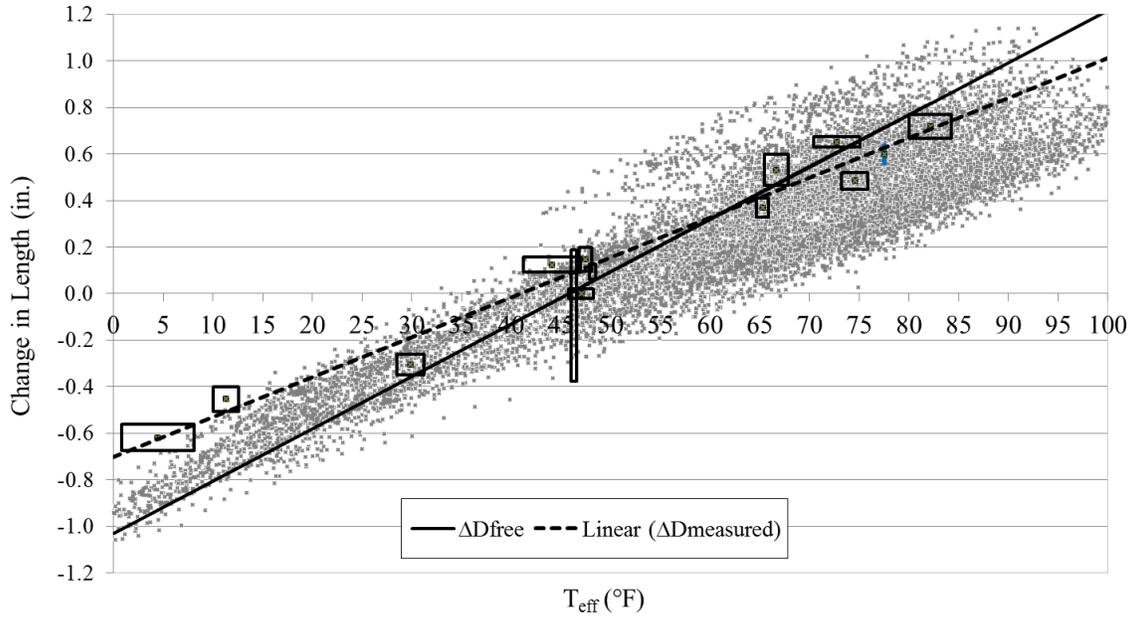
Figure 6.57. Bridge 309 total change in length
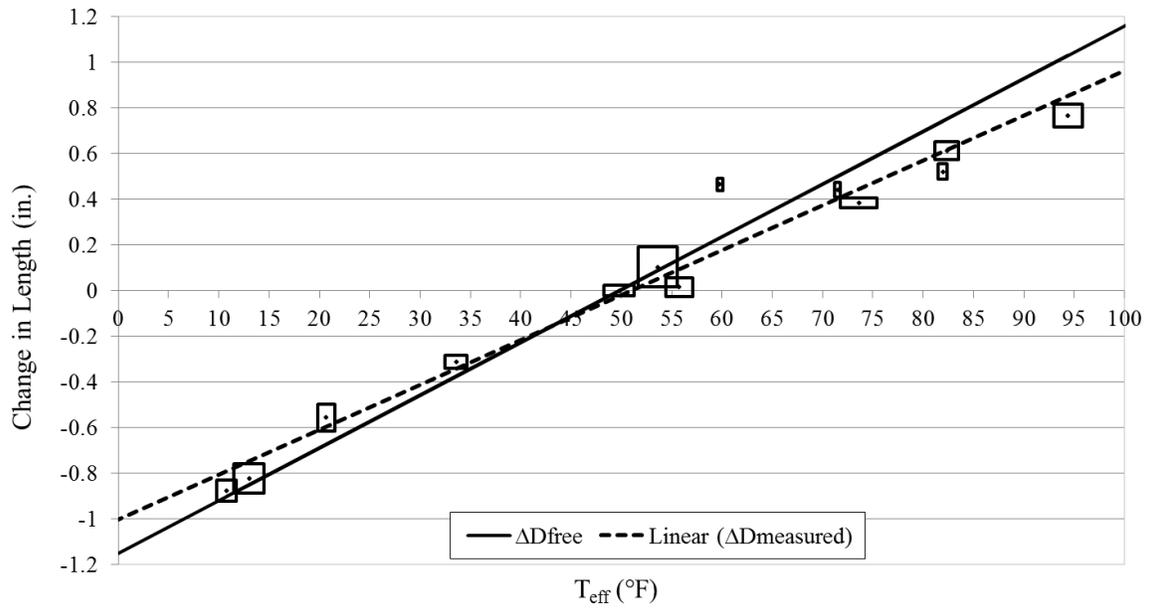
Figure 6.58. Bridge 2208 total change in length

100
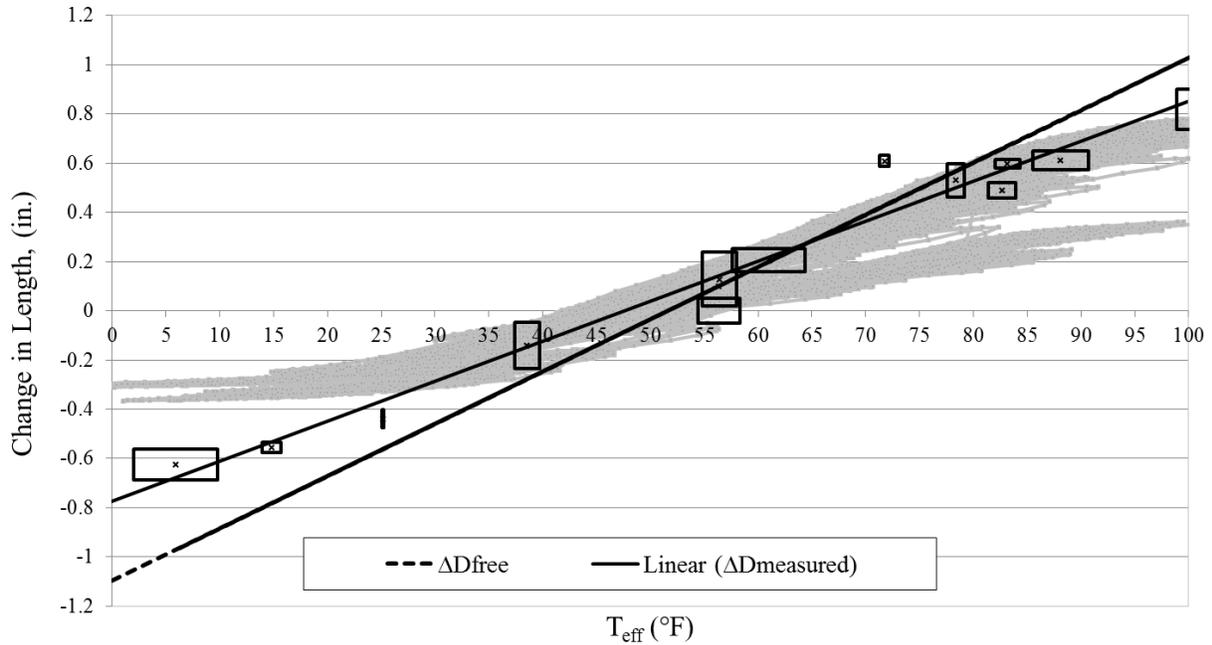
Figure 6.59. Bridge 2308 total change in length
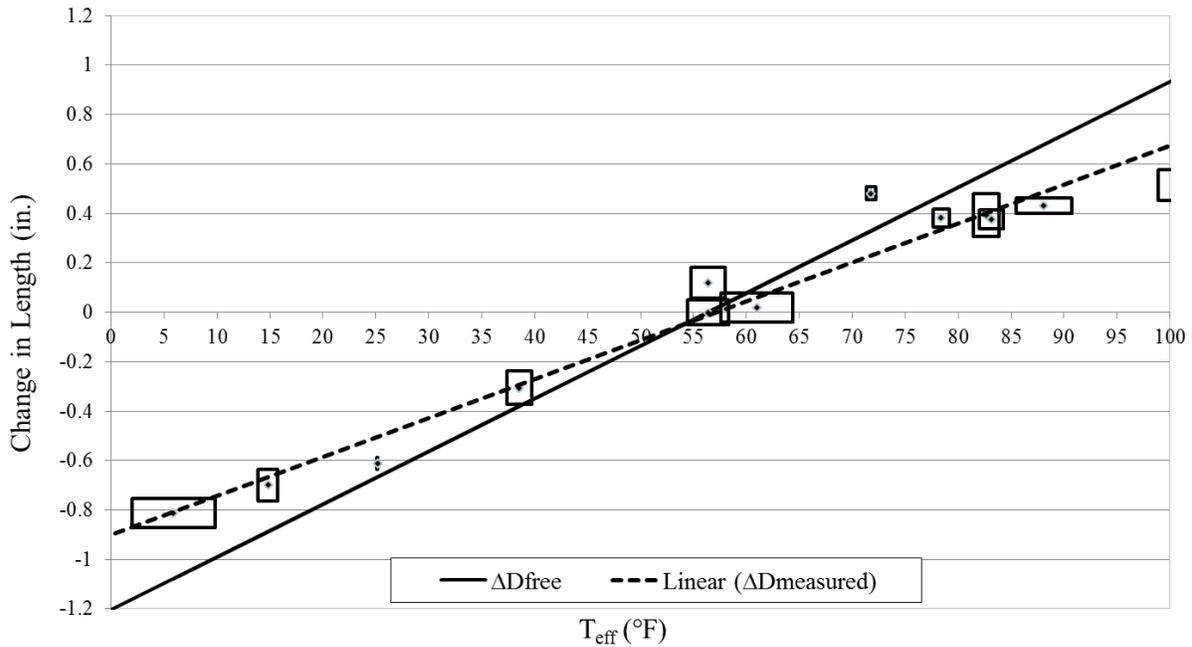
Figure 6.60. Bridge 2408 total change in length

Table 6.8 shows the total free expansion change in length, ΔL_{free}, and the total measured change in length, $\Delta L_{measured}$, for each bridge, which are equal to the differences between the maximum and minimum lengths in Figure 6.55 to Figure 6.60.

An axial strain as a result of expansion resistance was calculated from the difference between these two lines by Equation 6.30:

$$\Delta\varepsilon_r = (\Delta L_{free} - \Delta L_{measured})/L \qquad (6.30)$$

where,

   $\Delta\varepsilon_r$ = resistance axial strain, and
   L   = length of bridge along curve.

Table 6.8. Total free expansion and measured change in length

Bridge/Range	109	209	309	2208	2308	2408
ΔL_{free}	2.14	2.32	2.24	2.24	2.14	2.14
$\Delta L_{measured}$	1.54	2.15	1.7	2.00	1.65	1.58

Table 6.9 shows the results from Equation 6.33 as well as the average axial strain in the respective bridge from the strain gauge data.

Table 6.9. Calculated average axial strain versus measured average axial strain

Bridge/Strain	109	209	309	2208	2308	2408
$\Delta\varepsilon_r(\mu\varepsilon)$	141	43	141	61	135	154
$\Delta\varepsilon_a(\mu\varepsilon)$	180	169	165	108	153	NA

The resistance axial strain, $\Delta\varepsilon_r$, is similar to the strain gauge measured axial strain, $\Delta\varepsilon_a$, for Bridges 109, 309, and 2308. The resistance axial strain for Bridges 209 and 2208 are much lower than the strain gauge measured axial strain, and no comparison can be made for Bridge 2408, as there is no strain gauge data.

Total Change in Span Length

From the survey data, the change in span length was calculated from displacements along the respective t-axis at the abutments and piers, v′. Figures 6.61 through 6.66 show the change in span length for Girder A and Girder D of each span of Bridges 109, 209, 309, 2208, 2308, and 2408, respectively. Also shown in the figures are the average of Girder A and Girder D for each span and the total average of all spans.
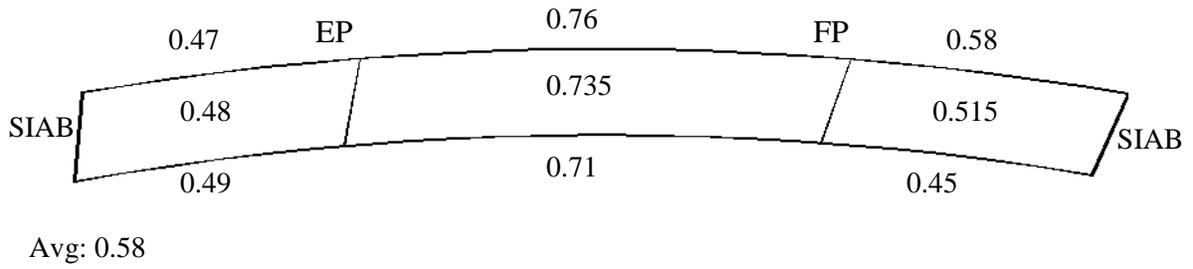
Figure 6.61. Bridge 209 change in length per span
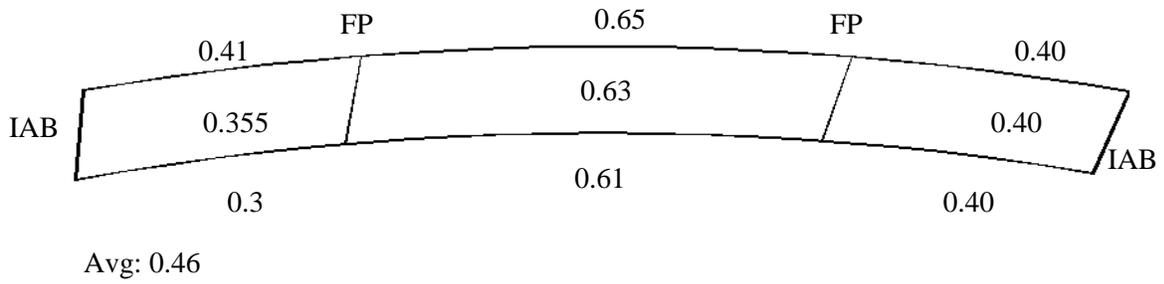
Figure 6.62. Bridge 309 change in length per span
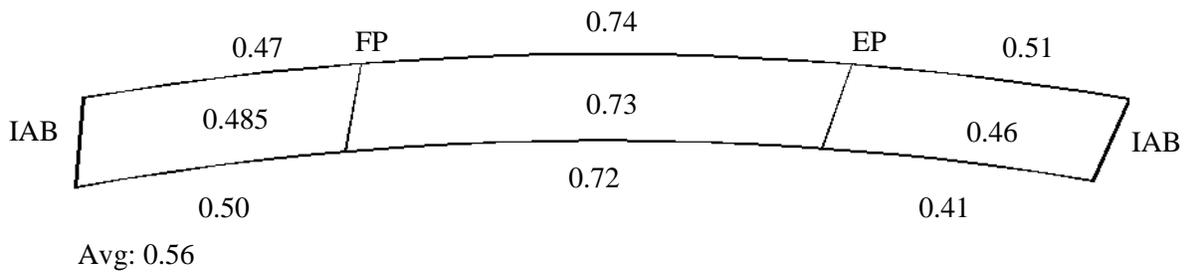
Figure 6.63. Bridge 2208 change in length per span

0.48   FP   0.66   FP   0.41

SIAB   0.425   0.625   0.41   SIAB

0.59

0.37   0.41

Avg: 0.49
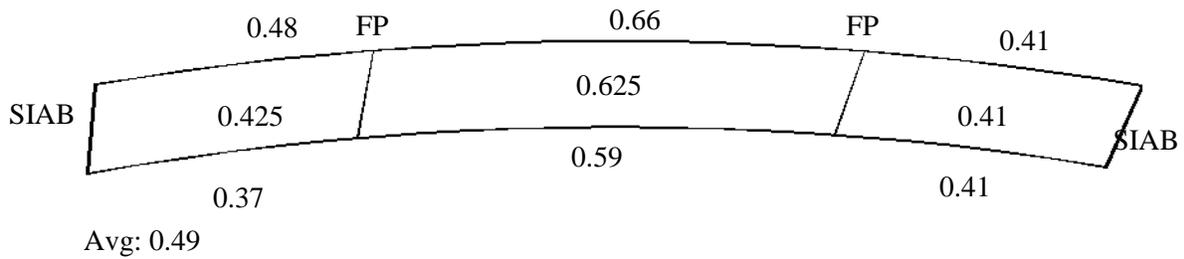
Figure 6.64. Bridge 2308 change in length per span

0.39   EP   0.73   FP   0.32

IAB   0.35   0.735   0.33   IAB

0.31   0.74   0.34

Avg: 0.47

Figure 6.65. Bridge 109 change in length per span

0.38   FP   0.74   EP   0.35

IAB   0.37   0.73   0.345   IAB

0.36   0.72   0.34

Avg: 0.48

Figure 6.66. Bridge 2408 change in length per span

As shown in Figures 6.60 through 6.66 the change in length of the center span is, as one might expect, largest for all bridges. With regard to the curved-girder bridges, Figures 6.60 through 6.64, the bridges with one fixed pier and one expansion pier, Bridge 209 and 2208, show higher values in the change in length of the center span compared to the two bridges with both piers fixed, Bridge 309 and 2308. With regard to the two straight bridges, Bridge 109 and 2408, the change in length of both end spans and the center span were similar between the bridges.

Bridge Movements Month to Month

The monthly reflector coordinates calculated from the survey data were input into a commercial drafting program. This allowed the research team to produce graphical images summarizing the

bridge movements with time. Because the movements were very small compared to the geometry of the bridges, the drawings had to be scaled. In the following the scale is shown in its respective figure.

Figures 6.67 through 6.72 display the location of the bridge, at the reflectors, for three months during the monitoring portion of the project life. The three months include February 2011, a cold month; April 2011, the reference month; and July 2011; a hot month. In the figures, the respective bridge is shortest during the cold month, at its longest during the hot month, and in the middle during the reference month.

Figures 6.73 through 6.96 track the monthly location of the abutments and piers reflectors on each bridge during the monitoring period. The west and east reflectors at each abutment and pier are positioned next to each other. Also, the figures are ordered starting with the north abutment and end with the south abutment, for each bridge respectively.

In general the reflector movements documented by Figures 6.73 through 6.96 show much larger longitudinal movements of the bridge superstructure compared to radial or transverse movements. As one might expect, the movement ranges of the superstructures near fixed piers are generally smaller than the movement ranges displayed near an expansion pier. The range of superstructure movements documented near IABs and SIABs show little difference between the two abutment configurations. Also, generally there is little noticeable difference between the movements in both the longitudinal and transverse direction of the two straight bridges and the four horizontal bridges when considering similar pier and abutment fixities.

Effective Thermal Length

One way to calculate longitudinal forces on piers from thermal expansion of girders is to establish a design length. The design length is the length of a girder whose expansion contributes to the development of forces on the pier. From here on, this report refers to this as the effective thermal length.

Table 6.6.2.12.4.1 of the Iowa DOT *LRFD Bridge Design Manual* specifies an effective thermal length based on abutment and pier fixity configuration. The table covers two- to four-span integral abutment bridges with expansion and fixed piers, and is used with bridges that do not have large variations in pier stiffness (Iowa DOT 2011). In this report, the research team used the survey data and Equation 6.31 to calculate an effective thermal length.

$$L_{eff} = \frac{\Delta d}{\alpha_{eff} \Delta T} \qquad\qquad (6.31)$$

where,
      Leff = effective thermal length,
       Δd = range on longitudinal movement of fixed pier or integral abutment, and
          ΔT is a temperature range of 100°F.

Table 6.10 shows the effective thermal length calculated by the research team as well as the effective thermal length given by the Iowa DOT. Iowa DOT values are in parentheses.

Table 6.10. Effective thermal length

Bridge/Location	S. Abut (ft)	S. Pier (ft)	N. Pier (ft)	N. Abut (ft)	Bearing
109	91		72	105	IAB-EP-FP-IAB
309	95	60 (74.5)	65 (74.5)	116	IAB-FP-FP-IAB
2208	142		113	150	IAB-EP-FP-IAB
209		51			SIAB-FP-EP-SIAB
2308		50 (71)	46 (71)		SIAB-FP-FP-SIAB
2408	155	115		101	IAB-FP-EP-IAB

As shown in Table 6.10, the effective thermal length approximation proposed by the Iowa DOT results in higher effective thermal lengths. As a result, there is a level of conservatism built into their design. Also, the results of the approach taken by the research team results in values for end spans that are larger than the actual length of the corresponding span.

Fixed Pier Displacement

The fixed pier of Bridge 109, the north pier, was instrumented with an expansion meter to measure the relative displacement between the bottom flange of Girder B and the pier cap. Figure 6.97 shows the displacement results from the expansion meter versus effective bridge temperature.

Figure 6.97 shows that there is little measurable relative displacement between the pier cap of the fixed pier and the bottom flange of Girder B. As a result, this figure helps to confirm pier fixity assumptions.

Along with the relative displacement between the pier cap and the bottom flange of Girder B, the absolute displacement of the bottom flange of Girder B perpendicular to the pier was calculated using the survey data. Figure 6.98 shows the results of the absolute movement of Girder B from the survey.

Combining the results of Figure 6.97 and Figure 6.98 implies that, although there is no relative movement between the pier cap and the bottom flange of Girder B, there is movement at the pier location. Thus, there must be flexure in the pier due to thermal girder movement induced forces.

Expansion Pier Displacement

The expansion pier of Bridge 209 and Bridge 2208 was instrumented with an expansion meter. This meter measured the relative displacement between the bottom flange of Girder B and the pier cap. Figure 6.99 shows the results of typical relative displacement of the expansion pier measured by the expansion meter and by the surveying results. Similar to the displacements measured by the expansion meters mounted on the semi-integral abutments, the expansion

106

meters mounted on the expansion piers start to plateau at the effective bridge approaches the hot and cold extremes.
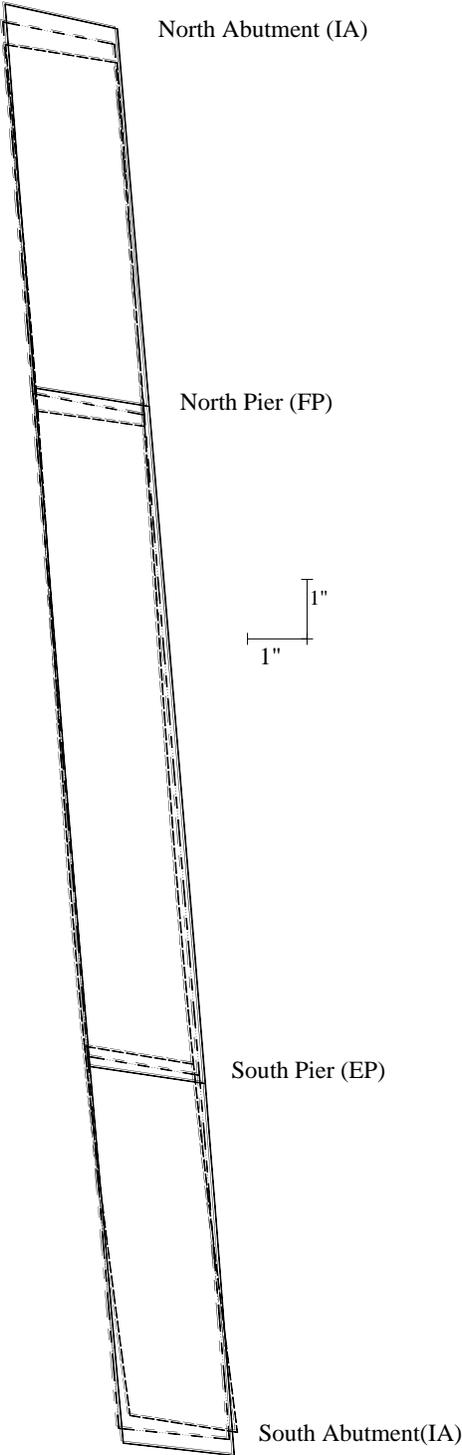
Figure 6.67. Bridge 109 deflected shape

North Abutment (SI)

North Pier (EP)

1"

1"

South Pier (FP)

South Abutment (SI)
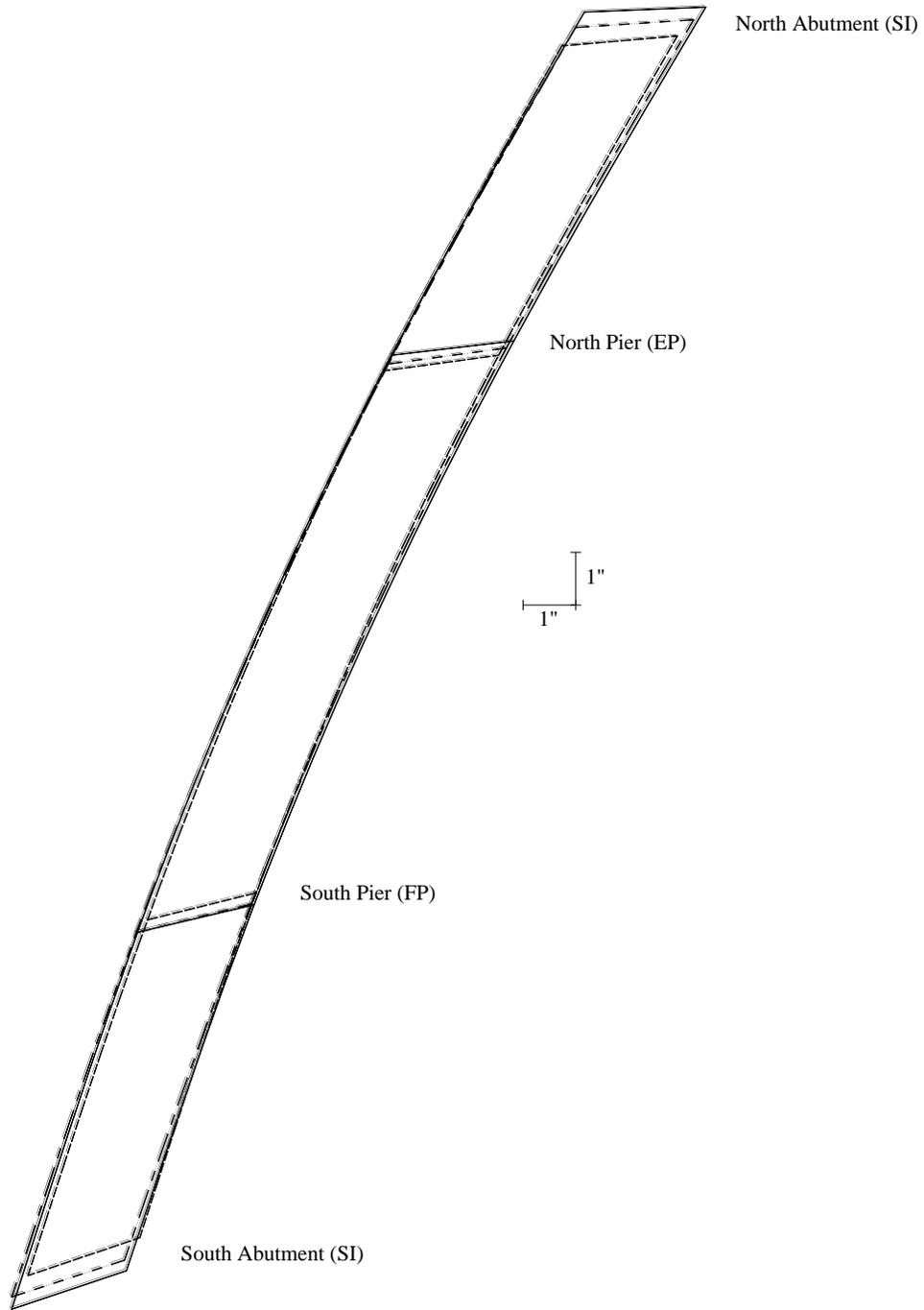
Figure 6.68. Bridge 209 deflected shape

North Abutment (IA)

North Pier (FP)

1"

1"

South Pier (FP)

South Abutment (IA)
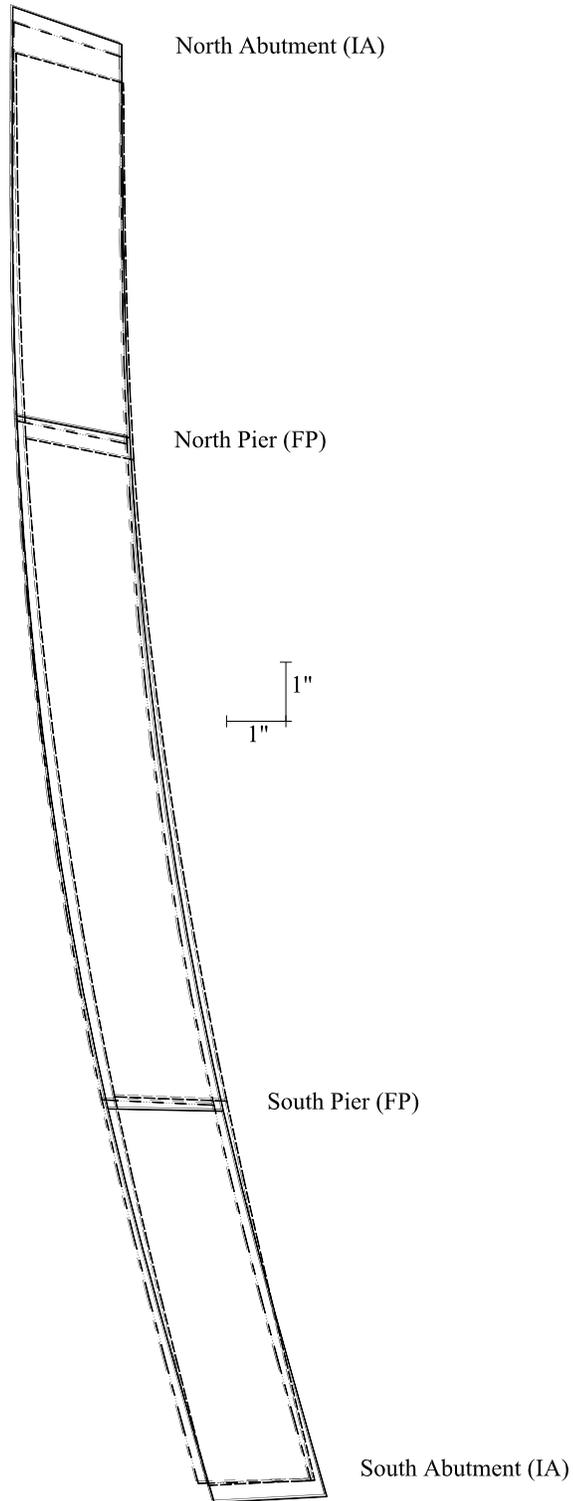
Figure 6.69. Bridge 309 deflected shape

North Abutment (IA)

North Pier (FP)

1"

1"

South Pier (EP)

South Abutment (IA)
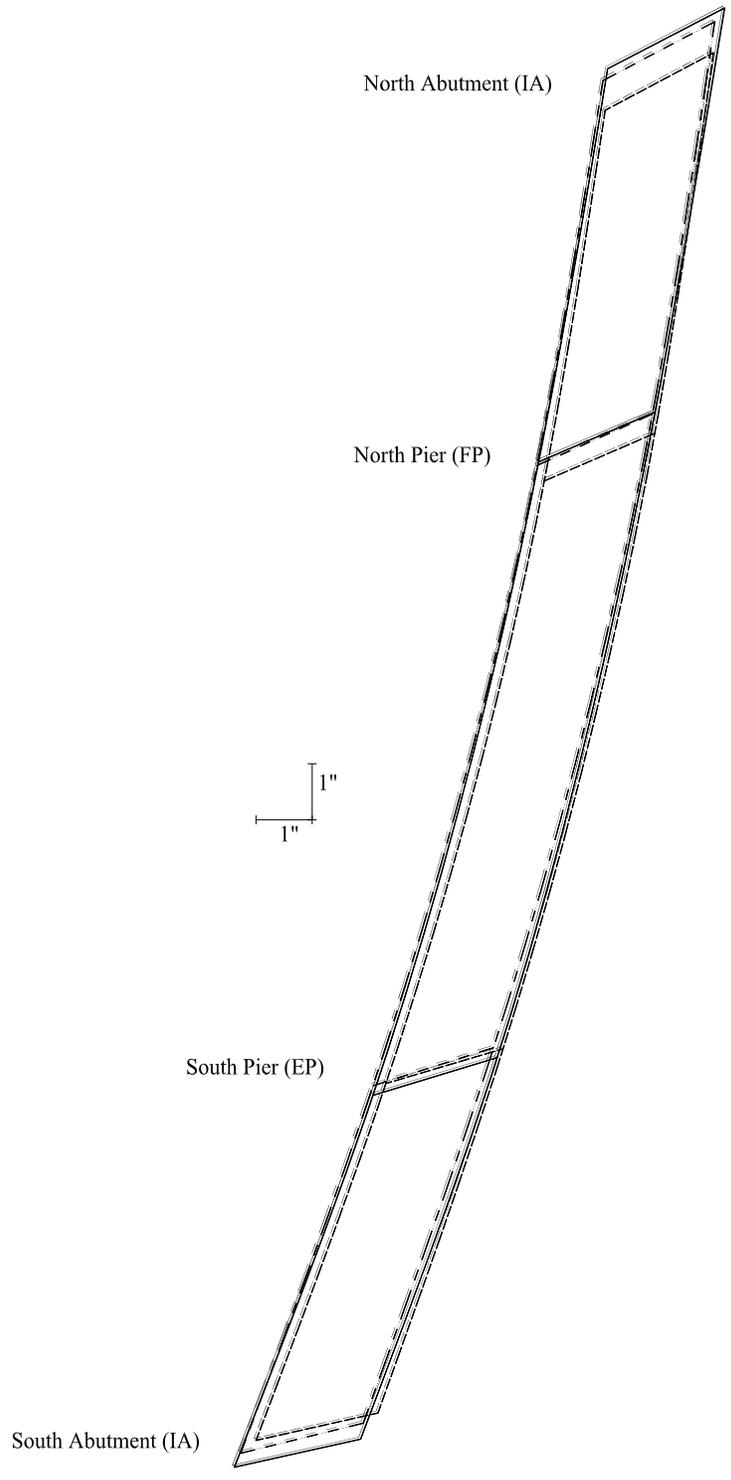
Figure 6.70. Bridge 2208 deflected shape

North Abutment (FP)

North Pier (FP)

1"

1"

South Pier (FP)

South Abutment (SI)
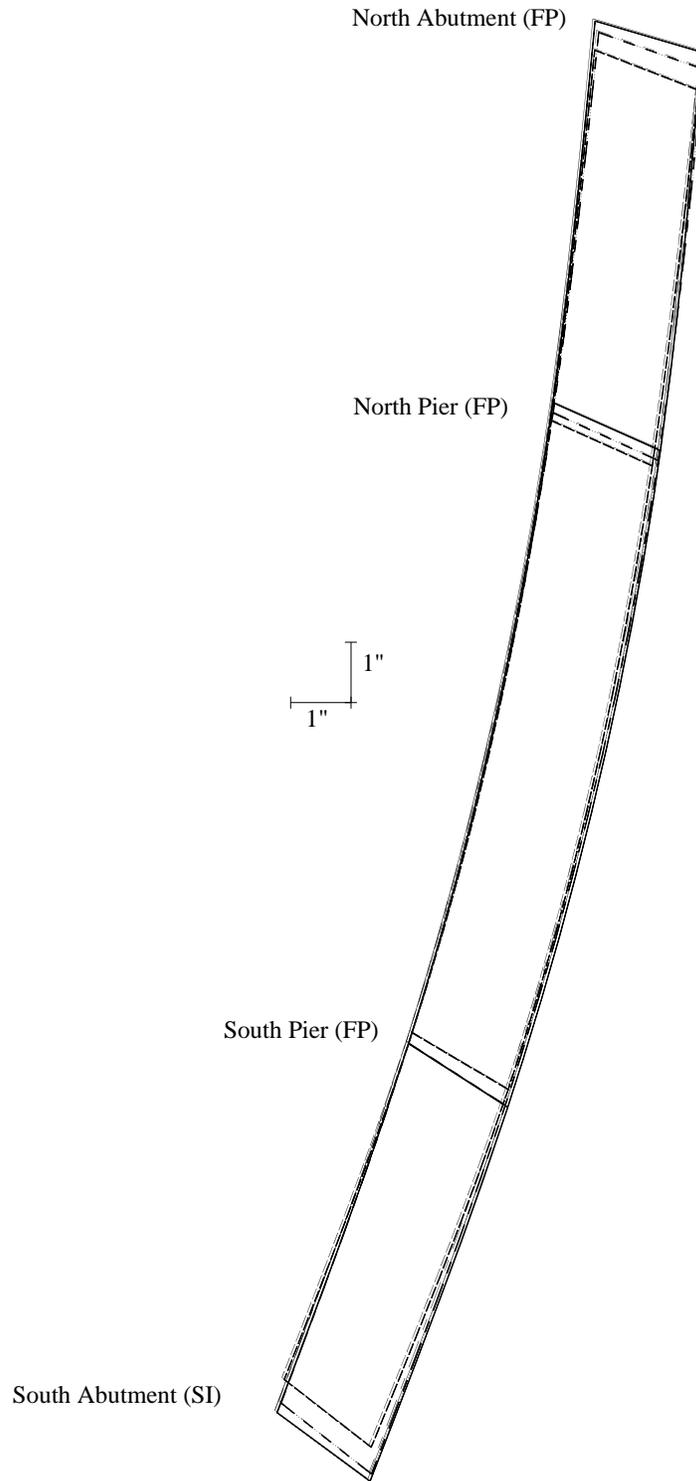
Figure 6.71. Bridge 2308 deflected shape

North Abutment (IA)

North Pier (EP)

1"

1"

South Pier (FP)
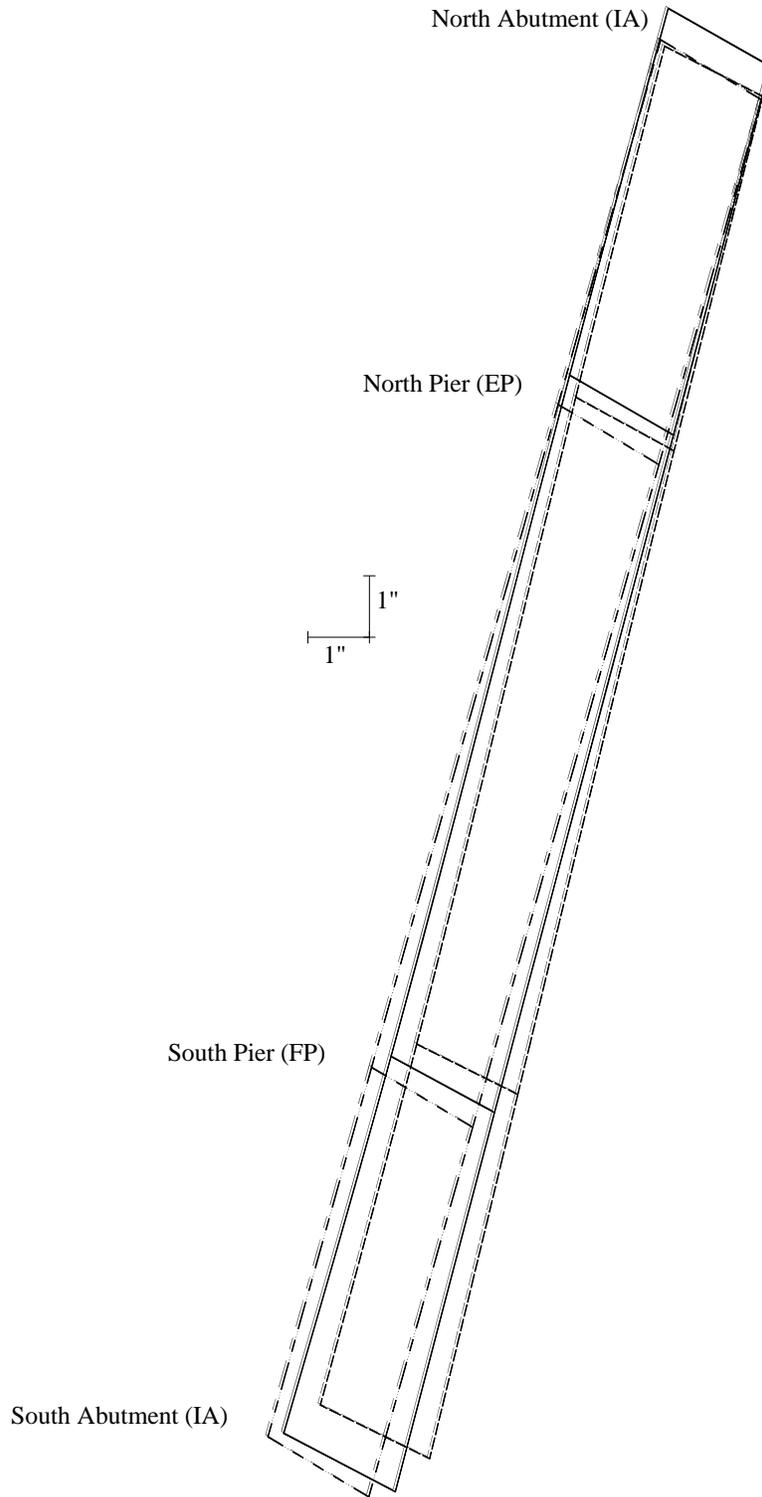
South Abutment (IA)

Figure 6.72. Bridge 2408 deflected shape

112
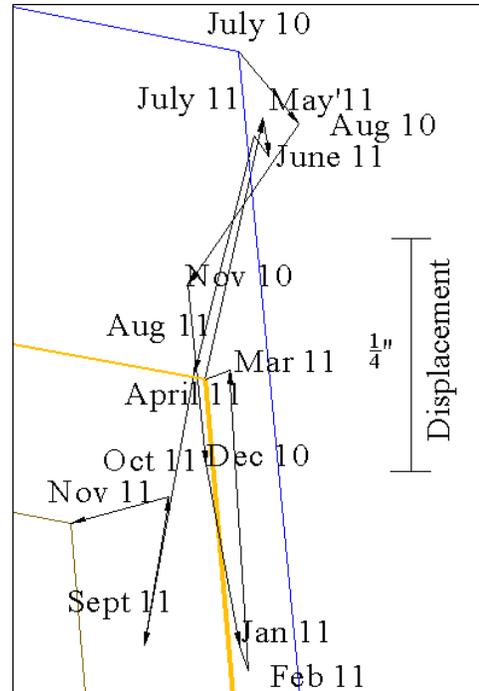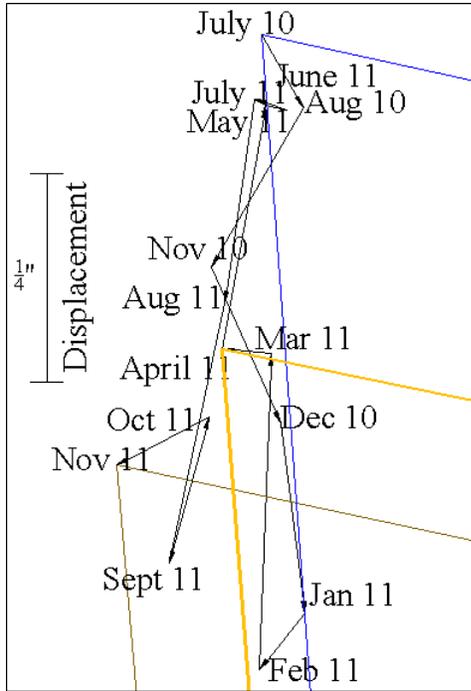
Figure 6.73. Bridge 109 movement at north abutment west and east reflectors
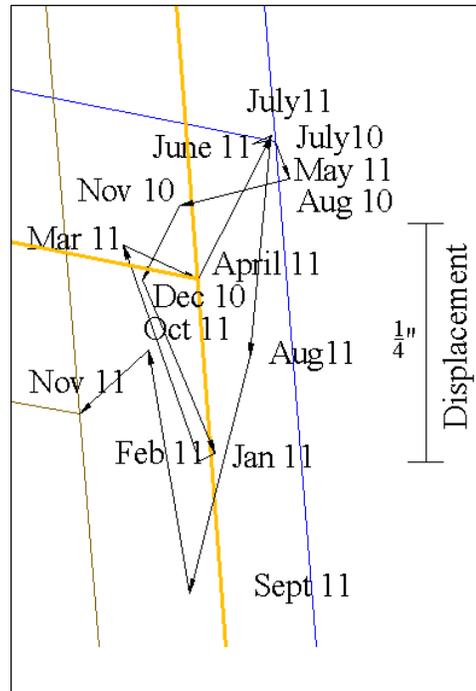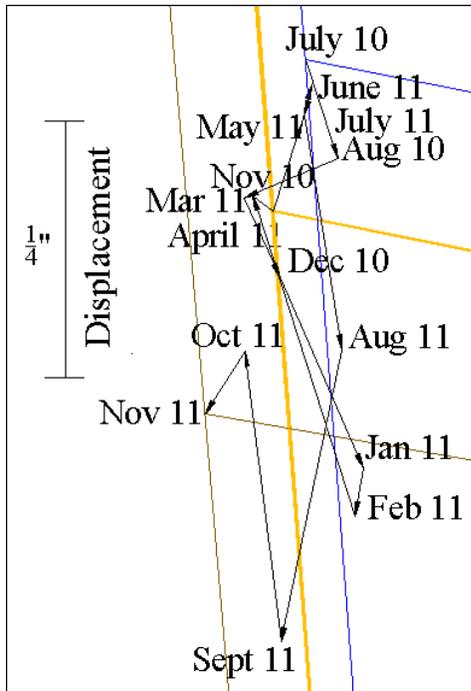
Figure 6.74. Bridge 109 movement at north pier west and east reflectors

113
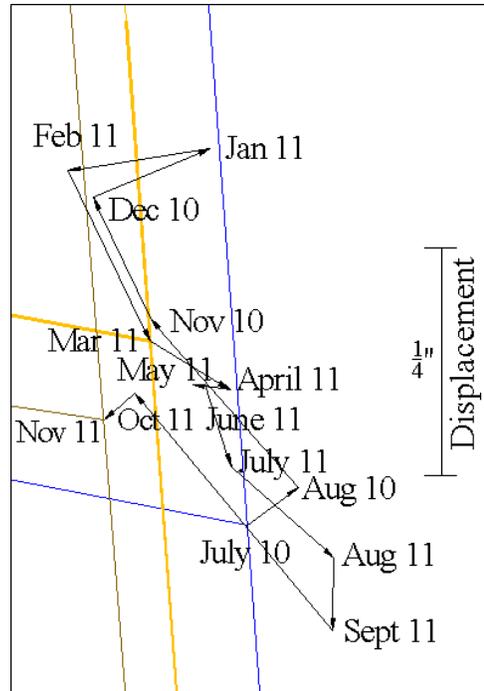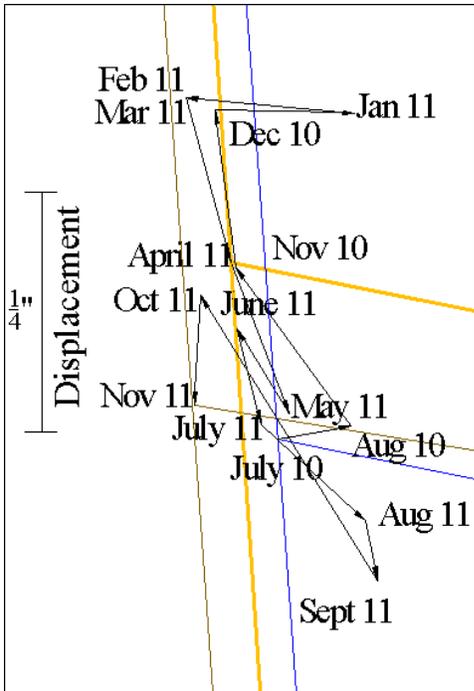
Figure 6.75. Bridge 109 movement at south pier west and east reflectors
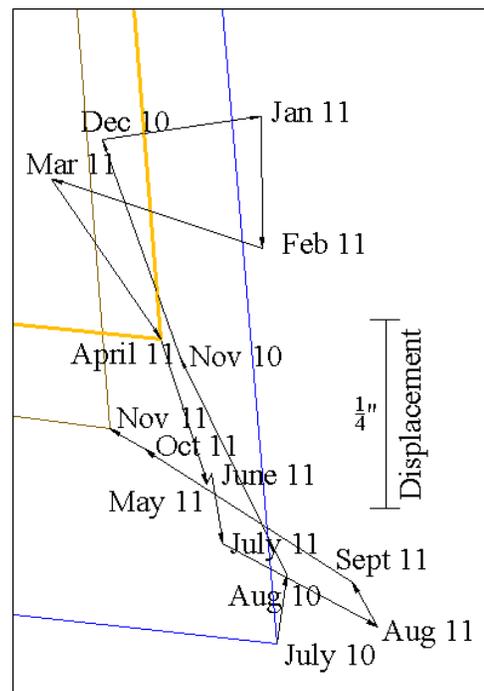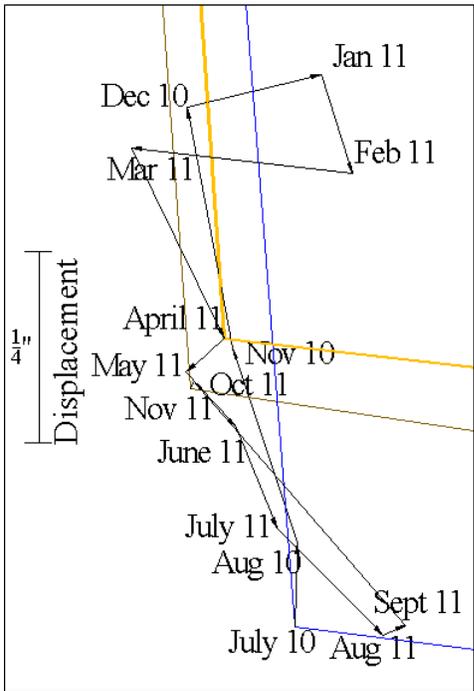
Figure 6.76. Bridge 109 movement at south abutment west and east reflectors
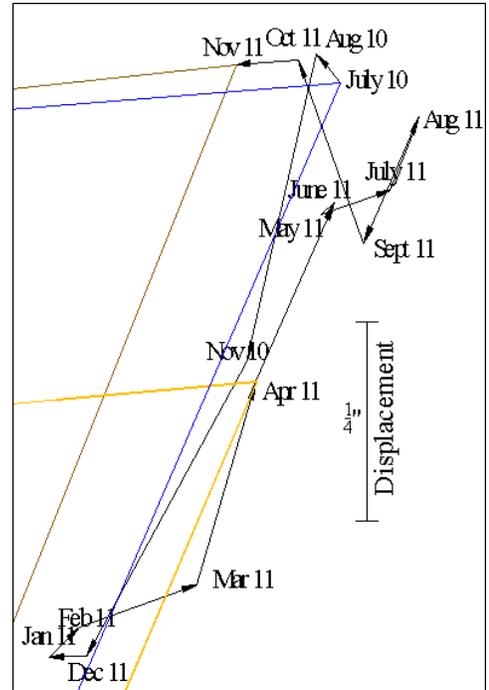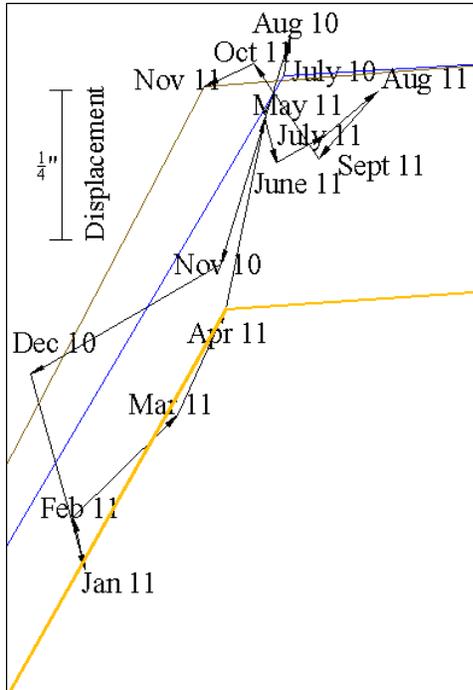
Figure 6.77. Bridge 209 movement at north abutment west and east reflectors
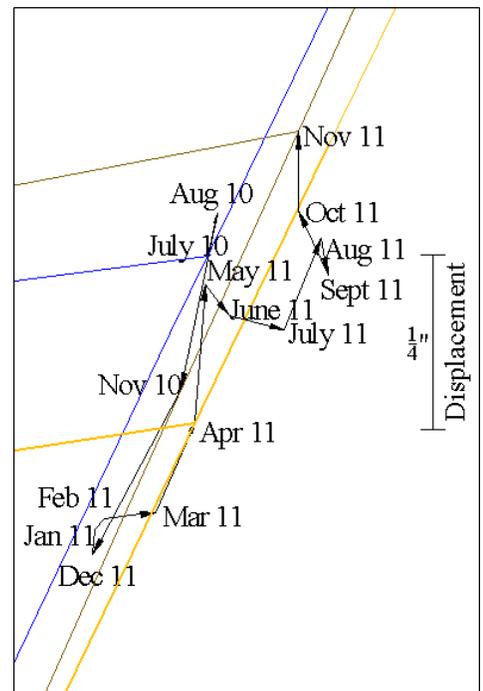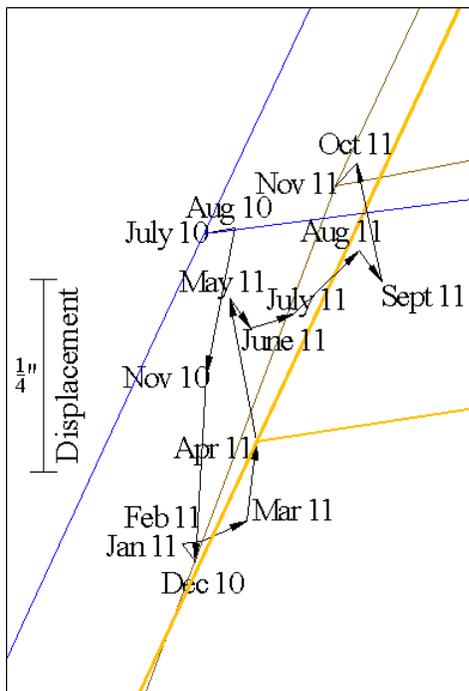
Figure 6.78. Bridge 209 movement at north pier west and east reflectors
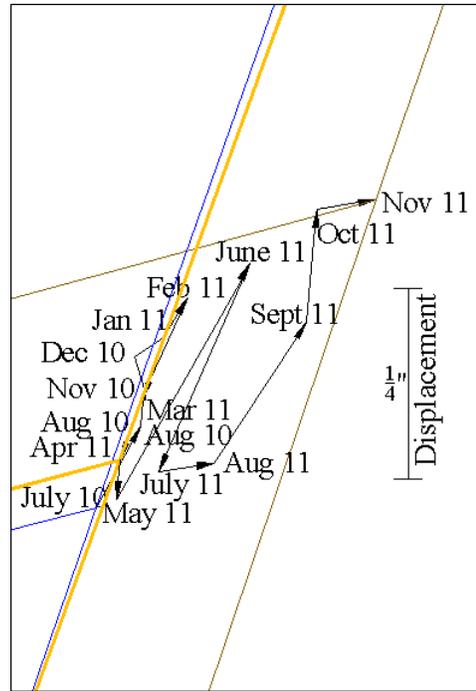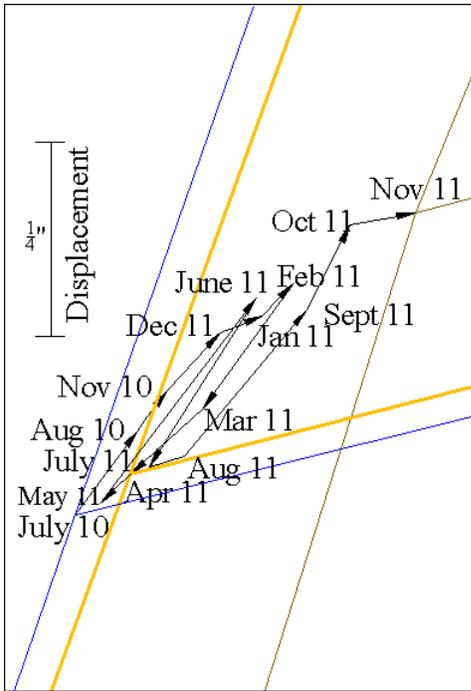
Figure 6.79. Bridge 209 movement at south pier west and east reflectors
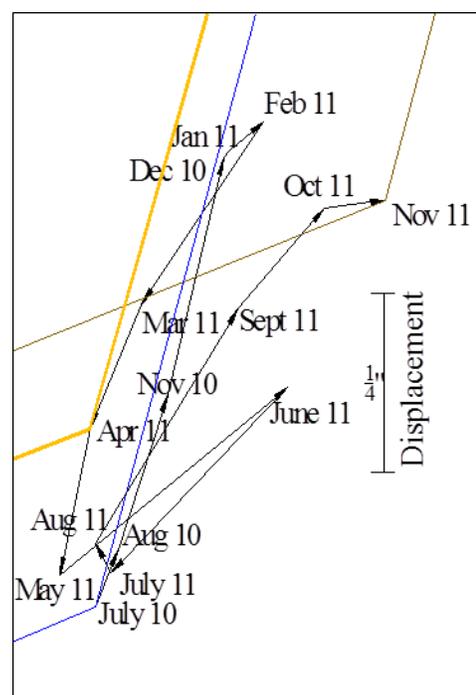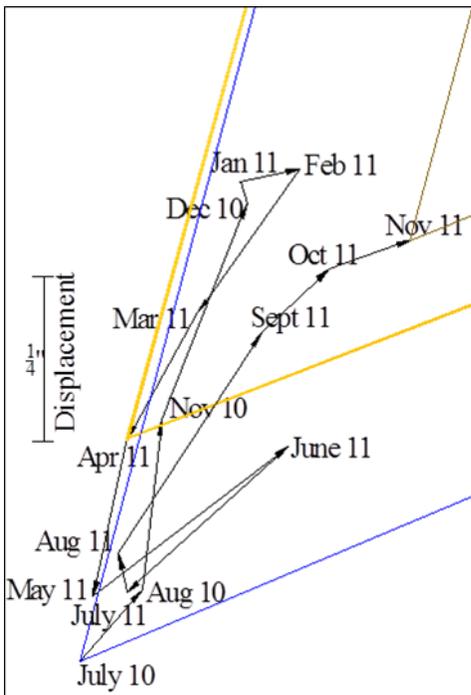
Figure 6.80. Bridge 209 movement at south abutment west and east reflectors

116
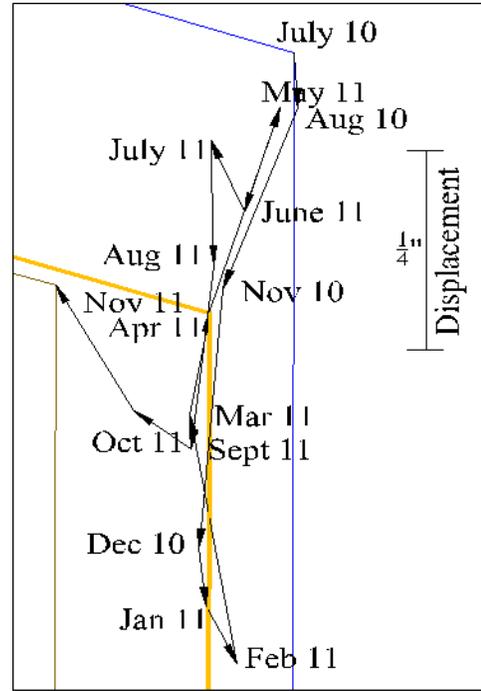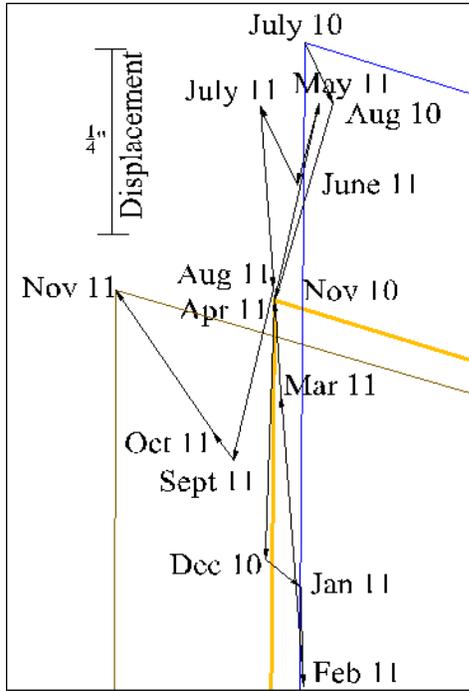
Figure 6.81. Bridge 309 movement at north abutment west and east reflectors
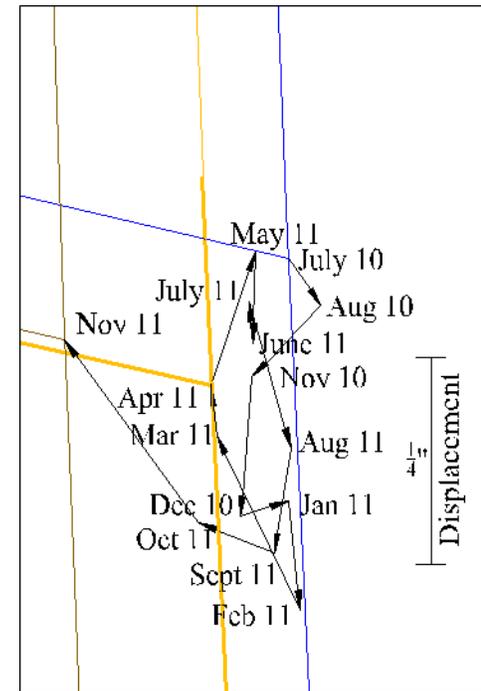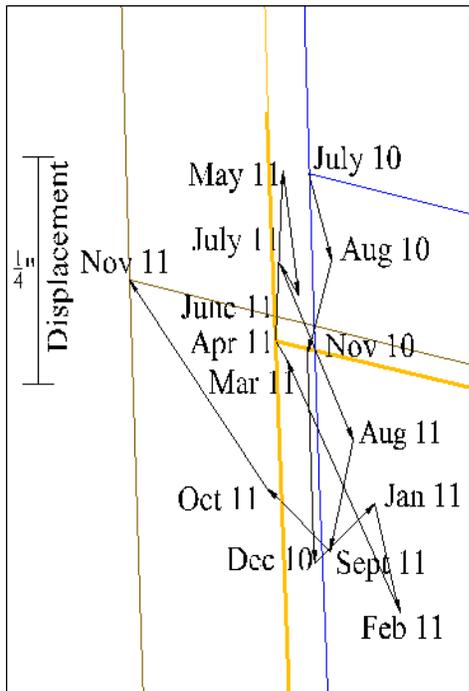
Figure 6.82. Bridge 309 movement at north pier west and east reflectors

117
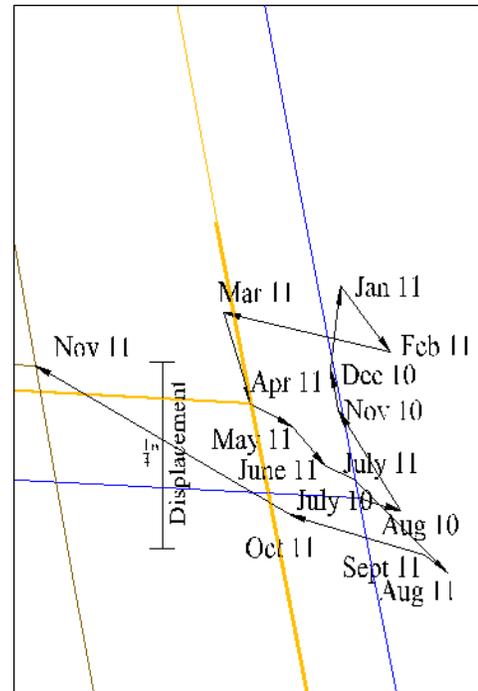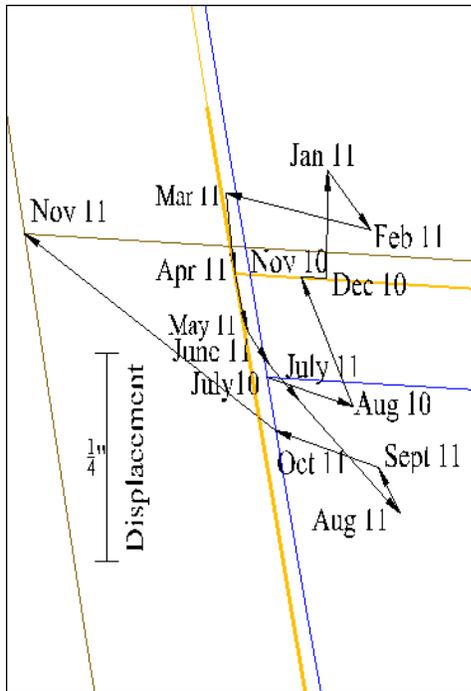
Figure 6.83. Bridge 309 movement at south pier west and east reflectors
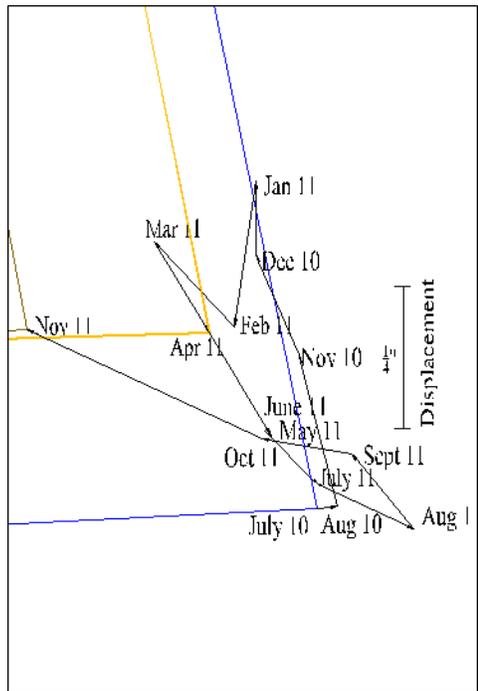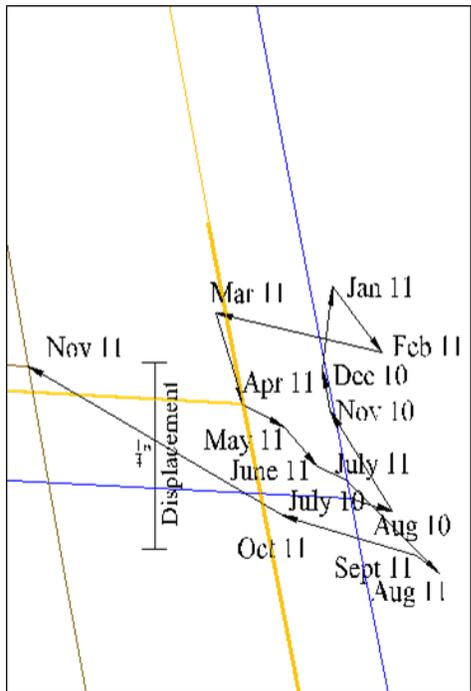
Figure 6.84. Bridge 309 movement at south abutment west and east reflectors

118
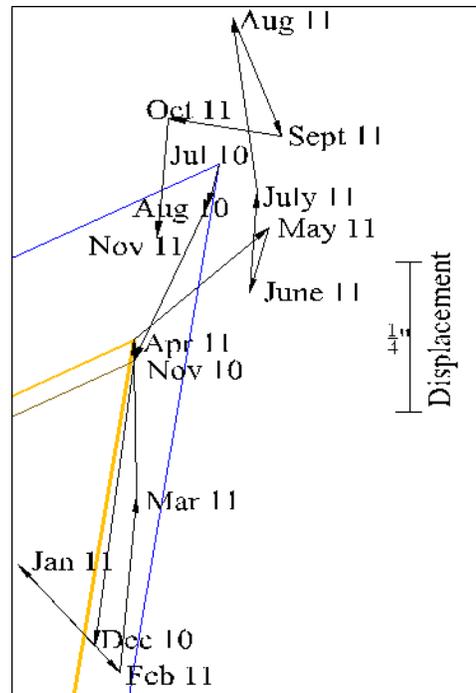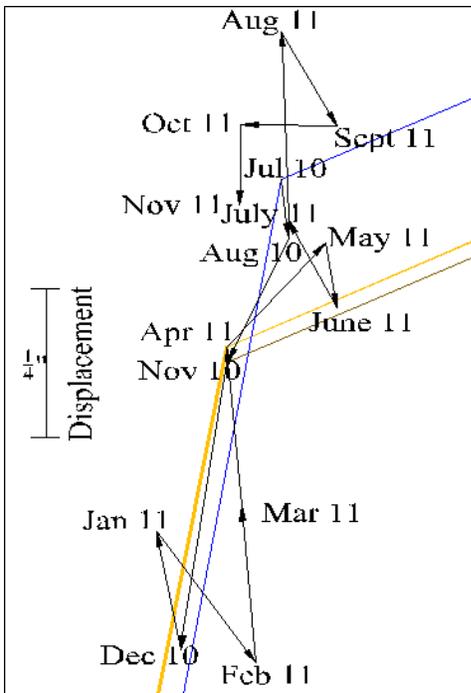
Figure 6.85. Bridge 2208 movement at north abutment west and east reflectors
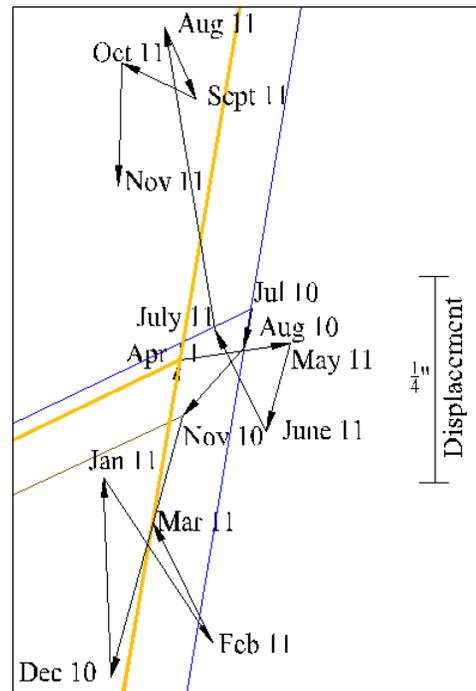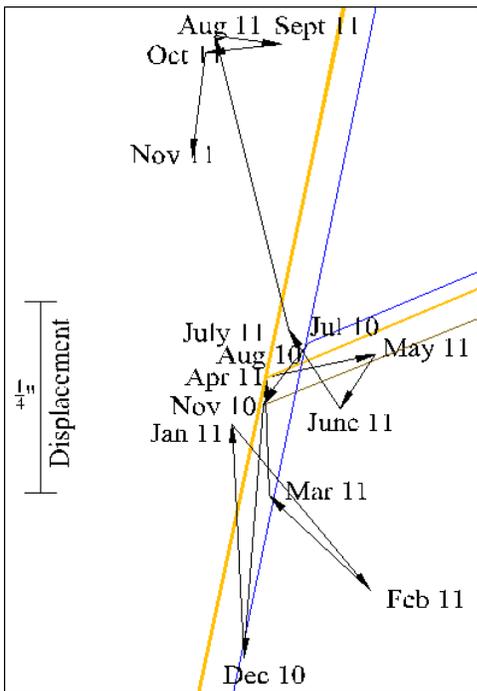
Figure 6.86. Bridge 2208 movement at north pier west and east reflectors

119
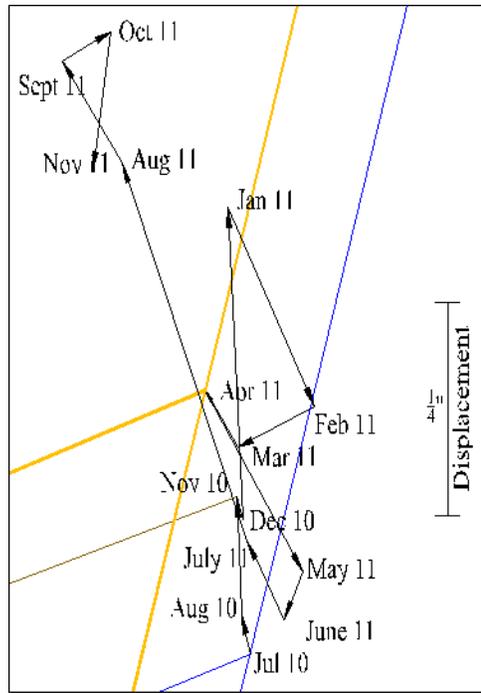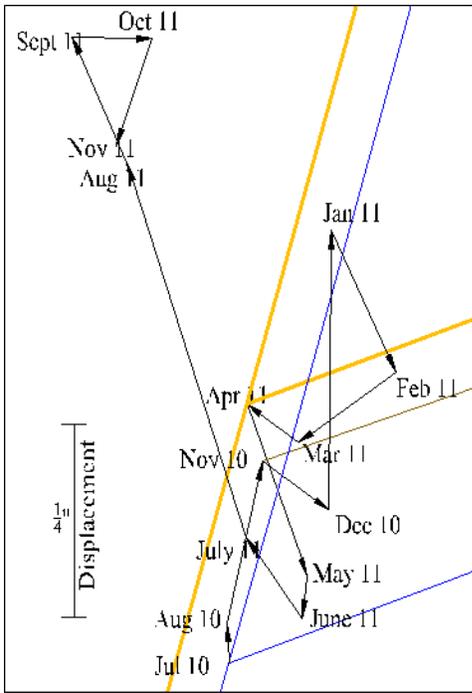
Figure 6.87. Bridge 2208 movement at south pier west and east reflectors
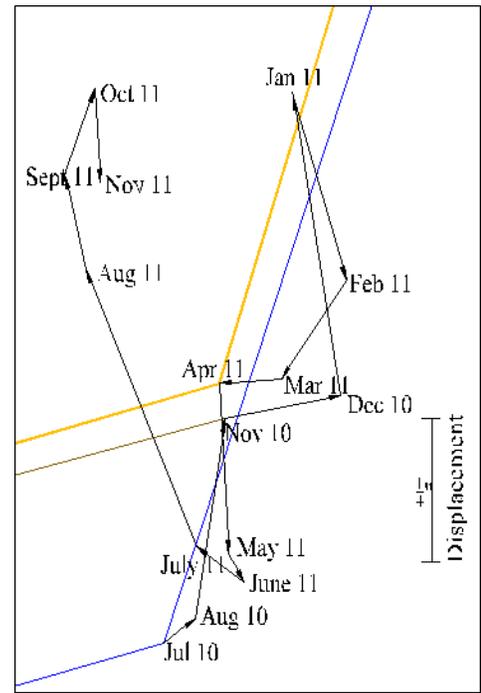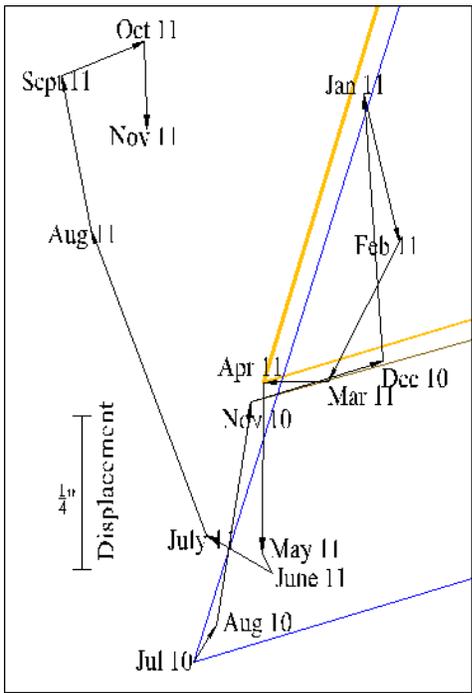
Figure 6.88. Bridge 2208 movement at south abutment west and east reflectors

120
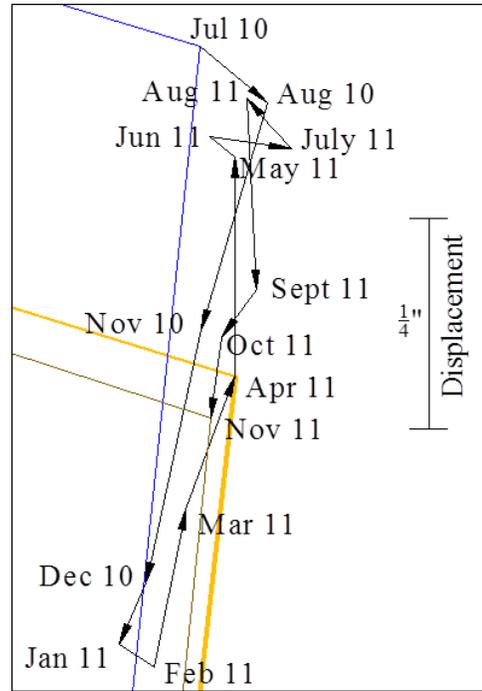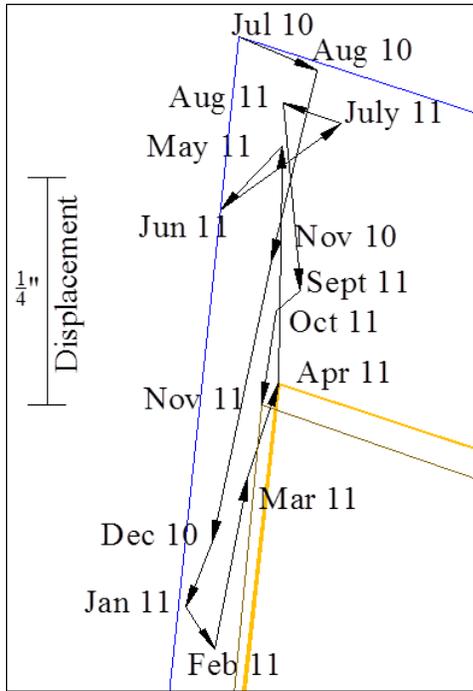
Figure 6.89. Bridge 2308 movement at north abutment west and east reflectors
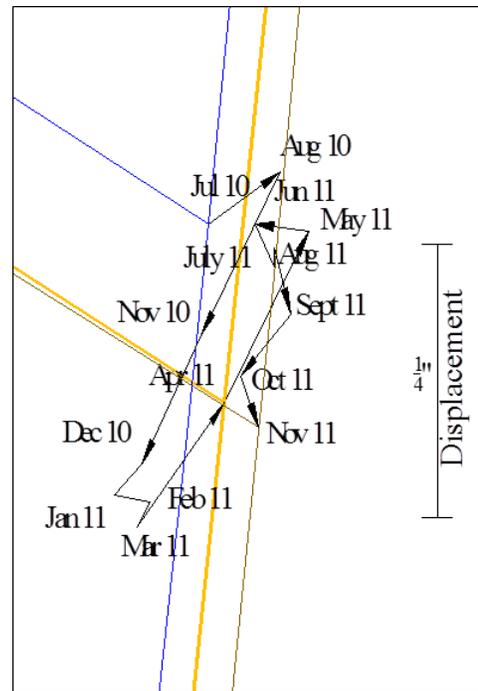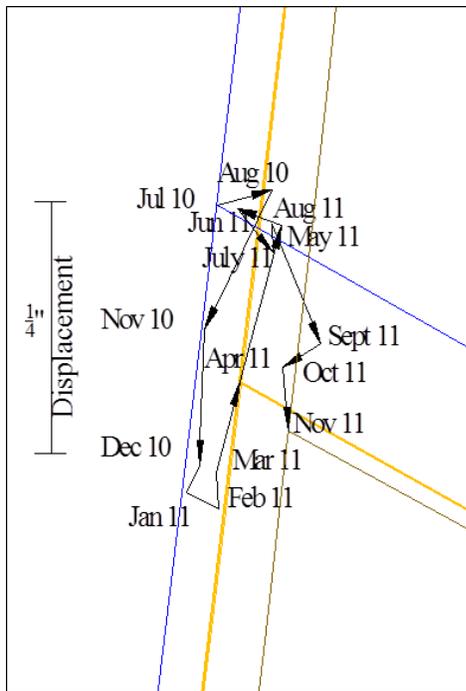
Figure 6.90. Bridge 2308 movement at north pier west and east reflectors

121
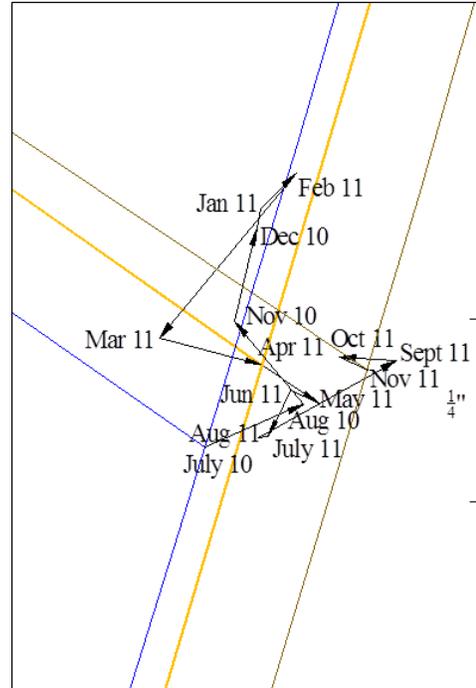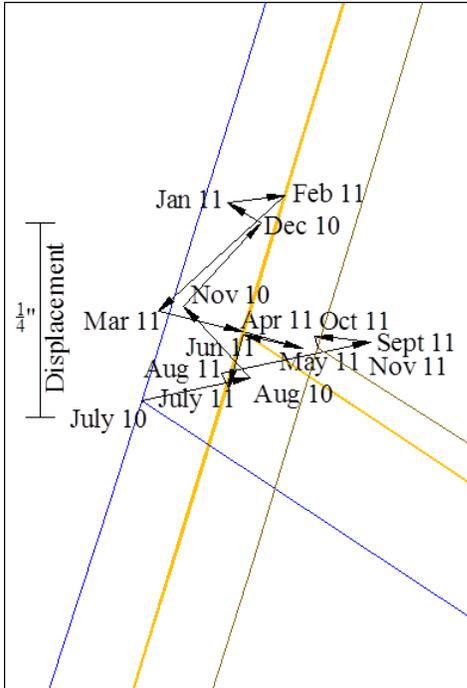
Figure 6.91. Bridge 2308 movement at south pier west and east reflectors
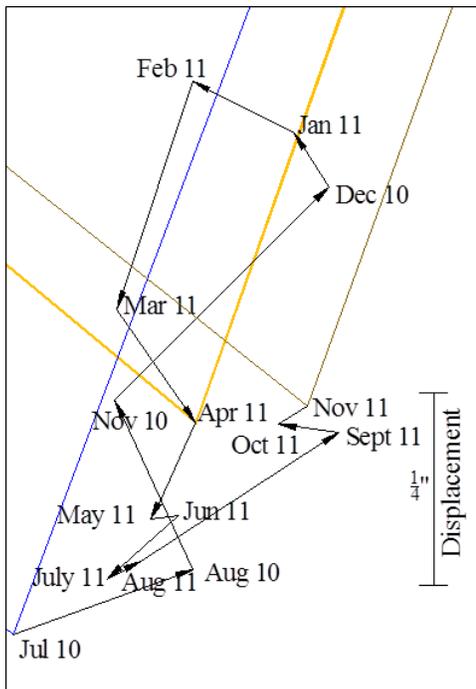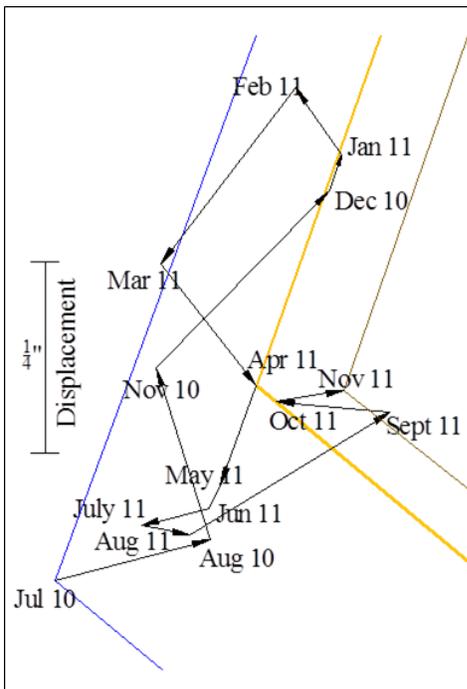
Figure 6.92. Bridge 2308 movement at south abutment west and east reflectors

122
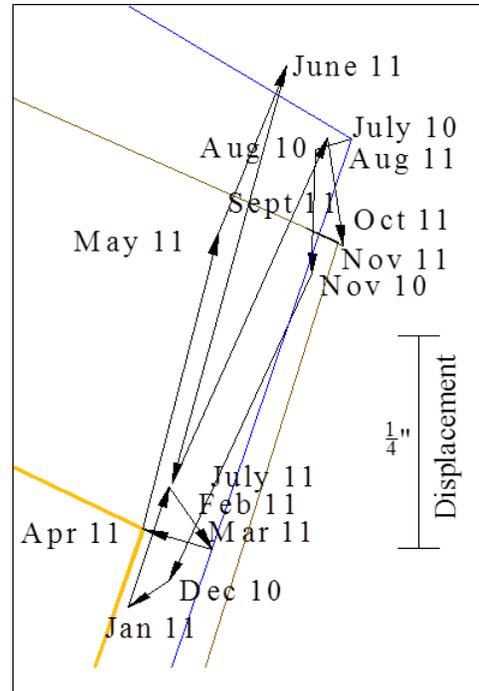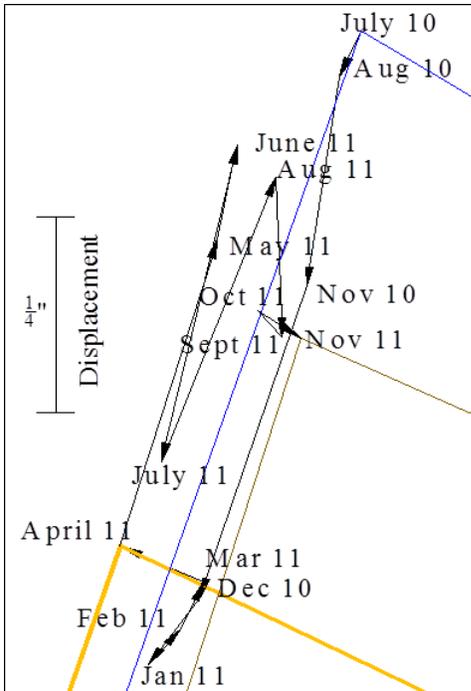
Figure 6.93. Bridge 2408 movement at north abutment west and east reflectors
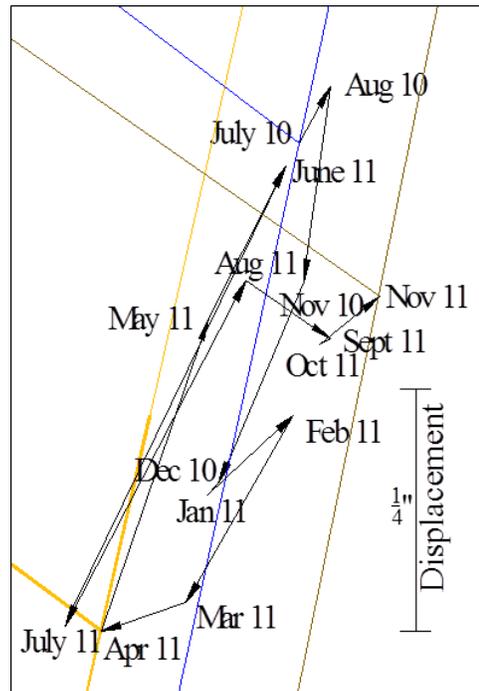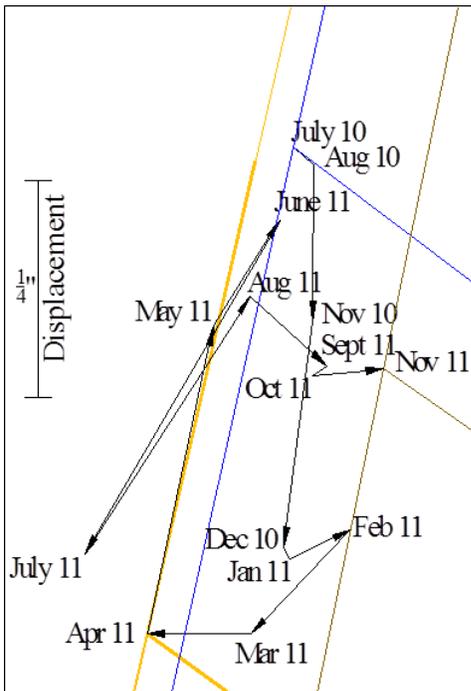
Figure 6.94. Bridge 2408 movement at north pier west and east reflectors

123
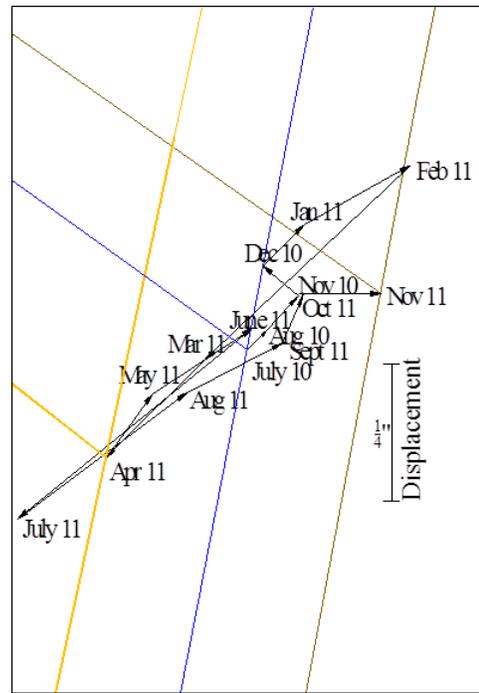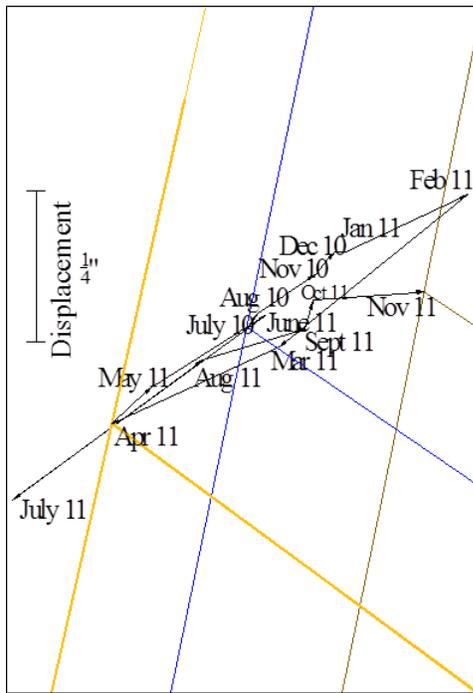
Figure 6.95. Bridge 2408 movement at south pier west and east reflectors
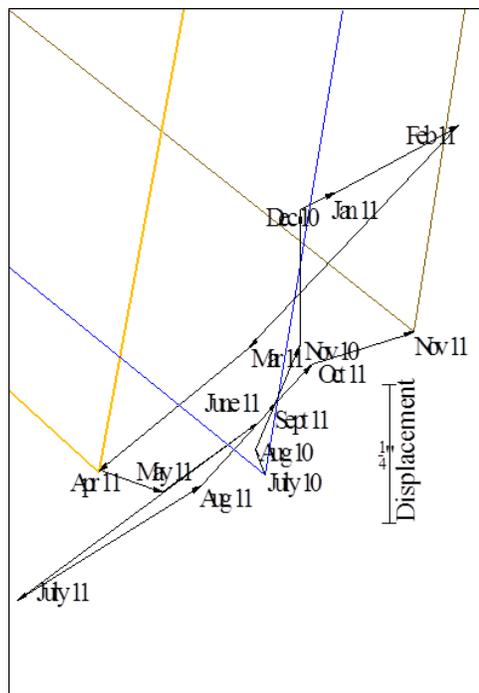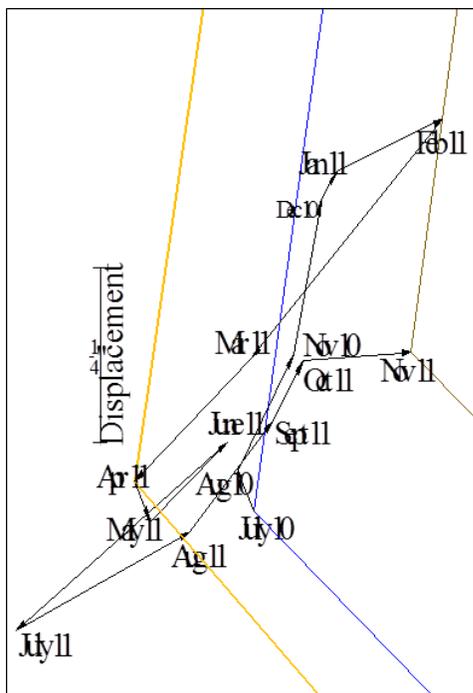
Figure 6.96. Bridge 2408 movement at south abutment east and west reflectors
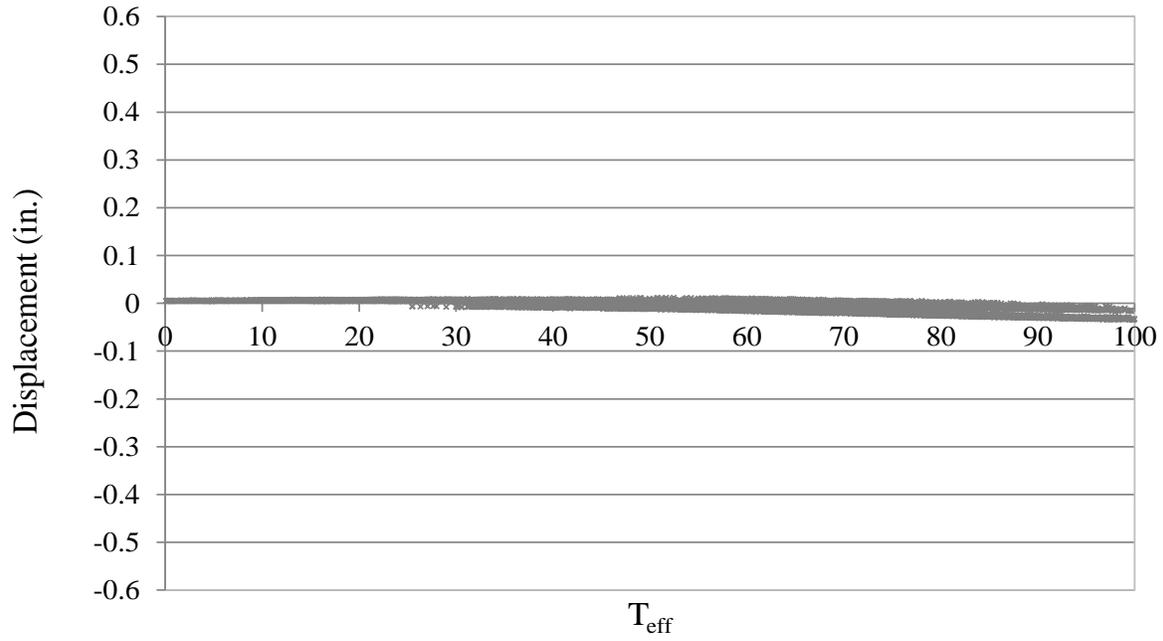
Figure 6.97. Bridge 109 relative displacement between fixed pier and Girder B
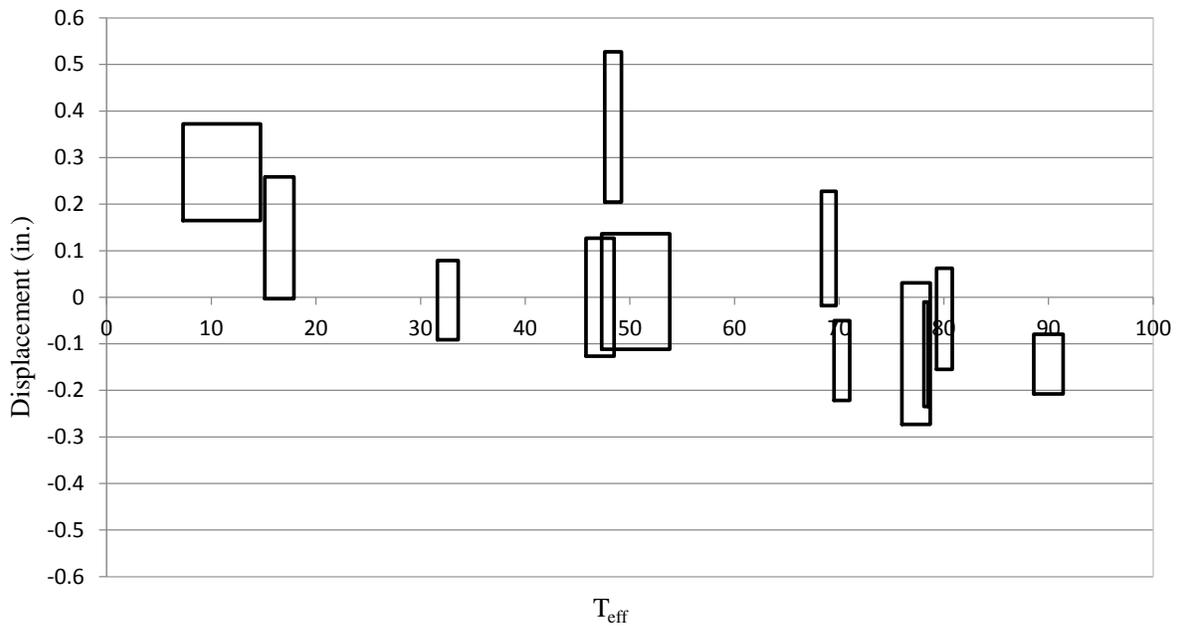
Figure 6.98. Absolute movement of bottom flange of Girder B at north pier reflector

125
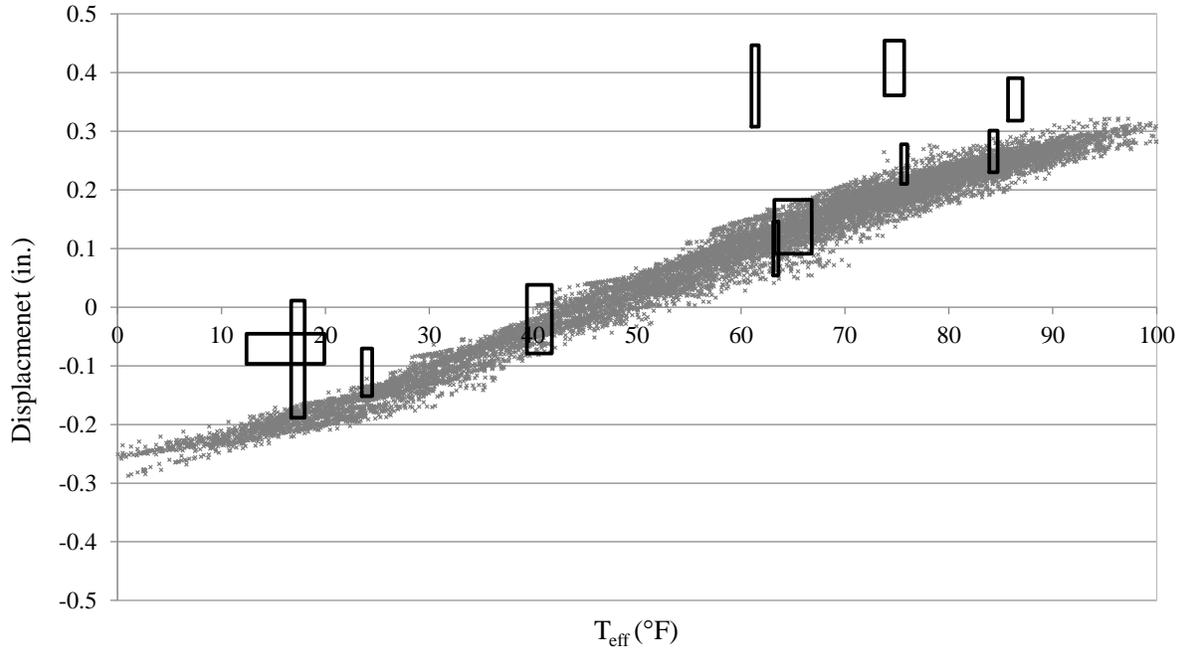
Figure 6.99. Expansion pier displacement

6.3.2 Steel Pile Behavior

Equivalent Cantilever Model

The equivalent cantilever analytical model shown in Figure 6.100 attempts to estimate the weak axis bending moment in an integral abutment steel pile (Abendroth 2005). In the model, the steel pile is idealized as an isolated column with an equivalent length, L, and rotationally fixed ends.

Equation 6.32 describes the relationship between the applied displacement, Δ, and the resulting end moment, M.

$$M = \frac{\Delta 6EI}{L_e^2} \tag{6.32}$$

Assuming a linear moment diagram for the pile because no intermediate forces exist, the end moment M can be calculated from M_g by Equation 6.33.

$$M = \frac{M_g L_e}{L_g} \tag{6.33}$$

The relationship between weak axis bending moment at the location of the strain gauges, M_g, and the weak axis bending strain at the location of the strain gauges, ε_g, is given by Equation 6.34.

126

$$\varepsilon_g = \frac{M_g c}{EI} \tag{6.34}$$

By combining Equations 6.32 through 6.34, the weak axis bending strain at the location of the strain gauges can be expressed by Equation 6.35.

$$\varepsilon_g = \frac{\Delta 6 L_g c}{L_e^3} \tag{6.35}$$
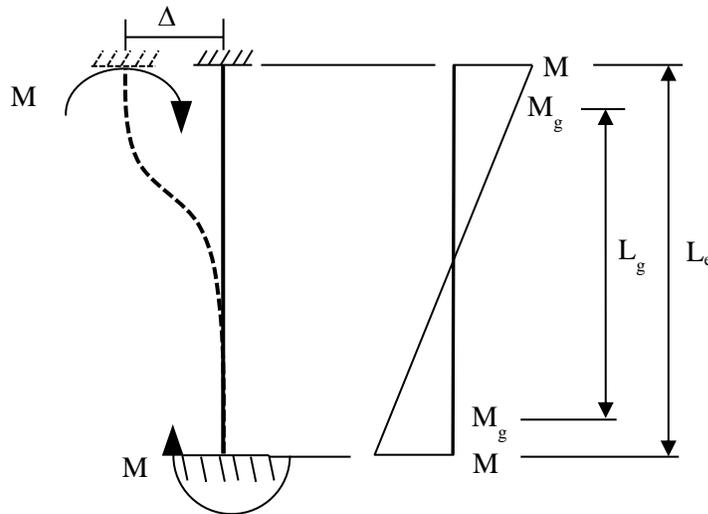
Figure 6.100. Equivalent cantilever pile model

where,
  Δ = applied lateral end displacement,
  M = resulting end moment,
  M_g = resulting moment at location of strain gauges
  L_e = equivalent cantilever length, and
  L_g = distance between equivalent M_g moments

Pile Expansion

Figures 6.101 through 6.106 show the weak axis bending strain versus displacement for the six instrumented piles of Bridge 309. The data in the figures come from the survey data and from the pile strain gauge data. Each rectangle in the figures represents a survey date. The horizontal sides of the rectangle represent the 95% confidence interval of pile displacement, at the top of the pile, for a given survey date. The vertical sides of the rectangle represent the change in the measured microstrain in the pile during the life of the respective survey, at the location of the strain gauge. The solid, diagonal lines represent the theoretical relationship between pile displacement and microstrain calculated using the analytical cantilever method. Based on the soil conditions shown

in the bridge plan set and following the work of Abendroth and Greimann, an equivalent cantilever length of 18 ft was calculated. From there, an approximate relationship between pile expansion and internal weak axis bending strain was plotted alongside the measured results.

In each of the figures there are a couple of survey months that show conflicting results with the rest of the data. One of the months has a very large confidence interval and two of the months show displacement without any resulting strain. These results have been unexplainable except for errors in the electronic and/or survey data.
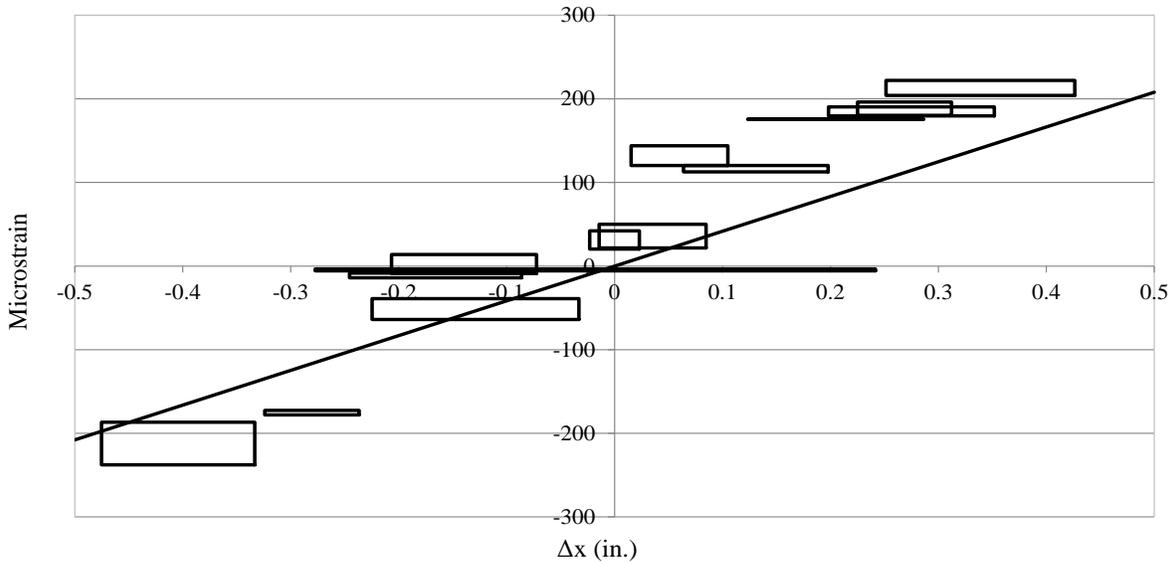
Figure 6.101. SAHP1 weak axis bending strain versus displacement
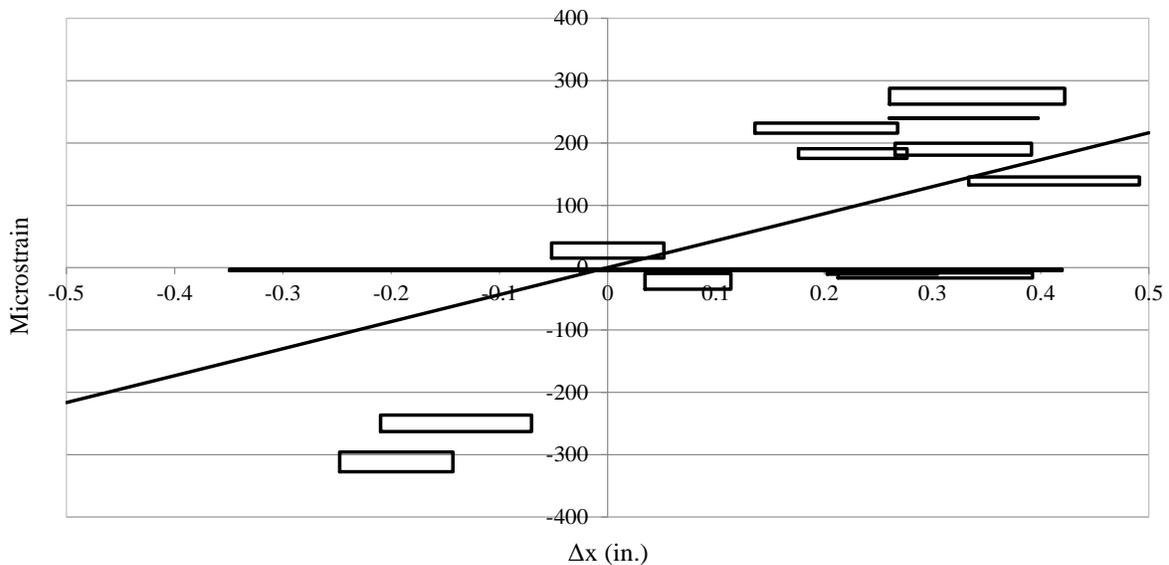
Figure 6.102. SAHP4 weak axis bending strain versus displacement
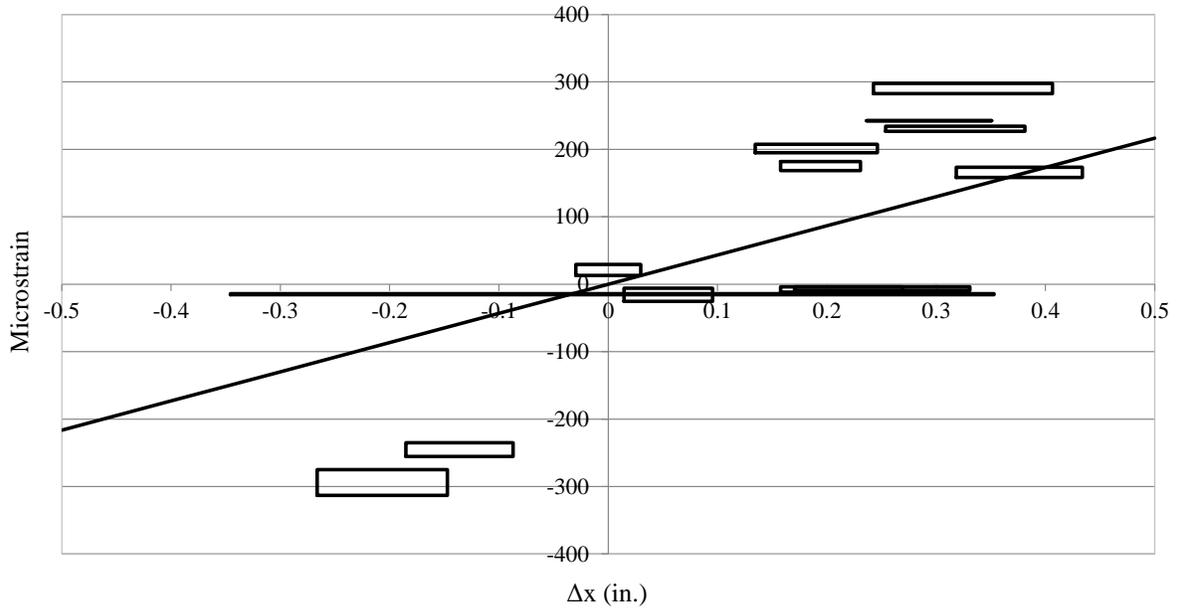
Figure 6.103. SAHP6 weak axis bending strain versus displacement
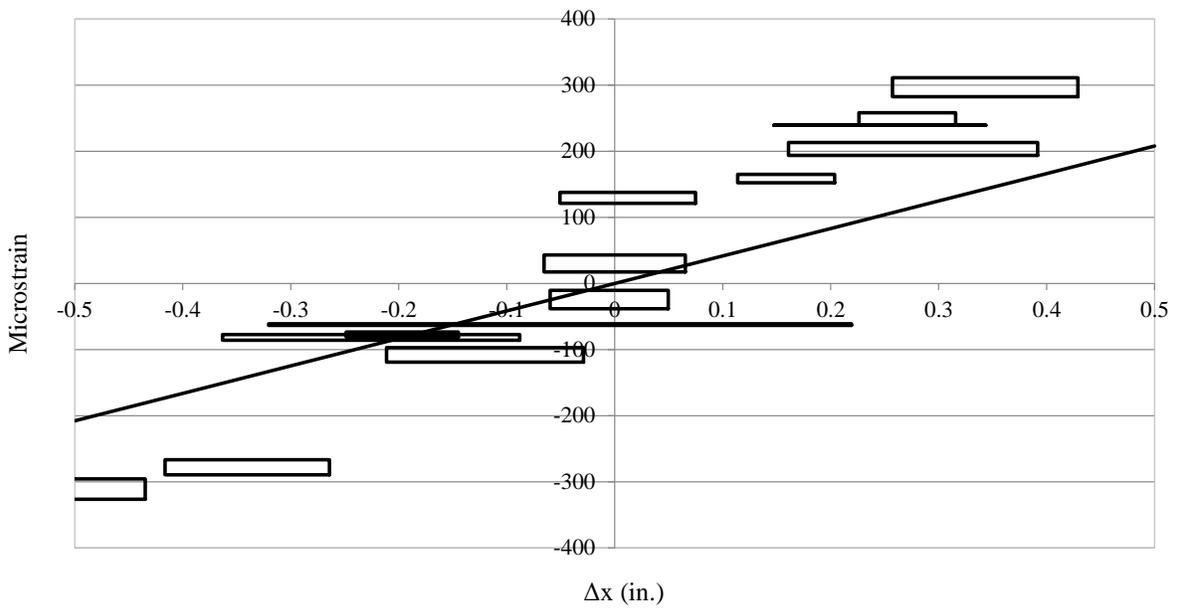
Figure 6.104. NAHP1 weak axis bending strain versus displacement
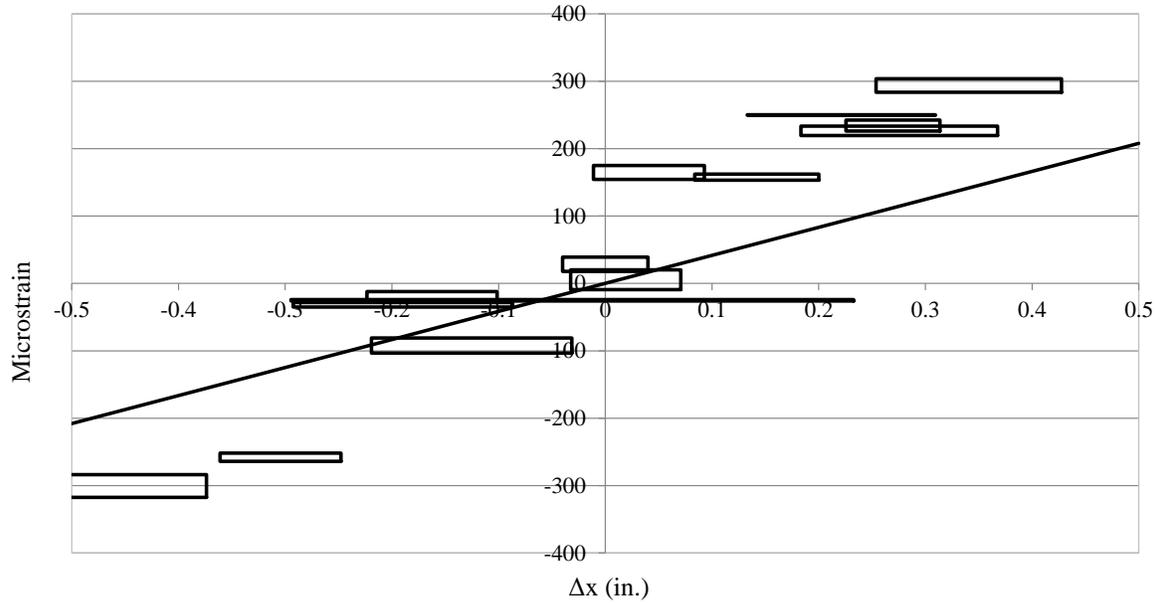
Figure 6.105. NAHP4 weak axis bending strain versus displacement
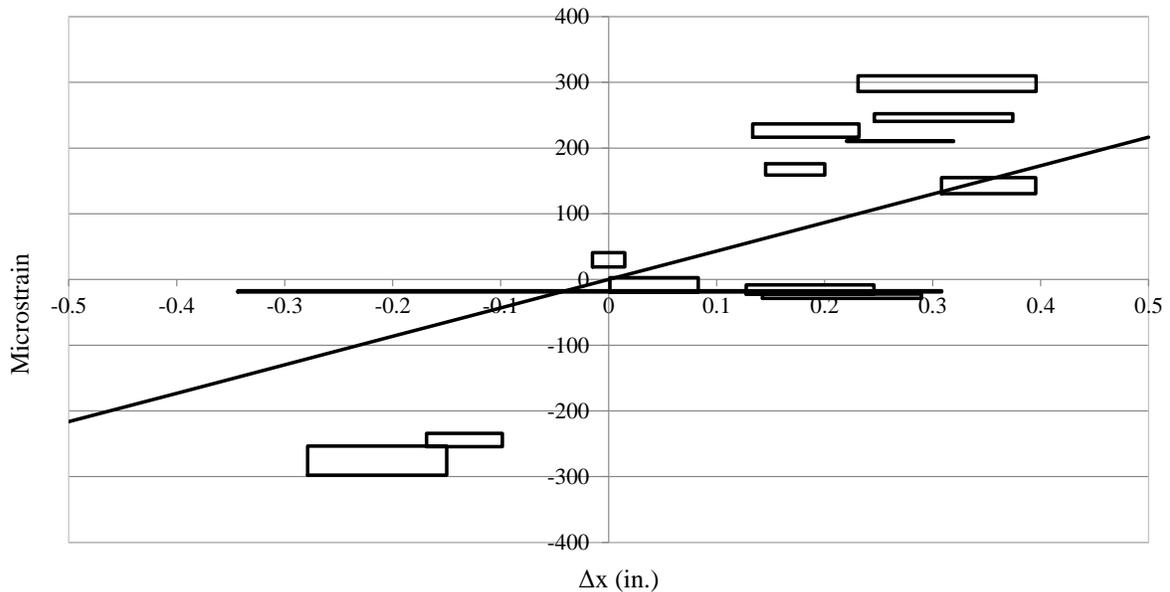
Figure 6.106. NAHP6 weak axis bending strain versus displacement

Based on the figures it appears that the analytical cantilever model was a better predictor of stress versus displacement for the HP1 piles, the piles closest to the outside curve. The equivalent length was too large to accurately reflect the measured results of the HP4 and HP6 piles, at both abutments. The equivalent length is directly related to the pre-bored depth of each pile as well as the soil conditions surrounding the piles. As a result, there are a number of explanations as to why the equivalent length was artificially large, none of which the research team could definitely narrow down.

CHAPTER 7 SHORT-TERM EXPERIMENTAL RESULTS

This chapter presents the measured strain and resolved superstructure forces from the static and dynamic live load field described in Chapter 5. The figures in this chapter display typical behavior of the five bridges and only represent a small amount of the total data evaluated during the course of the assessment. Section 7.1 briefly introduces the collected strain data that will be further interpreted in relation to superstructure forces, discussed in Section 7.2. Observations and conclusions throughout this chapter were based on values summarized in tables that were generated from analyses not always presented.

7.1 Strain Data

7.1.1 Girder Strains

The four girders in each bridge were one of the main focuses for assessing the superstructure behavior under live load. Initially, plots similar to Figure 7.1 through Figure 7.8 were produced for each of the five bridges for each of the three load paths, LP1, LP2, and LP3 (See Figure 5.39). The figures below plot the four strains measured in each girder for Bridge 309 (LP2). The top and bottom flange tips are designated by inner, for gauges located inside of the curve, and outer, for gauges located outside of the curve; recall Figure 5.37 for the strain gauge locations.
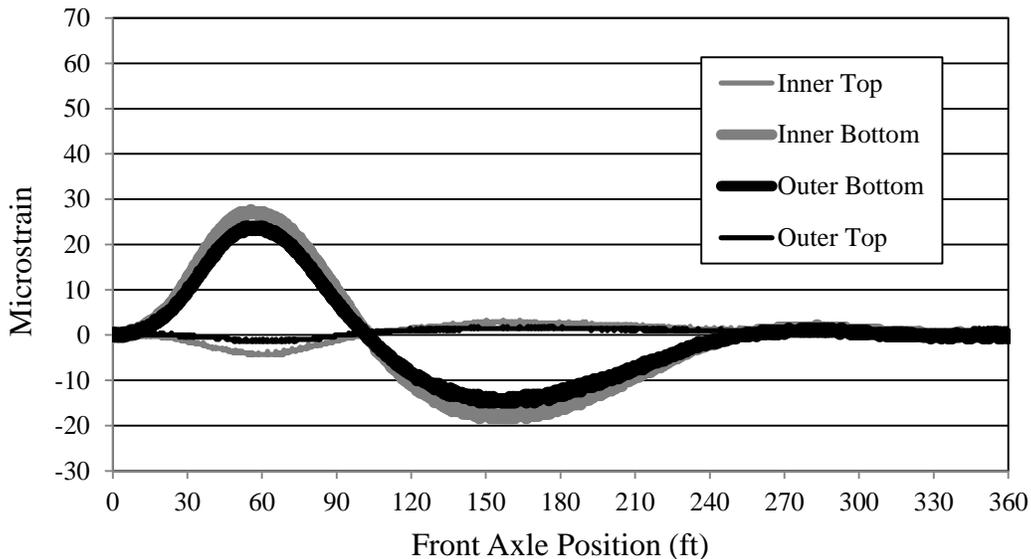
Figure 7.1. Bridge 309-S1 Girder A strain (LP2)
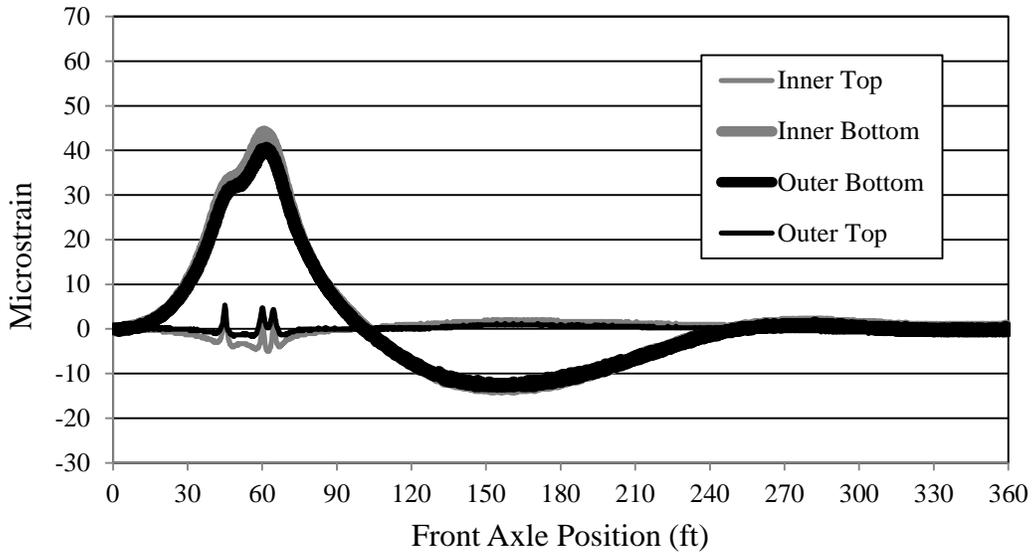
Figure 7.2. Bridge 309-S1 Girder B strain for (LP2)
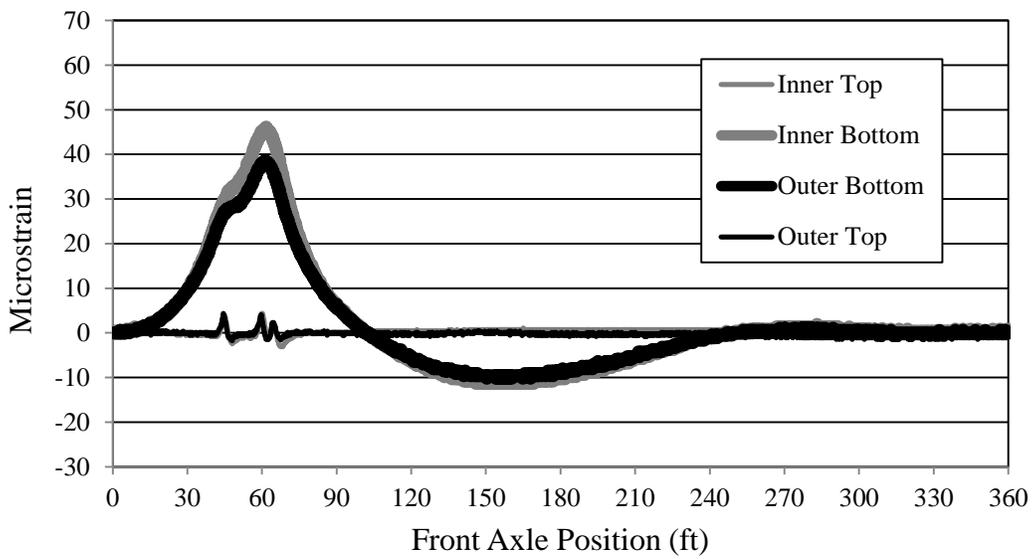
Figure 7.3. Bridge 309-S1 Girder C strain (LP2)

132
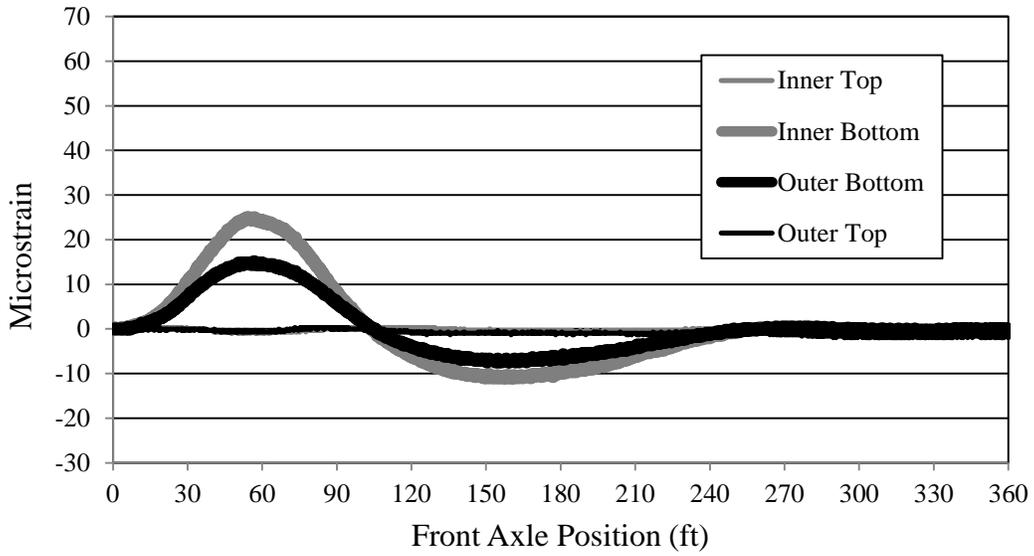
Figure 7.4. Bridge 309-S1 Girder D strain (LP2)
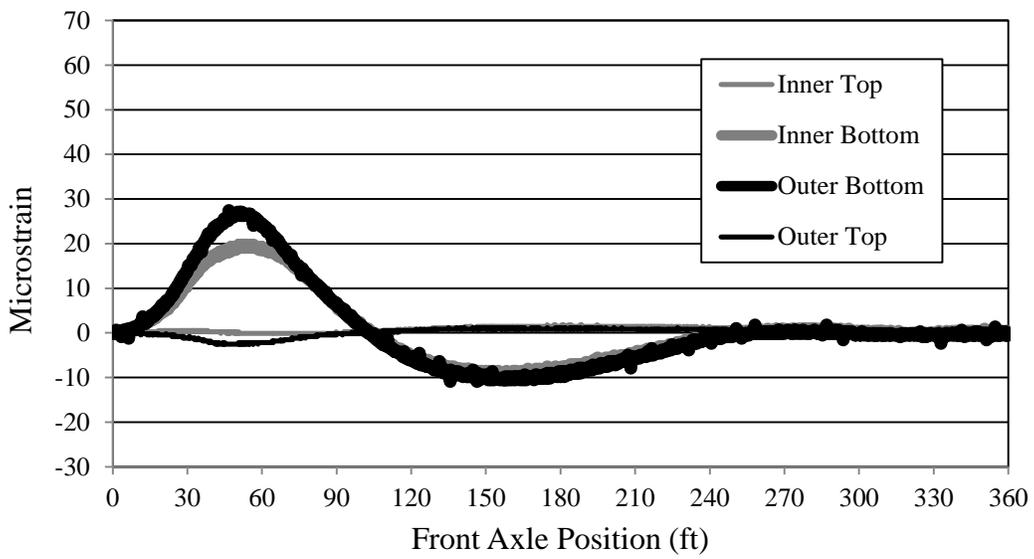
Figure 7.5. Bridge 309-S2 Girder A strain (LP2)

133
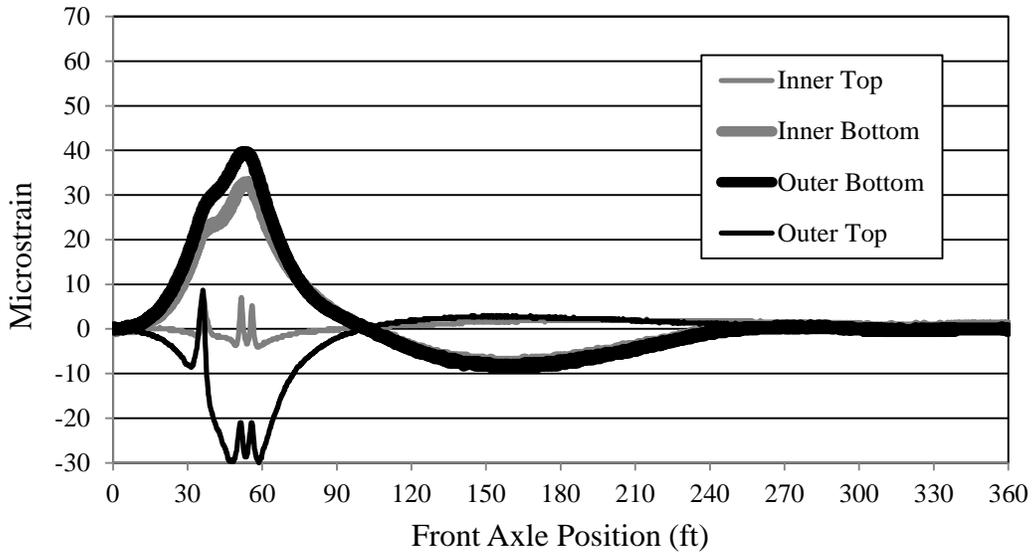
Figure 7.6. Bridge 309-S2 Girder B strain (LP2)
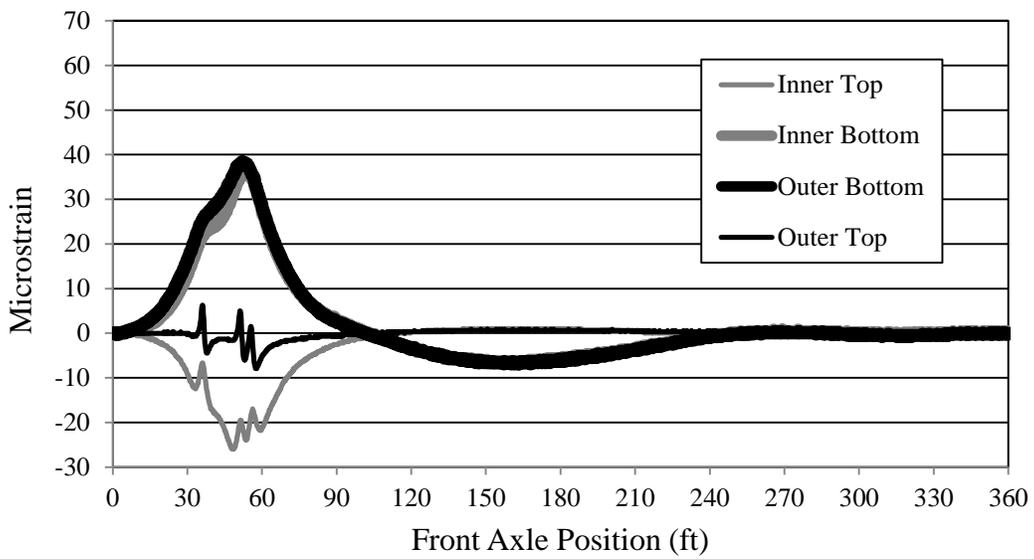
Figure 7.7. Bridge 309-S2 Girder C strain (LP2)

134
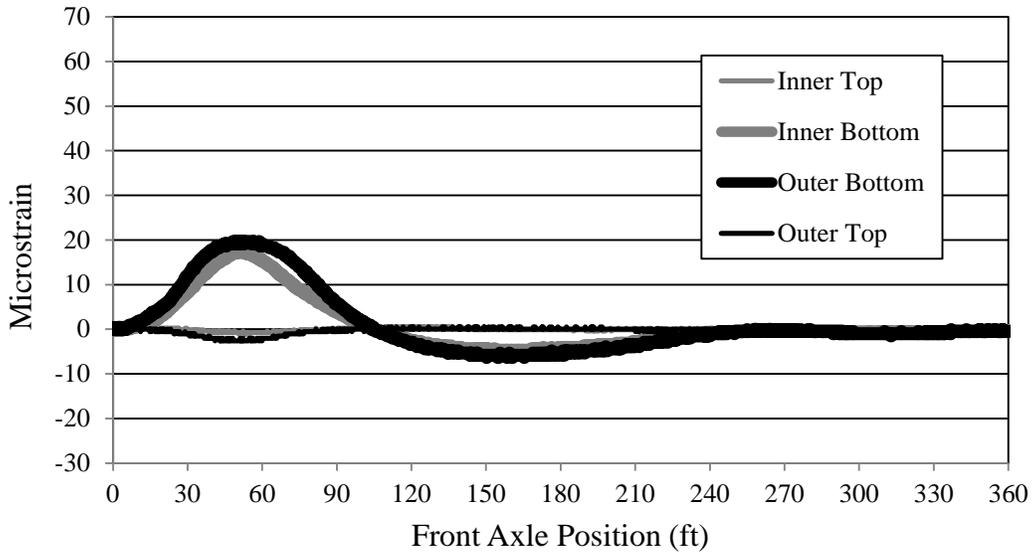
Figure 7.8. Bridge 309-S2 Girder D strain (LP2)

Strain values at the top and bottom of the girder webs were calculated by assuming linear strain variations through the flange width (equation 7.1).

$$\mu\varepsilon_{web} = (\mu\varepsilon_{inner} + \mu\varepsilon_{outer})/\ 2 \tag{7.1}$$

where,
$\mu\varepsilon_{inner}$ = flange strain measured at the gauge located on the inside of the curve
$\mu\varepsilon_{outer}$ = flange strain measured at the gauge located on the outside of the curve
$\mu\varepsilon_{web}$= flange strain measured at the web

Table 7.1 and Table 7.2 present the maximum strains found in each girder at each section due to one of the three load paths. Results are separated by girder section located at S1 and S2.

Table 7.1. Maximum strain ($\mu\varepsilon$) at bottom of web

	Girder	Bridge Section 1 (S1)				Bridge Section 2 (S2)			
		A	**B**	**C**	**D**	**A**	**B**	**C**	**D**
Bridge #	**309**	51	48	43	52	45	40	37	47
	2308	58	55	49	60	52	48	45	43
	2208	48	46	40	43	46	43	41	50
	209	53	52	45	52	52	49	41	41
	109	43	50	49	51	-	-	-	-

Table 7.2. Maximum strain (με) at top of web

Bridge #	Girder	Bridge Section 1 (S1)				Bridge Section 2 (S2)			
		A	B	C	D	A	B	C	D
	309	5	4	7	9	4	21	9	4
	2308	8	9	9	10	10	11	9	21
	2208	10	7	8	9	10	9	9	15
	209	7	8	6	9	26	9	6	22
	109	7	8	6	8	-	-	-	-

In examining the data, several observations were evident for the four curved bridges. First, maximum strains in the bottom flange typically occurred in the exterior girders, A and D, at S1. At S2, Bridges 309 and 2208, consisting of IABs, produced strains in Girder D that differed from Girder A by only 2 με and 4 με, respectively. Conversely, Bridges 209 and 2308, consisting of SIABs, produced slightly larger strains in Girder A than Girder D by 11 με and 9 με, respectively. Although these differences are quite small, they may indicate the distribution of live load at diaphragm sections may be influenced by the abutment type.

Strain magnitudes in the top flange were less in magnitude and often subject to the localized effect of the truck wheels crossing the instrumented section at maximum strain locations, represented by the spikes in strain measurements (Figure 7.6). The largest top flange strains were produced at S2. A maximum top flange strain was measured in Girder A (Bridge 209) equal to 26 με compared to the largest top flange strain at S1 equal to 10 με (Bridges 2308 and 2208).

Bottom Flange Strain Variations

The most notable trends relate to the variations in bottom and top flanges between the inner and outer strains. This typical behavior is not found in traditionally straight bridges, such as Bridge 109. Figure 7.9 and Figure 7.10 plot the bottom flange strains for the inner and outer flange tips for Girder A. The two figures represent the typically larger strain variation at S1 than at S2. Additionally, the largest strain variations typically occur in the exterior girders, A and D. These data also indicate that the strain variations reverse from S1 to S2. For example, in Figure 7.9 the inner strain is larger than the outer strain, while in Figure 7.10, the outer strain is larger than the inner strain. This illustrates the reversal in direction of lateral bottom flange bending found in horizontally curved bridges, which is influenced by the diaphragms. This is an important point as it relates to curved girder design.
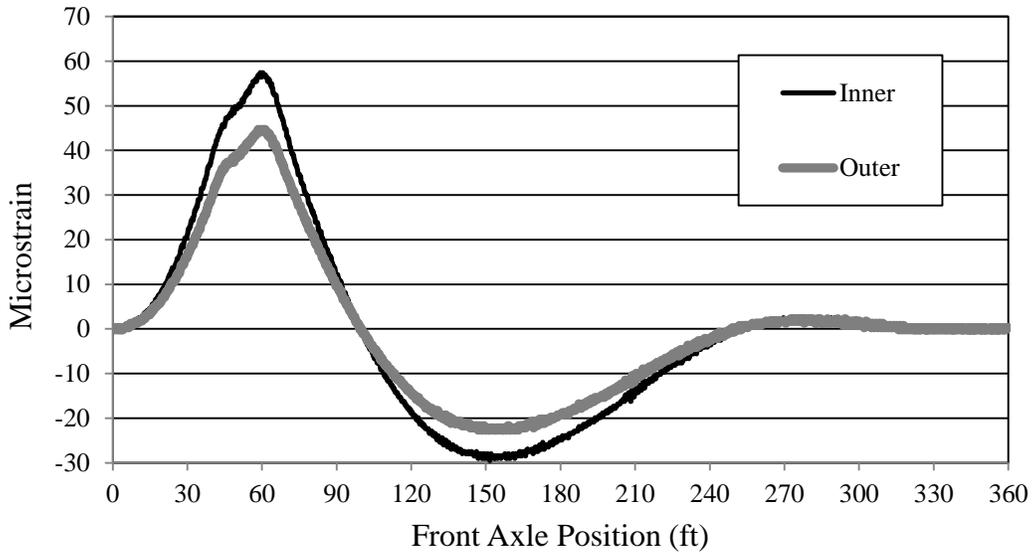
Figure 7.9. Bridge 309-S1 Girder A bottom flange strain (LP3)
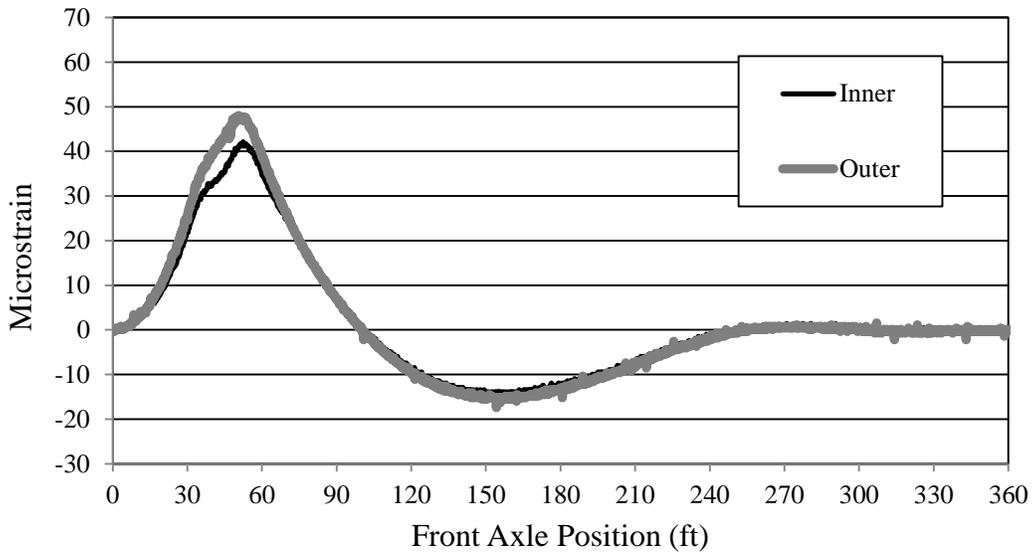
Figure 7.10. Bridge 309-S2 Girder A bottom flange strain (LP3)

Top Flange Strain Variations

Figure 7.11 and Figure 7.12 display the top flange strain variation in S1 and S2 in girder B, respectively. Conversely to the bottom flange, strains in the top flange typically varied most for the interior girders, B and C, at S2 for all three load paths. Figure 7.12 shows a maximum strain variation nearly equal to 30 $\mu\varepsilon$. This behavior may represent significant girder-diaphragm interactions transferring live loads to adjacent girders. This again emphasizes the proper consideration of curvature influences.

137
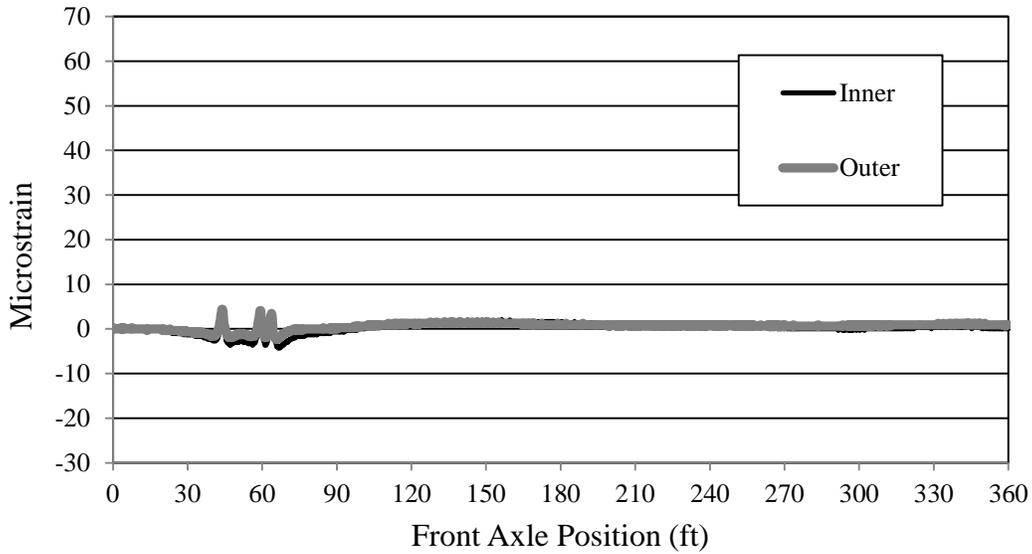
Figure 7.11. Bridge 309-S1 Girder B top flange strain (LP3)
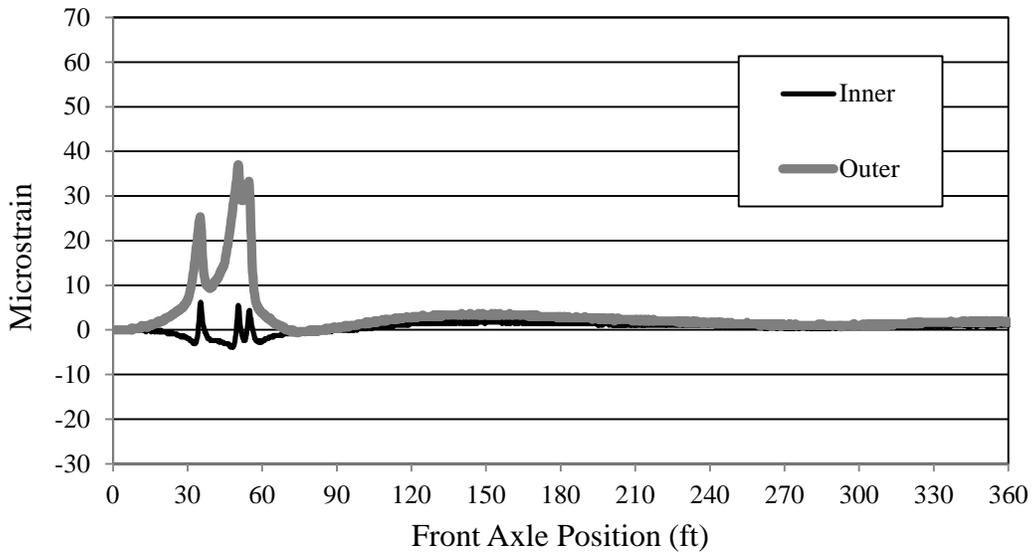
Figure 7.12. Girder B-S2 top flange strain (LP3)

7.1.2 Diaphragm Strains

Figure 7.13 through Figure 7.15 characterize typical strains recorded in the three diaphragms at S2 for LP2. As discussed in Chapter 5, strains were measured in the top and bottom flanges at mid points for the inner and center diaphragms. For the outer diaphragm, strains were measured in the top and bottom flanges at the one-third points. The letter A or B on the outer diaphragm designates that the one-third point was nearest to either Girder A or Girder B.

138
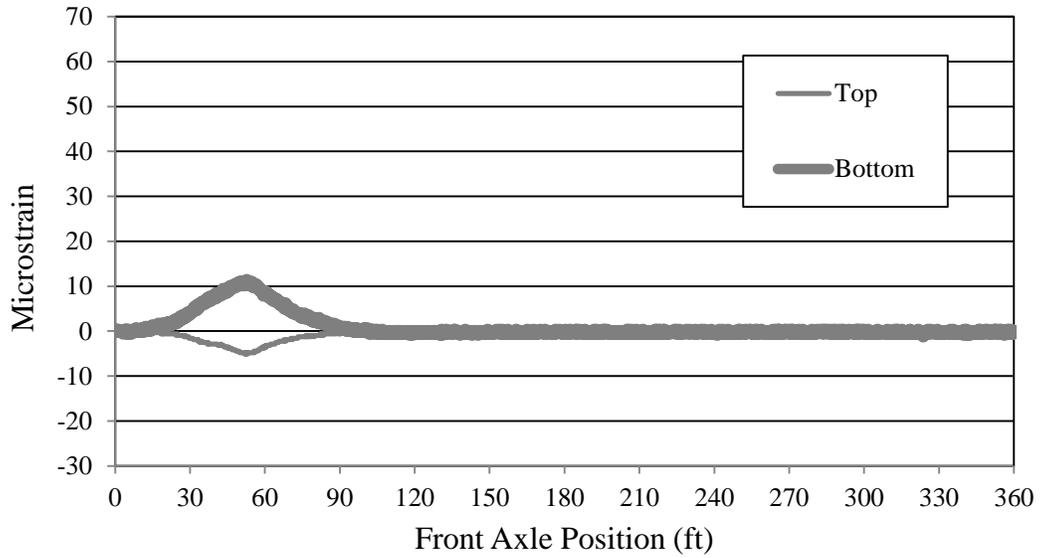
Figure 7.13. Bridge 309 inner diaphragm strain (LP2)
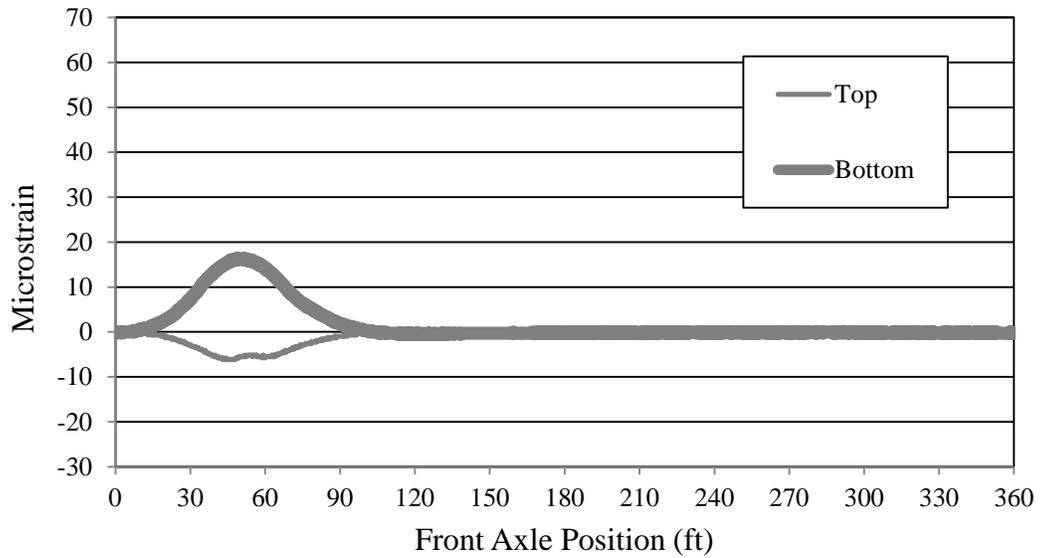
Figure 7.14. Bridge 309 center diaphragm strain (LP2)
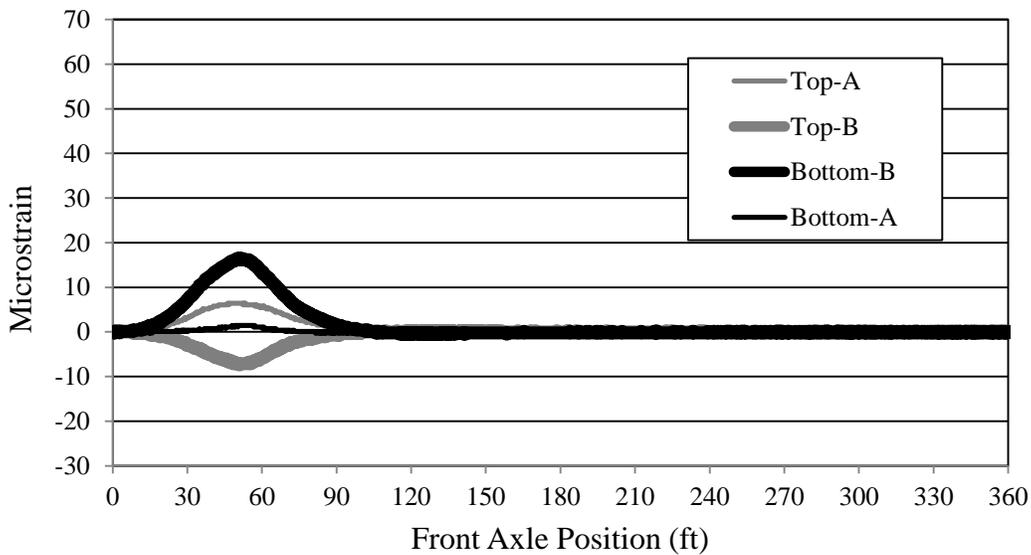
Figure 7.15. Bridge 309 outer diaphragm strain (LP2)

Note that regardless of the diaphragm or the cross-section, the maximum tensile strain exceeds the maximum compression strain. This indicates that in addition to being subjected to bending, the diaphragms must also resist a tensile force. These results indicate that the outermost girder is tending to expand radially more than the innermost girder. This is an important point as it relates to inner and outer girder design approaches.

Table 7.3 tabulates maximum diaphragm strains recorded for each of the four curved bridges. The maximum strain was 26 $\mu\varepsilon$ in the bottom of the center diaphragm (Bridge 209). The outer diaphragm experienced larger strains in the top and bottom flanges at the section nearest Girder B compared to the section nearest Girder A.

Table 7.3. Maximum diaphragm strains ($\mu\varepsilon$)

		Inner		Center		Outer-B		Outer-A	
	Diaphragm	**Top**	**Bot.**	**Top**	**Bot.**	**Top**	**Bot.**	**Top**	**Bot.**
Bridge #	**309**	-5	11	-6	16	-8	17	6	7
	2308	-5	7	-7	15	-6	21	6	3
	2208	-4	7	-7	12	-9	10	2	5
	209	-5	12	-6	26	-13	12	2	4

7.1.3 Dynamic Load Data

Recall from Chapter 5 that load testing also entailed at least two high speed test trials per bridge with truck speeds ranging from 35-45 mph using LP2. These speeds are typical of truck traffic on the bridges as they are located within an interchange. The truck driver monitored and reported his approximate entrance and exit speeds on the bridge.

140

Figure 7.16 represents typical dynamic strain measured at a bottom flange gauge location, where the position of the truck was estimated.
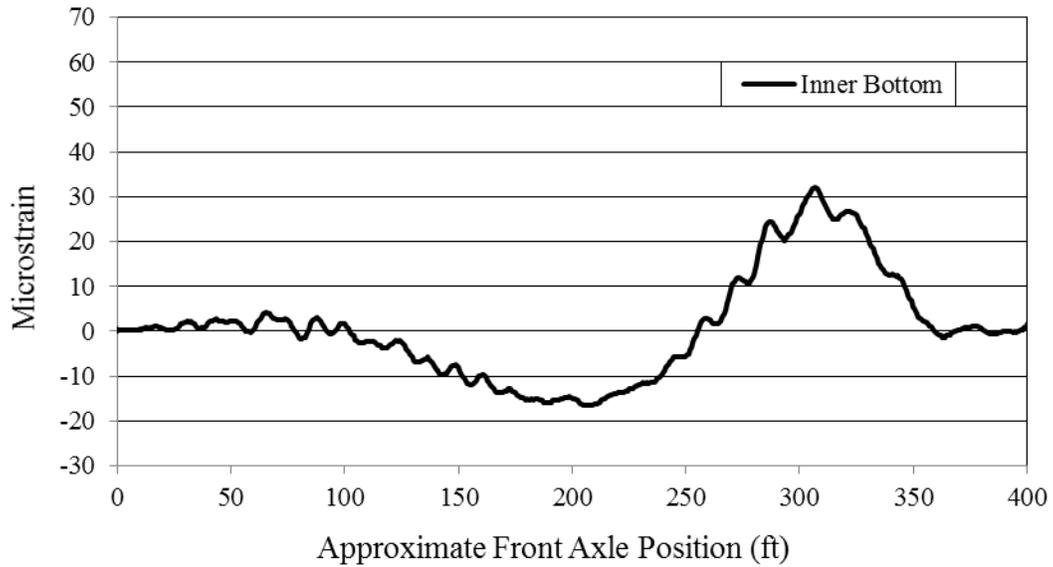
Figure 7.16. Bridge 209-S1 dynamic loading strain in Girder A

Figure 7.17 plots the strain measured during the static load testing, which corresponds to the same load path and location of measured strain as Figure 7.16. Figure 7.16 is superimposed onto Figure 7.17 to produce Figure 7.18. The difference between the magnitudes of the two lines in Figure 7.18 represents the dynamic load contribution to the overall response.
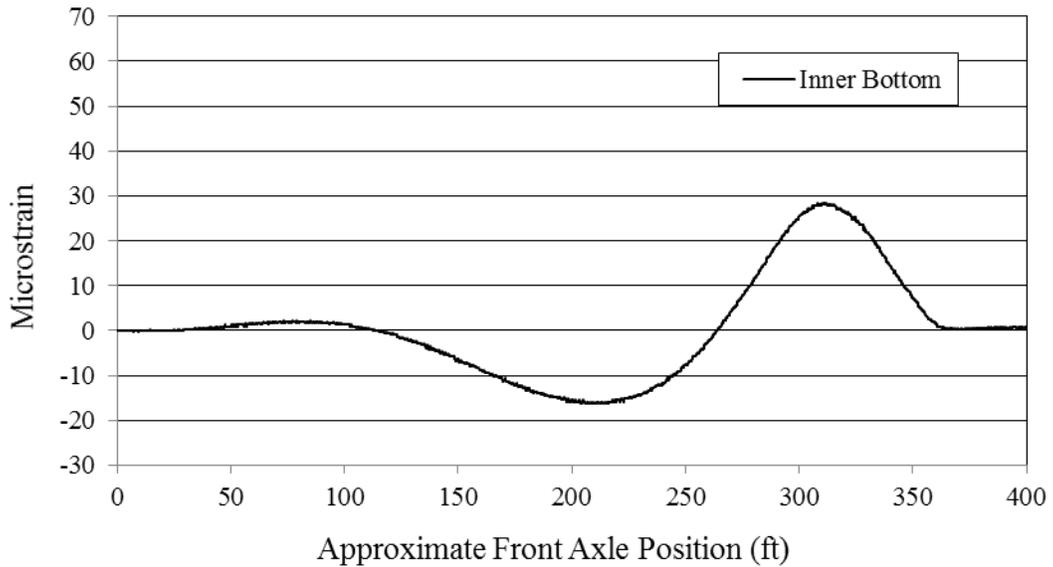
Figure 7.17. Bridge 209-S1 static loading strain in Girder A
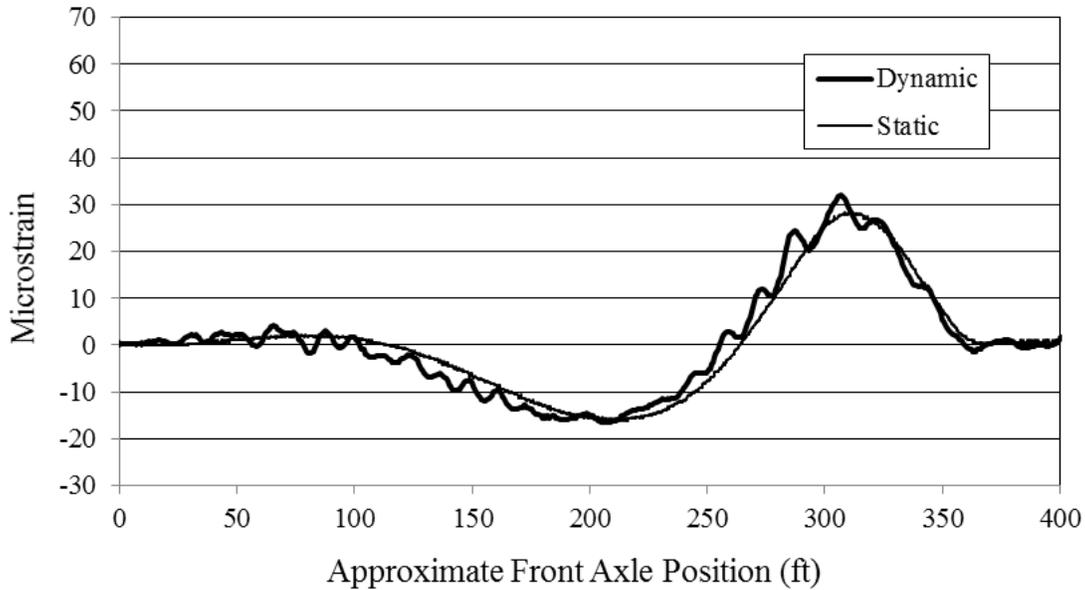
Figure 7.18. Superimposed static and dynamic load strains

Dynamic Amplification Factors

Dynamic amplification from live loading was assessed by comparing the differences in maximum strains from the static and dynamic load testing using LP2. Equation 7.2 was used to calculate the dynamic amplification factors with measured strains. Note that negative values were assumed equal to zero.

$$\text{DAF}(\%) = [(\mu\varepsilon_d - \mu\varepsilon_d)/\mu\varepsilon_s]*100 \tag{7.2}$$

where,
$\mu\varepsilon_s$ = maximum static strain
$\mu\varepsilon_d$ = maximum dynamic strain

Table 7.4 tabulates the maximum DAF in the bottom flanges of each bridge. The bottom flanges were of primary focus since the strains were the largest at this location in the girder.

Table 7.4. Maximum DAF (%) in bottom flange strain

	Girder	Bridge Section 1 (S1)				Bridge Section 2 (S2)			
		A	B	C	D	A	B	C	D
Bridge #	**309**	7	0	0	0	5	5	0	0
	2308	6	3	0	0	3	0	0	0
	2208	4	0	0	0	4	0	0	0
	209	13	0	0	8	7	11	7	1
	109	49	20	0	0	-	-	-	-

The most significant dynamic amplification factors were found in Girder A for all bridges at S1. A maximum of 13% was found in Bridge 209 for the four curved bridges, which was graphically shown in Figure 7.18. One of the high speed runs on Bridge 109 give a maximum DAF of 49% respectively. It should be noted that the transverse positioning of the truck during the dynamic testing was not as accurate as the static testing. This fact could contribute to some experimental error in the determination of the experimental DAF.

Table 3.6.2.1-1 in the *AASHTO LRFD* specifications provides a dynamic load allowance factor of 15% in girders for fatigue and fracture limit states and 33% in girders for limits states other than fatigue and fracture. The calculated DAFs for the curved bridges in Table 7.4 prove to be less than values that the *AASHTO LRFD* specifications used in design.

7.2 Superstructure Forces

This section utilizes the strain data, briefly shown in Section 7.1, to calculate forces in the girders and diaphragms. Further investigation of lateral flange bending, strong axis bending, axial load, live load distribution, and diaphragm behavior will be presented. Observations regarding superstructure results with respect to bridge type and geometry will be made appropriately.

7.2.1 Resolving Member Forces

The composite section girder forces for the live load study are determined using the same procedure outlined in Section 6.2.1 of this report. Refer to Figure 6.4 for the resolved girder forces and the matrix described in Figure 6.5 for the four equations and four unknowns associated with the cross-section. Equations 6.16 through 6.19 represent the relationships between internal strain components and internal forces calculated within the girder that will be used in the assessment of the live load girder response.

Similarly, Figure 7.19 depicts the forces considered in the analysis of the diaphragms for the horizontally curved bridges. P represents the internal axial force (tension is positive). M_x represents the internal strong axis bending moment in the diaphragm (positive when the top flange is in compression).
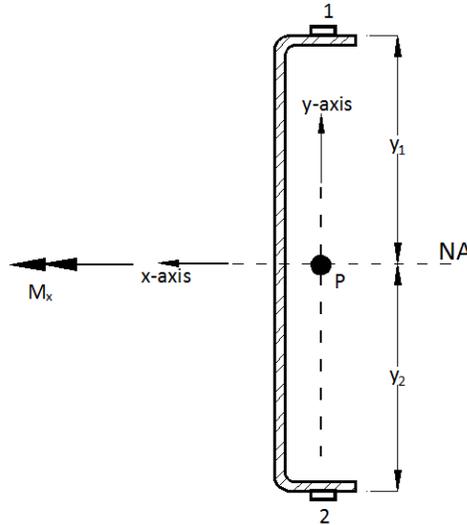
Figure 7.19. Diaphragm cross-section

Figure 7.20 shows the matrix used to calculated P and M_x from known diaphragm dimensions and measured field strains.

$$\begin{Bmatrix} \varepsilon_1 \\ \varepsilon_2 \end{Bmatrix} = \begin{bmatrix} 1 & y_1 \\ 1 & y_2 \end{bmatrix} \begin{Bmatrix} \dfrac{P}{(AE)} \\ \dfrac{M_x}{(EI_x)} \end{Bmatrix}$$

Figure 7.20. Two equations and two unknowns

where,

ε_i = strain reading at gauge i,

y_i = distance from neutral axis to strain gauge i along the y-axis

P = the internal axial force in the diaphragm.

M_x = strong axis bending moment in the diaphragm.

A = cross-sectional area of the diaphragm (24 in.^{2})

I_x = strong axis moment of inertia about the NA (3,834 in.^{4})

E = Young's modulus of elasticity for steel (29,000 ksi)

7.2.2 Girder Forces

Strong Axis Bending Moment

Figure 7.21 through Figure 7.23 displays typical strong axis moments calculated for each of the four girders in all bridges. The figures plot the strong axis moments in Bridge 309 versus truck position for load paths LP1 through LP3, respectively. In general, LP1 typically produced the

144

largest M_x in Girder D. LP2 typically produced the largest M_x in Girders B and C. And LP3 typically produced the largest M_x in Girder A.
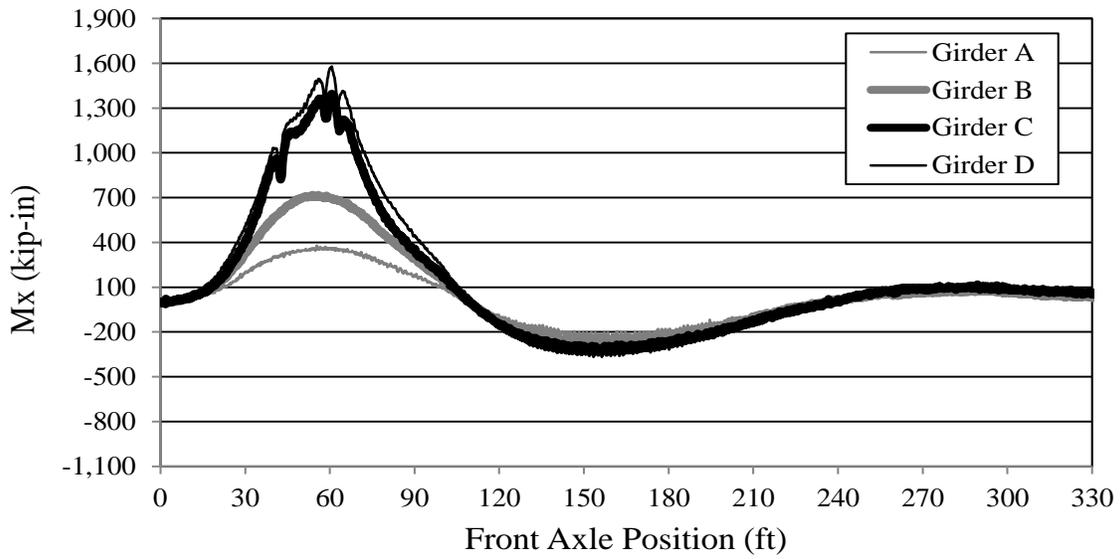
Figure 7.21. Bridge 309-S1 strong axis moments in girders (LP1)
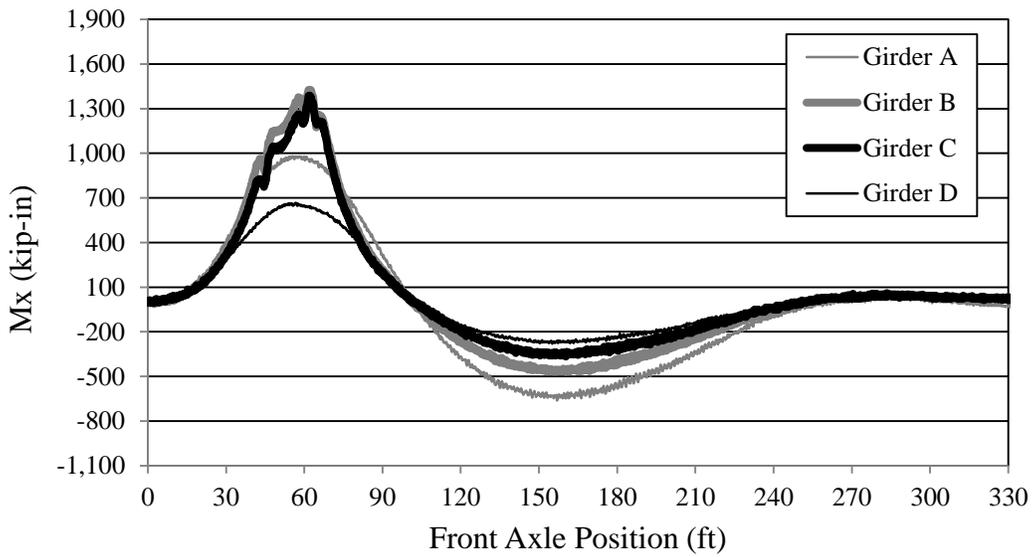
Figure 7.22. Bridge 309-S1 strong axis moments in girders (LP2)
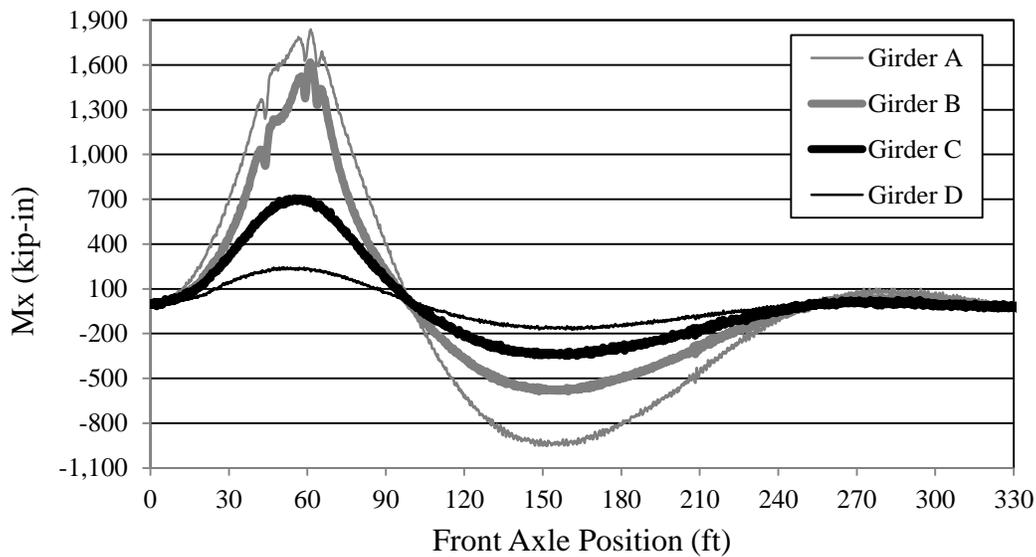
Figure 7.23. Bridge 309-S1 strong axis moments in girders (LP3)

Table 7.5 tabulates the maximum strong axis bending moments and the associated load path in each girder for the five bridges.

Table 7.5. Maximum M_x in girder (kip-in.)

	Girder	Bridge Section 1 (S1)				Bridge Section 2 (S2)			
		A	**B**	**C**	**D**	**A**	**B**	**C**	**D**
Bridge #	**309**	1840[LP3]	1620[LP3]	1400[LP1]	1580[LP1]	1510[LP3]	1680[LP2]	1670[LP2]	1530[LP1]
	2308	1870[LP3]	1530[LP3]	1350[LP2]	1570[LP1]	1510[LP3]	1350[LP2]	1240[LP2]	1130[LP1]
	2208	1340[LP3]	1340[LP3]	1210[LP2]	1210[LP1]	1300[LP3]	1320[LP2]	1340[LP2]	1180[LP1]
	209	1580[LP3]	1600[LP3]	1370[LP2]	1480[LP1]	1090[LP3]	1450[LP3]	1280[LP2]	820[LP1]
	109	1310[LP3]	1560[LP3]	1600[LP2]	1530[LP1]	-	-	-	-

Results show the largest strong axis moments occurred at S1 in Girder A for the two bridges with the most severe curvature, Bridges 309 and 2308. Also at S1, Girder C produced the least moment of all four girders for all curved bridges. For Bridges 209 and 2208, with less curvature, more uniform moments were produced throughout the four girders at S1.

Additionally, the moment in Girder A was less at S2 compared to S1 for all curved bridges. The straight bridge, Bridge 109, produced the largest moments in the interior two girders and the smallest moments in the exterior two girders.

These results indicate noticeable load distribution differences to the girders for various bridge geometries. The most significant factors influencing the distribution results may relate to bridge radius and diaphragm location. The effects of these will further be addressed under the live load distribution section.

Lateral Flange Bending Moment

Figure 7.24 and Figure 7.25 display the typical lateral bottom flange bending moments in Bridge 309. Note that the reversal in direction for the lateral bottom flange bending is illustrated by comparing Figure 7.24 to Figure 7.25. Recall from the resolved girder forces diagram (Figure 6.4) that positive lateral flange bending values occur when strain in the flange located on the outside of the curve is larger than the strain in the flange located towards the inside of the curve. The apparent direction of lateral bottom flange bending is related to the diaphragm location along the girder length, further discussed within the V-Load exploration section. A detailed summary of the maximum lateral bottom flange bending moments and associated load path for the tested bridges is presented in Table 7.6.
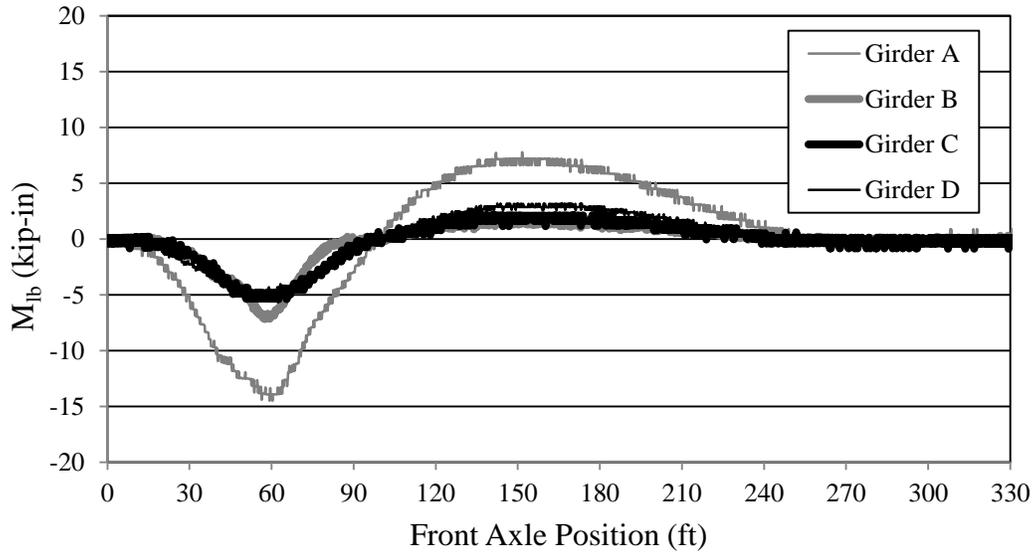
Figure 7.24. Bridge 309-S1 lateral bottom flange moments (LP3)
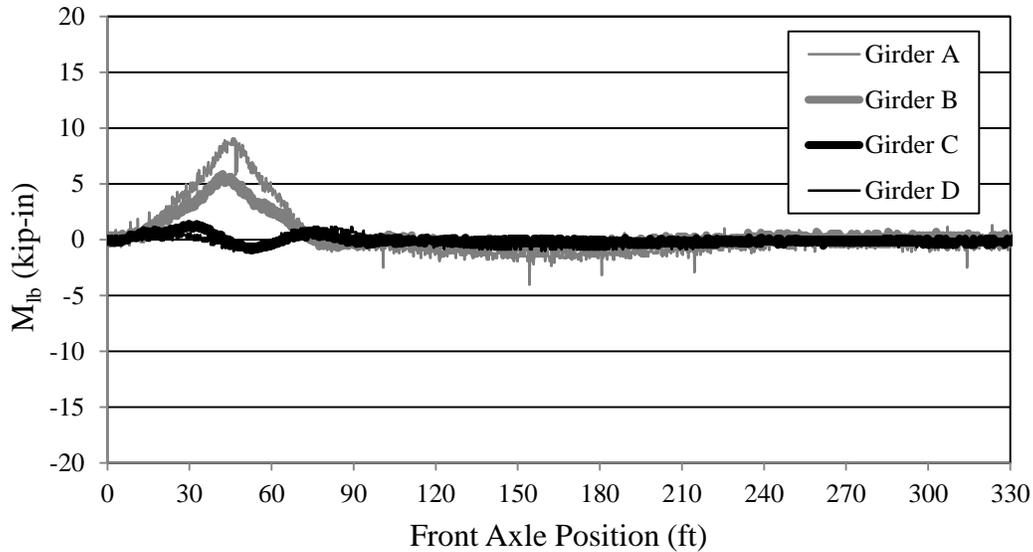
Figure 7.25. Bridge 309-S2 lateral bottom flange moments (LP3)

Table 7.6. Maximum M_{lb} in girders (kip-in.)

	Girder	Bridge Section 1 (S1)				Bridge Section 2 (S2)			
		A	**B**	**C**	**D**	**A**	**B**	**C**	**D**
Bridge #	**309**	-15[LP3]	-7[LP3]	-7[LP2]	-19[LP1]	11[LP2]	8[LP2]	8[LP1]	17[LP1]
	2308	-8[LP3]	3[LP1]	34[LP1]	-17[LP1]	8[LP2]	6[LP2]	10[LP1]	10[LP1]
	2208	-8[LP3]	-4[LP3]	-5[LP1]	18[LP1]	14[LP3]	15[LP2]	6[LP1]	-16[LP1]
	209	-6[LP3]	-6[LP3]	-8[LP3]	-5[LP2]	9[LP2]	-8[LP1]	-13[LP1]	-7[LP1]
	109	-3[LP1]	-12[LP3]	-5[LP1]	4[LP1]	-	-	-	-

As expected, lateral bottom flange bending proved to be more significant in the four curved bridges compared to the straight bridge. Maximum bottom flange moments ranged from -19 to 34 kip-in. in the curved girders versus only -12 to 4 kip-in. in the straight girders. Furthermore, the largest results were found in Bridges 309 and 2308, which have the largest curvature. These results indicate that increased skew and curvature have direct influences on lateral bottom flange bending.

Typical lateral top flange bending moments are illustrated in Figure 7.26, whereas a more detailed summary of results is tabulated in Table 7.7.
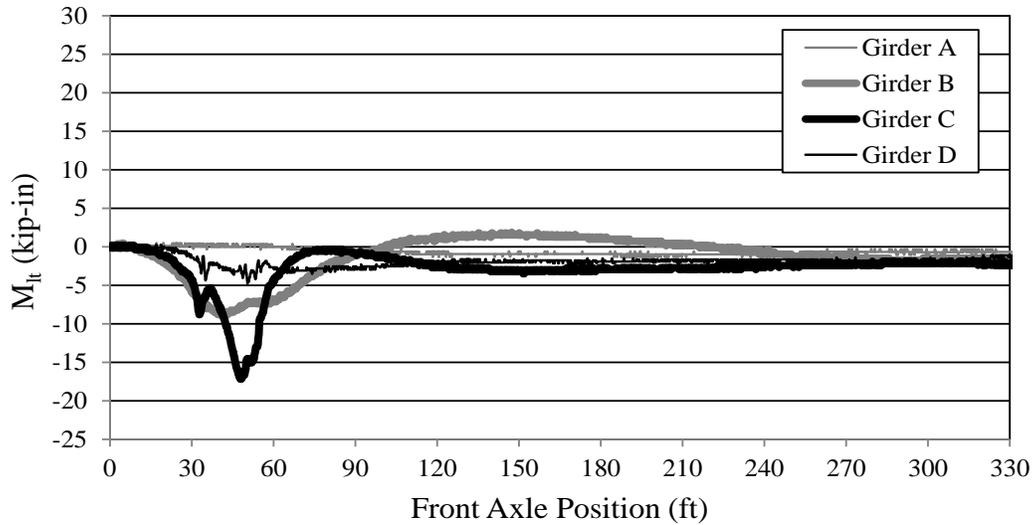
Figure 7.26. Bridge 309-S2 lateral top flange moments (LP3)

Table 7.7. Maximum M_{lt} in girders (kip-in.)

	Girder	Bridge Section 1 (S1)				Bridge Section 2 (S2)			
		A	B	C	D	A	B	C	D
Bridge #	309	7[LP3]	5[LP2]	4[LP1]	3[LP1]	4[LP3]	-34[LP2]	20[LP2]	-5[LP1]
	2308	-4[LP3]	-4[LP2]	3[LP1]	4[LP1]	5[LP1]	9[LP3]	8[LP2]	23[LP1]
	2208	-7[LP3]	6[LP3]	5[LP1]	8[LP1]	-5[LP3]	-13[LP2]	23[LP2]	20[LP1]
	209	-6[LP3]	-4[LP3]	-8[LP3]	-5[LP2]	-50[LP3]	5[LP2]	6[LP2]	-40[LP1]
	109	3[LP3]	-2[LP3]	-3[LP3]	-2[LP1]	-	-	-	-

First, lateral top flange bending moments were much smaller than lateral bottom flange bending moments for all bridges, particularly at S1. Lateral top flange bending moments increased at S2. The moments in the exterior girders for Bridge 209 increased by nearly ten times the moment found at S1 for Girder A. In Bridge 309, the largest increases were found in the interior girders. These results indicate that lateral top flange bending moments are most significant at diaphragm sections. However, the AASHTO LRFD Specifications permit lateral top flange bending moments to be neglected when designing the flexural resistance of a steel girder that has the top flange continuously braced through shear studs (6-105). Because of the smaller values produced and the *AASHTO LRFD* specifications permitting the moments to be neglected, lateral top flange bending will not be further addressed in this work.

Axial Forces

Figure 7.27 and Figure 7.28 plot the typical axial girder forces for Bridge 309 for a given load path at S1 and S2, respectively. Note the large increase in axial force found in Girder B when comparing S1 to S2. The maximum values are tabulated in Table 7.8.
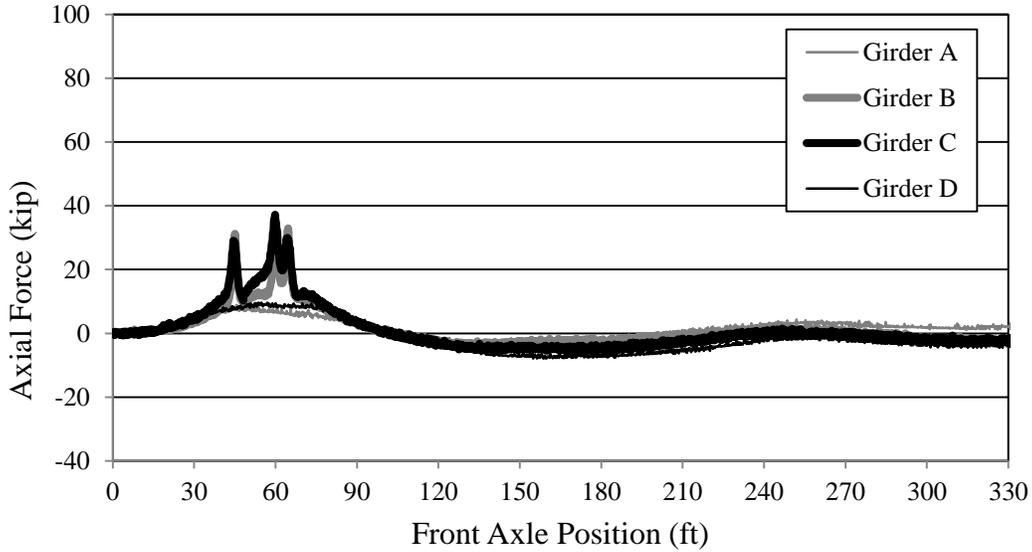
Figure 7.27. Bridge 309-S1 axial forces in girders (LP3)
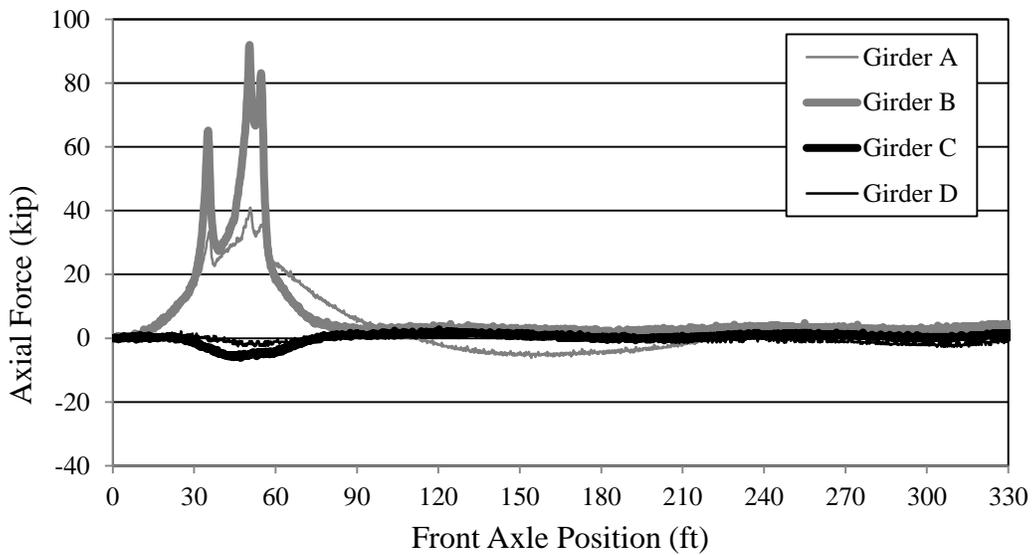
Figure 7.28. Bridge 309-S2 axial forces in girders (LP3)

Table 7.8. Maximum P in girders (kip)

	Girder	Bridge Section 1 (S1)				Bridge Section 2 (S2)			
		A	**B**	**C**	**D**	**A**	**B**	**C**	**D**
Bridge #	**309**	45[LP3]	41[LP3]	42[LP1]	57[LP1]	41[LP3]	92[LP3]	49[LP1]	38[LP1]
	2308	53[LP3]	54[LP3]	46[LP2]	59[LP1]	58[LP3]	56[LP3]	45[LP1]	101[LP1]
	2208	59[LP3]	50[LP3]	47[LP1]	55[LP1]	61[LP3]	54[LP3]	50[LP1]	76[LP1]
	209	55[LP3]	55[LP3]	42[LP2]	59[LP1]	122[LP3]	55[LP3]	37[LP2]	95[LP1]
	109	43[LP3]	48[LP3]	41[LP1]	50[LP1]	-	-	-	-

150

Results in Table 7.8 indicate that axial forces for the curved bridges are largest at S2. The forces produced at S1 for the curved bridges are relatively uniform between adjacent girders, similar to the straight bridge. Largest increases occurred in the exterior girders for Bridges 2308, 2208, and 209. The axial force in Girder A increased from 55 kips at S1, to 122 kips at S2 (Bridge 209).

7.2.3 Diaphragm Forces

Strong Axis Bending Moment

Figure 7.29 displays typical strong axis bending moments produced in the three diaphragms due to a particular load path. Note the large difference in values produced in the outer diaphragm near girder B compared to outer diaphragm near girder A. This trend is also apparent in the results listed for each curved bridge in Table 7.9.
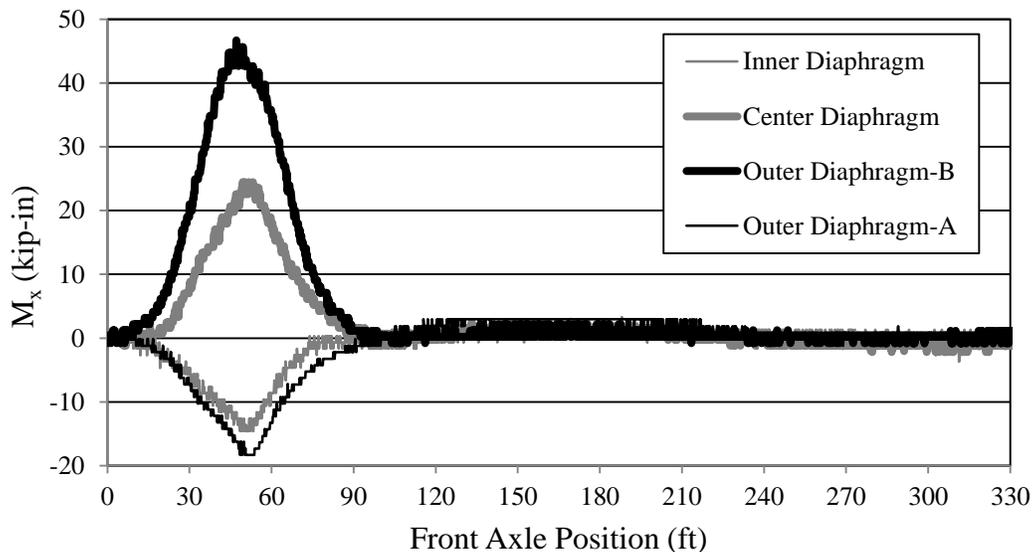
Figure 7.29. Bridge 309 strong axis moments in diaphragms (LP3)

Table 7.9. Maximum M_x in diaphragms (kip-in.)

	Diaphragm	Inner	Center	Outer-B	Outer-A
Bridge #	**309**	50[LP2]	70[LP2]	74[LP2]	-18[LP3]
	2308	35[LP2]	67[LP2]	82[LP2]	-16[LP3]
	2208	35[LP2]	55[LP2]	59[LP2]	18[LP2]
	209	51[LP2]	96[LP2]	80[LP2]	9[LP2]

The largest strong axis moments were found at the center diaphragm and at the one-third point nearest Girder B for the outer diaphragm. LP2 produced the maximum strong axis moments for all bridges. Conversely, the strong axis moments were significantly smaller at the one-third point nearest Girder A for the outer diaphragm. Overall, diaphragm strong axis moments in Bridge 209

151

and 2308, consisting of SIABs, were larger than the strong axis moments in Bridges 309 and 2208, consisting of IABs.

Axial Forces

Figure 7.30 depicts typical axial forces produced in the three diaphragms for the curved bridges due to a particular load path. Table 7.10 provides a summary of maximum axial forces reported in the diaphragms for the four curved bridges tested. Results for axial forces in the diaphragms were all governed by LP2 in all bridges. Bridge 209 produced the largest range of axial forces from 0.6 to 7.6 kip.
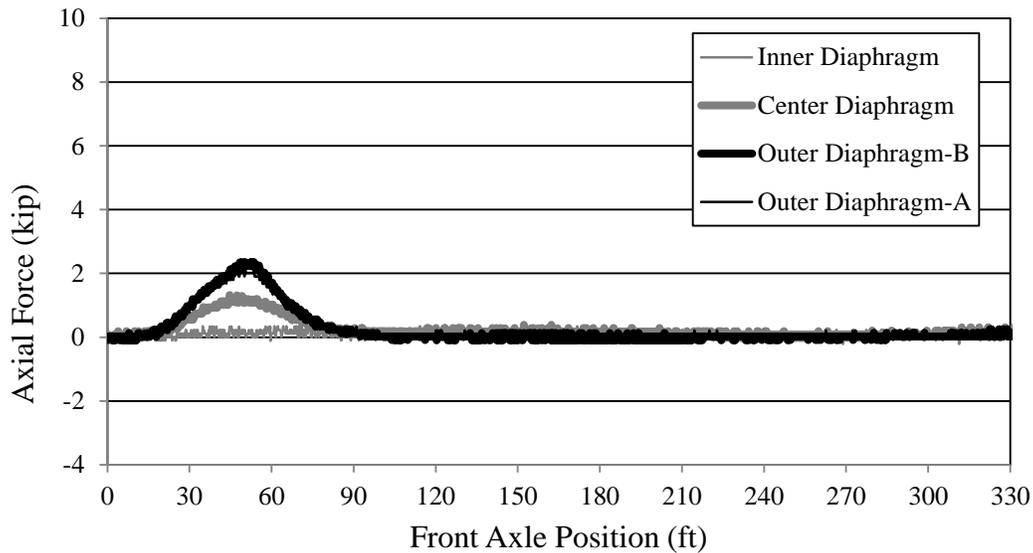
Figure 7.30. Bridge 309 axial forces in diaphragms (LP3)

Table 7.10. Maximum P in diaphragms (kip)

	Diaphragm	Inner	Center	Outer-B	Outer-A
Bridge #	**309**	2.3[LP2]	3.8[LP2]	3.3[LP2]	2.7[LP2]
	2308	0.9[LP2]	3.1[LP2]	5.5[LP2]	3.0[LP2]
	2208	1.3[LP2]	1.9[LP2]	0.9[LP2]	1.8[LP2]
	209	2.3[LP2]	7.6[LP2]	0.6[LP2]	1.1[LP2]

7.2.4 Live Load Distribution

Live load distribution to the girders was assessed by calculating moment distribution factors in the four girders for each bridge. Strong axis moments were used throughout this process. The moment distribution factors were determined for single lane and multi-lane loadings for LP1, LP2, and LP3.

152

Single Lane

The moment distribution factor for each girder due to individual load paths was calculated using equation 7.3.

$$MDF_i = M_{xi}/\Sigma M_x \tag{7.3}$$

where,

   M_{xi} = strong axis bending moment in girder i,
   MDF_i = moment distribution factor in girder i,
   ΣM_x = sum of strong axis moments in girders at section,

The results of equation 7.3 were then plotted versus truck position. Figure 7.31 represents an example of the moment distribution factors found in Bridge 309 at S2 due to LP1. This process was repeated for every load path at S1 and S2. Values were selected at a determined truck position, since results varied throughout the length of the span. To avoid the localized effect the concentrated wheel loads have on the data, values were selected at one truck length past the instrumented section. For example, one truck length past the gauge locations at S2 in Bridge 309 relate to a front axle truck position of roughly 68 ft, represented by the dashed line in Figure 7.31. The selected values in Figure 7.31 for LP1 were then plotted in Figure 7.32, represented by the × markers. In a similar fashion, values selected for LP2 and LP3 at S1 are represented by square and triangle markers, respectively. This process was repeated at S2 and results are as shown in Figure 7.33.
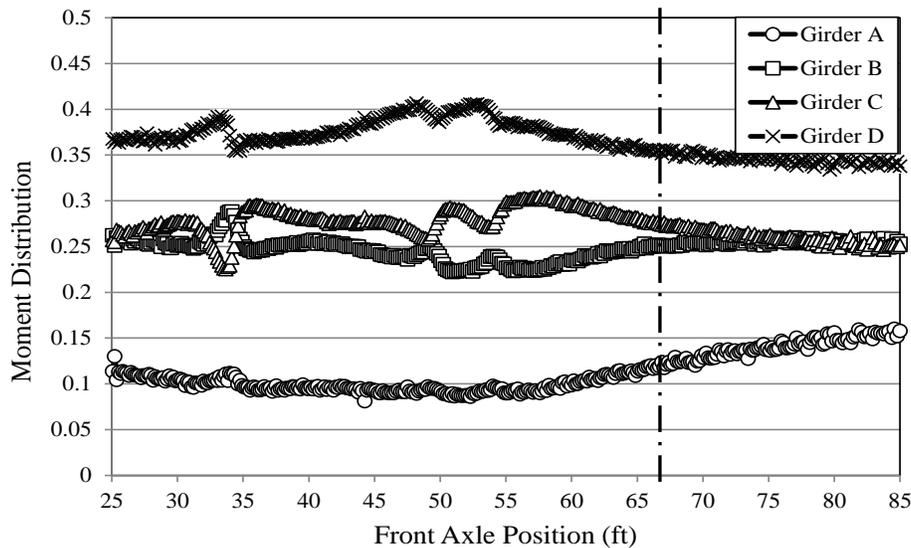
Figure 7.31. Bridge 309-S2 (LP1)

153
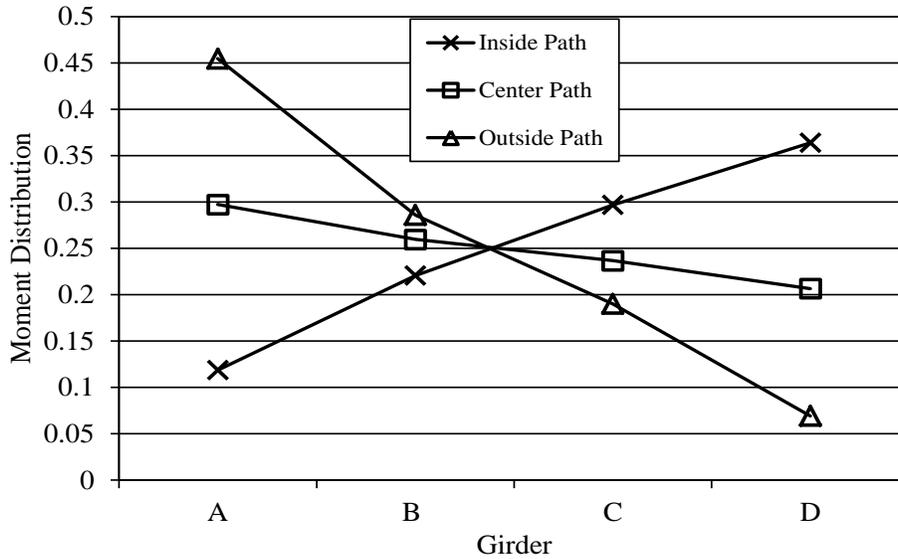
Figure 7.32. Bridge 309-S1 single lane moment distributions for three truck lanes
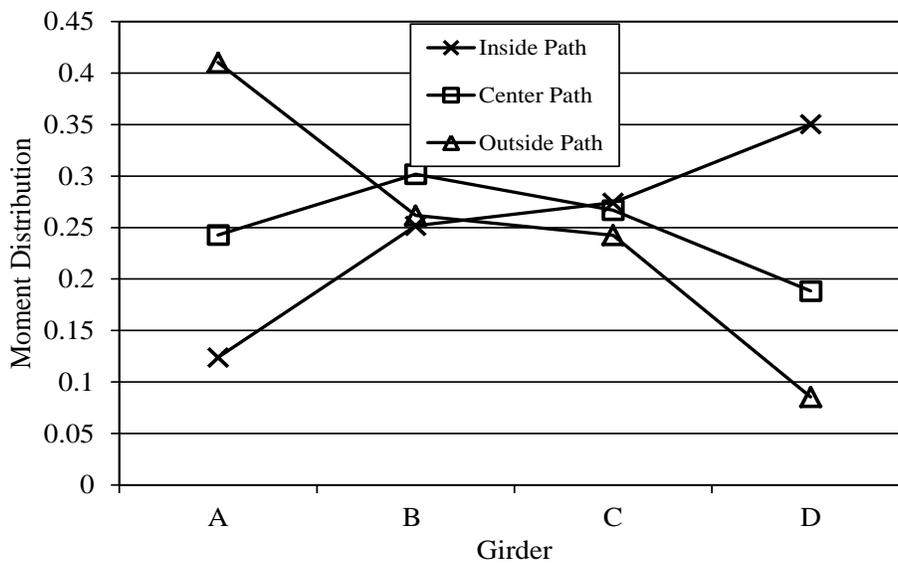
Figure 7.33. Bridge 309-S2 single lane moment distributions for three truck lanes

Multi-Lane

Since the roadway width was a constant 26 ft for all bridges, 12 ft design lane widths allows two trucks to be placed adjacent to one another. Consequently, multi-lane live load moment distribution factors were estimated by superimposing the results from LP1 and LP3. Similarly to the single lane moment distributions, the results from the multi-lane loading were plotted versus truck position. Figure 7.34 and Figure 7.35 display typical results for each girder for the curved Bridge 309 at S1 and S2, respectively. Again, individual values were selected at one truck length beyond the instrumented section. Figure 7.36 represents the selected values for Bridge 309.

154
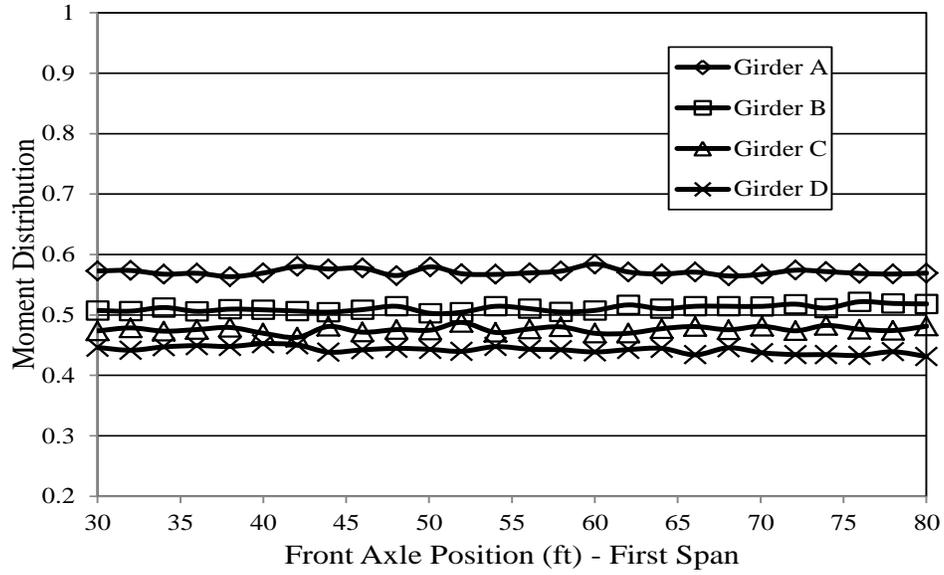
Figure 7.34. Bridge 309-S1 moment distributions versus truck position
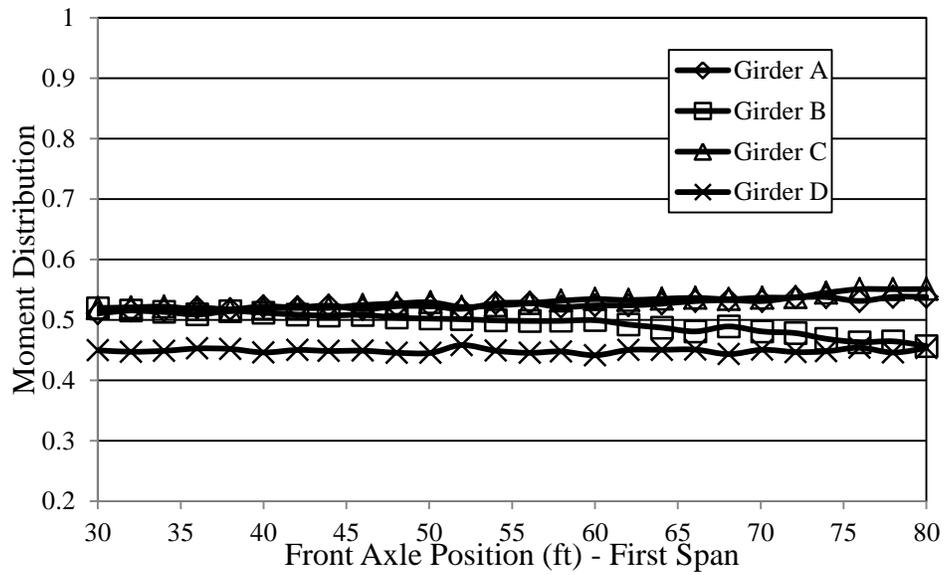
Figure 7.35. Bridge 309-S2 moment distributions versus truck position
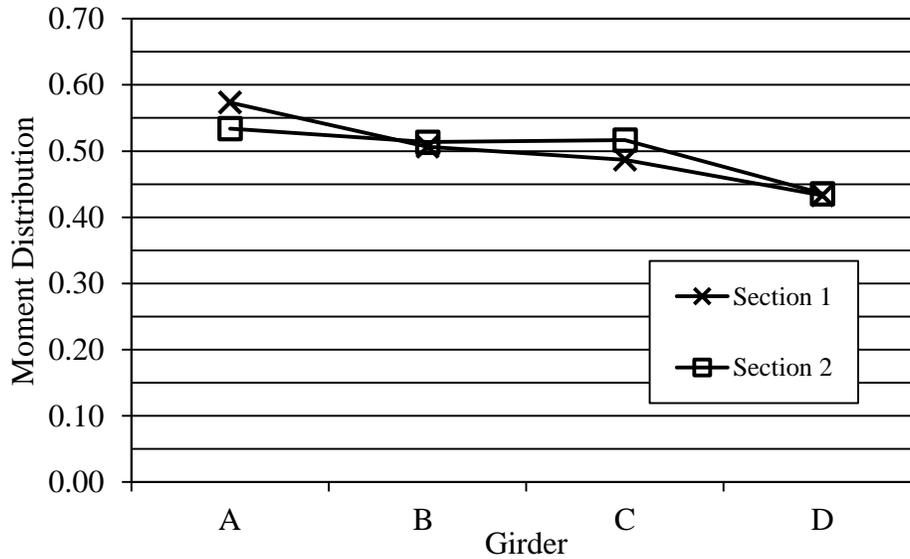
Figure 7.36. Bridge 309 maximum moment distribution factors

Tabulated results for multi-lane moment distribution factors are presented in Table 7.11. Results are separated by their respective section, S1 and S2. The controlling value is in bold for each girder based on the maximum value at either section and Figure 7.37 graphically represents the controlling values shown in Table 7.11.

Table 7.11. Moment distribution factors for multi-lane live loading

	Girder	Bridge Section 1 (S1)				Bridge Section 2 (S2)			
		A	**B**	**C**	**D**	**A**	**B**	**C**	**D**
Bridge #	**309**	**0.57**	0.51	0.49	0.43	0.53	**0.51**	**0.52**	**0.44**
	2308	**0.63**	0.47	0.44	**0.46**	0.58	**0.51**	**0.51**	0.40
	2208	**0.51**	0.53	0.53	0.43	0.50	**0.54**	**0.53**	**0.44**
	209	**0.53**	0.52	0.49	**0.47**	0.46	**0.56**	**0.58**	0.40
	109	**0.42**	**0.55**	**0.56**	**0.47**	-	-	-	-

156
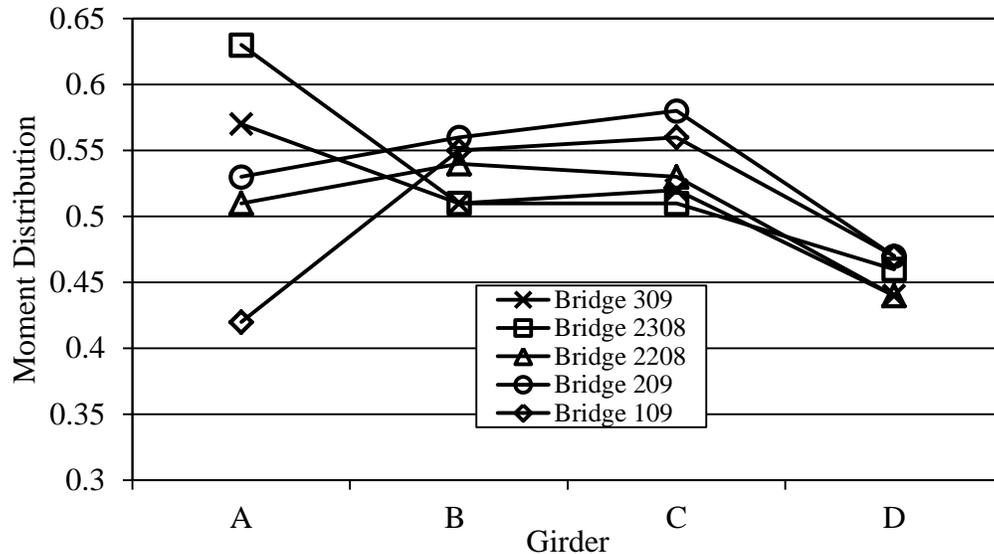
Figure 7.37. Maximum moment distribution factors in bridges

Results in Figure 7.37 indicate the largest MDFs were in Girder A for the two bridges with the most sever curvature, Bridges 309 and 2308 with values of 0.57 and 0.63, respectively. The interior girders produced MDF values ranging from 0.51 to 0.52 at S2. Lastly, Girder D produced the smallest moment distribution factors of 0.44 and 0.46 in Bridges 309 and 2308, respectively. Results show the bridges will the largest degree of curvature will distribute more load to the exterior girder located on the outside of the curve and the least amount to the exterior girder located on the inside of the curve.

For Bridges 2208 and 209, which consist of larger radii and skew angles, produced results more similar to Bridge 109 than the other two curved bridges. The largest MDF was found in the interior two girders for Bridges 2208, 209, and 109. Values for Girders B and C ranged from 0.53 to 0.58. The exterior girders in Bridges 2208 and 209 produced smaller MDFs, ranging from 0.44 in Girder D to 0.53 in Girder A. However, Girder A was found to produce larger MDFs than Girder D for these two bridges.

As a general comparison, the experimental MDFs were compared to approximate method of analysis as specified by Section 4.6.2.2.2 in AASHTO. Note that these bridges do not meet the criteria for applying the approximate level of analysis, because not all girders have the same stiffness and the degree of curvature exceeds the limits as required in Section 4.6.1.2.4. By applying appropriate bridge geometry, the multi-lane MDF for Bridge 309 equals 0.582 for exterior girders and 0.623 for interior girders. These results do not match experimental values, as the exterior girders do not have the same MDF in the curved bridges, proving in fact that the approximate method of analysis by AASHTO is not applicable for these curved bridges.

7.2.5 V-Load Exploration

The application of the V-Load method, which was introduced in Chapter 2 of this report, was explored for lateral flange bending. According to Section 4.6.1.2.4b-1 in AASHTO, the effect of curvature when calculating strong axis bending moments may be ignored when the following criteria are satisfied:

- Concentric girders
- Skews less than 10^0 from radial
- Equal girder stiffness
- Arc span length to radius ratio less than 0.06 radians

If the above criteria are met, then the bridge can be assumed straight and an approximate method of analysis can be used for the bridge. However, lateral flange bending effects still need to be considered regardless of the degree of curvature. AASHTO refers to equation 7.4, the V-Load equation, to adequately determine the lateral flange bending due to curvature for all curvatures. This method is sometimes used in place of a refined method of analysis. Note that the V-Load equation does not account for skew effects. This is important, as it has been observed here that increasing skew may increase lateral flange bending.

$$M_{lb} = M_x L^2 / NRD \qquad\qquad (7.4)$$

where,
$\quad M_x \quad$ = strong axis bending,
$\quad M_{lb}$ = lateral flange bending located at the presence of a diaphragm or cross frame,
$\quad L$ = length of the member,
$\quad N$ = a constant of either 10 or 12 (engineer's discretion),
$\quad R$ = the radius of the girder, and
$\quad D$ = the depth of the web.

Based on their geometry, the four curved bridges in this study fail to satisfy the requirements that AASHTO specifies for an approximate level of analysis for strong axis bending, because:

- Girders do not have equal stiffness
- Skew angles range from 15^0 to 35^0
- Arc length to radius ratios for the end spans range from 0.061 to 0.076 radians

Consequently, AASHTO requires that a refined analysis must be employed. However, the V-Load method still is applicable in the assessment of lateral flange bending due to curvature. The remaining results in this section evaluate the V-Load equation with respect to Bridges 309, 2308, 2208, and 209. Equation 7.4 was rearranged as equation 7.5 to produce the ratio of lateral flange bending to strong axis bending to ease comparison with experimental results. Table 7.12 provides the results in equation 7.5.

$M_{lb}/Mx=L^2/NRD$ (7.5)

Table 7.12. Results from AASHTO LRFD equation C4.6.1.2.4b-1

Bridge #	Radius, R (ft)	Web Depth, D (ft)	N (constant)	Diaphragm Spacing, L (ft)	M_{lb}/M_x (%)
309	950	4.0	10	18.75	*0.9*
2308	950	4.0	10	18.70	*0.9*
2208	1340	3.5	10	17.50	*0.7*
209	1340	3.5	10	17.20	*0.6*

The experimentally determined lateral bottom flange bending moments and strong axis bending moment were plotted as ratios. Figure 7.38 shows a typical example of the experimentally determined ratio.
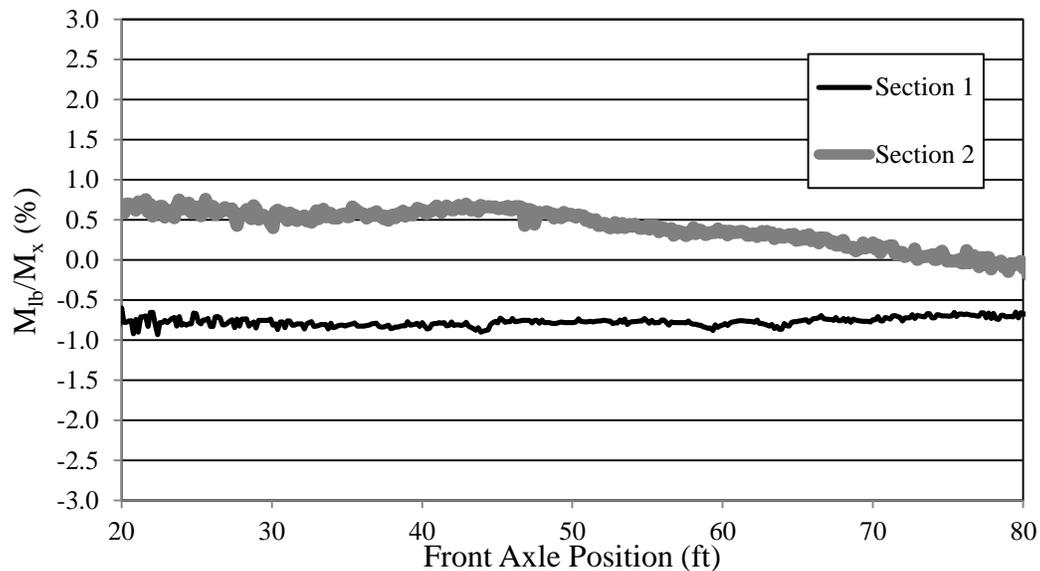
Figure 7.38. Bridge 309 Girder A ratio of M_{lb}/M_x

Table 7.13 and Table 7.14 summarize the field results for each girder of each bridge. Values shown under A-D are when the maximum lateral bottom flange moments occurred due to LP1, LP2, or LP3. An average value from the four girders is provided in the last column. Note this equation is only applicable at the diaphragm. Thus, only field results at S2 (Table 7.13) relate to the V-Load equation results (Table 7.12).

Table 7.13 S2: M_{lb}/M_x (%) from field results

	Girder	A	B	C	D	*Avg.*
	309	1.3	0.5	0.8	1.2	*1.0*
Bridge #	**2308**	0.6	0.4	0.8	1.3	*0.8*
	2208	1.1	1.1	0.6	1.1	*1.0*
	209	0.9	1.2	1.3	0.9	*1.1*

Table 7.14. S1: M_{lb}/M_x (%) from field results

	Girder	A	B	C	D	*Avg.*
Bridge #	**309**	0.8	0.5	0.6	1.3	*0.8*
	2308	0.5	0.5	0.4	1.2	*0.6*
	2208	0.7	0.3	0.5	1.5	*0.8*
	209	0.4	0.5	1.0	0.7	*0.6*

Average results in Table 7.13 and Table 7.14 indicate larger lateral bottom flange moment to strong axis moment ratios at S2 than ratios at S1. Additionally, results at S2 compare well with the V-Load equation results (Table 7.12) for Bridges 309 and 2308. These two bridges have smaller skews of only 15^0. On the other hand, average values in Bridges 2208 and 209 were greater than the results in Table 7.12. This increase could be a direct result of the 35^0 skew in Bridges 2208 and 209. Overall, results indicate that the V-Load equation provides a worthy preliminary assessment for the lateral bottom flange bending moment based on the strong axis moment produced in the girder. Additional analysis would need to be performed in order to address the effects of increased skew angles. In conclusion, the V-Load method may help a designer understand the basic behavior of the diaphragm and lower girder flange, even if the numerical results may not be accurate enough for final design. This fact likely becomes more imperfect for smaller radii and larger skews.

CHAPTER 8 ANALYTICAL STUDY

The purpose of the work described in this chapter is to analytically investigate the superstructure behavior of a horizontally curved bridge under design loading conditions. One bridge from the empirical field study was modeled using a commercial finite element model (FEM) analysis software package. The 3D rendering included main components of the superstructure system along with simplified components for the substructure.

8.1 Introduction

Structural analysis of a bridge, in accordance to the 2010 AASHTO LRFD Specifications, requires any method that satisfies equilibrium, compatibility, and proper stress-strain relationships for a given material. Examples of such methods include classical, finite difference, FEM, folded plate, finite strip, yield line, and grillage methods. Often, a horizontally curved girder bridge requires a refined method of analysis. Section 4.6.3.3.2 states:

Refined analysis methods should be used for the analysis of curved steel bridges unless the Engineer ascertains that approximate analysis methods are appropriate according to the provision of Article 4.6.2.2.4 (4-69).

A refined method of analysis is defined as one that includes the superstructure as an integral system providing adequate displacements and reactions. An engineer may neglect the horizontal curvature component and apply approximate methods of analysis if the geometry meets certain criteria outlined in Article 4.6.2.2.4. These criteria often pertain to limiting bridge skew, maintaining constant cross sections, and limiting radius to arc span length ratios. Approximate methods of analysis require significantly less effort as several assumptions are made throughout the process. Simplifications and assumptions made in the approximate methods greatly reduce time.

The four curved bridges of focus in this study do not meet the criteria established in Article 4.6.2.2.4 of AASHTO. Consequently, a refined analysis method must be employed. Chapter 2 of this report categorizes three levels of analysis. Levels 2 and 3 fall under the definition of a refined level of analysis. Based on the desired outputs from this study and relative accuracy provided as discussed, a Level 3 analysis was selected. According to Lydzinski et al. (2008), the finite element method is beneficial for multispan horizontally curved steel girders. Modeling certain details in order to capture structural behaviors cannot be completed any other way. Details such as bracing connections and element type combinations can play an important role when analyzing a complex structure similar to the horizontally curved bridges in this study.

8.2 Model Development

Bridge 309 was selected for a detailed analytical FEM study for a number of reasons. First, this bridge was equipped with the most instrumentation of the five bridges in the field study. This would prove beneficial in not only validating the analytical model, but evaluating the behavior of the structure to the fullest degree. Also, as mentioned in Chapter 5, Bridge 309 is the most

restrained bridge, consisting of two integral abutments and two piers fixed to translation. Lastly, Bridge 309 has the most severe curvature with a 950 ft radius. This section will address how the FEM attempts to represent the conditions of Bridge 309.

8.2.1 Geometry

Superstructure

Recall the Bridge 309 superstructure detailed in Chapter 5. Figure 8.1 illustrates a cross section of the simplified dimensions of the superstructure. Steel girder dimensions follow Figure 8.2 to include all flange thickness changes along the longitudinal length of the bridge. The concrete deck was assumed to have a constant thickness of 8 in. and was modeled directly on top of the steel girders. The connection between the deck and the girders is described under Section 8.2.4.

The following notable components of the superstructure were assumed to be insignificant and were neglected for the scope of this study:

- Superelevations
- Differential elevation changes
- Concrete haunches
- Field splices
- Plate stiffeners
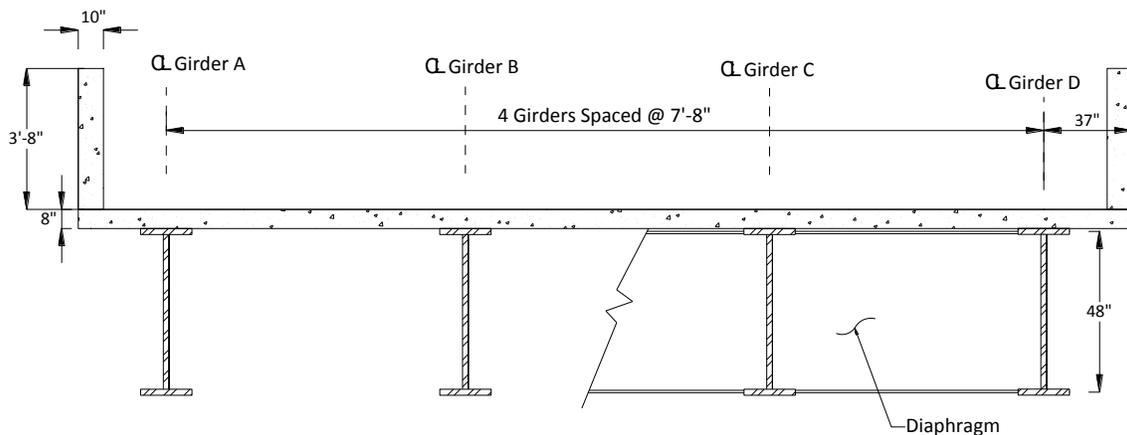
Figure 8.1. Model superstructure cross section

Diaphragms shown in Figure 8.1 were modeled as the entire 48 in. depth of the girder web. As indicated, web stiffeners were not included in the model, so the diaphragms were modeled as being directly connected to the girder. Additionally, parapets models were simplified by assuming an average constant thickness of 10 in. and directly attaching them to the deck, i.e. a jointless connection.
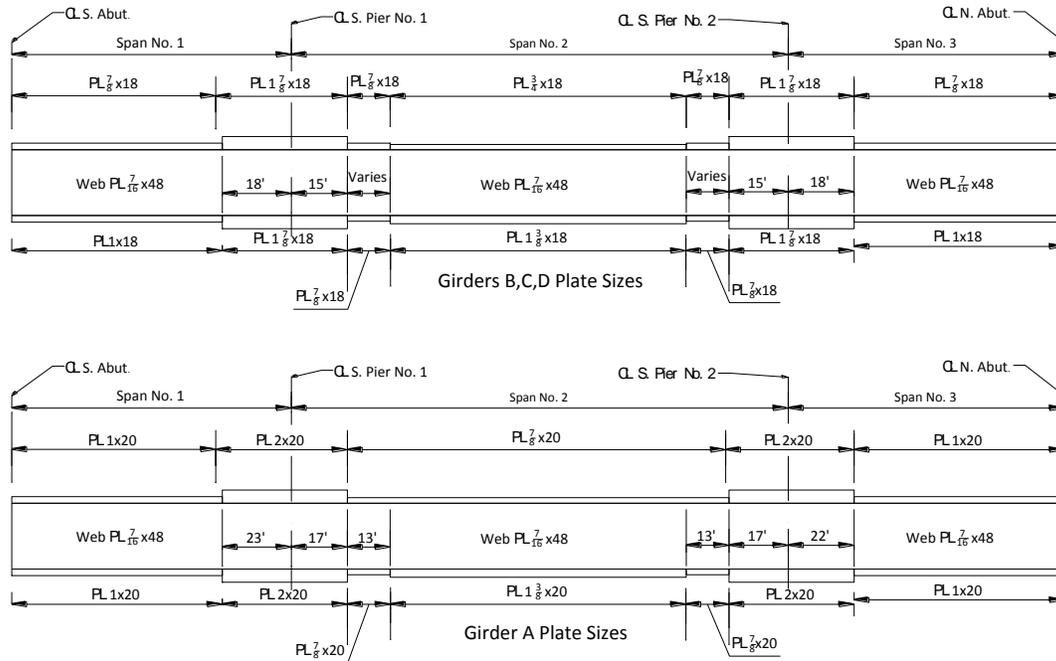
Figure 8.2. Plate girder sizes elevation view

Piers

Pier columns and beams were modeled about their centerlines. The pier columns were modeled using tapered members starting at the base cross section, 51 in. x 53in; and increasing to the top, 51in. x 74 in.. The pier cap heights and widths were 51 in. and 74 in., respectively. Thicknesses of the members were specified during the meshing process. Figure 8.3 illustrates the simplified typical frame pier geometry. Since superelevation was neglected, the average distance from the centerline of the pier cap to the bottom of the girders was determined to equal 37 ½ in.. Connections between the girders and the piers are described in Section 8.2.4.
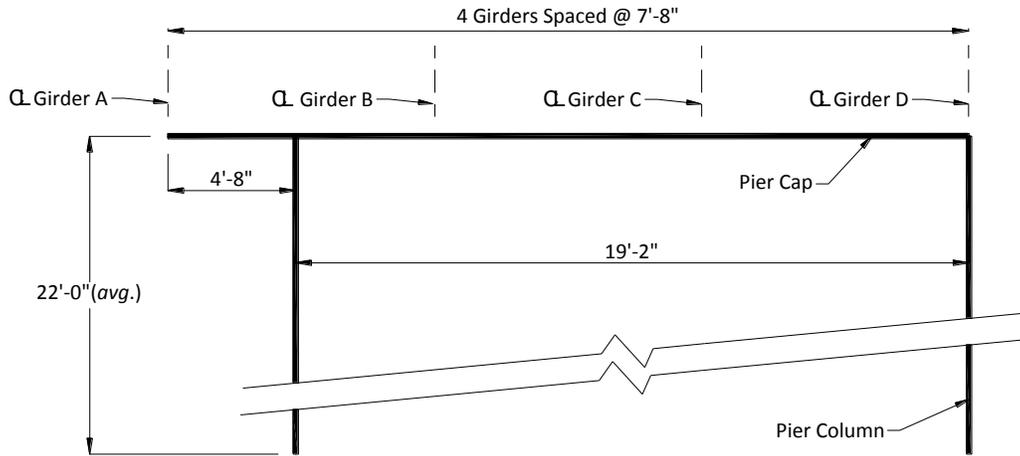
Figure 8.3. Typical pier geometry

Abutments

The analytical abutment model utilized the as-built north/south abutment dimensions. The top and bottom elevations, pile locations, pile cap, and backwall thicknesses were taken from the Bridge 309 plan sheets. Abutment piles were modeled using an equivalent cantilever length of 18 ft, previously calculated in Section 6.3.2. Figure 8.4 through Figure 8.6 depict the simplified geometry of the analytical south abutment. The north abutment geometry is identical.
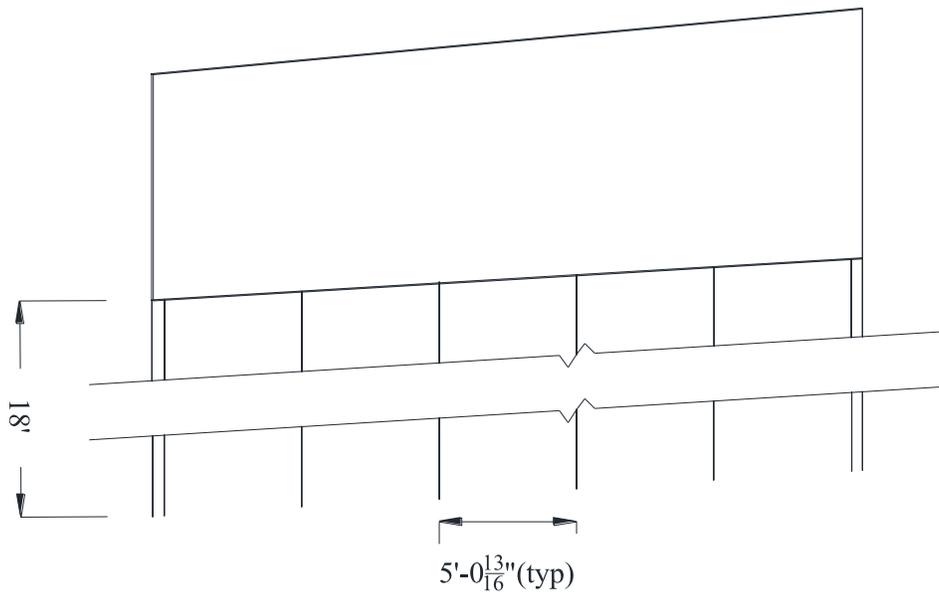
Figure 8.4. Analytical model elevation view
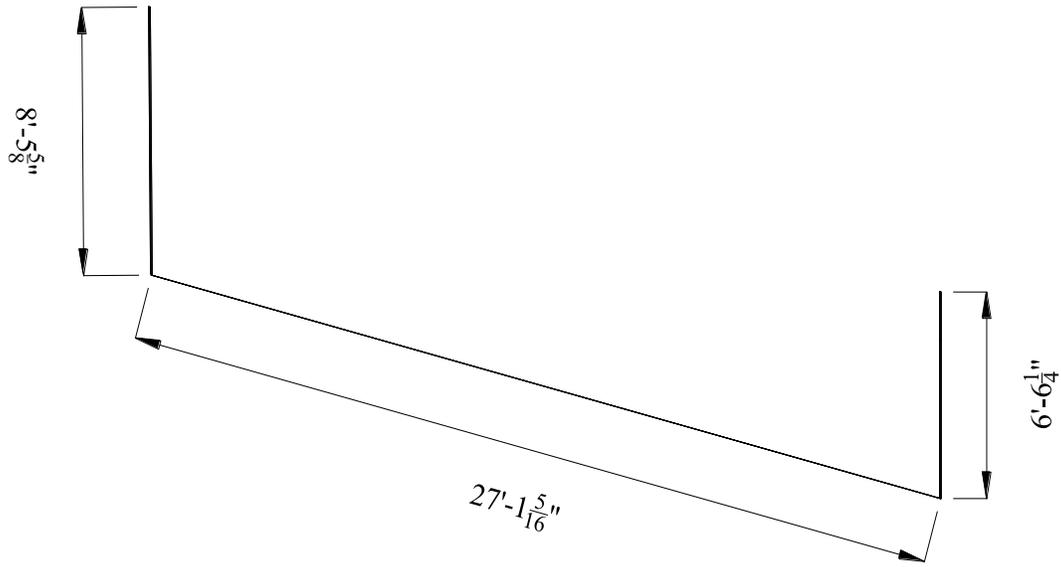
Figure 8.5. Analytical model plan view
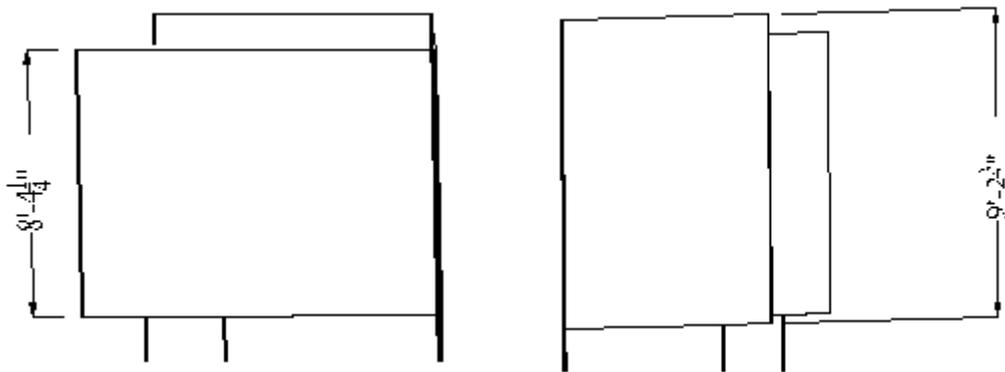
Figure 8.6. Analytical model end views

In order to simplify the analytical model, the wingwalls were extended the full height of the abutment backwall and the thickness of the abutment is a constant 36 in.. Also, the portion of the wingwall that extends forward, past the backwall was not included in the analytical model.

8.2.2 Elements

Three types of elements were used throughout the FEM, which are described below. The shell and beam elements used are described accordingly.

165

SHELL63

SHELL63 is a 3-D elastic shell element that has both bending and membrane capabilities. This element was used when meshing the abutment, deck, and web of the steel plate girders. In this analysis, the element geometry was defined by four nodes, a constant thickness, and the isotropic material properties. There are six degrees of freedom at each node: translations in the nodal x, y, and z directions and rotations about the nodal x, y, and z axes. Both in-plane and normal loads are permitted.

BEAM4

BEAM4 is a uniaxial 3-D elastic beam element with tension, compression, torsion, and bending capabilities. This element was used to model the abutment piles, pier caps, and flanges of the steel plate girders. In this analysis, the element was defined by two nodes, the cross sectional area, two moments of inertia (IZZ and IYY), two thicknesses (TKY and TKZ), an angle of orientation (θ) about the element x-axis, the torsional moment of inertia (IXX), and the material properties. At each node the element has six degrees of freedom: translations in the nodal x, y, and z directions and rotations about the nodal x, y, and z axes.

BEAM188

BEAM188 is also a uniaxial 3-D elastic beam element with tension, compression, torsion, and bending capabilities. This element was used when meshing the pier columns as it is associated with tapered cross sections. This element is often used for slender to reasonably stubby structures. A slenderness ratio greater than 30 is recommended. This element was defined by two end nodes, an orientation node, two section IDs, and the material properties. Six degrees of freedom exist at each node, the same as the BEAM4 element.

8.2.3 Material Properties

For the materials properties used in the FEM consisted of steel and concrete. Certain assumptions were made about the thermal and structural properties of the concrete and steel. Concrete material properties presented in Table 8.1 were applied to the piers, abutments, deck, and parapets. The modulus of elasticity of the concrete, E_c, was estimated from recommendations of ACI 318-08 section 8.5.1. The concrete's Poisson Ratio, ν_c; density, ρ_c; and coefficient of linear thermal expansion, α_c were selected from appropriate charts (The Engineer ToolBox 2012).

Table 8.1. ANSYS model concrete material properties

E_c (psi)	ν_c	ρ_c (lb/in.$^{-3}$)	α_c (10^{-6} in./in. °F)
3,372,165	0.2	0.08681	4.8

Steel material properties were applied to the girders, diaphragms, and abutment piles as listed in Table 8.2. The steel's modulus of elasticity, E_s; Poisson's ratio, ν_s; density, ρ_s; and coefficient of linear thermal expansion, α_s; were selected from Chapter 17 in the AISC Steel Construction Manual (AISC 2007).

Table 8.2. ANSYS model steel material properties

E_s (psi)	ν_s	ρ_s (lb/in.$^{-3}$)	α_s (10^{-6} in./in. °F)
29,000,000	0.3	0.2836	6.5

8.2.4 Boundary Conditions and Meshing

Boundary conditions varied throughout the FEM study in order to accomplish specific tasks and comparisons. Task outlines and reasoning for changes will be noted in appropriate proceeding sections of Chapter 8. This section discusses all boundary conditions and mesh arrangements used in the FEM.

Girders and Diaphragms

Considering that the girder and diaphragm responses were the main focus of the FEM study, much attention to detail went into determining their respective mesh sizes and connecting the two entities. As previously described, the diaphragms were directly attached to the girders along their full depth. Directly attaching these components required that girder elements and diaphragm elements share common nodes. The diaphragms and girders are shown sharing three common nodes in Figure 8.7. The top shared node is attached to the top flanges of the girder and diaphragm, as well as the webs of the girder and diaphragm. The middle shared node joins the webs of the girder and diaphragm. The bottom shared node is attached to the bottom flanges of the girder and diaphragm, as well as the webs of the girder and diaphragm.

Lydzinski et al. (2008) described that the number of elements per girder cross section has little influence on results. Conversely, the results are more sensitive to a finer mesh with respect to the longitudinal length of the bridge. Lydzinski et al. further suggested that the element length should roughly equal 2% of the span length. This percentage correlates to an element length of 20 in. for the shortest span of 85ft. Approximate element lengths of 12 in. were conservatively chosen to account for the location of flange thickness changes. Flange thickness changes are represented by the color changes in Figure 8.8. The web depth consisted of two elements to produce a desirable aspect ratio near 2:1.
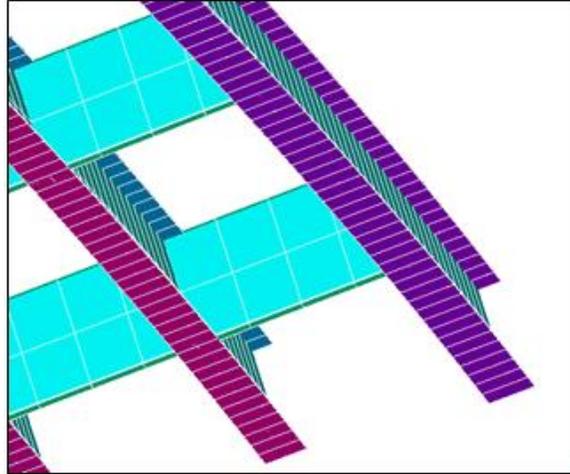
Figure 8.7. Meshed diaphragms and girders
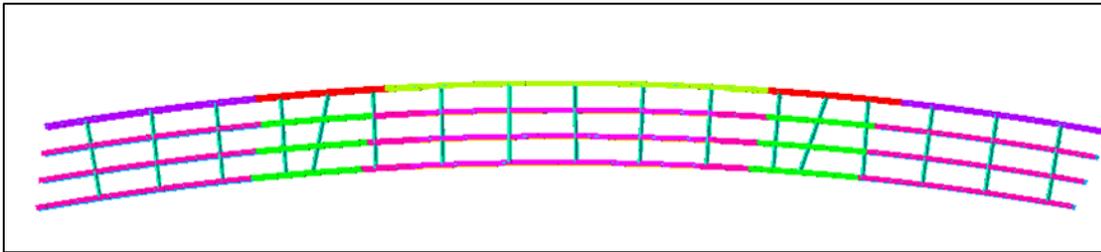
Figure 8.8. Meshed changes in girder bottom flange thicknesses

Deck and Parapets

Rigid links connected the girders to the deck. The top flange of the girder contained the master node, while the slave node was located in the deck. A 4 in. rigid link accounted for the difference in elevation between the top of the girder and the centerline of the deck.

Dunker (1985) explained that the mesh size of the deck has little effect on stress and deflection results of the superstructure. Consequently, the mesh size of the deck, shown in Figure 8.9, was determined based on the locations of the live load and a more sensitive girder mesh size. Point loads were used during loading, so the transverse locations of the nodes in the deck were critical in order to properly place the loading because the live loads followed predetermined radial truck paths. Furthermore, the longitudinal mesh size was determined by aligning nodes in the deck and the girder. This alignment was necessary in order to align the rigid links vertically.
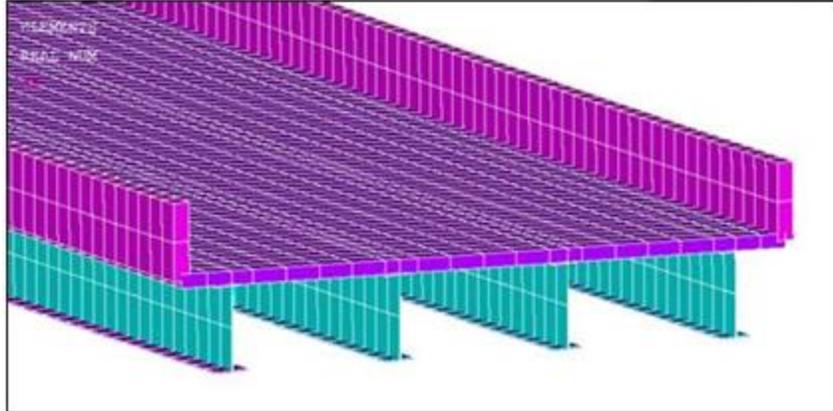
Figure 8.9. Typical meshed cross section with parapets

The parapets shown in Figure 8.9 were directly attached to the deck. Doing so requires equal mesh sizes along the shared line.

Abutments

Both abutments were directly attached to the girders, deck, and abutment piles. Shown in Figure 8.10, the mesh geometry is irregular. Few undesired tetrahedral element shapes were formed, but necessary in order to align the shared nodes with the correct geometry. These formations were deemed insignificant as the superstructure's response is assumed to be insensitive to the meshing in the abutment.

More importantly, the abutment piles would provide the rotational restraint of the abutment as a whole. The effective cantilevered piles were oriented such that their weak axis coincided with the abutment centerline. All rotation and translation degrees of freedom (DOF) were restrained at the base of the piles to represent the theorized effective cantilever.
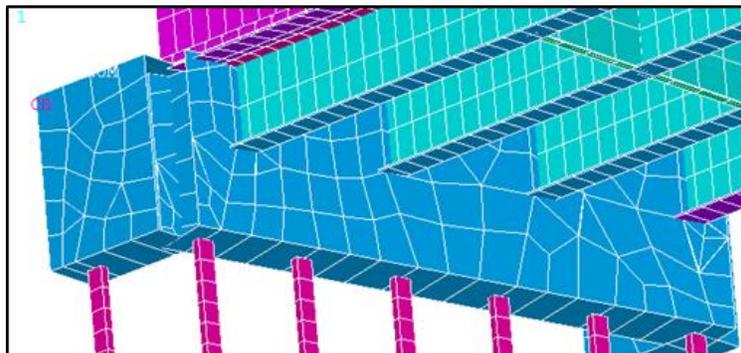
Figure 8.10. Meshed girders and abutment

Piers

Rigid links also connected the bottom of the girders to the center line of the pier caps. The rigid link nodes attached to the pier were restrained to all DOFs, while the nodes on the bottom of the girders released rotation in the plane tangent to the curvature about the strong axis of the girders. Releasing such the rotation represented the fixed pier condition, previously described in Chapter 5. Piers were assumed to be fixed at the base of the modeled columns. The piles and footings for the pier were assumed to be rigid for the scope of this study. Figure 8.11 shows the typical meshed pier, where the tapered columns can be noted. The sensitivity of the superstructure behavior to the mesh arraignment in the piers is assumed to be insignificant. Again, nodes were placed directly below proper girder node locations to ensure the rigid links were vertical.
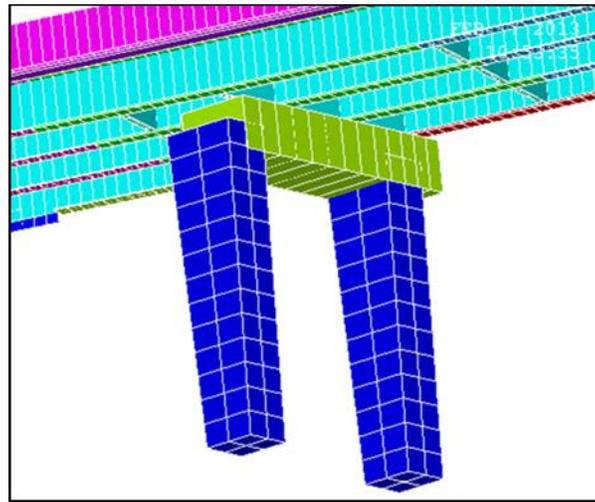
Figure 8.11. Meshed pier

Simply Supported Model

The simply supported model was constructed in order to validate the FEM results in this study to results from a consultant's modeling. Section 8.3.3 discusses the validation. The consultant's design model substituted simple supports for the substructure components modeled above. Additionally, the parapets were excluded in the consultant model, as they are not considered in design practice; however, the field results showed that they have an influence on the superstructure response as discussed in Chapter 6.
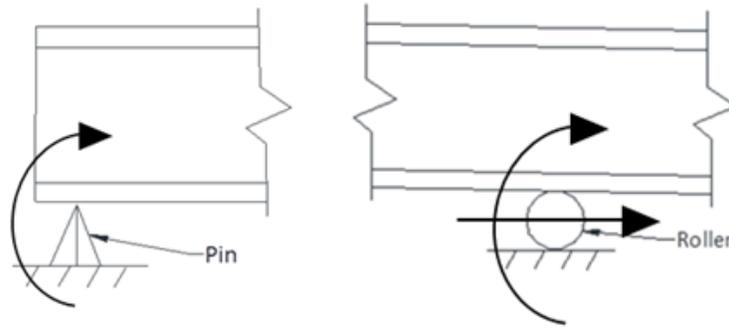
Figure 8.12. Simply supported abutment (left) and pier (right)

Abutments, piers, and parapets were removed for the simply supported FEM model. Boundary conditions were applied at nodes in the bottom of the girder ends, where the abutments and piers would be located (Figure 8.12). DOFs at these nodes were fixed for translation and released for the girder's x-axis rotation. These supports at the abutments represented classical pinned support condition. Supports at the piers were idealized as rollers, releasing the translational DOF in the girder's y-axis direction and the rotational DOF about the girder's x-axis.

8.3 Model Validation

Model validation will be achieved by comparing the FEM analysis results to two separate data sets. First, the FEM will be tailored to compare with the experimental results presented in Chapter 7, referred to as "field" hereafter. Additionally, a second FEM will be tailored to compare results provided from a consulting design firm, referred to as "consultant" hereafter. The consultant completed a 3D finite element analysis of Bridge 309 for design and agreed to provide their output to further aid this study. The alterations made to the completed FEM will be discussed in the accompanying subsections. Upon validation of this study's FEM, further exploration of design loading effects will be presented in Sections 8.4 and 8.5.

8.3.1 Data Reduction

Section 6.2.1of this report discusses the process of resolving internal composite section strains and forces from the four measured strains at each girder cross section. The data reduction and analysis for the analytical model will follow the same procedure outlined in Section 6.2.1. In order to do so, strains were linearly interpolated from the FEM output for the four strain gauge locations designated in the experimental field study.

8.3.2 Validation to Field Study

As previously mentioned, the field study comparison required the FEM to contain certain structural entities in the model for validation. Results from the field study indicate that the parapets influence the live load response in the superstructure, particularly the exterior girders. Therefore, parapets were included in the FEM for live load field comparisons. In addition, all

substructure entities and boundary conditions described in Section 8.2.4 were incorporated for the field study validation to simulate the as-is bridge conditions.

Live loading was applied according to the truck dimensions, axle weights, and transverse axle locations for the static field testing discussed in Chapter 5. Prior to processing data, deflected shapes of the model were verified at various truck positions. Figure 8.13 shows the deflected shape for a truck positioned in the first span for the outer load path. The plotted deflections are not to scale.
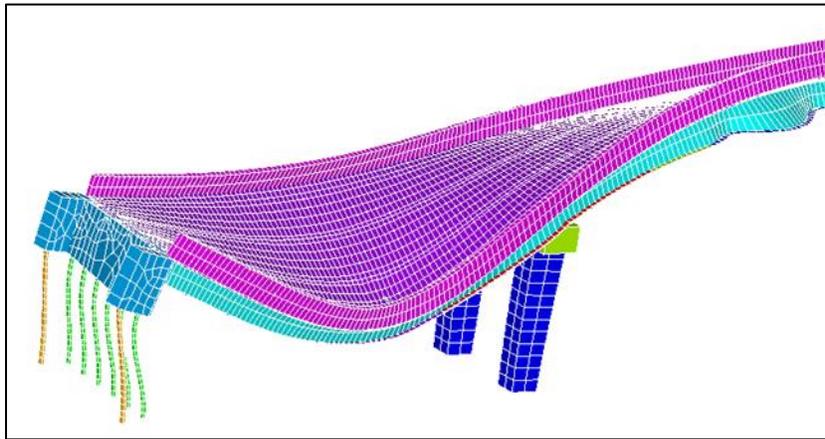
Figure 8.13. Deflected shape for outer truck position

Once several deflected shapes were plotted and reviewed, the girder strains were extracted at Bridge Sections 1 and 2. The FEM strains were then directly compared to the strains in the field. Directly comparing strains reduced the potential of discrepancies between FEM composite section calculations and existing field composite sections.

While comparing strains, girder bottom flange strains were of specific interest due to their large magnitudes relative to the top flange strains. Figure 8.14 and Figure 8.15 are typical graphs comparing bottom flange strains at Bridge Section 1 or 2, respectively.
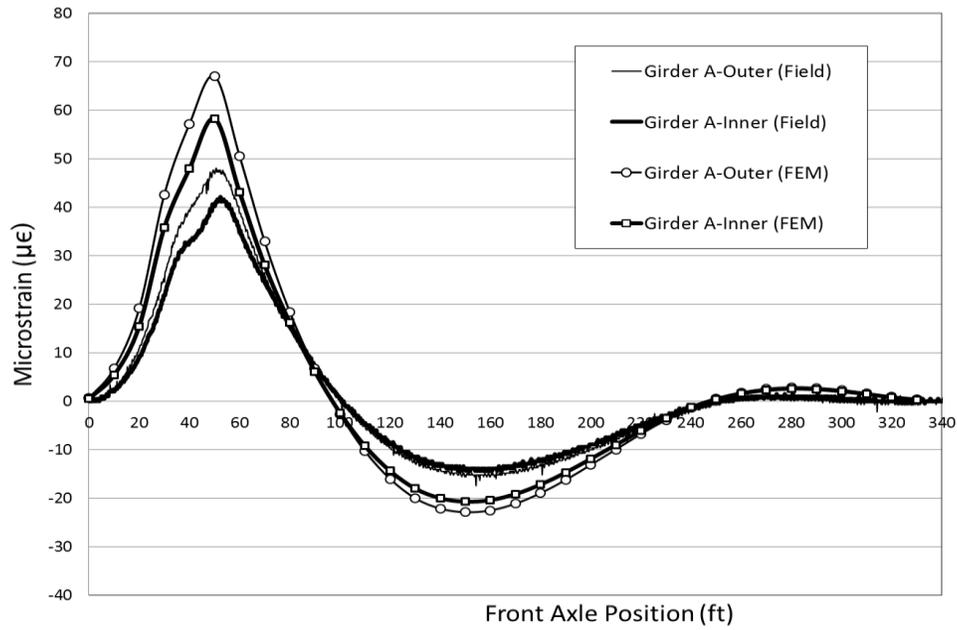
Figure 8.14. Outside path at Section 2 Girder A
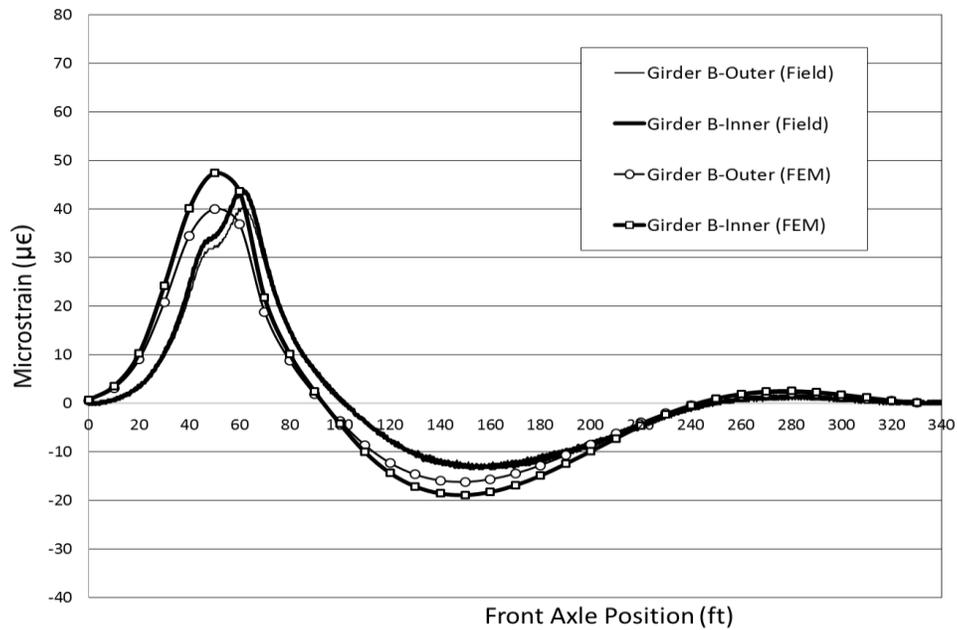
Figure 8.15. Center path at Section 1 Girder B

The comparisons typically shown in Figure 8.14 and Figure 8.15 indicate that the FEM predicted larger bottom flange strains at all girder locations for all three load paths. Upon summing the peak bottom flange strains of all girders at a given bridge section, the results produced

173

differences ranging from 12% to 22% between FEM and field strains. The magnitude of difference was least when the truck was centered and at Bridge Section 1. Since Bridge Section 1 is located between two diaphragm sets, results may indicate that the behavior of the modeled girder-diaphragm interaction diverges from the actual field condition.

In addition to the increased values presented by the FEM, another key behavior is also shown in Figure 8.14 and Figure 8.15. The FEM coordinated to the field with respect to outer versus inner flange tip strain variations. Results from the FEM show the outer and inner flange tips varying in strain magnitudes. This trend validates that the FEM not only predicted lateral bottom flange bending behavior that is present in horizontally curved girders, but also the correct direction of the lateral flange bending as it relates to the field results. Figure 8.16, viewed from the bottom of the superstructure, plots laterally deflected girders for a centered truck in the first span of Bridge 309.
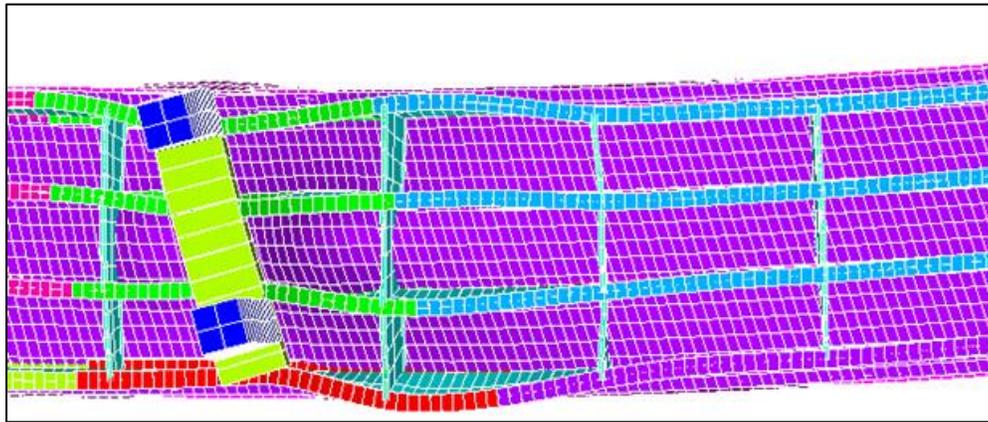
Figure 8.16. Laterally-deflected girders

A tabular summary is presented in Table 8.3 through Table 8.5, comparing maximum girder strains averaged across the bottom flange width for the three truck paths.

Table 8.3. Center load path average bottom flange strain ($\mu\varepsilon$)

Girder	Bridge Section 1				Bridge Section 2			
	A	**B**	**C**	**D**	**A**	**B**	**C**	**D**
FEM	33	44	43	30	34	38	37	29
Field	26	42	42	20	24	36	37	19
% Diff.	21	4	1	33	31	5	7	37

Table 8.4. Outside load path bottom flange strain ($\mu\varepsilon$)

Girder	Bridge Section 1				Bridge Section 2			
	A	**B**	**C**	**D**	**A**	**B**	**C**	**D**
FEM	63	54	25	8	63	48	28	8
Field	51	48	20	6	45	40	22	7
% Diff.	*19*	*11*	*18*	*25*	*28*	*15*	*19*	*22*

Table 8.5. Inside load path bottom flange strain ($\mu\varepsilon$)

Girder	Bridge Section 1				Bridge Section 2			
	A	B	C	D	A	B	C	D
FEM	11	25	53	62	12	27	43	57
Field	8	20	44	52	8	20	37	47
% Diff.	*33*	*21*	*18*	*18*	*32*	*25*	*12*	*19*

From the results presented in the previous tables, it was concluded analytical values match experimental field tests reasonably well. Based on these results, the FEM validation is considered acceptable with respect to the field results.

8.3.3 Validation to Thermal Analysis

Reported in Chapter 6, the field study measured the temperatures in the steel girders and the concrete deck, the strains in steel girders and backwall pressures at abutments. The measured field data at two time instants (i.e., 1/21/2011 6:00 and 7/19/2011 6:00) during cold and hot weathers respectively are selected to validate the FE model as shown in Table 1. The differences of strains between the two time instants were mainly induced by the change of temperatures in the concrete deck and steel girders and backwall pressures at abutments in Table 2. The ranges of temperatures and backwall pressures are calculated in Table 1. As indicated in Table 1, the temperature ranges are almost the same in all girders A and D at different spans. Thus, a uniform temperature change of the average value 86.7 ℉ is applied to all the steel sections of the superstructures in the FE model. The temperature change of 89.0 ℉ is applied to concrete deck and parapets. The average backwall pressure of 11.7 psi is applied to both south and north abutments.

The ranges of axial strains in the sections of girders A and D at mid-center span are calculated using the FE model and summarized in Table 2. As indicated Table 2, the strains in Girders A and D at the mid-center span predicted using the FE model compare well with the field data.

Table 8.6. Ranges of measured temperatures and strains in Girders A and D at different spans and backwall pressure at abutments

	Temperature Range (℉)							Back Wall Pressure Range (psi)	
	Mid-South Span		Mid-Center Span		Mid-North Span		Concrete Deck	South Abutment	North Abutment
	A	D	A	D	A	D			
1/21/2011 6:00	-1.5	-1.7	-1.2	-0.4	-0.9	-1.1	-1.6	0.2	0.1
7/19/2011 6:00	85	85.3	85.1	85.8	86.2	85.8	87.4	13.6	10
Differences	86.5	87.0	86.3	86.2	87.1	86.9	89.0	13.4	9.9
Average	86.7						89.0	11.7	

Note: *A* – Girder A; *D* – Girder D

Table 8.7. Strain range comparison between field data and FEM results

	Strain Ranges in Mid-Center Span (10^{-6})	
	Girder A	Girder D
Field Data	-95	-151
FEM Results	-122	-133

8.3.4 Validation to Consultant Model

Similar to the field study comparison, changes in the FEM needed to be made to compare with the consultant model. The goal was to create a FEM that closely resembled the geometry of the consultant design model for Bridge 309. In practice, designers do not consider the parapets to contribute to the structural stiffness of the superstructure. Therefore, the parapets were removed for this stage of validation. Substructure entities were also removed for the consultant comparison. Simply supported conditions, discussed in Section 8.2.4, were applied in place of the substructure abutments and piers to correlate with the design practice of the consultant. With these changes, the only known differences between the consultant model and the FEM pertained to mesh sizes. The consultant meshed one element through the depth of the girder webs and diaphragm webs with aspect ratios near 1:1. Also, deck elements were approximately twice the size in the consultant model, compared to the FEM.

Once geometric model comparisons were finished, live loading was then applied in similar fashion to the field study model for both the FEM and consultant analyses. Only the center and outside load paths were considered. In post-processing, deflected shapes of the model were verified at various truck positions. Figure 8.17 illustrates the deflected shape for a truck positioned in the first span for the center load path. The simple supports are represented by triangles at the abutment and first pier. All deflected shapes for the live load positions, similar to Figure 8.17, agreed with the assumed overall structural behavior of the bridge.
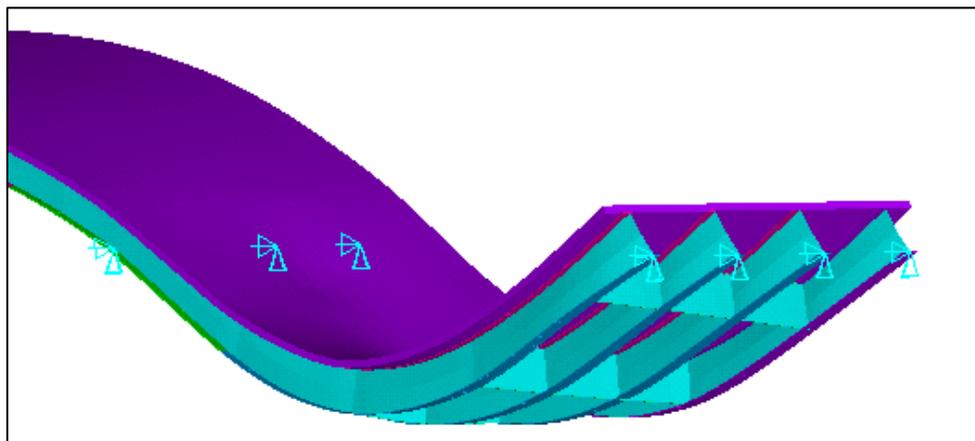
Figure 8.17. Deflected shape for center truck position

Next, the FEM output was compared to the supplied output from the consultant design model. The consultant presented results in terms of strong axis bending moments and lateral bottom flange bending moments. The consultant determined strong axis bending moments based on nodal force extractions in the composite section, Figure 8.18. Element nodal forces for the top and bottom flange, top and bottom node of the web plate, and one nodal force in the deck plate on each side of the girder were extracted. With the extracted forces and known locations, the moment of the section could be summed about the section's neutral axis.
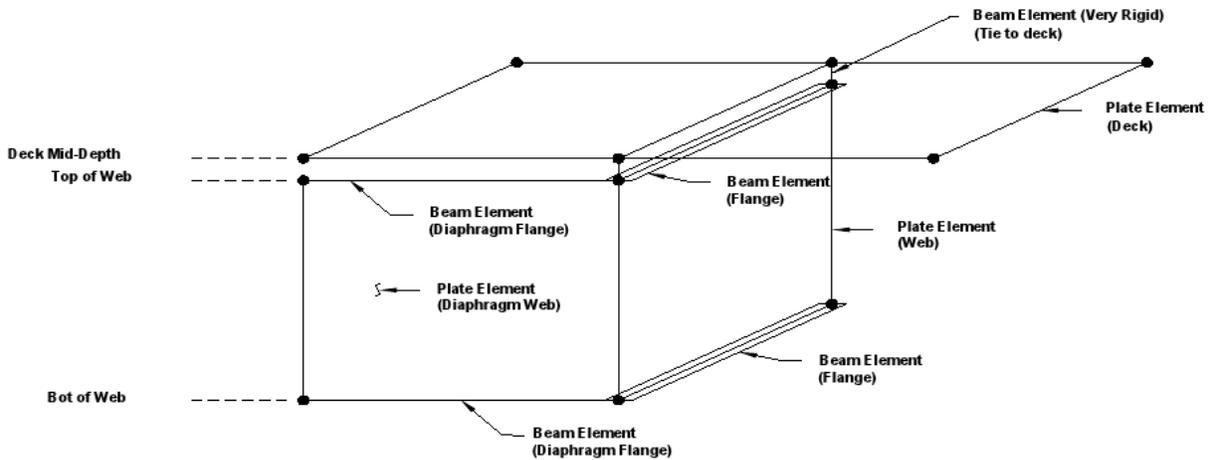
Figure 8.18. Composite section presented by consultant

The consultant's procedure of determining strong axis bending moments in the composite section differed from those used in this study. Recall that moments were calculated from internal composite section forces, described in Section 6.2.1. The results from the consultant's procedure would give the opportunity to validate the data reduction procedure in this study.

The validation compared calculated moments at Bridge Sections 1 and 2 for the two indicated load paths. Typical strong axis moments and lateral bottom flange moments calculated in the FEM are represented in Figure 8.19 and Figure 8.20, respectively, for all four girders. Each of the four girders was then directly compared to the consultant's results. Figure 8.21 and Figure 8.22 represent typical comparisons to lateral flange bending moments and strong axis bending moments for Girder A.
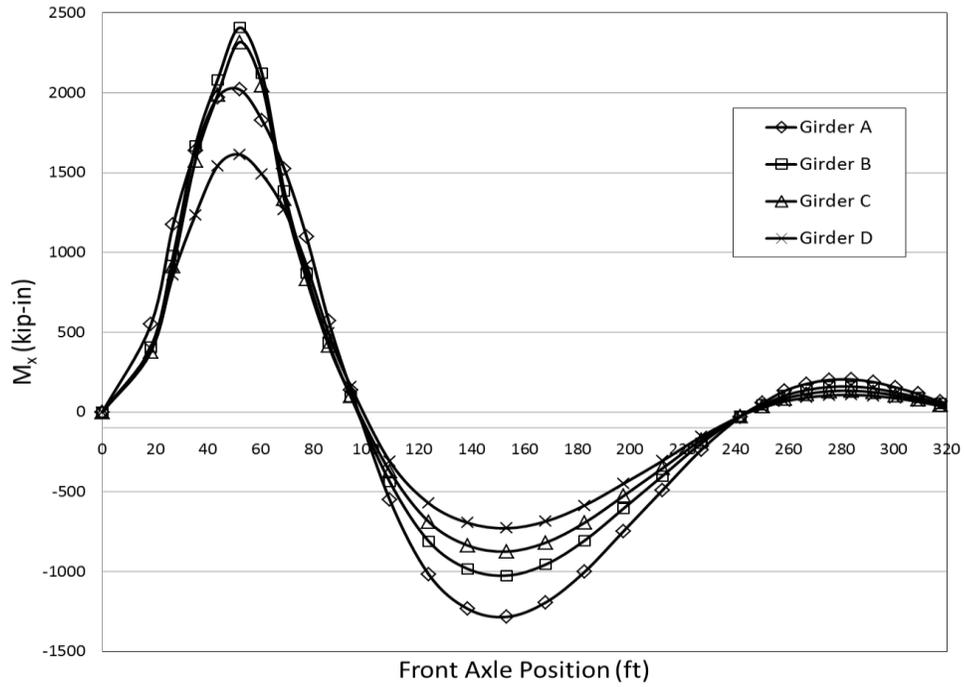
Figure 8.19. FEM center path at Section 1
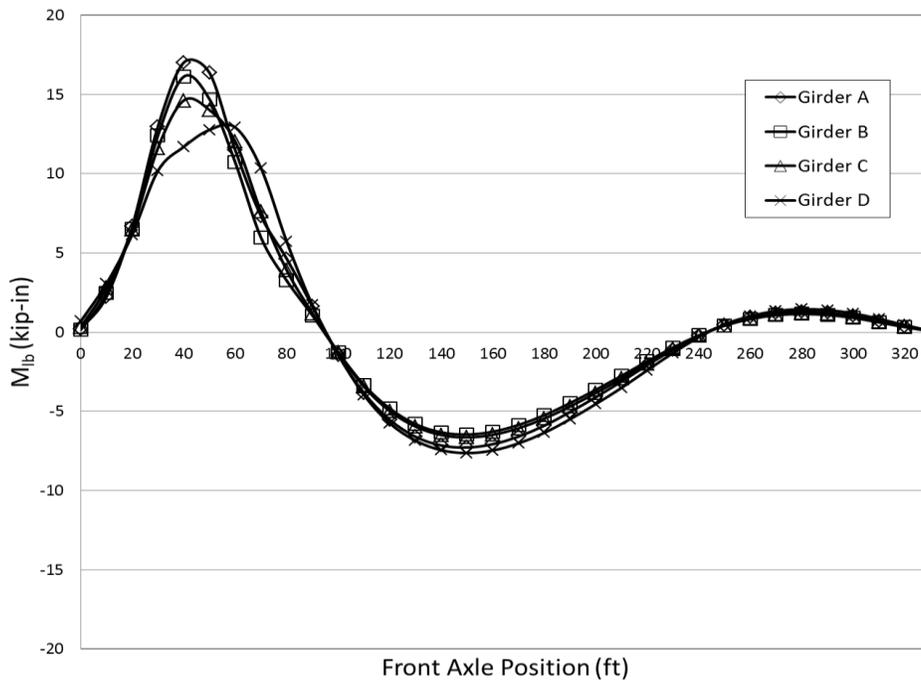
Figure 8.20. FEM center path at Section 2

178
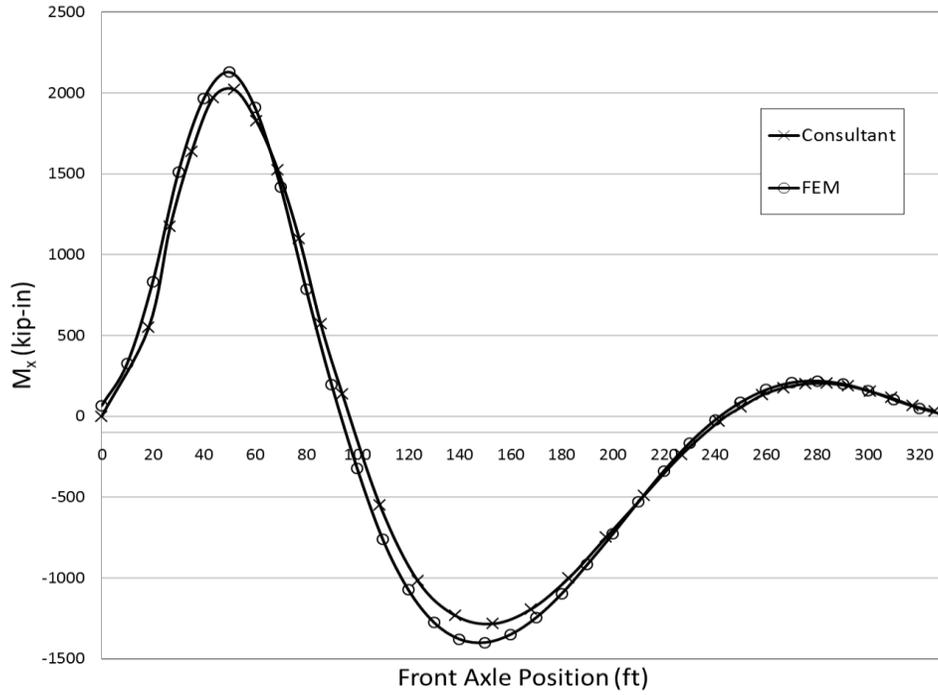
Figure 8.21. Girder A center path at Section 1
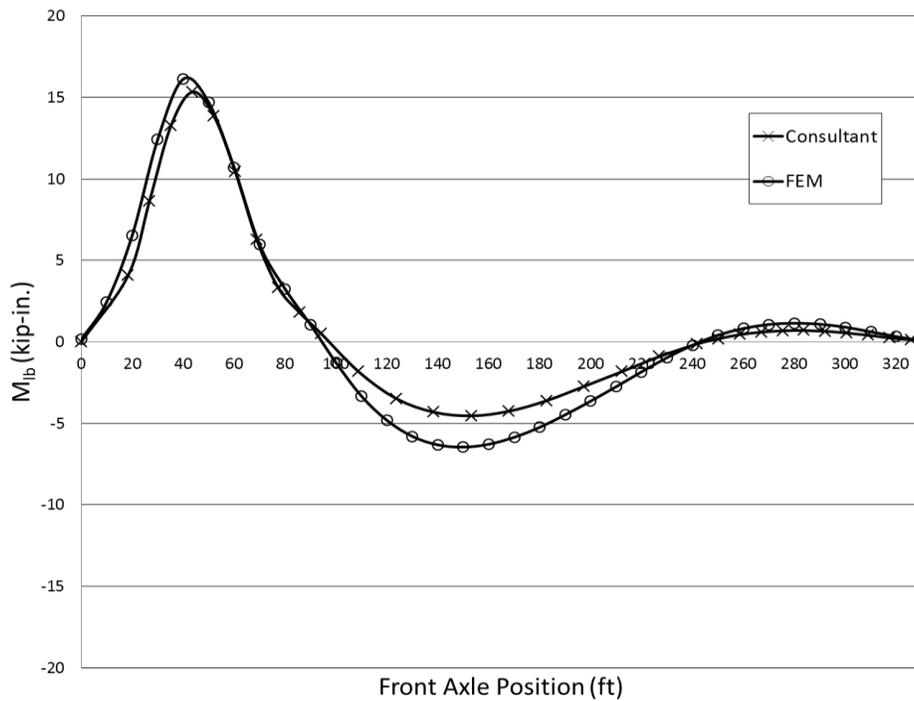
Figure 8.22. Girder C center path at Section 2

179

Strong axis moments differed between the FEM and consultant by an average 6.0% at peak truck locations in all girder sections. Furthermore, lateral bottom flange moments differed by less than 4.0 kip-in at peak truck locations in all girder sections. The FEM validation is considered acceptable with respect to the consultant's design model.

8.4 Design Loading

8.4.1 Load Factors and Combinations

With the validation complete, the study then investigated design loading conditions. The loading conditions selected were based on the design limit states in accordance with the *AASHTO LRFD* specification. For the scope of this study, the Strength I and Service I load combinations from Table 3.4.1-1 in *AASHTO LRFD* were assumed to govern the design. These load combinations included components for dead load, live load, water load, thermal load, wind load, settlement, and friction load. However, for the scope of this study, only the dead, live, and thermal loads were considered. In reference to Table 3.4.1-1, the following variables will be used.

DC=*dead load of structural components and nonstructural attachments*
LL=*vehicular live load*
IM=*vehicular dynamic load allowance*
TU=*force effect due to uniform temperature*
TG=*force effect due to temperature gradient*
γ_p=*load factor for permanent loads*
γ_{TG}=*load factor for temperature gradient*
γ_{TU}=*load factor for uniform temperature*

Equations 8.1 and 8.2 represent the load combinations considered throughout Chapter 8. Values for the given load factors will be addressed in Sections 8.4.2 through 8.4.4.

$$\text{Strength I} = \gamma_p DC + 1.75 LL(1+IM/100) + \gamma_{TU}TU + \gamma_{TG}TG \tag{8.3}$$

$$\text{Service I} = 1.00DC + 1.00LL(1+IM/100) + \gamma_{TU}TU + \gamma_{TG}TG \tag{8.4}$$

8.4.2 Dead Load

Dead loads from the structural components included the weights of the deck, steel girders, steel diaphragms, and parapets. Material densities from Table 8.1 and Table 8.2 were assigned to the proper structural components in the model. In addition to the self-weight of the modeled components, the weights of the parapets were calculated based on their average cross sectional area of 440 in^2. A distributed weight of 0.268×10^{-2} k/in^2 was applied over the length of the bridge in place of their footprint on the bridge deck.

Maximum and minimum load factors, γ_p, of 1.25 and 0.90 were applied for the Strength I load combination. The minimum load factor was used when the force results from the live load were not additive to the dead load results.

8.4.3 Live Load

Vehicular live loading was designated by the HL-93 load case, consisting of the combination of a design truck or design tandem in both lanes, and the design lane load. The combination of the design truck with the design lane load were assumed to govern for this work. Design lanes are 12.0 ft wide and the number of design lanes is based on the roadway width. Bridge 309 has a 26.0 ft roadway width, so the number of design lanes equals two.

The 0.64 klf uniformly distributed design lane load occupies a 10.0 ft transverse width within the design lane. The load was distributed over the entire length of the bridge and superimposed on top of the design truck load. Axle spacing and weights for the design truck load are specified in Figure 8.23. Rear axle spacing varies between 14.0 ft and 30.0 ft to produce maximum force effects. For the scope of this study, the 14.0 ft axle spacing was assumed to control. Since Bridge 309 has two design lanes, two design trucks were placed side by side at increments of 10.0 ft along the bridge centerline. Placing the trucks side by side would produce maximum responses to live load.
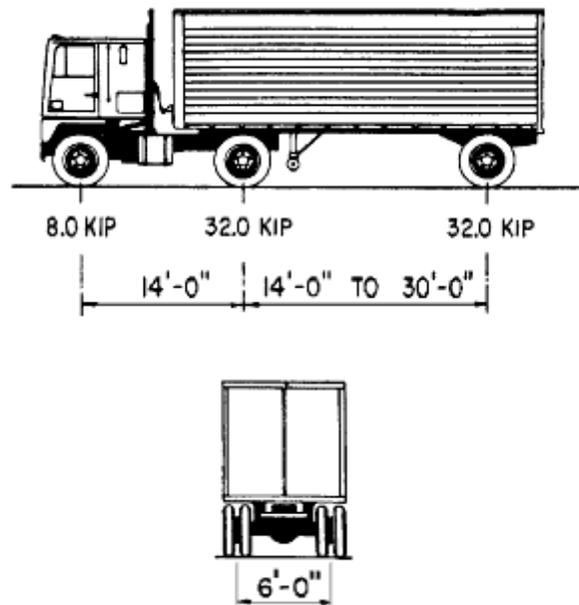
Figure 8.23. Design truck specifications (from Figure 3.6.1.2.2-1 AASHTO 2010)

Load factors for Strength I and Service I load combinations were taken as 1.75 and 1.00, respectively. A vehicular dynamic load allowance of 33% was applied to the static live load application for both load combinations. Note that only the design truck is subject to the *IM*.

181

8.4.4 Thermal Load

Design loads also considered two thermal loads, uniform temperature and temperature gradient. Shown in Figure 8.24, uniform temperature is applied to the entire depth of the superstructure. Procedure A from Section 3.12.2.1 in AASHTO LRFD was used to determine the maximum and minimum temperatures for the model. Table 8.8 lists the temperature ranges Bridge 309 experiences. Temperature ranges are based on the classification of the bridge due to material type and location. Bridge 309 classifies as a steel or aluminum structure located in a cold climate. A cold climate is defined as having more than 14 days with average temperatures less than 32°F.
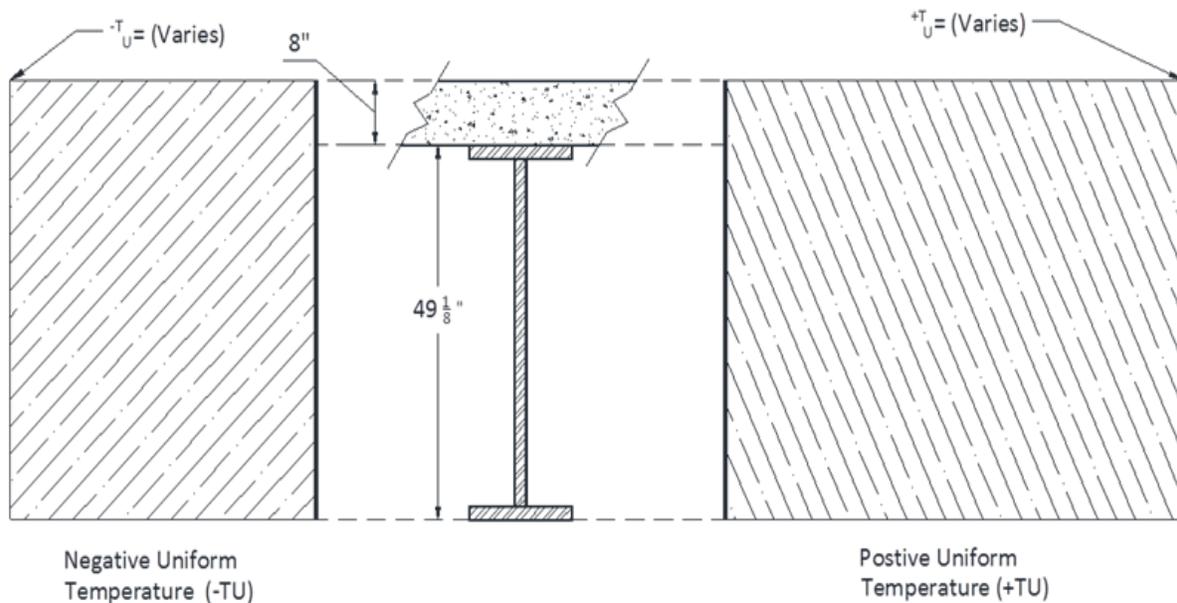
Figure 8.24. Uniform temperature distribution

Table 8.8. Uniform temperature values

Temperature Range	Lock-in Temperatures	+TU	-TU
-30 to 120^{0}F	40 and 80^{0}F	80^{0}F	-110^{0}F

The thermal analysis assumed two lock-in temperatures for a positive (+TU) and negative (-TU) temperature change. Lock-in temperatures were based on acceptable temperatures for placing concrete during construction. By choosing the upper and lower bounds for acceptable pouring temperatures, the positive and negative uniform temperatures changes could then be chosen accordingly, listed in Table 8.8. For a positive uniform temperature change, the lock-in temperature was assumed to be 40°F; yielding +TU equal to 80°F to reach the upper temperature range of 120°F. For a negative uniform temperature change, the lock in temperature was assumed to be 80°F; yielding -TU equal to -110°F to reach the lower range of -30°F.

Figure 8.25 diagrams the temperature gradients applied to the superstructure. Temperature 1 (T_1) and temperature 2 (T_2), for the positive temperature gradient, were selected based on the geographic bridge location in Section 3.12.3 in the *AASHTO LRFD* specification. Temperature 3 (T_3) was calculated from the cross section depth shown in Figure 8.25. For steel superstructures, A=12.0 in. and the location of T_2 is 4.0 in. from the top of the deck. Negative values were obtained by multiplying the positive values by -0.30 for plain concrete decks with no asphalt overlay.
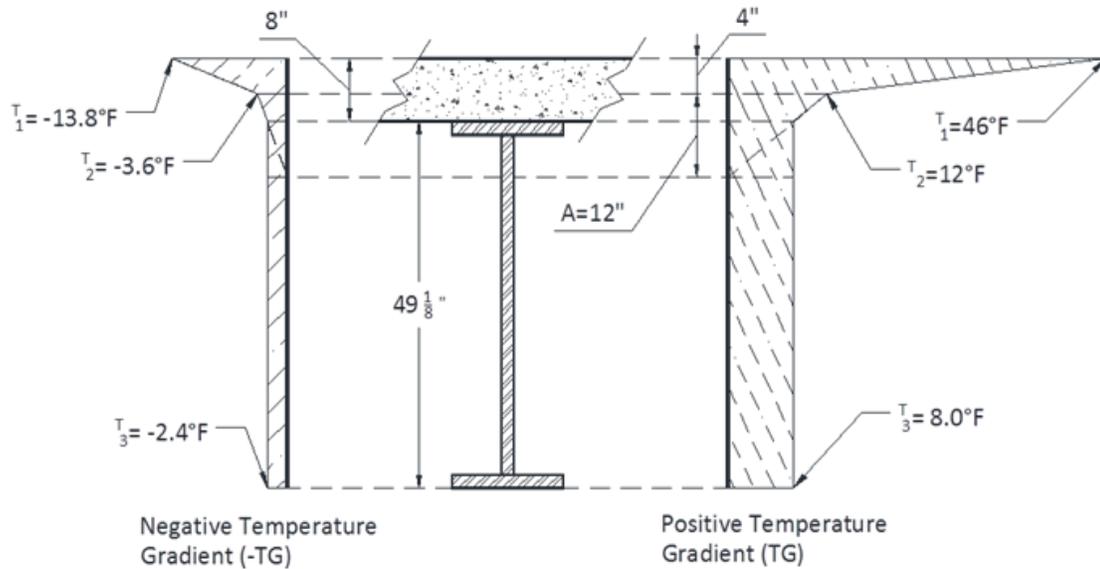
Figure 8.25. Temperature gradient

8.5 Results and Observations

In order to narrow the exploration of the design loading conditions, the study focused on results near approximate maximum positive and maximum negative moment regions. Strains were extracted for each of the four girders at seven cross sections along Bridge 309. Three mid-span cross sections representing positive moment regions and four support cross sections for negative moment regions. The sections located at mid-span are parallel to the bridge radius while the sections near supports are parallel to the bridge skew. Recall that the supports align with the bridge skew and intermediate diaphragms align with the radius.

8.5.1 Preliminary Results

A preliminary review of results indicated that typical trends could be characterized by two of the seven cross sections. The center span cross section represented girder behavior for maximum positive moment regions. The cross section at the fixed north pier represented girder behavior for maximum negative moment regions. Initial results concentrated on relative magnitudes of strong axis bending, lateral bending in the bottom flange, and axial forces for each loading condition.

Girder A, the outside girder, typically produced the maximum results at the center span and north pier cross sections. Table 8.9 and Table 8.10 tabulate the unfactored internal forces for each of the design loads in Girder A.

Table 8.9. Girder A unfactored internal forces at north pier

N. Pier	DL	LL	T(+)	T(-)
M_x (kip-ft)	-1730	-745	98.4	-172
M_{lb} (kip-ft)	8.9	5.7	-23.3	31.0
P (kip)	24.0	10.7	-150.2	328

Table 8.10. Girder A unfactored internal forces at center span

C. Span	DL	LL	T(+)	T(-)
M_x (kip-ft)	1480	1030	-78.4	150
M_{lb} (kip-ft)	-6.0	-4.7	1.2	-2.4
P (kip)	-72.2	-53.3	-70.2	224

Note that live load results were recorded from peak truck positions for each respective cross section. Also, thermal results were separated into positive and negative temperature changes. Each temperature change combined both uniform and gradient temperatures, previously specified.

Influences of thermal loadings proved to be present upon further assessment of Table 8.9 and Table 8.10. A negative temperature change produced a strong axis moment nearly one-quarter of the moment due to live loading at the north pier. Furthermore, lateral flange moments were over six times greater than the lateral flange moments produced by the live load. Finally, thermal axial loads were significantly greater than that of dead and live load results for all girder cross sections.

Even though the contributions of temperature are to be included in Strength I and Service I limit states according to AASHTO LRFD, bridge designers sometimes neglect the influences of thermal loadings. The designers may make conservative assumptions for boundary conditions and degrees of fixity within the structure to offset the omission of possible internal thermal forces. Increased efforts and uncertainty in thermal analysis leads designers away from assessing thermal loads because their influence is assumed insignificant. Regarding superstructure design, temperatures are only taken into account in extreme design cases, deemed necessary by designer or owner. However, since the above tables suggest that thermal loads may have contributions to design load conditions, the study further investigated the matter. The proceeding figures in this chapter help determine the significance of including thermal loading and/ or modeling substructure entities.

To determine the significance, two different models will be compared in this section. This study attempted to decide whether that assumption is appropriate by plotting the load effects for the simply supported model, referred to as the "Simple" model, versus the model that included the abutments and piers, referred to as the "Full" model. In summary, the models are as follows:

- Full model: includes abutments, piers, and applies thermal, dead, and live loads (results represented by solid lines in accompanying figures)
- Simple model: assumes simple supports and applies only dead and live loads (results represented by dashed lines in accompanying figures)

8.5.2 Service I Load Conditions

Strong Axis Bending

Girder responses to individual Service I load conditions were plotted for all four girders at the north pier and center span cross sections. Figure 8.26 and Figure 8.27 plot the strong axis moment results for the Service I load cases. Service I strong axis moments due to thermal loads prove to be noticeable but less influential compared to the dead and live load results. Thermal strong axis moments contributed a maximum of 8.8% to the total negative moment at the north pier in Girder C. Temperature had an even less significant influence at the center span where the maximum contribution to the total moment is 5.8% in Girder A.

Replacing substructure entities with the simply supported model produced negligible differences in results. Less than a 3% increase in strong axis moments (center span) due to dead load and live load were present. This slight increase may suggest the simply supported conditions do not increase results due to dead and live load as assumed by consultant
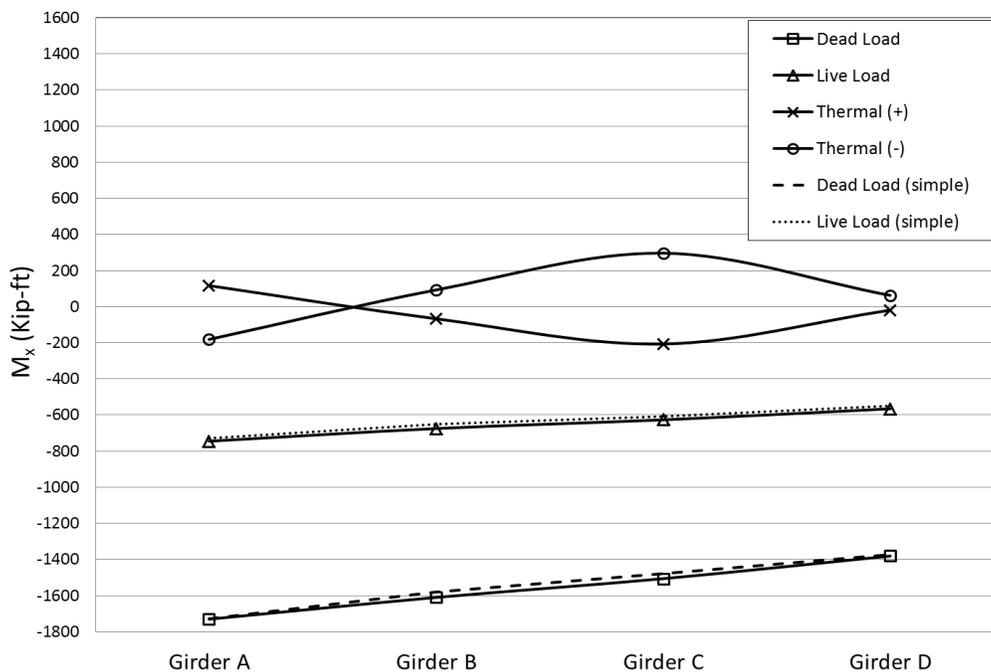
Figure 8.26. North pier Service I loads

185
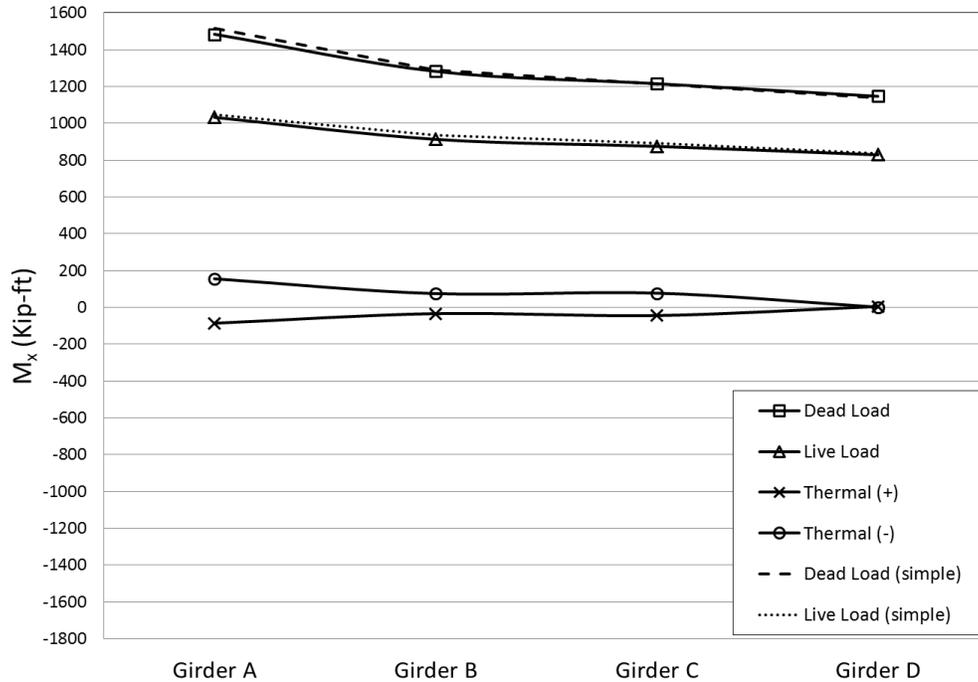
Figure 8.27. Center span Service I loads

Lateral Bottom Flange Bending

Figure 8.28 and Figure 8.29 show the lateral bending moment in the bottom flange for factored Service I level loads. Results indicate that thermal lateral bending moments in the bottom flanges ranged from -57 kip-ft to 43 kip-ft at the north pier. Lateral bending moments in the bottom flanges for thermal loads were greater than dead or live loads in Girders A, B, and D at the north pier. The exterior two girders, A and D, had the largest responses to temperature. After combining dead, live, and thermal lateral moments in Girder D, a positive temperature increase contributed to nearly 50% of the sum. Conversely, thermal lateral bending moments were rather insignificant at the center span.

Replacing the substructure entities with simply supported conditions yielded smaller lateral bending moments in the bottom flanges for dead and live load conditions. Figure 8.28 and Figure 8.29 illustrate that the simply supported model produced smaller lateral moments in the bottom flanges in all girders at both negative and positive moment regions. The simply supported assumption proves to be unconservative with respect to lateral bending in the bottom flange, particularly at the pier.

186
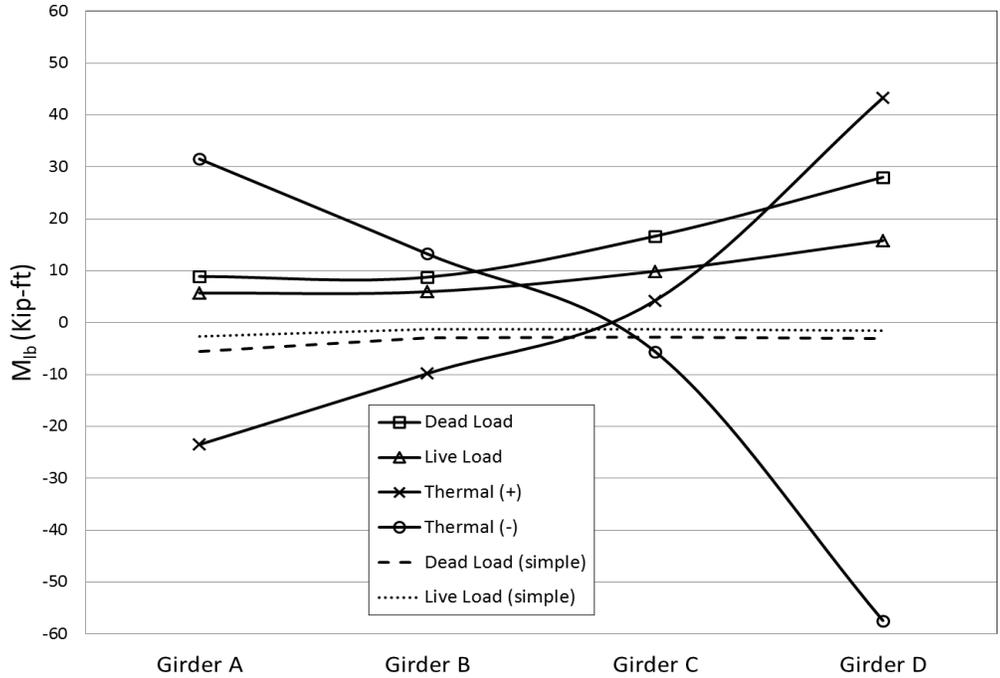
Figure 8.28. North pier Service I loads
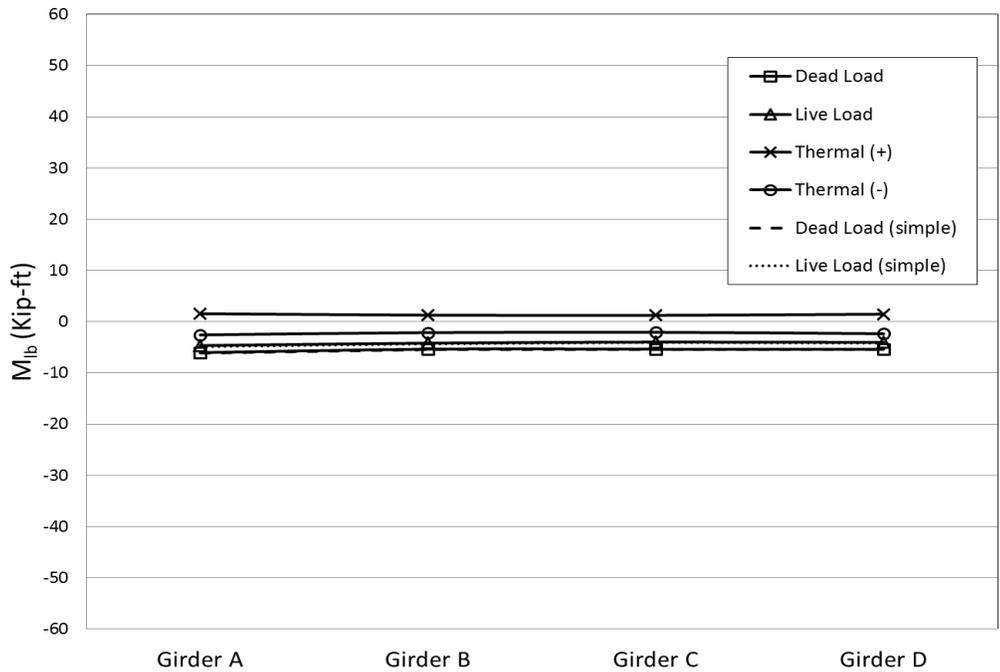
Figure 8.29. Center span Service I loads

Figure 8.30 demonstrates the cause of increased lateral bending in the bottom flanges at support locations based on simple mechanics of materials. A non-composite undeformed curved member

187

subjected to a constant increase in temperature will uniformly increase in overall length and radius of curvature. Support conditions at the piers and abutments in Bridge 309, represented in Figure 8.30, restrain translational movement. Thus, the piers hinder the uniform deformation of the member, especially the lower flange, which is connected directly to the pier.
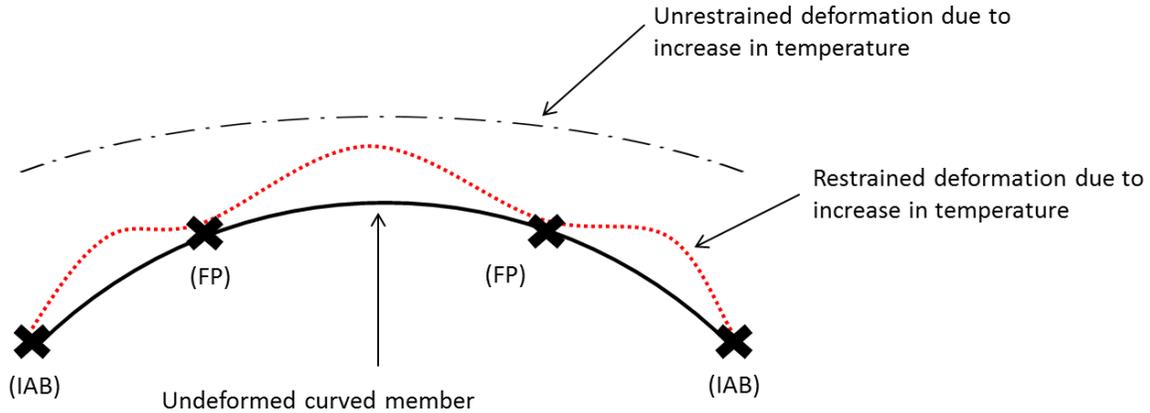
Figure 8.30. Curved member subjected to temperature increase

Figure 8.31 plots the FEM deformed shape of Girder A at the north pier due to an increase in temperature. Restraining the deformation of the horizontally curved member increased lateral bending, particularly in the bottom flange, at the fixed pier location. The development of Figure 8.30 and the results presented in Figure 8.28 and Figure 8.31 call special attention to lateral bottom flange bending due to temperature changes at fixed pier locations.
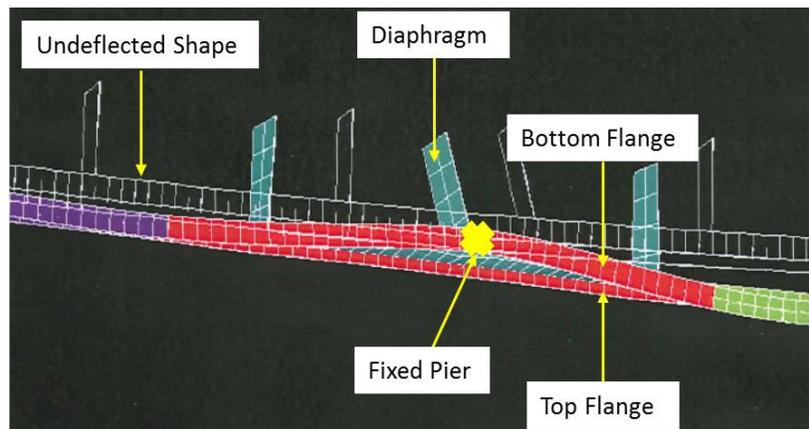
Figure 8.31. Girder A deflected shape due to T(+)

Axial Forces

Figure 8.32 and Figure 8.33 plot the axial forces from Service I loading conditions. Axial forces due to thermal loads are much greater compared to the dead and live load conditions at both the north pier and center span. Temperature changes produced average girder axial forces ranging from -217 to 358 kips and -195 to 326 kips at the north pier and center span, respectively. The

axial forces produced at the north pier due to dead and live loads are small in comparison to the thermal results. At the center span, girder axial forces due to combined dead and live loads had a greater influence with an average of -141 kips.

Incorporating simply supported conditions had little effect on axial forces at the north pier due to the negligible results produced from dead and live loads. However, at the center span, girder axial forces from the simply supported model produced an average -67 kips due to combined dead and live load. Only 48% of the axial forces produced by incorporating the substructure model were present in the Simple model. Again, the assumption of replacing substructure entities with simply supported conditions proves to be unconservative with respect to axial forces produced from design loads in the superstructure.
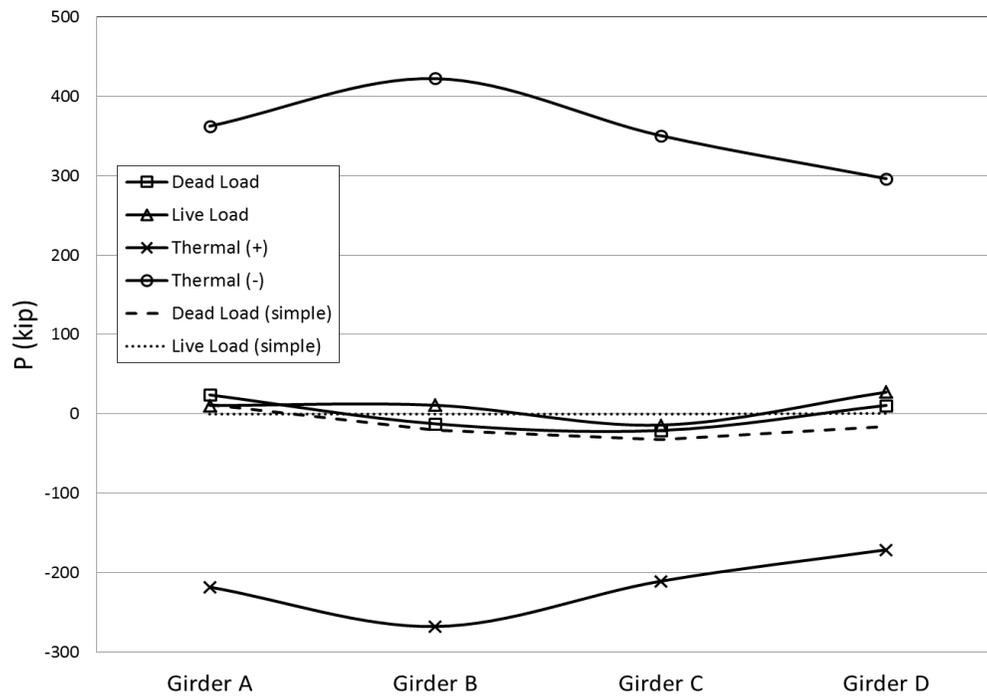
Figure 8.32. North pier Service I loads
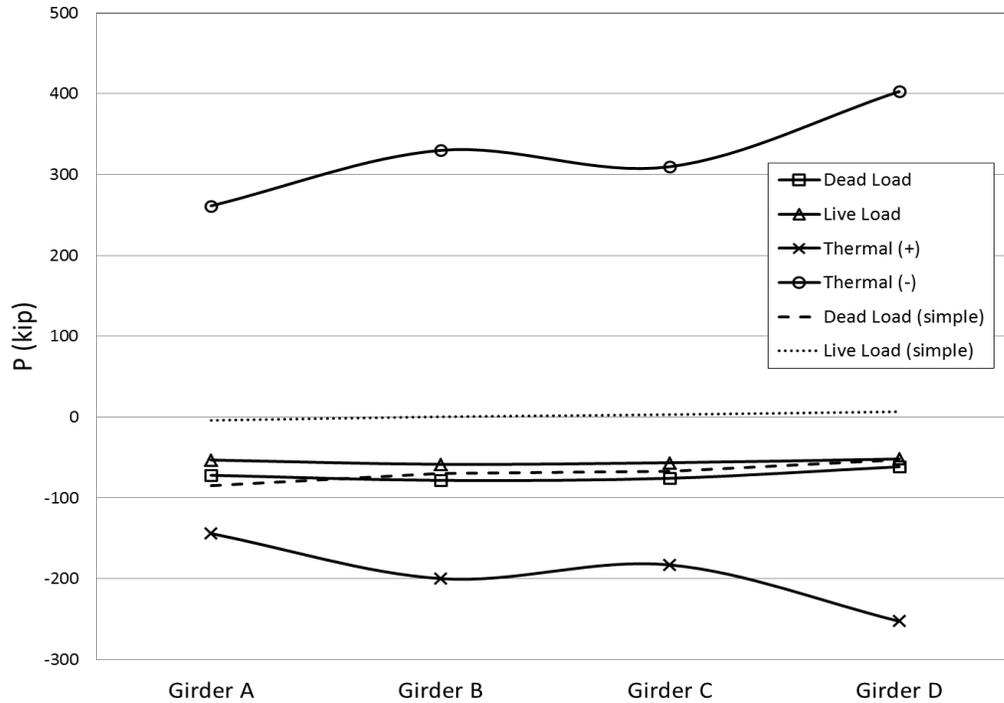
Figure 8.33. Center span Service I loads

Summary

According to the results presented in Figure 8.26 through Figure 8.33, temperature appeared to influence the substructure behavior for Service I level loading conditions. Axial loads due to temperature produced the most significant results as they often accounted for most of the total force at all cross sections along the bridge. Lateral bending moments in the bottom flange proved to be most influential for temperature changes at fixed pier locations, accounting for up to 50% of the total lateral moment in bottom flanges. Strong axis bending moments due to temperature were less influential; however, their presence was still noticeable as they contributed up to 8.8% of the total moment in the composite section. Lastly, removing substructure entities and replacing boundary conditions with the simply supported model proved to be unconservative for the axial forces and lateral bottom flange bending moments.

8.5.3 Load Combinations

Service I level results suggest that thermal loads may be critical in the design of Bridge 309. However, Strength I load conditions often govern the design of girder members. The accompanying graphs of this section compare Service I and Strength I load combinations.

Strong Axis Bending

Figure 8.34 and Figure 8.35 plot the combinations of Strength I and Service I strong axis moments in the composite sections. As noted, a thermal analysis was conducted for both negative and positive temperature changes. The load combinations account for only the thermal analysis that yielded the critical loading combination. In other words, the thermal load results were to be additive to the dead and live load results. The solid lines represent the model that includes the substructure entities and accounts for the thermal loads, referred to as the "Full" model. The dashed lines represent the simply supported model that does not include thermal loads, referred to as "Simple" in the associated figures.

Results in Figure 8.34 and Figure 8.35 show that strong axis moment magnitudes were up to 5.6% more for the Strength I Full model at the north pier compared to the Simple model. Overall, including the substructure and incorporating thermal loads in the analysis provide only slight variances with regards to strong axis composite section moments.

Strength I load factors produced larger moments over the Service I load factors. Magnitudes of Strength I moments were on average 35% and 43% larger than Service I moments for each of the four girders at the north pier and center span, respectively. Therefore, for this case the Strength I load combination governs over the Service I load combinations for strong axis moments, as assumed.
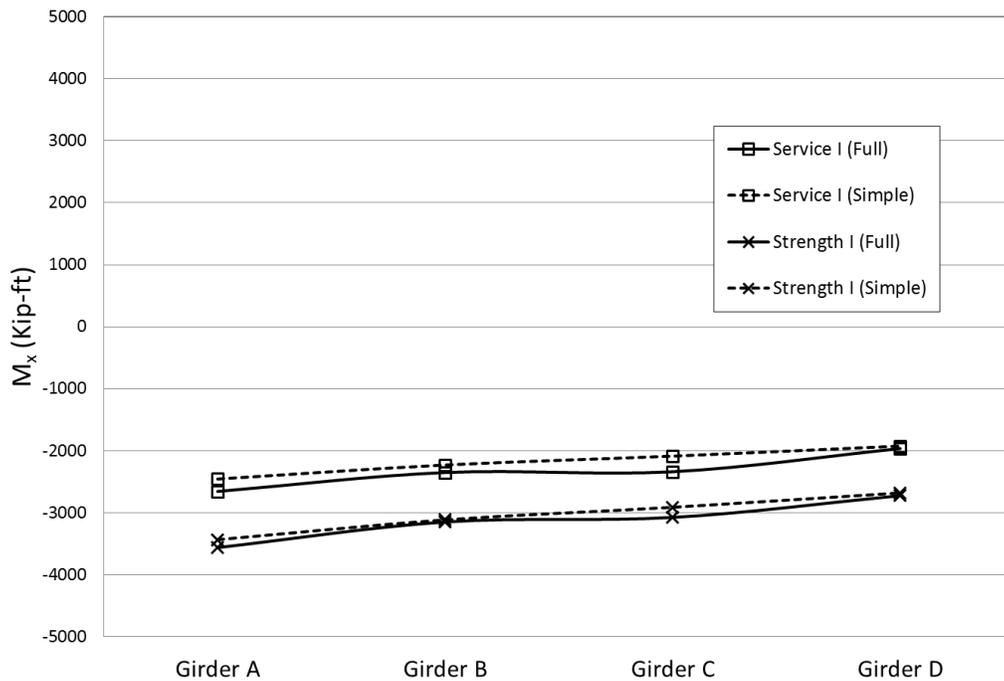
Figure 8.34. North pier load combinations
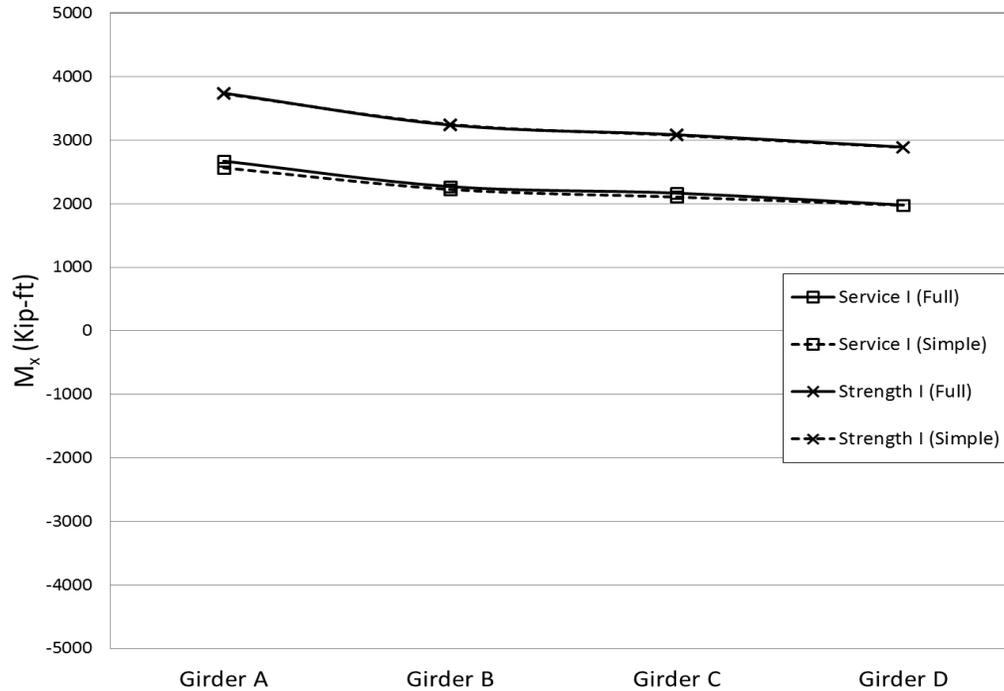
Figure 8.35. Center span load combinations

Lateral Bottom Flange Bending

Figure 8.36 and Figure 8.37 plot the combined loads for the lateral bottom flange bending moments. Again, including thermal loads and substructure entities yield the largest lateral moments. The impact of temperature loads in the Full model is most profound at the fixed pier location. Lateral flange bending moments at the center span are negligible for all loading conditions when compared to the pier locations. Service I produced slightly larger lateral moments in the exterior girder flanges while Strength I produced larger lateral moments in the interior girders. Because the relatively large lateral bottom flange moments are not present in the Simple model, the Full model exemplifies the unique behavior a curved member exhibits from thermal loads at restrained support locations.
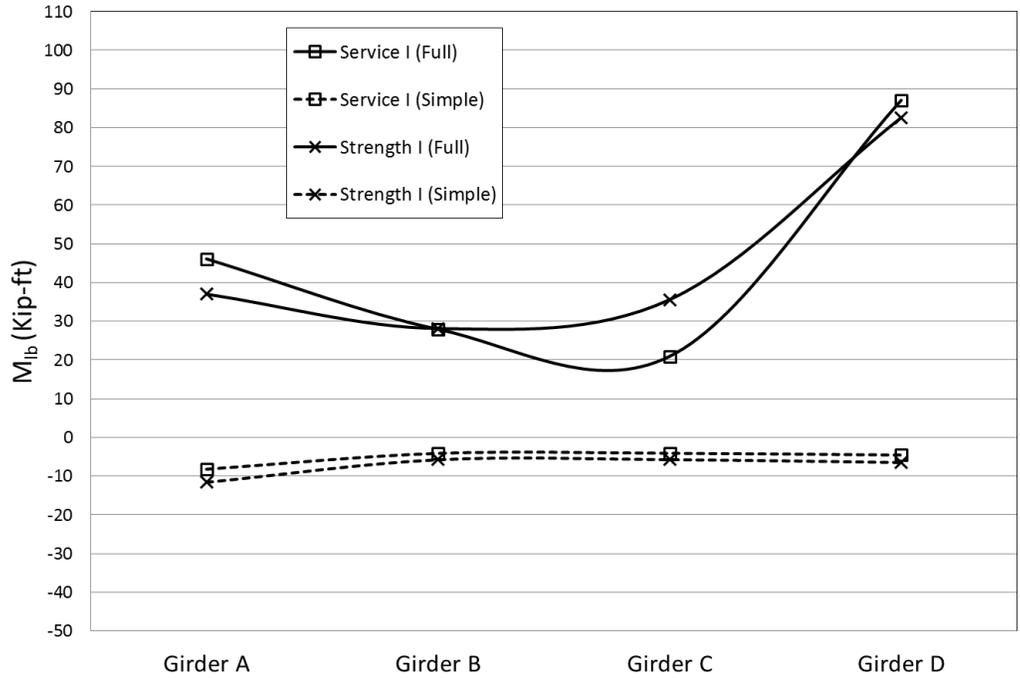
Figure 8.36. North pier load combinations
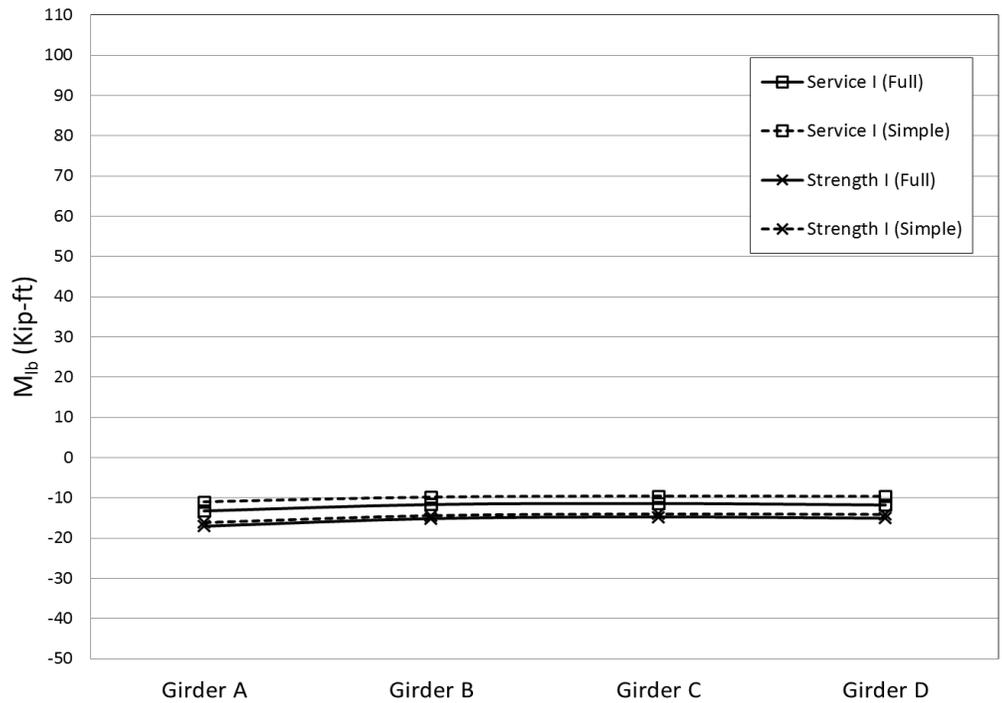
Figure 8.37. Center span load combinations

Axial Forces

Figure 8.38 and Figure 8.39 plot the Service I and Strength I axial load combinations. Service I produced the largest axial forces in all four girders at the north pier and in only Girders A and C at the center span. More importantly, inclusion of the substructure model and thermal effects yielded axial load magnitudes up to 12 times greater than the Simple model. This large increase emphasizes the significance of a thermal analysis for determining axial loads.
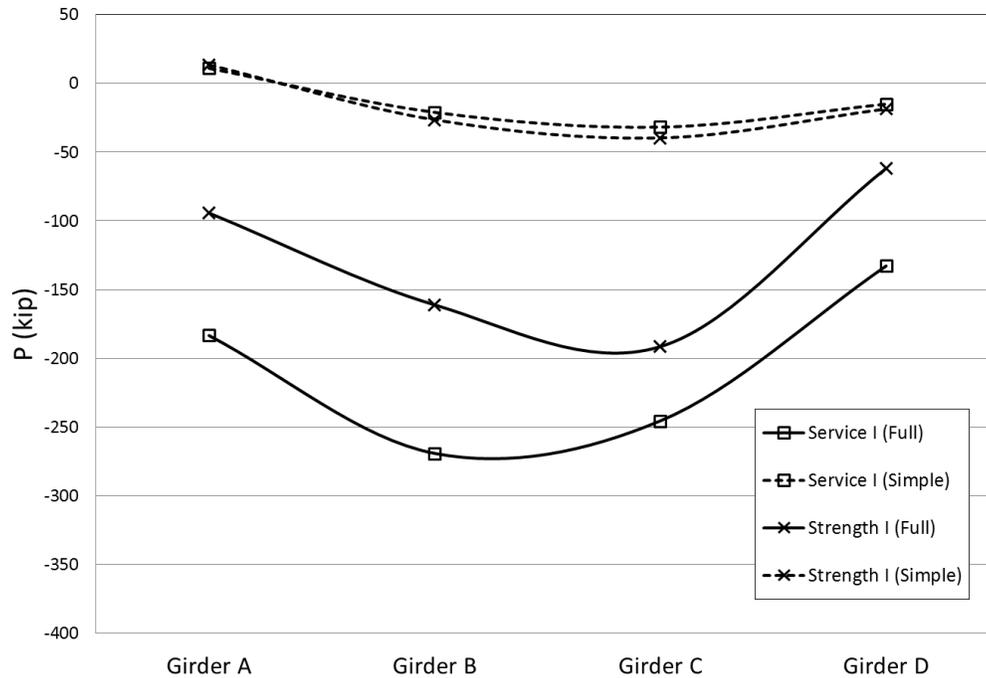
Figure 8.38. North pier load combinations

194
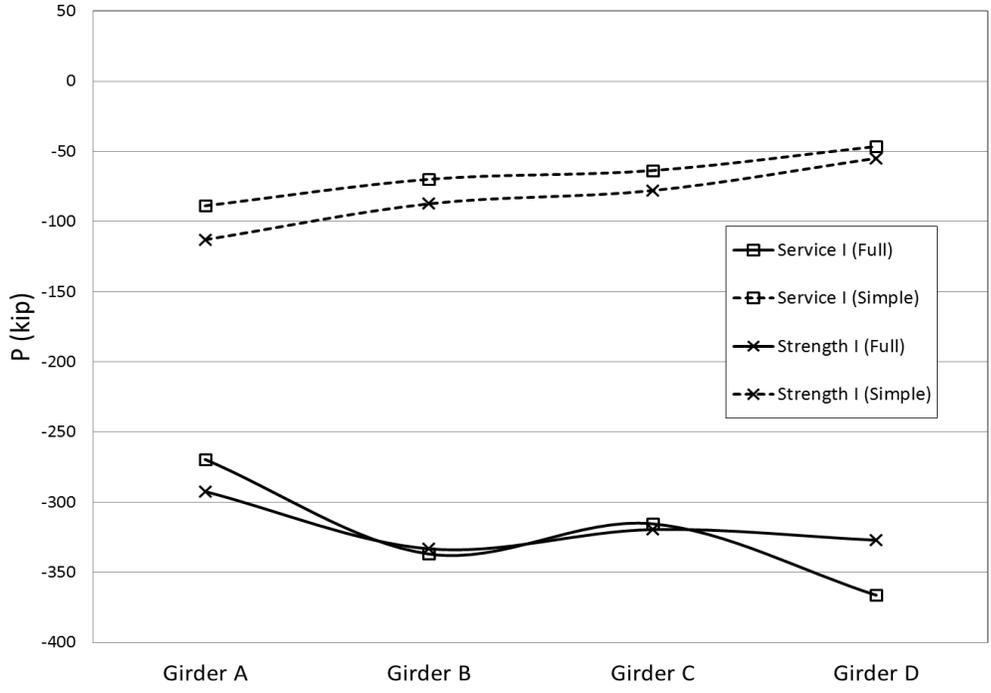
Figure 8.39. Center span load combinations

Stresses

Observations from Figure 8.34 through Figure 8.39 indicate that both Strength I and Service I load combinations are highly dependent on including a thermal analysis to assess strong axis moments, lateral bottom flange moments, and axial forces in a girder section. Even though the internal moments and forces, i.e., stress resultants, produced from temperature changes are noteworthy, it was deemed necessary to study the effects temperature has on the stress levels. So, for example, even though the effect of temperature on bottom flange bending moment may be large, the effect of the bottom flange bending stress may be small relative to the major axis bending stresses produced from dead and live load.

Table 8.11 and Table 8.12 tabulate the Strength I design load stresses at the north pier and center span cross sections from the Full model. Results are in terms of internal components consisting of strong axis bending stress, σ_x; lateral bottom flange bending stress, σ_{lb}; and axial stress, σ_a. Additionally, the last four rows in Table 8.11 and Table 8.12 provide the total individual girder stress, $\Sigma\sigma_{total}$, for each loading case as well as the stresses from combined loading.

As previously stated, the stresses presented in Table 8.11 and Table 8.12 represent only two locations--a small portion of the design stresses that are considered in practice for all cross sections. The purpose of this portion of the study is to merely evaluate the effect that temperature changes may have on a horizontally curved steel I-girders. In doing so, the dead and live load results provide references to assess the relative magnitudes of the thermal results. (For this study, the dead load stresses are based on the composite section.)

195

Table 8.11. North pier Strength I stresses

	Girder	DL	LL	T(+)	Combined Loads
σ_x (ksi)	A	-10.2	-6.1	0.3	*-16.0*
	B	-11.0	-6.4	-0.2	*-17.5*
	C	-10.2	-6.0	-0.5	*-16.7*
	D	-9.4	-5.4	-0.1	*-14.8*
σ_lb (ksi)	A	-0.9	-0.8	-0.9	*-2.6*
	B	-1.1	-1.0	-0.5	*-2.6*
	C	-2.1	-1.7	-0.2	*-4.0*
	D	-3.5	-2.7	-2.0	*-8.2*
σ_a (ksi)	A	0.2	0.1	-0.8	*-0.5*
	B	-0.1	0.1	-0.9	*-0.9*
	C	-0.2	-0.1	-0.8	*-1.1*
	D	0.1	0.3	-0.7	*-0.4*
Σσ_total (ksi)	A	*-10.9*	*-6.8*	*-1.4*	***-19.0***
	B	*-12.1*	*-7.3*	*-1.6*	***-21.1***
	C	*-12.4*	*-7.8*	*-1.5*	***-21.7***
	D	*-12.8*	*-7.8*	*-2.7*	***-23.3***

Table 8.12. Center span Strength I stresses

	Girder	DL	LL	T(-)	Combined Loads
σ_x (ksi)	A	12.4	12.1	0.5	*25.1*
	B	11.9	11.9	0.3	*24.0*
	C	11.3	11.4	0.3	*22.9*
	D	10.6	10.8	0.0	*21.4*
σ_lb (ksi)	A	0.8	0.9	0.2	*1.9*
	B	0.9	1.0	0.2	*2.0*
	C	0.9	0.9	0.2	*2.0*
	D	0.9	1.0	0.2	*2.0*
σ_a (ksi)	A	-0.6	-0.6	1.0	*-0.2*
	B	-0.7	-0.7	1.2	*-0.1*
	C	-0.7	-0.7	1.2	*-0.2*
	D	-0.5	-0.6	1.5	*0.4*
Σσ_total (ksi)	A	*12.7*	*12.4*	*1.7*	***26.8***
	B	*12.1*	*12.1*	*1.7*	***25.9***
	C	*11.5*	*11.6*	*1.6*	***24.7***
	D	*11.0*	*11.1*	*1.6*	***23.8***

Notice that Table 8.11 and Table 8.12 only provide results for one thermal load case, T(+) or T(-). The controlling thermal load at the individual section was selected based on the critical total stress produced in the section. An increase in temperature, T(+), was found to be the controlling thermal case at the north pier; while on the other hand, a negative temperature change, T(-), controlled the thermal loading at the center span in Table 8.12.

The tabulated results indicate that the strong axis bending stresses contribute most to the total stress (for DL and LL). Strong axis bending from combined loading accounts for an average 92% and 77% of the total stress from combined loading at the center span and north pier, respectively. Thermal loads contribute only up to 3% of the combined strong axis bending stress in Girder C at the north pier.

Contrarily, thermal loads had more influence at the fixed pier location for bottom flange bending. In the most extreme case of Girder D, lateral bending stresses in the bottom flanges were greatest at the north pier. After applying Strength I load factors, combined loading produced a lateral bottom flange bending stress magnitude of 8.2 ksi. Thermal loads produced maximum lateral flange bending stresses of 2.0 ksi. Though this quantity is less than the lateral stress produced from the dead and live load of 3.5 ksi and 2.7 ksi, respectively, the thermal contribution to the stress in the flange may be significant enough to account for in design. At the center span, lateral bending stresses were less at only 2.0 ksi, due to combined loading.

Recall that significantly higher axial loads were present due to the temperature changes. However, the constant axial force was found to be relatively small for the size of the composite cross sectional area. Therefore, the stresses yielded less influential results. The maximum axial stress equaled -1.1 ksi, in compression, for Girder C at the north pier due to combined loading. Thermal axial stress accounted for -0.8 ksi of the total -1.1 ksi, indicating that temperature does indeed account for most of the axial effects. However, axial loads only contribute minimal stresses to the section.

After summing the stresses in individual girders for each load case, thermal loads contribute average magnitudes of 1.8 ksi and 1.7 ksi to the total combined stress for the north pier and center span, respectively. For Grade 50 steel, 1.8 ksi correlates to only 4% of the yield stress. As mentioned, the maximum case existed in Girder D at the north pier. Thermal loads produced a total stress magnitude of 2.7 ksi, or 5% of the yield stress. In conclusion, thermal stresses for these curved bridges are small and may only add up to near 3 ksi.

CHAPTER 9 SENSITIVITY STUDY

In this chapter, a sensitivity study is described that was performed to investigate the influence of bridge curvature and skew on the stresses induced in girders of an integral abutment bridge, in particular Bridge 309. The goal of this sensitivity study is to determine the amount of curvature that does not result in bridge behaviors significantly different from straight integral abutment bridges. Further, the impact of having two fixed piers (as opposed to one fixed pier and one expansion pier) on the design of these curved girder bridges will be investigated.

9.1 Curvature and Skew Effects

9.1.1 Established FE Models

To achieve the study goal, the FE modeling techniques described in Chapter 8 were utilized to establish the components of the superstructure and substructure systems. Then, different bridge models were established by systematically changing the degree of curvature and skew. To allow for comparison, all other parameters of the bridge models - such as the dimensions of bridge components, spacings of girders and diaphragms, material properties and boundary conditions, etc. - were kept the same as the Bridge 309 model. Following analysis, the internal stresses in the girders at different locations were studied to understand how they might be influenced by skew and curvature.

A total of twelve FE models were established with the range of values for curvature and skew as tabulated in Table 9.1. Note that Bridge 309 (which was the baseline for this study) has a curvature radius of 950 ft and a skew of 15 degrees. All bridge models with a curvature radius of 20950 ft (very high curvature radius) are deemed to essentially represent the straight bridge case.

For the entire sensitivity study, the Strength I load combination was considered and included dead load, live load, and thermal loads associated with the load factors illustrated in Section 8.4.1. Accordingly, the dead load, live load and thermal loads were applied to the bridge models based on Sections 8.4.2, 8.4.3, and 8.4.4, respectively. Note that an average back wall pressure of 11.7 psi was applied to both the south and north abutments when considering positive temperature change effects.

Table 9.1. Variable values of the curvature and skew

Skew, degrees	Curvature Radius, ft (Curvature, 1/ft)			
0	350 (0.00303)	550 (0.00182)	950 (0.00105)	20950 (0.00005)
15	350 (0.00303)	550 (0.00182)	950 (0.00105)	20950 (0.00005)
30	350 (0.00303)	550 (0.00182)	950 (0.00105)	20950 (0.00005)

9.1.2 Results and Discussion

Similar to the analytical work described in Chapter 8, this study focused on results near the approximate maximum positive and negative moment regions. Strains were extracted for each of the four girders at seven cross sections along the bridge length. Specifically, three mid-span cross sections representing positive moment regions and four support cross sections representing the negative moment regions were considered. Given the different curvatures and skew, the mid-span cross sections were selected to be parallel to the bridge skew so that the cross sections are all located the same distance from the two piers. Taking the model of Bridge 309 as an example, the mid-span and support cross sections considered are circled in Figure 9.1. Recall that the supports align with the bridge skew and that the intermediate diaphragms align with the radius.
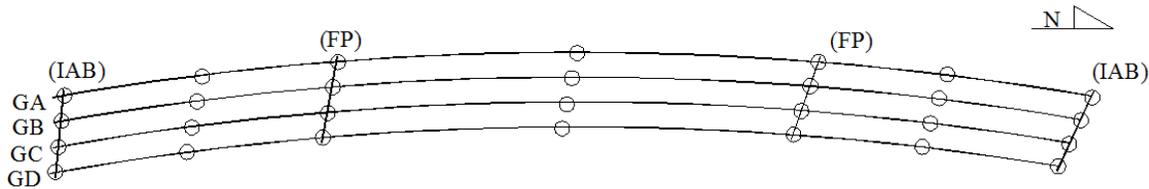
Figure 9.1. Bridge 309 circled locations of extracted results

The FE results indicated that the mid-center span section and the north pier section are representative of the locations where the most critical stresses exist. As was done previously the stress results for Girders A and D were the focus of the sensitivity study. In the previous experimental and analytical work, the stresses at four points (i.e., 1, 2, 3, and 4) in the girder cross-section, as shown in figure 9.2 (similar to Figure 6.4), were discussed. As the stresses at Points 3 and 4 were larger than Points 1 and 2, Points 3 and 4 are the focus here. Note that Points 3 and 4 are located at the outer and inner curvature of the girders, respectively (See Figure 9.2).
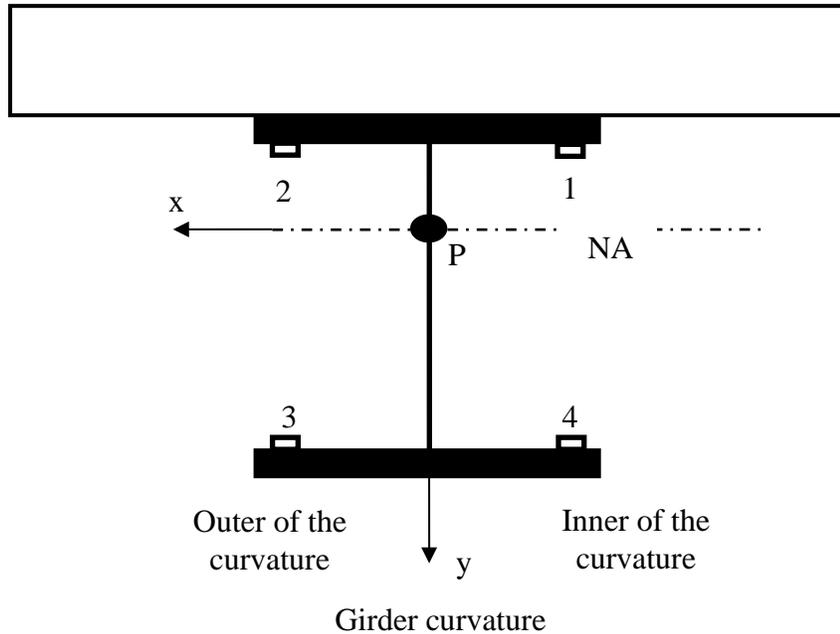
Figure 9.2. Stress points in girder section

The critical stresses in the mid-center span and north pier sections of Girders A and D are plotted in Figure 9.3 and Figure 9.4, respectively. Critical stress in this discussion refers to the largest sum of stresses (vertical bending plus lateral bending plus axial) in the cross section. Figure 9.3 shows that at the mid-center span section the stress in Girder A increases and the stress in Girder D decreases with an increase of curvature regardless of the skew; further, the stresses in Girder A and Girder D both decrease with an increase of skew regardless of the curvature. Figure 9.4 shows that for the north pier section, the stresses in Girder A and Girder D generally increase with an increase of curvature, except for the girder D at a 0 degree skew; the stresses in Girder A and Girder D increase with an increase of skew.

According to Section 4.6.1.2.4b-1 in the AASHTO LRFD Bridge Design Code, the effect of curvature, when calculating strong axis bending moments, may be ignored when the following criteria are satisfied:

- concentric girders;
- skews less than 10^0 from radial;
- equal girder stiffness;
- arc span length to radius ratio less than 0.06 radians.

In addition to showing the actual critical stresses, Figure 9.3 and Figure 9.4 show the percentage of the critical stress obtained for the bridge with the zero skew and 20950 ft curvature radius (i.e., a baseline condition). For the bridge with 10^0 skew and 0.06 radians arc span length to radius ratio (i.e., a bridge meeting the geometrical requirements to ignore curvature for strong axis bending), the critical stresses in Girder A at the mid-center span, Girder D at the mid-center

span, Girder A at the north pier, and Girder D at the north pier are 107%, 97%, 99%, 110% of those in the straight bridge, respectively, as shown in Figure 9.3(a), Figure 9.3(b), Figure 9.4(a), and Figure 9.4(a).

Figure 9.3 indicates that the maximum critical stress occurs at the mid-center span section of Girder A. Additionally, the sensitivity study results indicated that the maximum lateral bending stress occurs at the north pier section of Girder D (also indicated in Chapter 8). As a result, these two sections were selected for further, more detailed analysis.
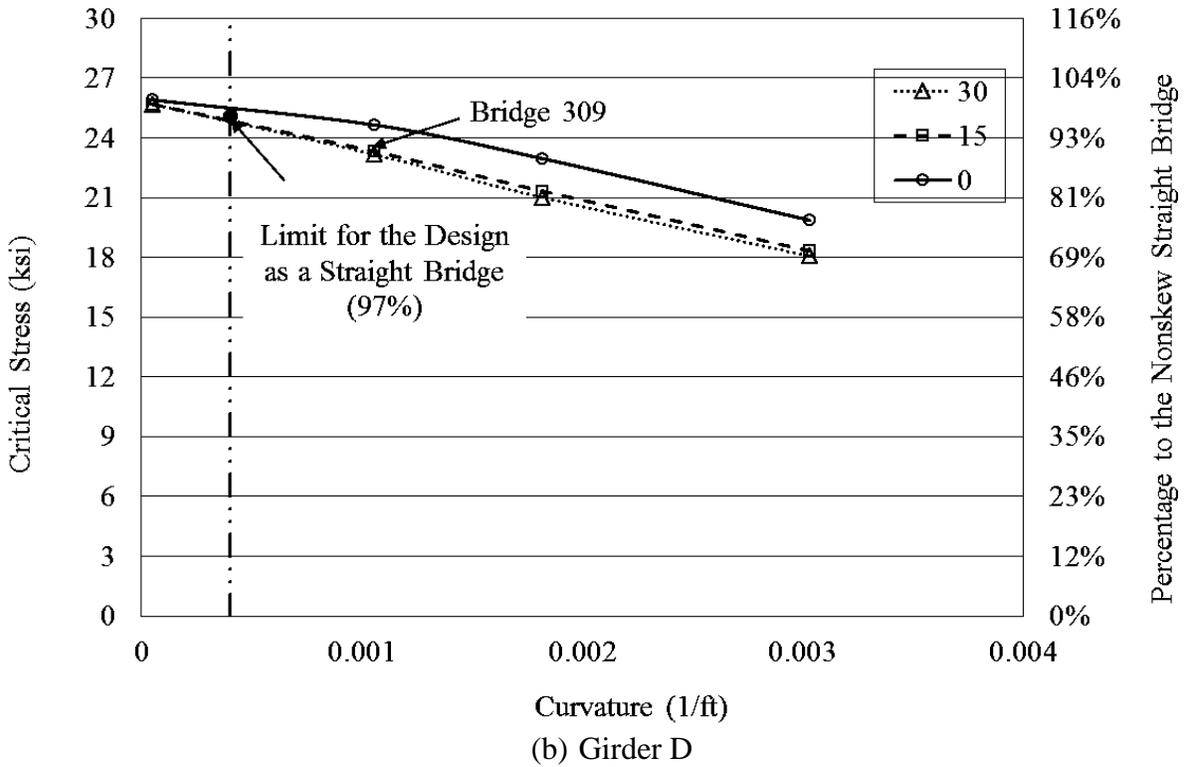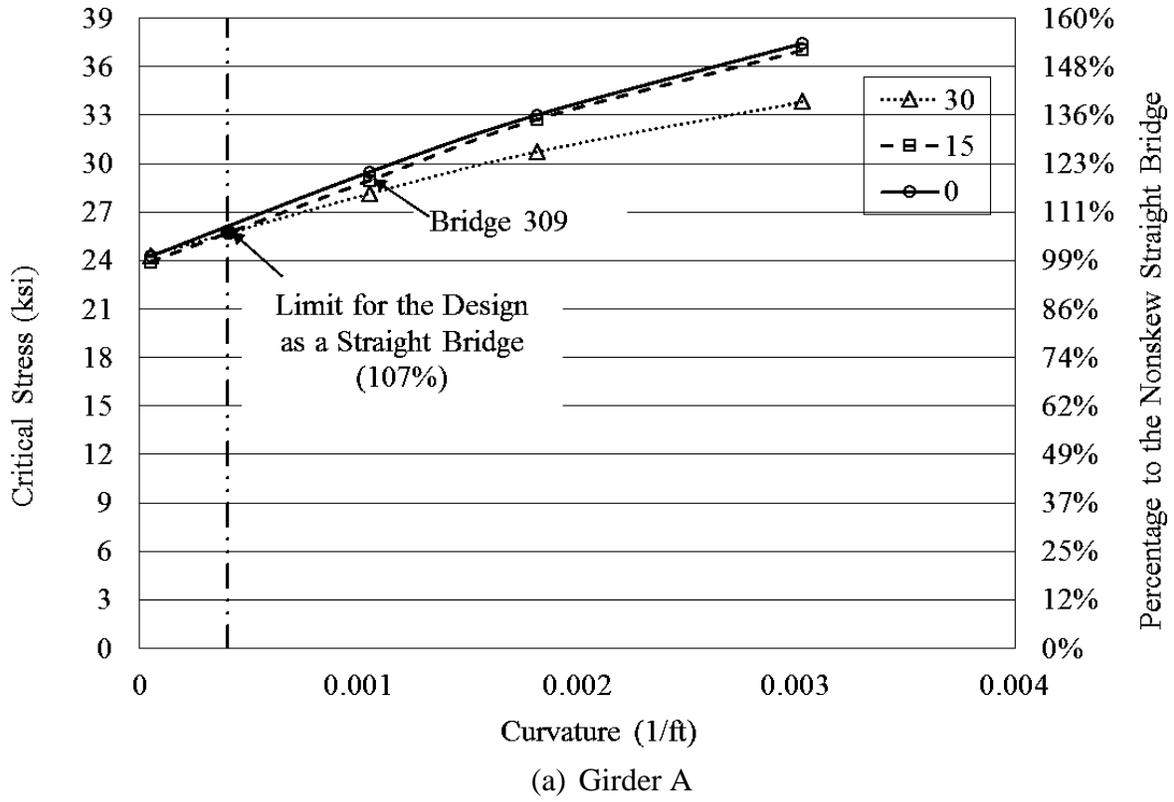
(a) Girder A

(b) Girder D

Figure 9.3. Critical stresses in Girder A and D at mid-center span with varying skew and curvature
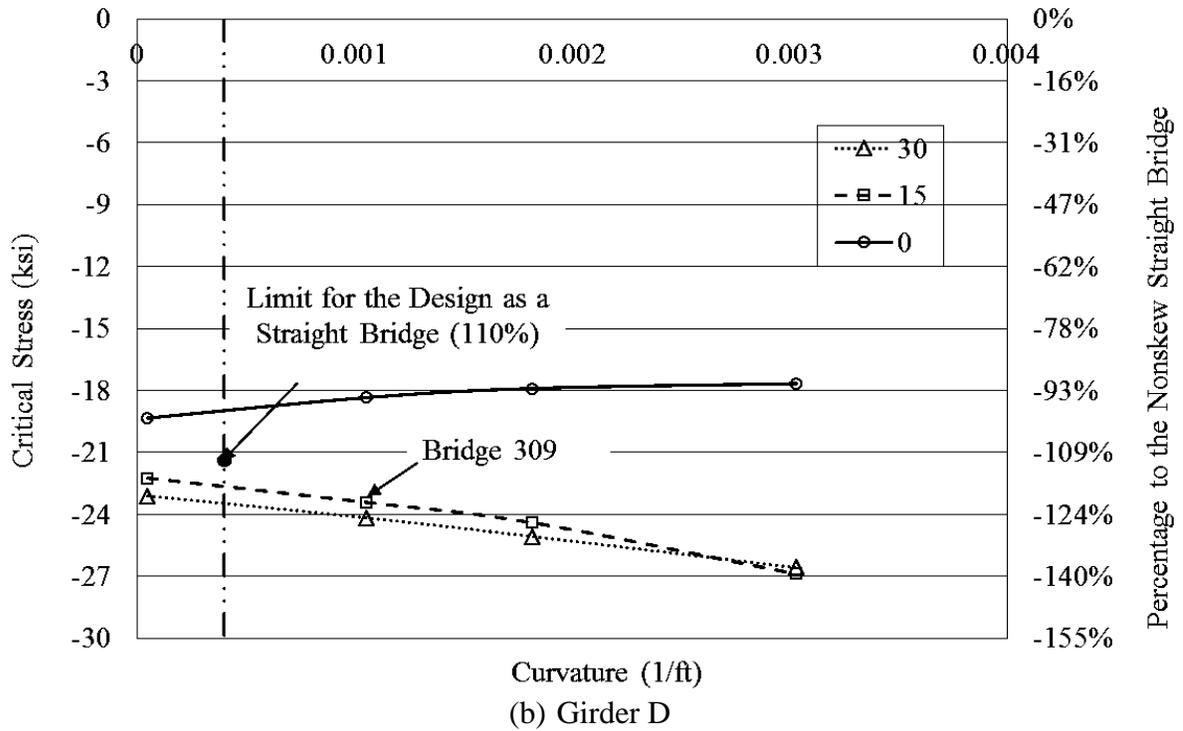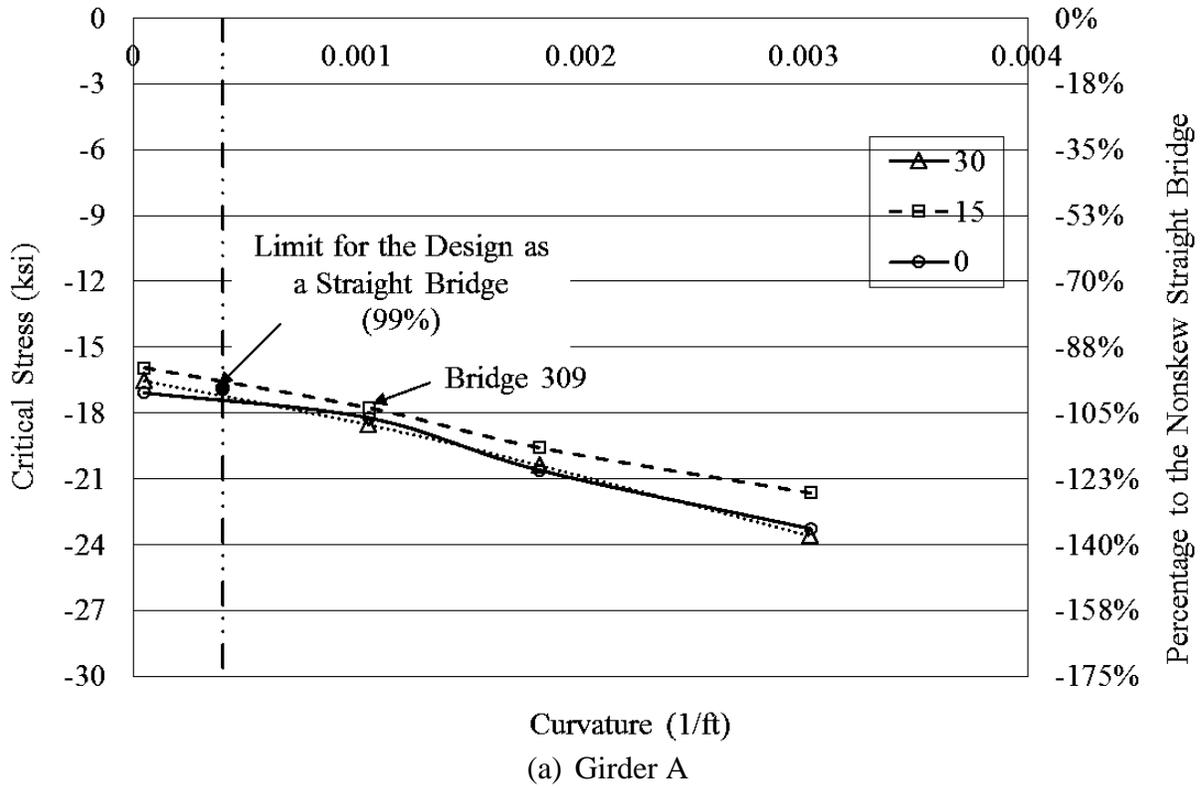
(a) Girder A

(b) Girder D

Figure 9.4. Critical stresses in Girder A and D at north pier with varying skew and curvature

203

Stresses in Girder A at Mid-Center Span

Figure 9.5 indicates that the change of the total stress at Point 3 of the girder Mid-Span section is similar to that of the stress at Point 4. However, the total stress at Point 3 is bigger for skews of 0 and 15 degrees while the total stress at Point 4 is smaller for skews of 0 and 15 degrees. Thus, the stress at either Point 3 or 4 was selected for further analysis depending on which one is bigger. Specifically, the stress at Point 3 was selected for Girder A at the mid-center span and the stress at Point 4 was selected for Girder D at the north pier for further analysis. Further analysis focused on studying the influence of different loads: dead load (DL), live load (LL), positive temperature change (T(+)), and negative temperature change (T(-)) and the changes in various stress components consisting of vertical bending stress, lateral bending stress, and axial stress as they were specifically influenced by changes in curvature and skew.

The total stress and stress components at Point 3 of the mid-center span section of Girder A due to the load combination of DL+LL+T(+) are shown in Figure 9.6(a) and Figure 9.6(b), respectively. The total stress is similar for the 0 and 15 degree skews but the total stress is significantly smaller for the 30 degree skew case due to the increase in lateral bending stress shown in Figure 9.6(b). The vertical bending stress does not vary much for different skews and increases with an increase in curvature as shown in Figure 9.6(b). Overall, the vertical bending stress is significantly larger than the lateral bending and axial stresses as shown in Figure 9.6(b). The lateral bending stress tends to increase when the curvature increases for the all skew cases as shown in Figure 9.6(b). The axial stress maintains a constant value of about 3 ksi regardless of the curvature and skew as shown in Figure 9.6(b).

The load combination of DL+LL+T(-) induces similar stress change patterns as the DL+LL+T(+) case except that the sign of the thermal stresses are reversed as shown in Figure 9.7. Thus, future discussion will focus on the positive temperature change effects (T(+)) only. DL and LL induce similar stress change patterns as DL+LL+T(+) as shown in Figure 9.8 and Figure 9.9, respectively. However, T(+) induces a different stress change patterns as shown in Figure 9.10, respectively. The total stress and component stresses at Point 3 of Girder A at the mid-center span due to T(+) are shown in Figure 9.10(a) and Figure 9.10(b), respectively. The total stress is generally less than about 3 ksi as shown in Figure 9.10(a). The stress components vary slightly with skew and the lateral bending stress increases with curvature shown in Figure 9.10(b).

Note that Figure 9.6(b), Figure 9.7(b), Figure 9.8(b), Figure 9.9(b), and Figure 9.10(b) show the percentage of the vertical bending stress in the secondary vertical axis obtained for the bridge with the zero skew and 20950 ft curvature radius (i.e., a baseline condition).
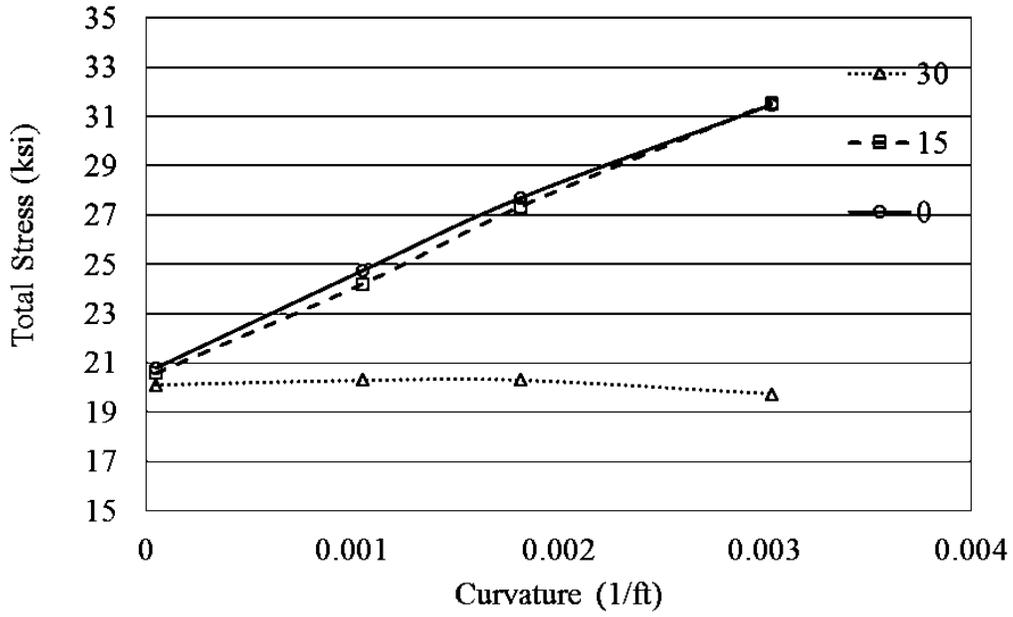
(a) Point 3
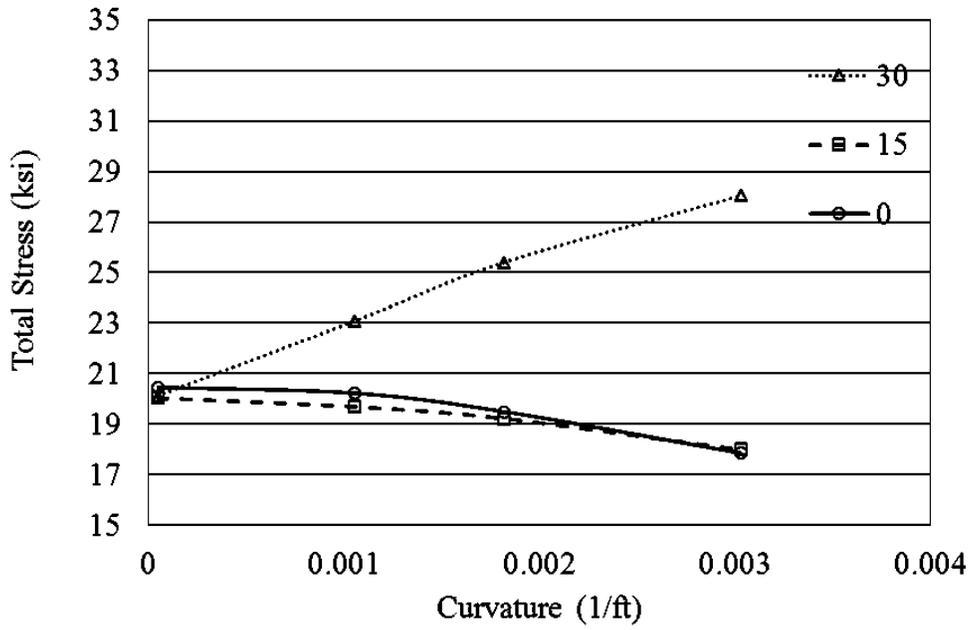
(b) Point 4

Figure 9.5. Total stresses at Points 3 and 4 of Girder A at mid-center span
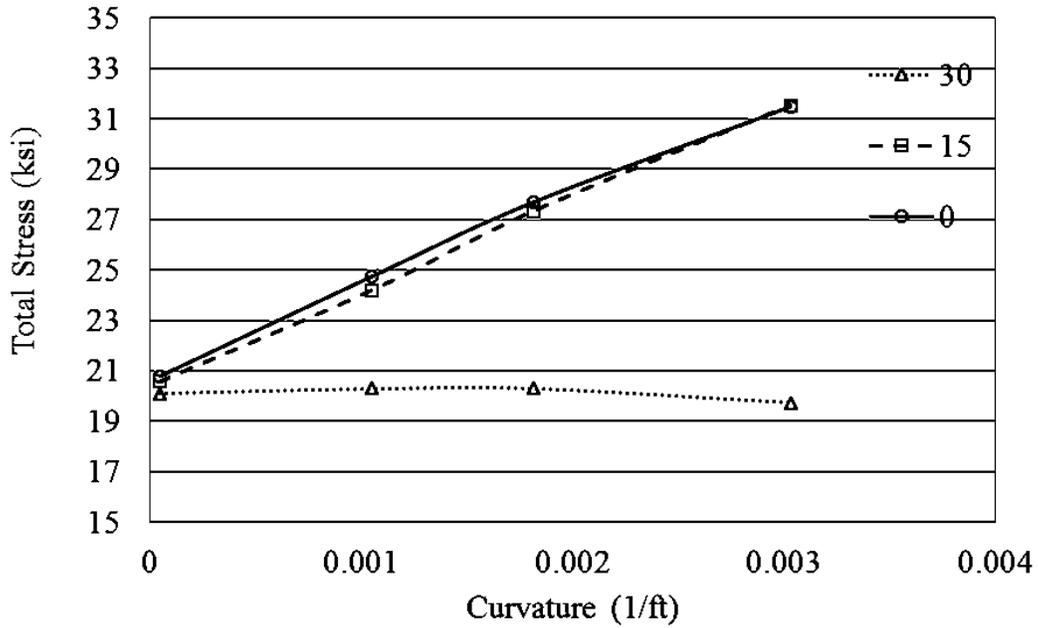
(a) Total Stress
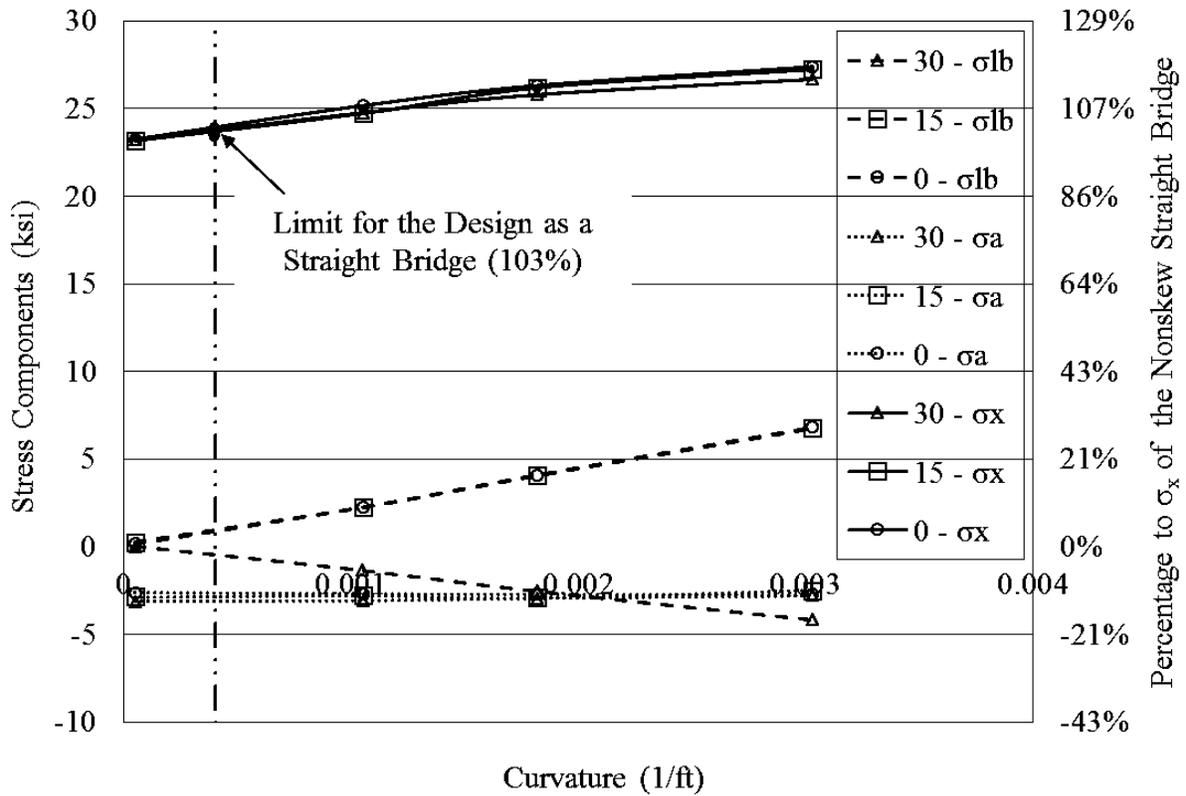
(b) Stress Components

Figure 9.6. Total and component stresses in Girder A at mid-center span due to DL+LL+T(+)
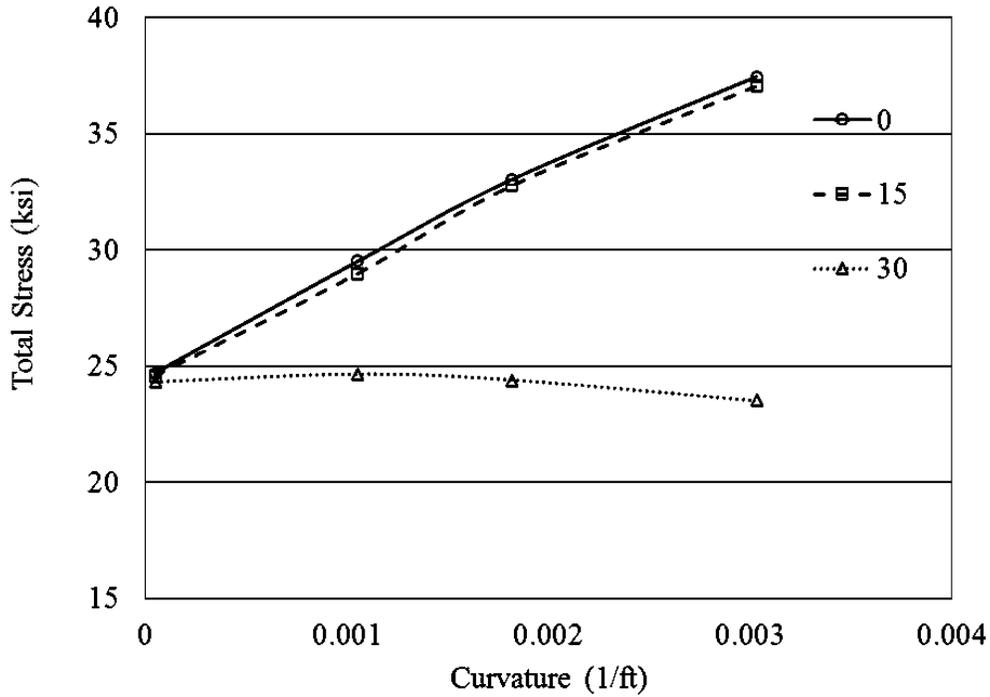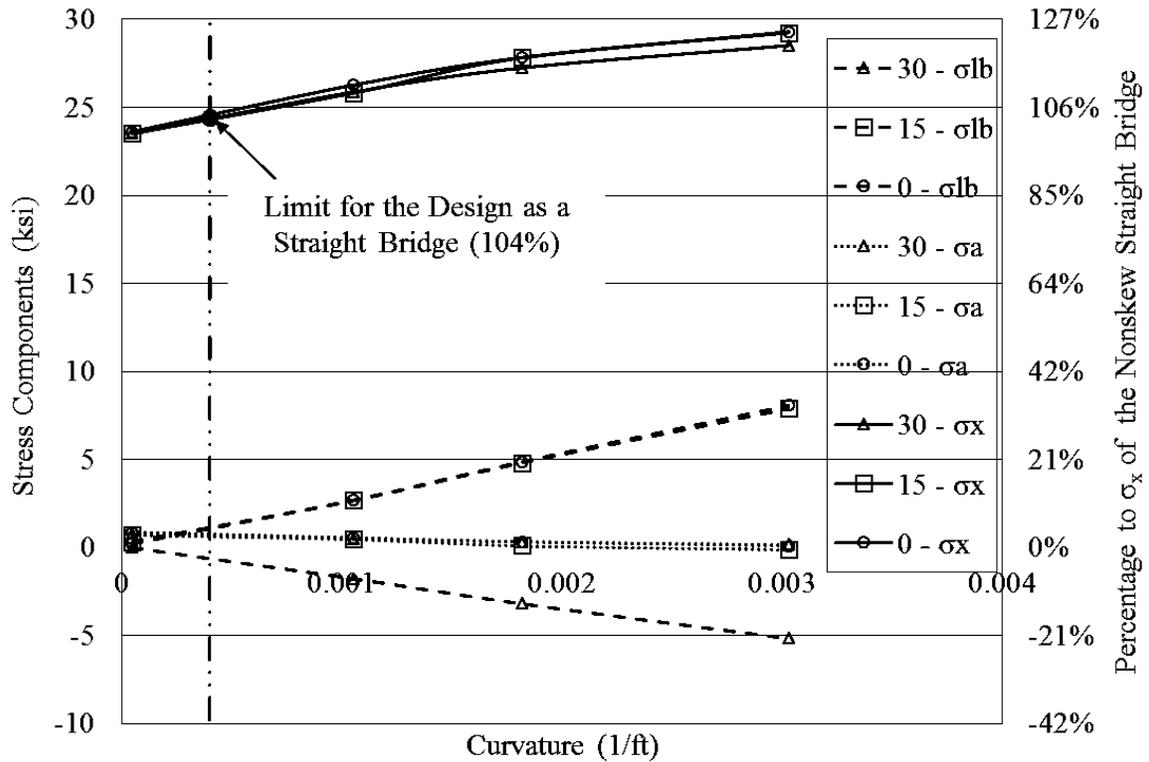
(a) Total Stress

(b) Stress Components

Figure 9.7. Total and component stresses in Girder A at mid-center span due to DL+LL+T(-)
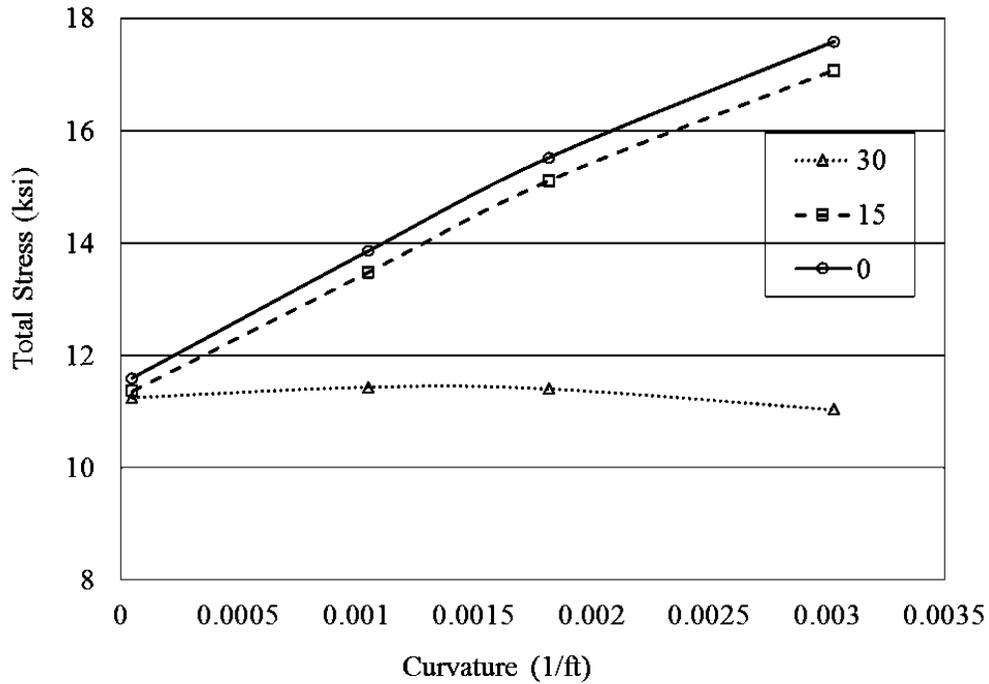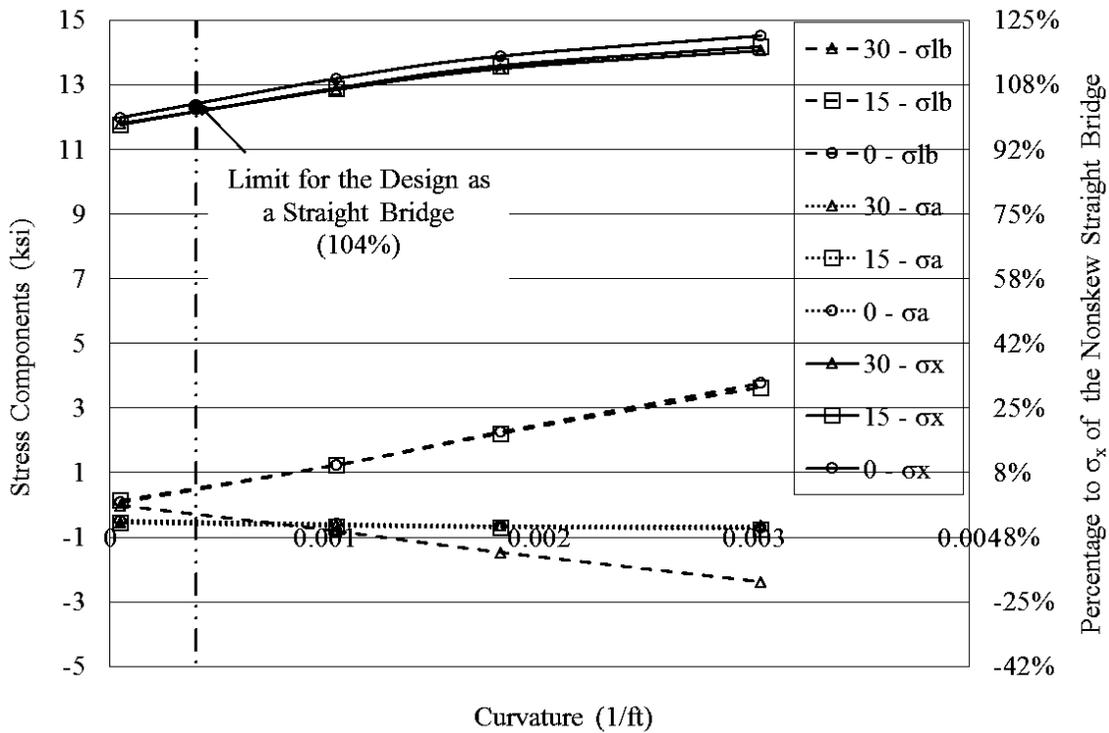
(a) Total Stress

(b) Stress Components

Figure 9.8. Total and component stresses in Girder A at mid-center span due to DL

208

(a) Total Stress

(b) Stress Components
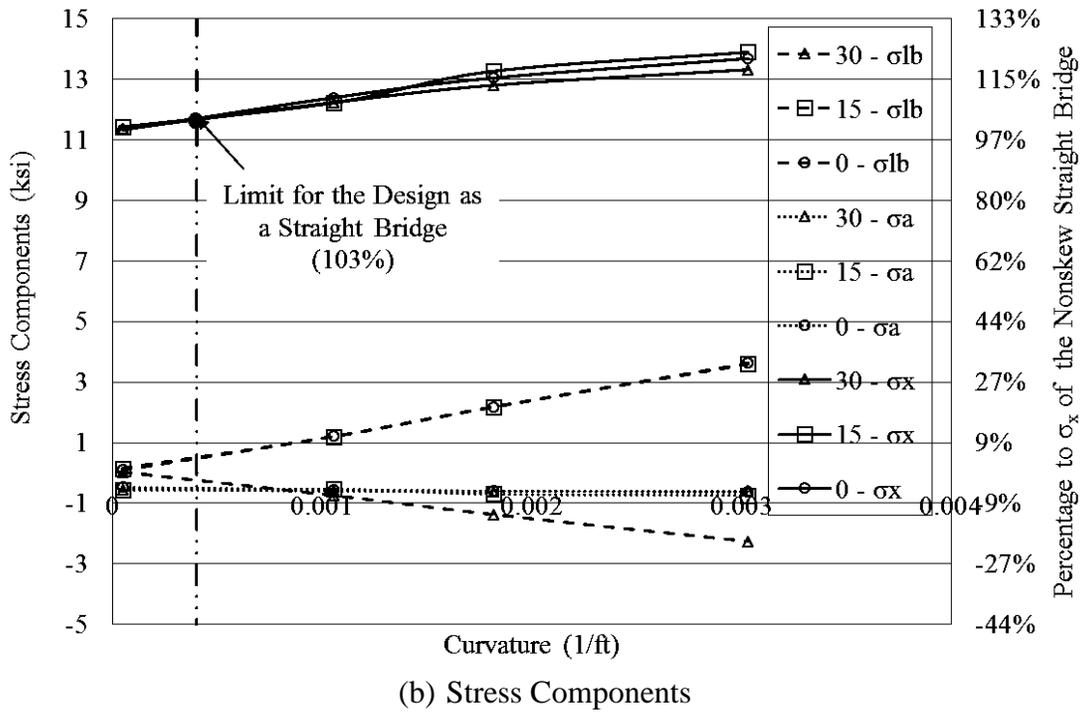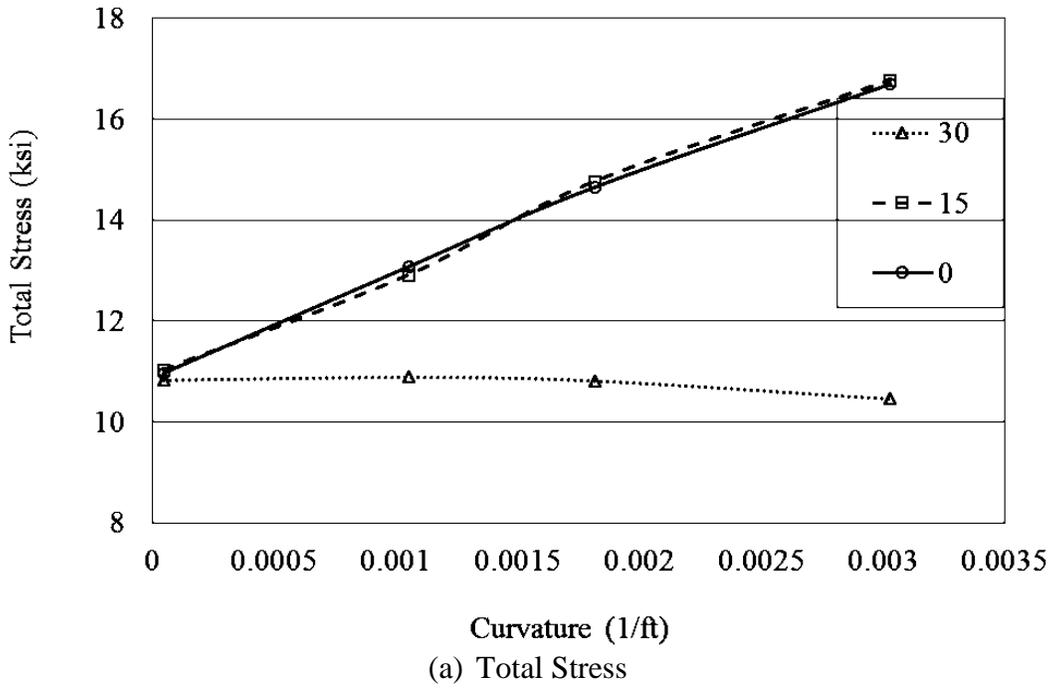
Figure 9.9. Total and component stresses in Girder A at mid-center span due to LL
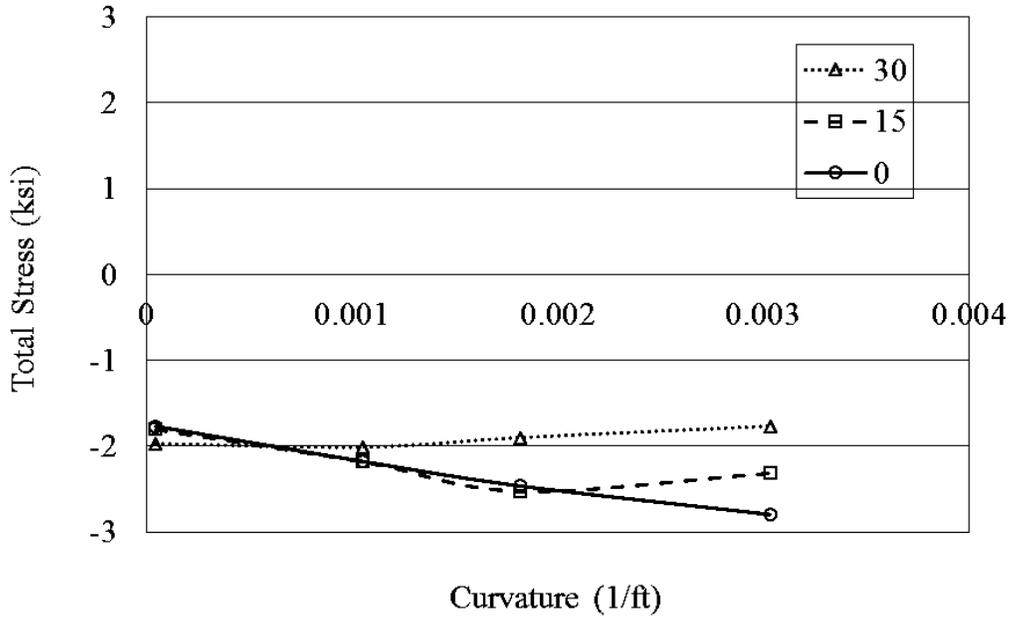
(a) Total Stress
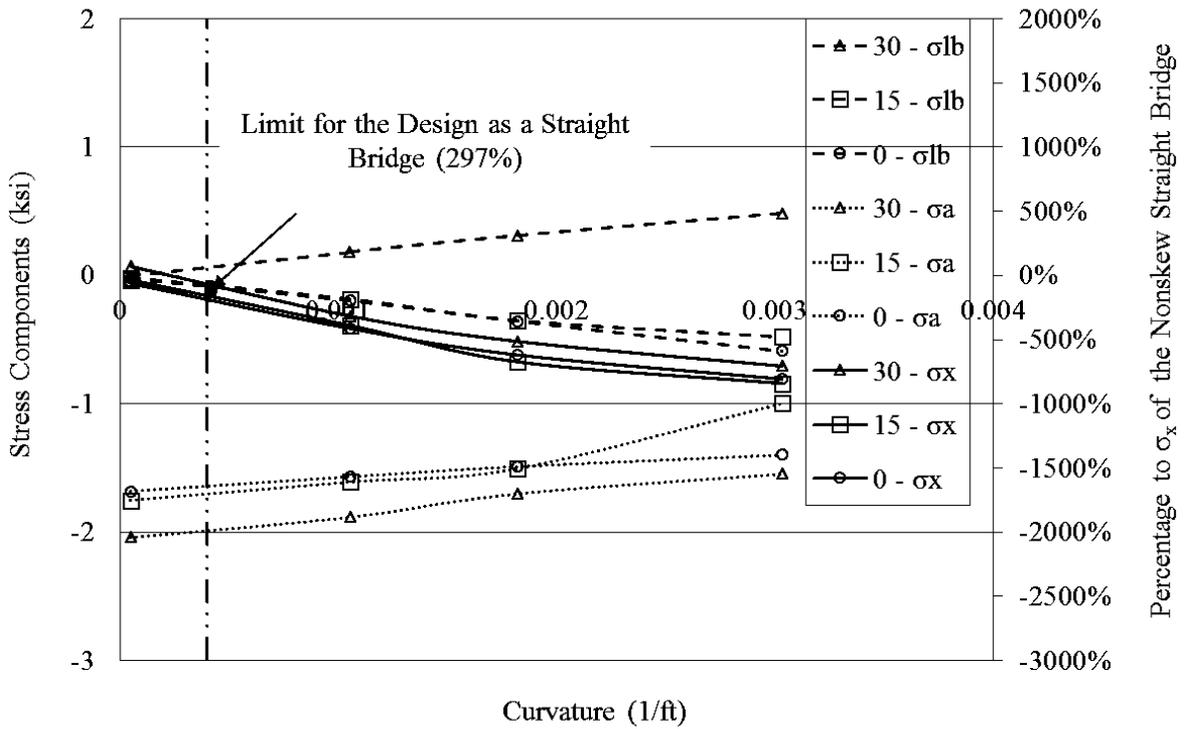
(b) Stress Components

Figure 9.10. Total and component stresses in Girder A at mid-center span due to T(+)

210

Stresses in Girder D at North Pier

The total stress and stress components at Point 4 of Girder D due to the load combination DL+LL+T(+) are shown in Figure 9.11(a) and Figure 9.11(b), respectively. The total stress in Girder D at the north pier increases for the 15 and 30 degree skews case due, principally, to an increase in the lateral bending stress as shown in Figure 9.11(a) and Figure 9.11(b). The vertical bending stress does not change significantly for different skews and decreases with an increase in curvature. The lateral bending stress increases with curvature especially for the 15 and 30 degree skew cases as shown in Figure 9.11(b). The vertical bending stress and the lateral bending stress are significantly larger than the axial stress as shown in Figure 9.11(a). The lateral bending stress increases when the curvature increases for all skews as shown in Figure 9.11(b).

DL and LL induce similar stress change patterns as DL+LL+T(+) as shown in Figure 9.12 and Figure 9.13, respectively. However, T(+) induces a different stress change patterns from DL+LL+T(+); this indicates that the sum seems to be dominated by DL+LL. The total stress and component stresses at Point 4 of Girder D at the mid-center span due to T(+) are shown in Figure 9.14(a) and Figure 9.14(b) respectively. The total stress is generally less than 2 ksi as shown in Figure 9.14(a). The stress components vary slightly with skew and the lateral bending stress decreases with an increase in curvature as shown in Figure 9.14(b).

Note that Figure 9.11(b), Figure 9.12(b), Figure 9.13(b), and Figure 9.14(b) show the percentage of the vertical bending stress in the secondary vertical axis obtained for the bridge with the zero skew and 20950 ft curvature radius (i.e., a baseline condition).

(a) Total Stress

(b) Stress Components
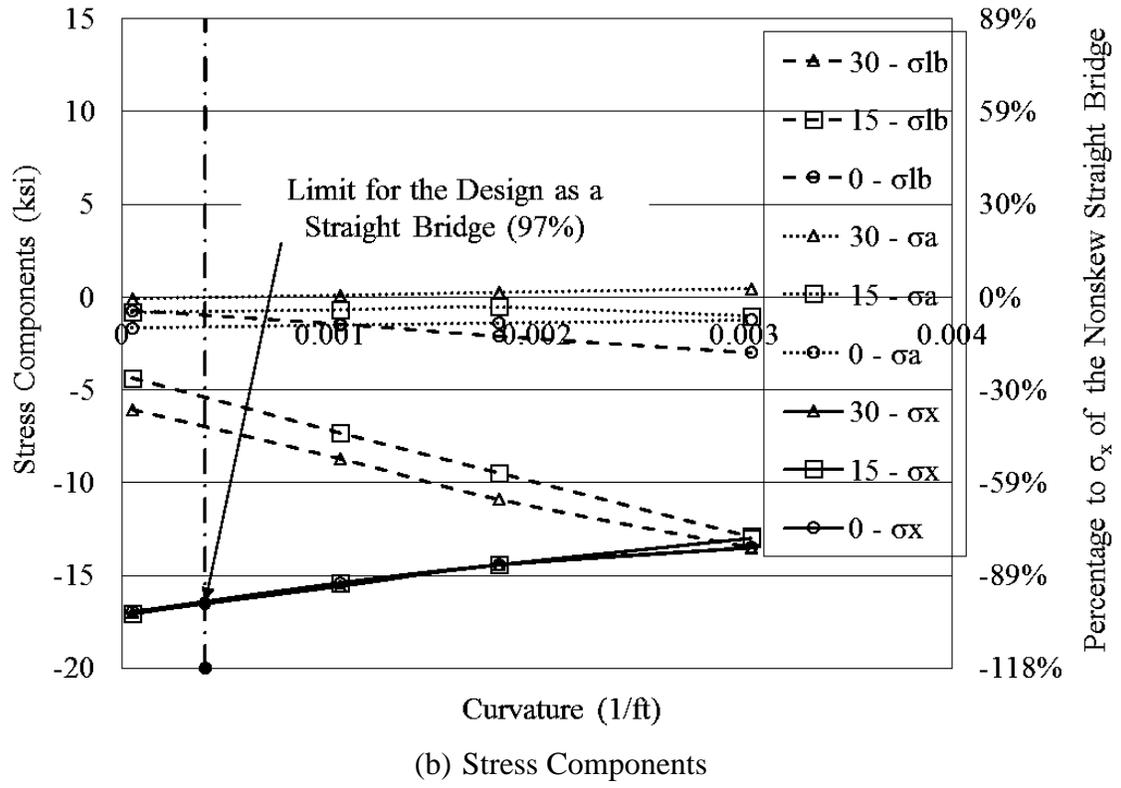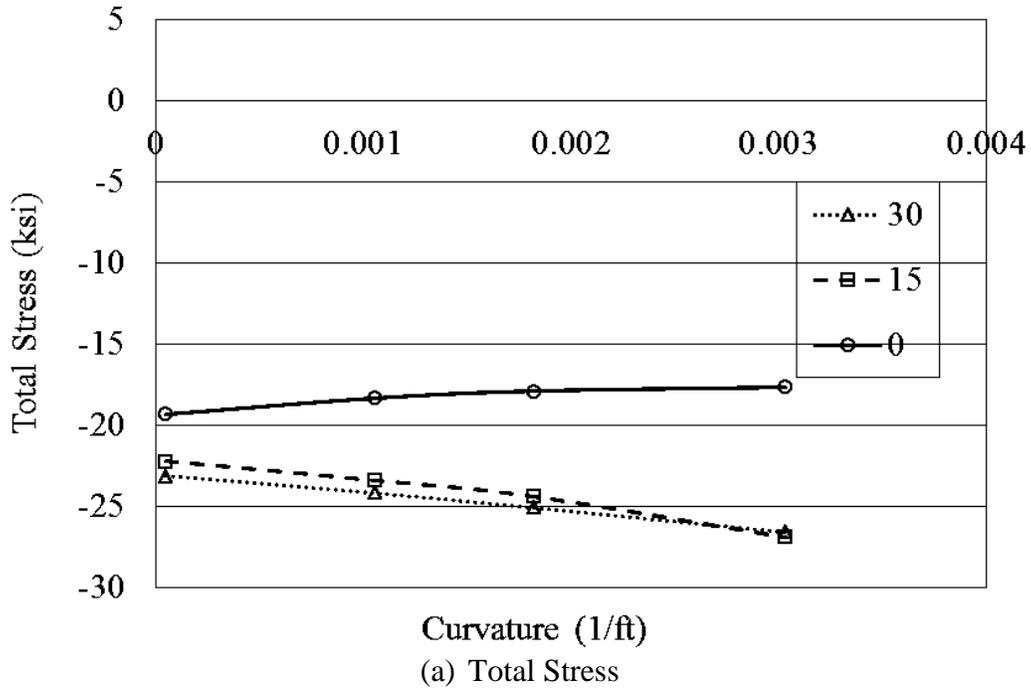
Figure 9.11. Total and component stresses in Girder D at north pier due to DL+LL+T(+)

(a) Total Stress

(b) Stress Components
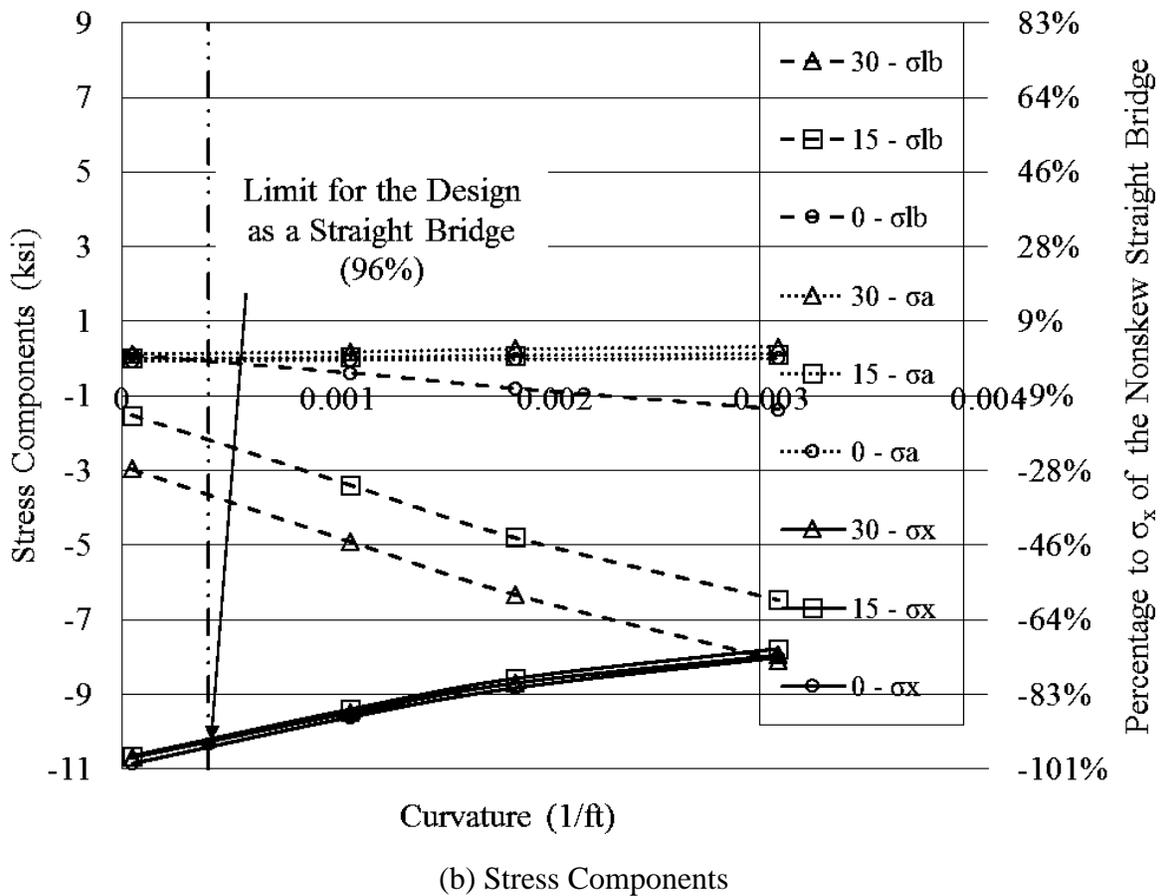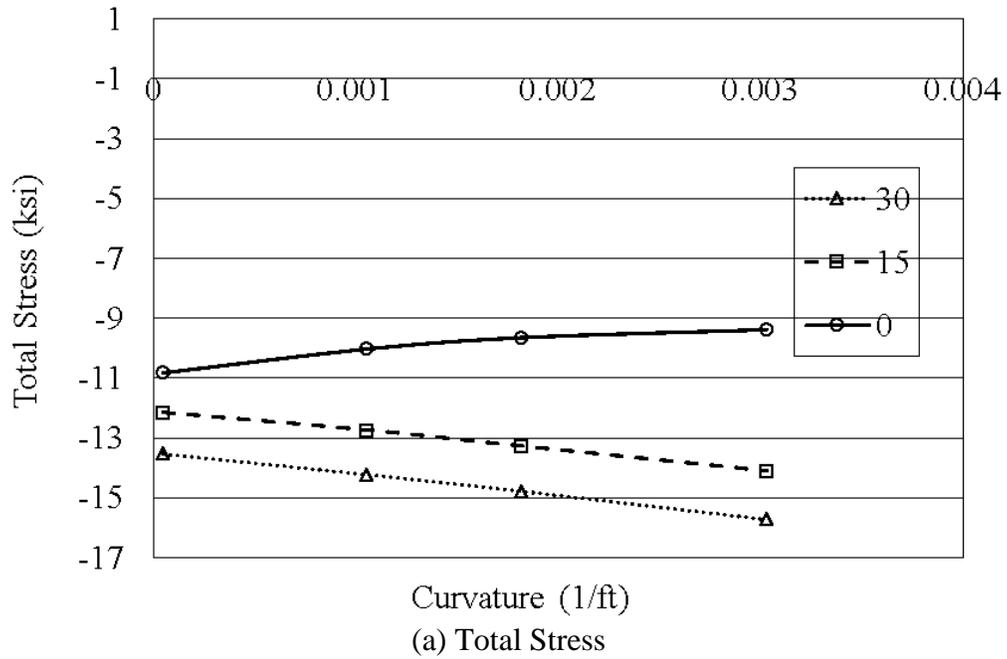
Figure 9.12. Total and component stresses in Girder D at north pier due to DL
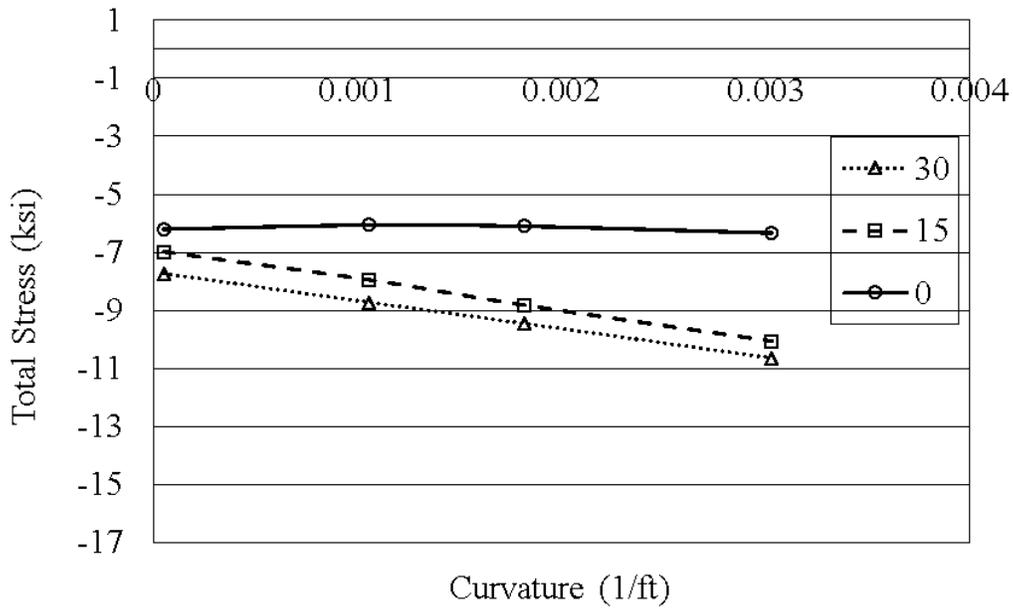
(a) Total Stress
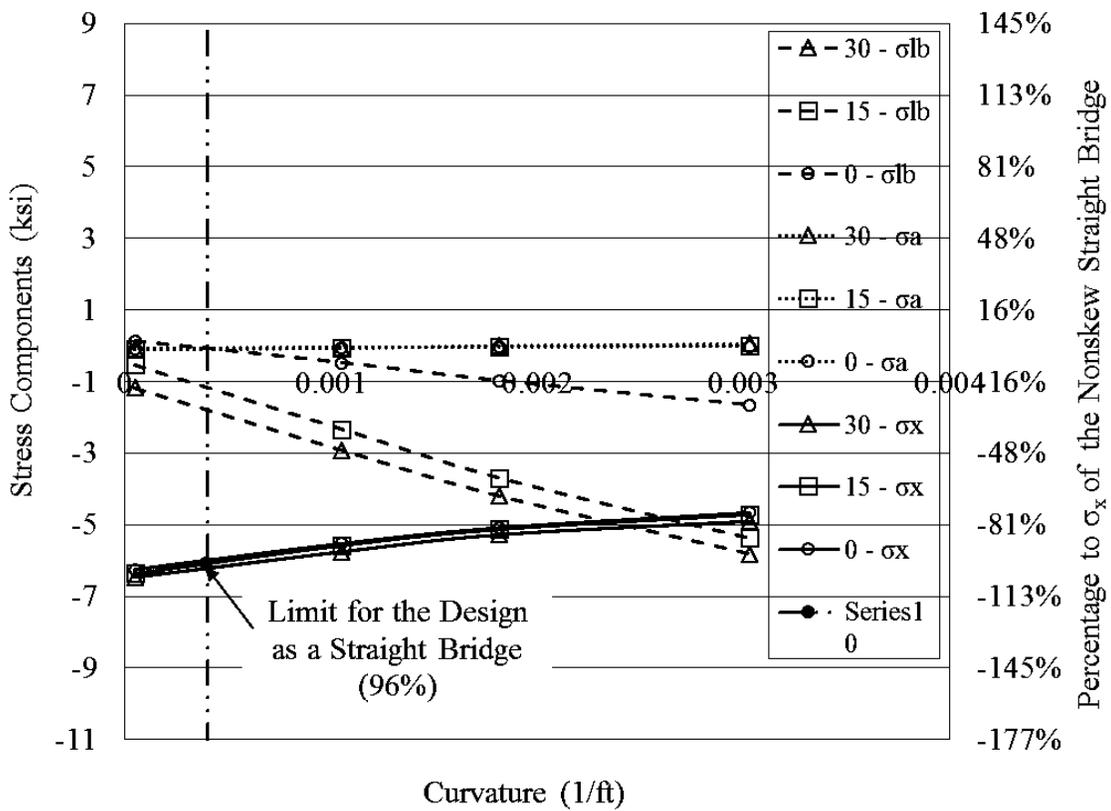
(b) Stress Components

Figure 9.13. Total and component stresses in Girder D at north pier due to LL
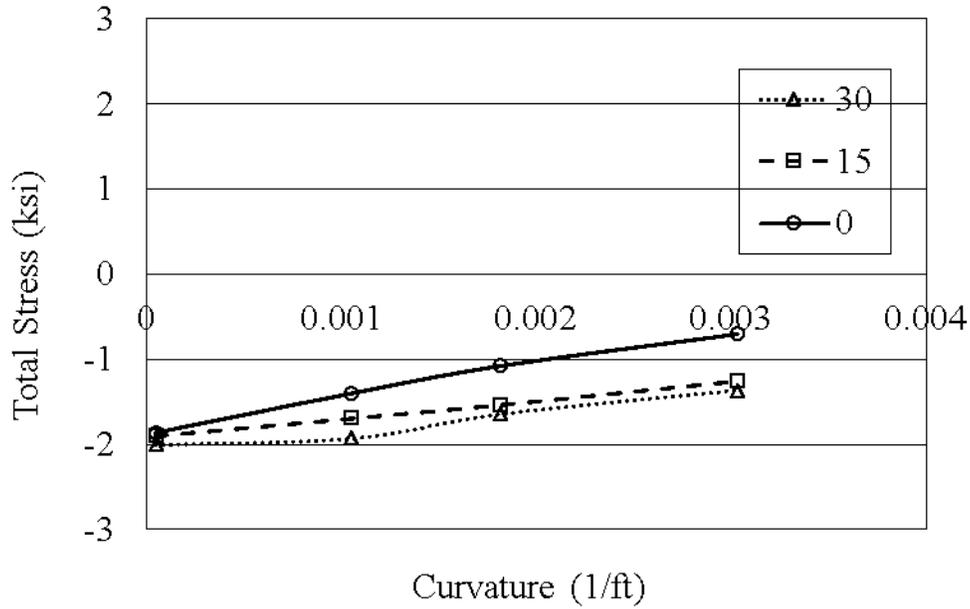
(a) Total Stress
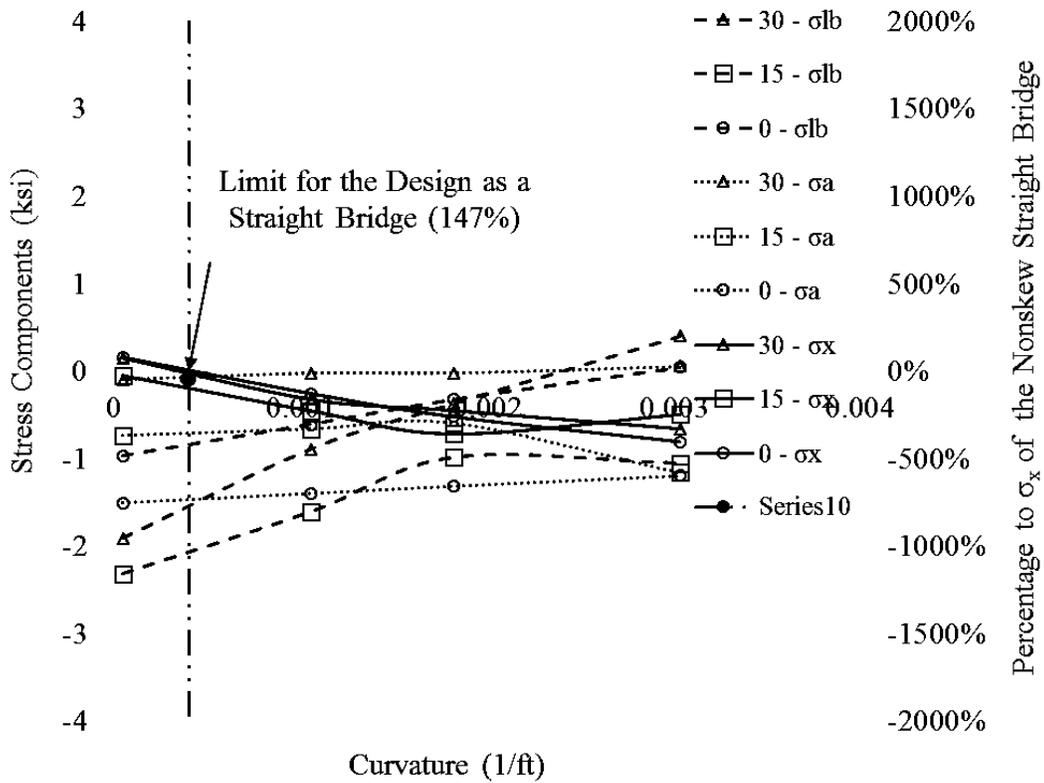
(b) Stress Components

Figure 9.14. Total and component stresses in Girder D at north pier due to T(+)

215

9.2 Pier Fixity Effects

The purpose of using expansion piers is to reduce overall bridge restraint and thereby reduce thermal stresses. Bridge 309, which was the basis for much of the study in this project, has a structural system consisting of two fixed piers. As a result, a question was raised regarding the impact of this particular geometry. To evaluate the impact on thermal restraint a positive temperature change was introduced to several analytical models. Two bridge models established for this part of the sensitivity study included (1) a straight bridge with a skew of 0 degree and (2) a curved and skew bridge (Bridge 309) with a skew of 15 degrees and a curvature radius of 950 ft for evaluating the skew and curvature effects. For each of the two bridge models, two types of pier fixity (i.e., fixed south pier-fixed north pier (fixed-fixed) and fixed south pier-expansion north pier (fixed-expansion)) were studied. Note that for the fixed pier case, the girder and pier tangential, radial and vertical displacements are coupled; for the expansion pier case, only the vertical displacement is coupled. Similar to Section 9.1, stresses at Point 3 of the mid-center span section of Girders A and Point 4 of the north pier section of Girder D are used for comparisons (See Figure 9.2).

The stress results for the straight bridge with two types of pier fixity are tabulated and compared in Table 9.2. Table 9.2 indicates:

- The vertical bending stresses slightly increased and the lateral bending stresses and the axial stresses decrease in all girder sections when a fixed-expansion pier system is used compared to those obtained using two fixed-fixed piers.
- The critical stresses in all sections (i.e., the bigger thermal stress at Points 3 and 4) also decrease when using a fixed-expansion pier system.

In short and as expected, using an expansion pier reduced the thermal stresses in the girders of the straight bridge due to the reduced restraints from the supports.

The stress results for the curved and skew bridge with two types of pier fixity are tabulated and compared in Table 9.3. Table 9.3 indicates that:

- For the fixed-expansion piers, the highest thermal stresses decrease in the mid-center span section of the girder and increase at the north pier section of the girder as compared to the fixed-fixed condition.
- The vertical bending stresses obtained using the fixed-expansion piers is larger than the fixed-fixed condition at the mid-center span section of Girder A and the north pier section of Girder D.
- Lateral bending stresses decrease in the two sections when the fixed-expansion piers are used.
- Axial stresses using fixed-expansion piers are larger than a fixed-fixed condition at the mid-center span section of Girder A and increase in the north pier section of Girder D.

Consequently, using an expansion pier does not appear to absolutely reduce the stresses in the girders of the curved and skew bridge even though the overall restraint is reduced. This is likely due to the complex interaction of skew, curvature, and restraint.

Table 9.2. Bridge model with a skew of 0 degrees and a curvature radius of 20,950 ft

Girder Section	Pier Fixity Type	Thermal Stress (ksi)		Vertical Bending Stress (ksi)		Lateral Bending Stress (ksi)		Axial Stress (ksi)	
		3	**4**	**3**	**4**	**3**	**4**	**3**	**4**
Girder A - Mid-Center Span	Fixed-fixed	-1.8	---	-0.1	---	0.0	---	-1.7	---
	Fixed-Expansion	-1.5	---	0.1	---	0.0	---	-1.6	---
Girder D - North Pier	Fixed-fixed	---	-2.4	---	0.2	---	-1.0	---	-1.6
	Fixed-Expansion	---	-1.2	---	0.3	---	-0.1	---	-1.4

Note: --- – not used for comparison

Table 9.3. Bridge model with a skew of 15 degrees and a curvature radius of 950 ft

Girder Section	Pier Fixity Type	Thermal Stress (ksi)		Vertical Bending Stress (ksi)		Lateral Bending Stress (ksi)		Axial Stress (ksi)	
		3	**4**	**3**	**4**	**3**	**4**	**3**	**4**
Girder A - Mid-Center Span	Fixed-fixed	-2.2	---	-0.4	---	-0.2	---	-1.6	---
	Fixed-Expansion	-1.8	---	-0.5	---	-0.1	---	-1.2	---
Girder D - North Pier	Fixed-fixed	---	-2.7	---	-0.5	---	-1.5	---	-0.7
	Fixed-Expansion	---	-4.5	---	-1.0	---	-1.4	---	-2.1

Note: --- – not used for comparison

CHAPTER 10 SUMMARY, CONCLUSIONS, AND RECOMMENDATIONS

This chapter presents a summary of the project approach, a discussion of the measured and analytical results, conclusions drawn from those results, and recommendations developed by the research team.

10.1 Long-Term Experimental Study

10.1.1 Summary of Procedure

The reconstruction of the NEMM provided the opportunity to monitor the behavior of straight and horizontally curved, steel-girder, integral-abutment bridges. There were six 26 ft wide roadway bridges included in this work. The interchange design was such that two straight-girder bridges were constructed with integral abutments, two curved-girder bridges were constructed with semi-integral abutments with expansion joints, and two curved-girder bridges were constructed with integral abutments.

The typical instrumentation plan for each bridge consisted of four girder strain gauges at the mid-span of exterior girders on select spans, temperature sensors embedded into the concrete deck, and expansion meters strategically placed between the bottom flange of the girders and the pier cap and the abutment cap. On Bridge 309, six abutment piles were also instrumented with strain gauges approximately ten inches below the bottom of the pile cap, long-range displacement meters were installed at each abutment and pier, and pressure cells were installed on the back face of the abutment backwalls. The bridges were monitored for a period of approximately 15 months.

Along with the electronic instrumentation placed on the bridges, each of the six bridges was outfitted with eight prismatic reflectors for the purpose of performing monthly surveys of the bridges. These reflectors were placed on the bottom flange of the exterior girders near both abutments and both piers.

10.1.2 Summary of Results

Composite Girder Strains and Forces

The axial-strain range, $\Delta\varepsilon_a$, at measured locations was between 70 $\mu\varepsilon$ and 220 $\mu\varepsilon$ for all six bridges, with an average value of 153 $\mu\varepsilon$. Axial thermal strains were somewhat larger for SIAB.

The strong-axis-bending strain range, $\Delta\varepsilon x$, at the monitored girder locations was measured between 20 $\mu\varepsilon$ and 110 $\mu\varepsilon$, with an average value of 73 $\mu\varepsilon$. The monitored lateral-bending strain range for the top and bottom flanges were measured between 10 $\mu\varepsilon$ and 100 $\mu\varepsilon$ and 10 $\mu\varepsilon$ and 120 $\mu\varepsilon$, respectively. The top flange lateral-bending strain range had an average value of 31 $\mu\varepsilon$ and the bottom flange lateral-bending strain range had an average value of 21 $\mu\varepsilon$. Strong axes bending and lateral bending thermal strains were similar for IAB and SAIB. Thermal axial and

major axis bending strains for straight and curved bridges were similar, though inside and outside girders varied slightly for curved bridges.

The axial-force range, ΔP, for all six bridges ranged from 70 kip to 770 kip with an average value of 596 kip. Axial forces were somewhat larger for SIAB. The strong-axis-bending moment ranged from 1200 kip-in. to 6300 kip-in. with an average value of 4400 kip-in. The lateral-bending strain range for the top and bottom flanges were between 13 kip-in. and 260 kip-in. and 12 kip-in. and 260 kip-in. with an average value of 43 kip-in. and 42 kip-in., respectively. Strong axes bending and lateral bending thermal moments were similar for IAB and SAIB. Axial forces and strong axis bending moments for straight and curved bridges were similar, though inside and outside girder varied slightly for curved bridges

Abutment Steel Pile Strains

The axial-strain range, $\Delta \varepsilon_a$, in the six abutment pile instrumented locations was measured between 60 $\mu\varepsilon$ and 120 $\mu\varepsilon$, with an average value of 83 $\mu\varepsilon$. The strong-axis-bending strain range, $\Delta \varepsilon_x$, was measured between 140 $\mu\varepsilon$ and 240 $\mu\varepsilon$, with an average value of 198 $\mu\varepsilon$. The weak-axis-bending strain range, $\Delta \varepsilon_y$, was measured between 590 $\mu\varepsilon$ and 900 $\mu\varepsilon$, with an average value of 750 $\mu\varepsilon$. The torsional-warping strain range, ε_t, measured from 20 $\mu\varepsilon$ to 60 $\mu\varepsilon$, with an average value of 39 $\mu\varepsilon$.

The strain ranges in the piles show only a few discernible relationships with the geometry of Bridge 309. The strong-axis bending-strain ranges are highest for HP6s, closest to Girder D. HP4s, closest to the interior girders; show the next highest strong-axis-bending strain ranges, followed by HP1s, closest to Girder A. The weak-axis-bending strain ranges are highest for HP1s, followed first by HP4s, and then HP6s. This result might be expected since Girder A is nearly eight feet longer than Girder D.

Abutment Backwall Pressure

The measured backwall soil pressure ranges were higher at the north abutment than those at the south abutment. For the north abutment the range in the west pressure cell and the east pressure cell were approximately 10 psi and 20 psi, respectively. For this abutment, the soil pressure range at the obtuse side of the skewed abutment shows a greater soil pressure range than at the acute side of the skewed abutment. This result is consistent with work presented in Abendroth and Greimann (2005). Both the west and east pressure cells on the south abutment measured approximately 8 psi for the soil pressure range against this abutment backwall.

The estimated axial forces in the girders due to the soil pressures against the abutments were much lower than these forces that were computed from the measured girder strains. The discrepancy in the girder axial forces can be explained by other restraining forces, such as forces from the piers, piles, and pavement. Also, by assuming linear soil pressure on the abutment backwall and equal girder force distribution made during the calculation can lead to errors in these results as well.

Bridge and Span Change in Length

The measured total change in length, $\Delta L_{measured}$, of the six bridges ranged from 1.54 in. to 2.15 in., with an average value of 1.77 in. The total change in length values by free expansion theory, ΔL_{free}, ranged from 2.14 in. to 2.32 in. The total change in length by free expansion theory provides a conservative estimate, on average 0.43 in. or 26% higher than the measured value. The average axial girder strain calculated from the difference between ΔL_{free} and $\Delta L_{measured}$, $\Delta \varepsilon_r$, ranged from 43 $\mu \varepsilon$ to 154 $\mu \varepsilon$ with an average value of 113 $\mu \varepsilon$. This average is 51 $\mu \varepsilon$ or 34% lower than the measured value.

For each three span bridge, the center spans experienced the greatest change in length. For all six bridges, the change in their center span lengths range from 0.59 in. to 0.75 in. with an average value of 0.70 in. The average difference for the change in the center span length between the inside and outside girders was 0.03 in. or 5%. The change in length of the center span for the bridge with an acute skew angle at the outside girder ranged from 0.32 in. to 0.58 in. with an average value of 0.43 in. The average difference in this span length between the inside and outside girders was 0.043 in. or 10%. The change in length of the center span for the bridges with an obtuse skew angle at the outside girder ranged from 0.30 in. to 0.50 in. with an average value of 0.41 in. The average difference in this span between the inside and outside girders was 0.06 in. or 18%. For all six bridges, the difference in the span length between the two end spans, for all six bridges, ranged from 0.015 in. to 0.045 in. with an average value of 0.03 in. or 7%.

Abutment and Pier Displacements

As shown in the bridge deflected shape figures presented earlier, the girders typically expanded during warmer temperatures and contracted during colder temperatures. Generally, longitudinal bridge displacement at expansion piers would show a larger displacement range than that at fixed piers. One of the semi-integral abutment bridges, Bridge 209, shows a larger displacement range at the abutments than that for all of the integral abutments, but the other semi-integral abutment bridge, Bridge 2309, shows a displacement range similar in value to most of the integral abutments.

Effective Thermal Length

An effective thermal length was calculated for all fixed bearing locations. The effective thermal lengths for the integral abutments were all longer than the length of their respective adjoining span. The effective thermal lengths for the fixed piers were all shorter than the longest adjacent span. In situations where the center span is between two fixed piers, the Iowa DOT uses half the length of the center span for the effective thermal length. The effective thermal length used by the Iowa DOT is conservatively longer when compared to the effective thermal lengths obtained from this study.

Fixed and Expansion Pier Displacement

According to collected data, the maximum range in the girder-to-expansion pier relative displacements were around 0.6 in. The displacements essentially show a linear relationship with regard to the effective bridge temperature until the temperatures approached 100 °F and 0 °F at which point they behave nonlinearly. A correlation between the survey and expansion meter results varied from month to month. In some cases the two data sets overlap one another and in some cases they show a difference of up to 0.2 in. This inconsistency most likely stems from accuracy issues within the survey data.

Abutment Steel Pile Cantilever Model

The results from the abutment steel pile equivalent cantilever model, as described by Abendroth and Greimann (2005), fell short of accurately predicting the relationship between the weak axis bending strain in the piles and the pile head displacement. According to the strain gauge data and the survey results, the measured strain was anywhere between 50 and 150 $\mu\varepsilon$ higher than the values predicted by the model. The accuracy of the survey data could be a possible explanation for the difference in results, as well as a possible difference between the actual pile pre-bore depths and the pre-bore depths shown on the plan, effectively shortening the effective length and increasing the resulting strains.

Abutment Steel Pile Strain versus Expansion

According to the measured strains and displacements, the abutment steel pile strains and the bridge expansion show a linear relationship. According to the data, the SAHP1 pile shows a strain range of approximately 470 $\mu\varepsilon$ under roughly 0.95 in. displacement, the SAHP4 pile shows a strain range of approximately 600 $\mu\varepsilon$ under 0.75 in. displacement, and the SAHP6 pile shows a strain range of approximately 620 $\mu\varepsilon$ under a 0.75 in. displacement. Also according to the data, the NAHP1 pile shows a strain range of approximately 650 $\mu\varepsilon$ under a 0.95 in. displacement, the NAHP4 pile shows a strain range of approximately 620 $\mu\varepsilon$ under a 0.95 in displacement, and the NAHP6 pile shows a strain range of approximately 610 $\mu\varepsilon$ under a 0.70 in. displacement.

10.1.3 Conclusions and Recommendations

Instrumentation

All of the electronic instrumentation (vibrating wire strain gauges, vibrating wire displacement meters, vibrating wire displacement meters, thermistors, and vibrating wire pressure transducers) performed acceptably with few problems occurring. The displacement data obtaining using surveying techniques were acceptable for this study but not as accurate as hoped with errors of the order of 0.3 in.

Internal Composite Girder Strains and Forces

The internal axial girder strain showed the largest ranges of all the resulting strains from the measured girder strain gauge data, with the largest range being 220 με. For Grade 50 steel the resulting stress is 6.4 ksi or roughly 13% of the yield stress. By superimposing the four calculated internal strains, the results can exceed 400 με, giving 11.6 ksi or 23% of yield stress for Grade 50 steel. Although the composite girders have substantial resistance to the effects of thermal loading, this does not consider the effects of other loading conditions.

Abutment Steel Pile Internal Strains

The relationship between abutment steel pile internal axial strain and effective bridge temperature varied depending on the pile location with respect to the abutment pile cap. The measured results showed either a proportional, inversely proportional, or erratic relationship between internal axial strain and effective bridge temperature. This behavior could impact design and further investigation into the phenomena should be undertaken.

The greatest weak axis bending strain, in fact the greatest of all the measured strains, to be resisted by any of the monitored abutment piles was the NAHP1 pile at 900 με. The stress in the section because of the strain equals 26.1 ksi, which amounts to 52% of the yield stress for Grade 50 steel. When considering just weak axis bending, the HP 10x57 piles used as support for the integral abutments in this study had appropriate resistance.

By superimposing the four different abutment pile internal strain ranges on one another, the largest possible strain felt by any of the piles was 1225 με. The stress in the section equates to 36 ksi or 72% of the yield stress of Grade 50 steel. From the results of this study, the piles used for support of the integral abutments at the NEMM had sufficient resistance to thermal expansion; however, this is without considering the effects of other loading conditions. Further investigation into the behavior of abutment piles of horizontally curved integral abutment bridges is suggested.

10.2 Short-Term Experimental Study

10.2.1 Summary of Procedure

Five of six bridges at the NEMM were selected to be live load tested. Static and dynamic truck loads were applied to the bridge using varying load paths. Monitoring the response of each bridge due to the various truck positions was prepared by instrumenting the girders and diaphragms of the bridge superstructures. Each of the four curved bridges was equipped with 40 strain transducers at two radial cross sections and one straight bridge was equipped with 16 strain transducers at a single cross section. Four strain transducers were placed on both the top and bottom flanges of each girder at the instrumented cross section. Strain transducers for the diaphragms, in the curved bridges, were placed on the top and bottom flanges at mid and one-third points for the purpose of monitoring girder-diaphragm interactions.

10.2.2 Summary of Results

Girder Forces

The largest strong axis moments occurred at S1 in Girder A for the two bridges with the most severe curvature, Bridges 309 and 2308. Maximum values reached almost 1900 kip-in. The other two curved bridges produced more uniform strong axis moments and the straight bridge produced larger strong axis moments in the interior girders compared to the exterior girders. Additionally, the moment in Girder A was less at S2 compared to at S1 for all curved bridges.

Lateral bottom flange bending moments proved to be more significant in the four curved bridges compared to the straight bridge as maximums ranged from -19 to 34 kip-in. in the curved bridges. The reversal in the lateral bending direction for the bottom flange was also noted when comparing results at S1 to S2. This trend was expected as curved bridges exhibit an S-shaped bending behavior, which is related to the diaphragm location along the girder.

Lateral top flange bending moments were much smaller than bottom flange bending moments at S1, ranging from -8 to 7 kip-in. Results at S2 produced outliers as the top flange was subject to the localized effect of the concentrated wheel loads.

Axial forces for the curved bridges were largest at S2. An axial force increase of 67 kip in Girder A was produced from S1 to S2 in Bridge 209 under LP3. Similar trends were consistent throughout the four curved bridges.

Dynamic Amplification Factors

A maximum DAF equal to 13% for the four curved bridges was found in Bridge 209. Bridge 109, the straight bridge, produced a 49% DAF in an exterior girder that may have been due to experimental errors during the dynamic testing. Overall, the experimental DAFs for the curved bridges proved to be less than the values specified by the AASHTO LRFD Specifications for all limit states.

Moment Distribution Factors

Experimental results produced the largest MDFs in Girder A for the bridges with the most severe curvature, Bridges 309 and 2308, equal to 0.57 and 0.63, respectively. The interior girders, Girders B and C, ranged from 0.51 to 0.52 and the innermost exterior girder, Girder D, ranged from 0.44 to 0.46. For Bridges 2208 and 209, the two exterior girders ranged from 0.44 in Girder D to 0.53 in Girder A.

Calculating MDFs for Bridge 309 using the approximate method of analysis in AASHTO produced MDFs equal to 0.58 in both exterior girders and 0.62 in both interior girders.

V-Load Exploration

The experimental ratios of M_{lb}/M_x for each girder produced average results ranging from 0.8 to 1.1% for the four curved bridges at S2. These values correspond to ratios calculated from the V-Load equation. Based on bridge geometry, the V-Load equation produced ratios ranging from 0.6 to 0.8%. Experimental values for Bridges 309 and 2308 matched well with the V-Load equation results, while experimental values for Bridges 209 and 2208 were larger than the V-Load equation results.

Diaphragm Forces

The largest strong axis bending in the diaphragms were recorded due to LP2 in the center diaphragm and the outer diaphragm sections located nearest Girder B for all curved bridges. Axial forces reached maximums of nearly 8 kips in tension in the center diaphragm in Bridge 209.

10.2.3 Conclusions and Recommendations

Based on the results from the live load field testing and assessment, it was concluded that live load moment distribution factors were primarily influenced by the degree of curvature. The largest MDFs were found in Girder A for the two bridges with the most severe curvature, Bridges 309 and 2308. The MDFs for Girder A in Bridges 2208 and 209, which have less severe curvature, were in between the results for the straight bridge and the results for the two bridges with more severe curvature. No conclusions were drawn related to support conditions or skew angles. Furthermore, the live load field testing results found that the V-Load equation provided a decent preliminary estimate of M_{lb} based on the magnitude of M_x and the degree of curvature in the girder near a diaphragm. However, as the skew increased in Bridges 2208 and 209, the V-Load equation under predicted the magnitude of M_{lb}.

Dynamic amplification values were well below specified code values for all curved girders. The DAFs in Bridge 109 may very well be due to experimental error and contain no amount of confidence.

Diaphragms were found to be subjected to both bending and tensile axial forces. This indicates that the outermost girder is tending to expand radially more than the innermost girder, an important point to note in outer versus inner girder design approaches.

10.3 Analytical Study

10.3.1 Summary of Procedure

A single bridge of the empirical field study at the NEMM was subject to further analytical study. A FEM static analysis was performed to investigate the superstructure behavior under design

loading conditions, particularly the thermal loads. Bridge 309 was selected because it had the most severe curvature, greatest level of restraints, and it was equipped with the most field instrumentation. The FEM used a combination of 3-D beam shell elements to model key superstructure and substructure entities. Once the model was completed, results from the empirical field study were used to validate the model and increase the confidence of the analytical output. Finally, design loading conditions were applied to the FEM in order to complete the investigation.

10.3.2 Summary of Results

FEM Validation

Girder strains were used as a basis for comparison with the measured field results. For the live load comparison, after summing the peak bottom flange strains of all girders at a given bridge section, the FEM produced strains 12% to 22% larger than the live load field results. Next, the FEM was compared with the thermal field results through proportioning effective bridge temperatures. Axial strains were approximately 18% larger in the outside girder, Girder A, for the FEM versus thermal field results comparison. Lastly, computed girder forces in the FEM were compared with the provided consultant FEM results. The FEM in this study produced strong axis moments that differed by an average 6.0% and lateral bottom flange bending moments that differed by less than 4.0 kip- in. at peak truck locations in all girder sections when compared to the consultant's results.

Strong Axis Bending

Strength I load conditions governed over Service I load conditions, producing larger strong axis bending moments by up to 43%. When comparing the Full model to the Simple model, Strength I strong axis bending moments were 5.6% greater for the Full model at the north pier.

With regards to girder stresses, Strength I strong axis bending due to only DL and LL contributed most to the total stress in the bottom flange. At the center span, the DL and LL accounted for 92% of the total stress in the bottom flange. The addition of thermal loads contributed only 3% more stress to the combined strong axis bending stress in a single girder.

Lateral Bottom Flange Bending

Lateral bottom flange bending was most noticeable at the fixed north pier as moments reached near 90 kip-ft. Service I produced slightly larger lateral moments in the exterior girder flanges while Strength I produced larger lateral moments in the interior girders. On the other hand, the simple model produced negligible lateral bottom flange bending results at both the center span and north pier as moments were less than 20 kip-ft.

Considering that Strength I load combinations produced such dominate strong axis bending stresses in the Full model, only the Strength I lateral bottom flange bending stresses were

calculated. At the north pier, lateral bottom flange bending produced stresses up to 2.0 ksi due to thermal loads alone.

Axial Forces

Axial forces were much greater in the Full model compared to the Simple model along the entire length of the bridge. Service I produced the largest axial forces at the center span and similar forces to Strength I at the North Span. Despite the large axial forces, axial stresses were deemed less significant. Thermal axial stresses were less than or equal to 1.5 ksi in each girder at both sections.

10.3.3 Conclusions and Recommendations

Based on analytical analysis results, Strength I lateral bottom flange bending moments were nearly 10 times greater when including temperature effects at the fixed pier. Moreover, Strength I axial forces were nearly three times greater when accounting for temperature effects compared to only DL and LL. These results indicate that temperature is an essential consideration when addressing member forces. However, in design it is more important to determine the level of stress produced in the section.

With regards to stresses, thermal-induced stresses in horizontally curved steel I-girder bridges similar to Bridge 309, with radii greater than 950 ft, are small. Thermal stresses may only add an additional stress of up to 3 ksi in the bottom flange. However, special attention has been drawn to translationally-restrained locations, such as fixed piers, for exterior girders as lateral bottom flange bending has become more prevalent. In conclusion, the findings from this investigation are not alarming; however, thermal loading may require further consideration in the future design of horizontally curved bridges that incorporate restrained supports with increasing degrees of curvature and skew.

10.4 Sensitivity Study

10.4.1 Summary of Procedure

A sensitivity study was performed to investigate the influence of curvature and skew on the stresses induced in the girders of an integral abutment bridge, in particular Bridge 309. A total of twelve bridge models were established by changing the degree of curvature and skew and keeping all other parameters of the bridge models the same as the as-constructed Bridge 309. Following analysis, the internal stresses in the girders at different locations were studied to understand how they might be influenced by skew and curvature.

Further, the impact of having two fixed piers (as opposed to one fixed pier and one expansion pier) on the behavior of these curved girder bridges was investigated. Two pairs of models were established for this portion of the sensitivity study and included (1) a straight bridge and (2) a curved plus skewed bridge. For each of the two bridge models, two types of pier fixity (i.e., fixed

south pier-fixed north pier (fixed-fixed) and fixed south pier-expansion north pier (fixed-expansion)) were evaluated.

10.4.2 Summary of Results

Critical Stresses

The FE results indicated that the mid-center span section and the north pier section are representative of the locations where the most critical stresses exist. For the mid-center span section, the critical stress in Girder A increases and the critical stress in Girder D decreases with an increase of curvature regardless of the skew; furthermore, the critical stresses in Girder A and Girder D both decrease with an increase of skew regardless of the curvature. For the north pier section, the critical stresses in Girder A and Girder D generally increase with an increase in curvature, except for girder D at a 0 degree skew; the critical stresses in Girder A and Girder D both vary with different skews regardless of the curvature. For the bridge with 10^0 skew and a 0.06 radians arc span length to radius ratio (i.e., a bridge meeting the geometrical requirements allowing curvature to be ignored for determining strong axis bending), the stresses in Girder A at the mid-center span, Girder D at the mid-center span, Girder A at the north pier, and Girder D at the north pier are 107%, 97%, 99%, 110% of those in the straight bridge, respectively.

Stresses in Girder A at Mid-Center Span

Due to the load combination of DL+LL+T(+), the total stress is similar for the 0 and 15 degree skews but the total stress is significantly smaller for the 30 degree skew case due to an increase in lateral bending. The vertical bending stress does not change significantly for different skews but increases with an increase in curvature. Overall, the vertical bending stress is significantly larger than the lateral bending and axial stresses. The lateral bending stress tends to increase when the curvature increases for all skews. The axial stress maintains a constant value of about 3 ksi regardless of the curvature and skew. The load combination of DL+LL+T(-) induces similar stress change patterns as the DL+LL+T(+) case except that the sign of the thermal stresses are reversed.

Stresses in Girder D at North Pier

Under load combination of DL+LL+T(+), the total stress in Girder D at the north pier increases for the 15 and 30 degree skews due to an increase in the lateral bending stress. The vertical bending stress does not change much for different skews and decreases with an increase in curvature. The lateral bending stress increases with curvature especially for the 15 and 30 degree skew cases. The vertical bending stress and the lateral bending stress are significantly larger than the axial stress. The lateral bending stress increases when the curvature increases for all skews. Due to T(+), the total stress, is generally less than 2 ksi and the stress components vary slightly with skew and the lateral bending stress decreases with an increase in curvature.

Pier Fixity Effects

For the straight bridge, the vertical bending stresses slightly increased and the lateral bending stresses and the axial stresses decrease in all girder sections when a fixed-expansion pier system is used compared to those obtained using two fixed piers. The critical stresses also decrease when using a fixed-expansion pier system.

For the curved and skew bridge, the maximum thermal stresses decrease at the mid-center span section of Girder A and increase in the north pier section of Girder D, respectively, when using fixed-expansion piers as opposed to fixed-fixed piers. The vertical bending stresses obtained using the fixed-expansion piers increase in the mid-center span section of Girder A and the north pier section of Girder D. When the fixed-expansion pier configuration is used, the lateral bending stresses decrease in the two sections and axial stresses decrease at the mid-center span section of Girder A and increase at the north pier section of Girder D.

10.4.3 Conclusions and Recommendations

The stresses in the girders of integral abutment bridges significantly vary with changes in skew and curvature. Due to dead and live loads, the change in pattern of the vertical bending stress and axial stress are easy to follow and the change in pattern of the lateral bending stress varies significantly with respect to different skews and curvature. Due to temperature change, the patterns of all stress components vary significantly with respect to different skews and curvature. The largest critical stress occurs in the outer girder at mid-center span and the largest lateral bending stress occurs at the inner girder at the pier. With a 10^0 skew and 0.06 radians arc span length to radius ratio (i.e., meeting the geometrical requirements to ignore curvature for strong axis bending), the curved and skew integral abutment bridges can be designed as a straight bridge if a stress tolerance of 10% is acceptable. If a designer cannot accept an apparent 10% error in stress estimation (even when meeting the geometrical requirements outlined in AASHTO), the designer is advised to use a more discretized modeling approach.

Using an expansion pier reduces the thermal stresses in the girders of the straight bridge due to the reduced restraints from the supports but does not appear to absolutely reduce the stresses in the girders of the curved and skew bridge even though the overall restraint is reduced.

10.5 Design Suggestions

- Thermal stresses should be included in all appropriate load combinations as per the AASHTO Bridge Design Specifications.
- For preliminary member sizing of curved bridges, thermal axial stresses and movements in a straight bridge of the same length are a reasonable first approximation.
- For preliminary member sizing, thermal major axis bending and lateral bending stresses in curved bridges are about the same as for straight bridges.

- Stresses for other loadings other than thermal should follow AASHTO recommendations and guidelines. However, designers should realize that even if AASHTO Specifications allow simpler bridge models that internal forces may be underestimated.
- The choice between IAB and SIAB should be based on life – cycle costs, e.g., construction and maintenance. Differences in thermal stresses are not significant for the bridges studied in this work.
- An expansion pier does reduces the thermal stresses in the girders of the straight bridge but does not appear to absolutely reduce the stresses in the girders of the curved and skew bridge even though the overall restraint is reduced.
- Since AASHTO requires a three-dimensional analytical model of the bridge and support conditions to calculate lateral bending stresses for the final design of all curved bridges, this model should also be used to calculate thermal stresses for final design of the curved bridge. However, with a 10^0 skew and 0.06 radians arc span length to radius ratio (i.e., meeting the geometrical requirements to ignore curvature for strong axis bending), the curved and skew integral abutment bridges can be designed as a straight bridge if a stress tolerance of 10% is acceptable.

REFERENCES

Abendroth, E. R., and L. F. Greimann. 2005. *Field Testing of Integral Abutments*. Center for Transportation Research and Education. Iowa State University. Ames, IA.

American Institute of Steel Construction Inc. 2007. *Steel Construction Manual Thirteenth Edition*. United States: American Institute of Steel Construction, Inc.

Barker, R. M., J. M. Duncan, K. B. Rojiani, P. S. K. Ooi, C. K. Tan, and S. G. Kim. 1991. *Manuals for the Design of Bridge Foundations*. NCHRP Report 343. Washington, DC: Transportation Research Board, National Research Council.

Barr, P. J., N. Yanadori, M. W. Halling, and K. C. Womack. 2007. "Live-Load Analysis of a Curved I-Girder Bridge." *Journal of Bridge Engineering*. ASCE, 11(2), 160-168.

Coduto, Donald P. 2001. *Foundation Design Principles and Practices: Second Edition*. New Jersey: Prentice Hall.

Doust, S. 2011. *Extending Integral Concepts to Curved Bridge Systems*. PhD dissertation. University of Nebraska.

Dunker, K. 1985. *Strengthening of Simple Span Composite Bridges by Post-Tensioning.* PhD dissertation. Iowa State University.

Geokon 2004. *Instruction Manual Model 4700 VW Temperature Gage*. Lebanon, NH: Geokon.

Geokon 2008. *Instruction Manual Model 4420 VW Crackmeter*. Lebanon, NH: Geokon.

Geokon 2009a. *Instruction Manual 3800/3810 Thermistors & Thermistor Strings*. Lebanon, NH: Geokon.

Geokon 2009b. *Instruction Manual Model 4427 VW Long range Displacement Meter*. Lebanon, NH: Geokon.

Geokon 2009c. *Instruction Manual Model VK-4100/4150 Vibrating Wire Strain Gages*. Lebanon, NH: Geokon.

Geokon 2010. *Instruction Manual Model 4800, 4810, 4820, and 4830 VW Earth Pressure Cells*. Lebanon, NH: Geokon.

Hall, D. H., M. A. Grubb, and C. H. Yoo. 1999. *Improved Design Specifications for Horizontally Curved Steel Girder Highway Bridges*. NCHRP Report 424. Washington, DC: Transportation Research Board, National Research Council.

Hassiotis, S., Y. Khodair, E. Roman, and Y. Dehne. 2006. *Final Report Evaluation of Integral Abutments*. Hoboken, New Jersey Department of Transportation, Division of Research and Technology.

Iowa DOT. 2011. *LRFD Bridge Design Manual*. Ames, IA: Iowa Department of Transportation Office of Bridges and Structures.

Kim, W. S., J. A. Laman, and D. G. Linzell. 2007. "Live Load Radial Moment Distribution for Horizontally Curved Bridges." *Journal of Bridge Engineering*. ASCE, 12(6), 727-736.

LaViolette, M. 2009. *Design and Construction of Curved Steel Girder Bridges*. Presentation.

Linzell, D., D. Hall, and D. White. 2004. "Historical Perspective on Horizontally Curved I Girder Bridge Design in the United States." *Journal of Bridge Engineering*. ASCE, 9(3), 218-229.

Lydzinski, J. and T. Baber. 2008. *Finite Element Analysis of the Wolf Creek Multispan Curved Girder Bridge*. Virginia Transportation Research Council, FHWA/VTRC 08-CR8. Charlottesville, Virginia.

Miller, J. and T. Baber. 2009. *Field Testing of the Wolf Creek Curved Girder Bridge: Part II: Strain Measurements.* Virginia Transportation Research Council, FHWA/ VTRC 09-CR14. Charlottesville, Virginia.

Mistry, Vasant C. Integral Abutment and Jointless Bridges. Conference of High Performance Steel Bridges. Baltimore, MD. Nov. 30-Dec. 1, 2000. 1-10. Accessed May 2011 at: http://www.nabro.unl.edu/articles/20002012/download/vasant.pdf.

Moorty, S., and C. W. Roeder. 1992. "Temperature-Dependent Bridge Movements." *Journal of Structural Engineering* 118: 1090-1105.

Nevling, D., D. Linzell, and J. Laman. 2006. "Examination of Level of Analysis Accuracy for Curved I-Girder Bridges through Comparisons to Field Data." *Journal of Bridge Engineering*. ASCE, 11(2), 160-168.

Priestley, M. J. N., F. Sieble, and G. M. Calvi. 1996. *Seismic Design and Retrofit of Bridges*. New York. John Wiley & Sons, Inc.

Richardson, Gordon and Associates. 1976. *Curved Girder Workshop*. Pittsburgh, PA: Federal Highway Administration, Office of Research and Development.

Salmon, C., J. Johnson, and F. Malhas. 2009. *Steel Structures: Design and Behavior*. Fifth Edition. New Jersey: Prentice Hall.

Shah, B. 2011. *3D Finite Element Analysis of Integral Abutment Bridges Subjected to Thermal Loading*. MS thesis. Kansas State University.

Thanasattayawibul, N. 2006. *Curved Integral Abutment Bridges*. PhD dissertation. University of Maryland.

Tennessee Department of Transportation. 1996. *Highway Structures Design Handbook. Volume II, Chapter 5. Integral Abutments for Steel Bridges*. U.S.A: American Iron and Steel Institute, National Steel Bridge Alliance.

The Engineering ToolBox. 2012. *Material Properties.* http://www.engineeringtoolbox.com/material-properties-t_24.html.

Topcon Corporation. 2007. *Pulse Total Station GPT-7500 Series*. Instruction Manual. Tokyo, Japan.

APPENDIX - QUESTIONNAIRE FOR CURVED INTEGRAL ABUTMENT BRIDGE PROJECT

Questionnaire

Questionnaire for Curved Integral and Semi-Integral Abutment

Background Information

Definitions:

Integral Abutment Bridge (IAB) is a bridge that has integral construction between the bridge deck, girders, abutment backwall, and the abutment pile cap. Typically, one row vertical of piles supports the abutments, and expansion joints do not occur within the bridge length.

Semi-integral Abutment Bridge (SIAB) is a bridge that has integral construction between the bridge deck, girders, and abutment backwall with a moment and shear release between the abutment and pile cap. Typically, there are two rows of piles with one row battered, and an expansion joint exists between the top of the pile cap and bottom of the abutment backwall.

1. Respondent Information:

First Name:

Last Name:

Title:

Agency:

Email Address:

Work Phone:

Questionnaire for Curved Integral and Semi-Integral Abutment

Questions 2 - 10 address curved integral and/or semi-integral abutment brid...

2. How many curved integral abutment bridges has your agency designed and constructed?

◯ 0

◯ 1 to 5

◯ 6 to 10

◯ over 10

3. Does your agency have or continue to have a desire or need to construct a curved bridge with integral abutments?

◯ Yes

◯ No

4. Briefly describe why your agency chooses to construct or not to construct curved integral abutment bridges.

[text input box]

5. How many curved semi-integral bridges has your agency designed and constructed?

◯ 0

◯ 1 to 5

◯ 6 to 10

◯ over 10

6. Does your agency have or continue to have a desire or need to construct a curved bridge with semi-integral abutments?

◯ Yes

◯ No

7. Briefly describe why your agency chooses to construct or not to construct curved semi-integral abutment bridges.

8. What unanswered questions does your agency have with regard to the design of curved integral and semi-integral abutment bridges?

9. What unanswered questions does your agency have with regard to performance of curved integral and semi-integral abutment bridges?

10. Are you aware of any published or unpublished reports or current or contemplated research that addresses the performance, monitoring, or design of curved or semi-integral abutment bridges? (please provide reference information)

Questionnaire for Curved Integral and Semi-Integral Abutment

Questions 11 – 13 address curved bridges that do not have integral or semi-...

11. What limitations does your agency place on the design of curved bridges that do not have integral or semi-integral abutments regarding skew, radius, span length, total length, steel girder, pc girder?

12. What AASHTO recommended method(s) does your agency follow for preliminary design and final design of curved bridges that do not have integral or semi-integral abutments?

☐ V Load Method

☐ M/R Method

☐ Grillage Method

☐ FE Method

☐ Other

13. Please rate the level of satisfaction your agency has with the performance curved girder bridges that do not have integral or semi-integral abutments?

	Low	Meduim	High
Satisfaction	○	○	○

Questionnaire for Curved Integral and Semi-Integral Abutment

Question 14 addresses straight bridges with integral and/or semi-integral a...

Much of the state of art and recent research in regard to integral abutment bridges up to 2005 is presented in the following references:

Abendroth, R.E. and Greimann, L.F. 2005. Field Testing of Integral Abutments. Iowa Department of Transportation. Project HR-399. Ames, Iowa. 2005, pp. 102-149.
<http://www.intrans.iastate.edu/reports/hr399.pdf>

Maruri, R., and S. Petro. Integral Abutments and Jointless Bridges (IAJB) 2004 Survey Summary. Proceedings of the 2005 – FHWA Conference: Integral Abutment and Jointless Bridges, Baltimore, Maryland. 2005, pp. 12-29. <http://www.cemr.wvu.edu/cfc/conference/Proceeding.pdf>

14. In the last five years, what significant advances has your agency made in regard to research, analysis, or design of straight integral and/or semi-integral abutment bridges? If possible, please provide references.

Responses

3. Briefly describe why your agency chooses to construct or not to construct horizontally curved, integral abutment, bridges.

Summary:

For the most part, the agencies that choose to construct horizontally curved, steel girder bridges with integral abutments have chosen to do so for joint elimination and the elimination of expansion joints, expansion bearings, and guides. Some also consider having restrained girder ends a benefit for both uplift and torque. Those agencies that choose to not construct horizontally curved, steel girder bridges with integral abutments have a variety of reasons each of which is unique to the state. These reasons include poor local soil conditions, extreme temperature range, unfamiliarity with design, additional forces on the girders, and a general lack of need.

~Alaska~

Alaska generally avoids integral abutments because of poor past performance. The combination of large temperature extremes (-60 to +100 degrees) and pile rotations prevented in frozen ground results in girders pulling out of the abutment walls.

~Arkansas~

Joint elimination

~Colora

do~

CDOT does not prohibit the use of integral abutments with curved bridges. CDOT encourages designers to explore the use of integral abutments for all bridges. The issues related to integral abutments with curved bridges are similar to those that can occur with skewed bridges, the significant issues being unbalanced earth pressures and direction of movement at approach slab expansion joints. The severity and certainly the frequency of these issues tend to be largest for skewed bridges. For the CDOT's guidance on integral abutments see Subsection 7.2 of the CDOT Bridge Design Manual. Skew is addressed in the second to last paragraph. Steps to control the affects of earth pressures is also partially addressed in the 3rd to last paragraph where using MSE to create a gap at the abutment interface is mentioned.

http://www.dot.state.co.us/Bridge/DesignManual/dm_s07.pdf

~Delaware~

We are a small state and have only a handful of curved girder bridges to begin with. We are just now getting into designing and constructing integral abutments for straight girder bridges.

~Florida~

Florida does not design integral abutments due to the fact that we do not have de-icing salts.

~Hawaii~

Our goal is to construct bridges that are jointless. The majority of our bridges are being designed with integral abutments. Generally our bridges are relatively short spans and a few may be on curves, however, its effect appears to be relatively insignificant compared to the degree of skew at the abutments.

~Idaho~

We do have a few integral abutment bridges on curved alignments. The girders (primarily prestressed concrete) girders are on chords between the abutments and piers and the concrete deck is placed on the curve. We have not constructed any steel bridges with the girders fabricated with a horizontal curve with the abutments placed radial to the curve.

~Iowa~

The answer to Q2 includes mostly chorded bridges, curved bridges made up of straight prestressed concrete or steel beams. Iowa approves integral abutments for chorded bridges because they have minimal curvature. Curved bridges with curved steel girders generally are not approved for integral abutments. The concerns for those bridges are lateral bending of girders and movements at bearings.

~Kentucky~

Haven't had right foundation conditions. There is shallow rock present at sites.

~Maryland~

We have generally avoided combining horizontally curved superstructures with integral abutments. This is not necessarily due to any specific technical or performance issue(s).

~Michigan~

Curved or large skewed alignments add out of plane forces not considered in developing the integral abutment details.

~Minnesota~

We do not restrict their use however but the geometric constraints for IA use (length, skew) have set limitations.

~Missouri~

We do allow IAB construction for horizontally curved bridges. Typically these are steel girders. It is preferred to use IAB construction and no expansion joints even for curved systems.

~Nebraska~

We don't have concerns constructing horizontally curved girders on integral abutments since it's has been established that the bridge will expand radial. But we do have some questions about skew limitations. Our policy is to limit integral abutment use to 45 degrees based on the assumption that the pile is in double curvature.

~New York State~

Concerns about additional axial forces from earth pressure being introduced into curved girders.

~New Hampshire~

NHDOT has a small number of straight integral bridges but we have not extended the use of integral abutment to the support of curved girders due to unfamiliarity.

~North Dakota~

Integral abutment bridges are our first choice for bridge type. They are used unless there is a reason we cannot use them.

~Ohio~

ODOT chooses to avoid the complex analysis required to resolve the axial loading placed on the curved superstructure. Typical curved girder analysis software applications do not address this loading.

~Pennsylvania~

Curved bridges are not permitted to guard against the possibility of flange buckling caused by the beams trying to expand between the restrained abutments.

~South Dakota~

We have very little, if any, need for curved structures.

~South Carolina~

Decision is based on span arrangement and project geometry.

~Tennessee~

Integral abutments for horizontally curved girders: 1) Provide beneficial restoring torques to otherwise simple supports; 2) Provide uplift restrain, if needed; 3)Provide protection from water intrusion; 4) Eliminate the need for expansion joints, expansion bearings and guides.

~Texas~

Texas has very limited soil and foundation conditions that are appropriate for integral abutments. We use drilled shaft foundations on a majority of or bridge projects so using integral abutments would be problematic and expensive compared to conventional abutments.

~Vermont~

We constructed one last construction season. We are interested in doing more but are moving ahead slowly. We have instrumented the one bridge and are awaiting some results on the seasonal and load responses.

~Virginia~

Not enough information/research in this area.

~Washington State~

Integral abutments inhibit movement at bridge ends. This movement is necessary to dissipate energy during seismic events.

~Wyoming~

Good past performance, no joints, constrained girder ends, direction of movement due to expansion and contraction does not appear to be as critical regarding the bearing layout.

5. Briefly describe why your agency chooses to construct or not to construct horizontally curved, semi-integral abutment, bridges.

Summary:

For the most part, the agencies that choose to construct horizontally curved, steel girder bridges with semi-integral abutments have chosen to do so for joint elimination and corrosion protection. Washington State also mentions their benefits during seismic events. Those agencies that choose to not construct horizontally curved, steel girder bridges with semi-integral abutments have a variety of reasons each of which is unique to the state. As with the responses regarding integral abutments, these reasons include poor local soil conditions, extreme local temperature range, additional forces on the girders, and a general lack of need.

~Alaska~

We construct very few horizontally curved bridges to start with. Further, we anticipate poor performance of a semi-integral abutment due to our large design temperature range.

~Arkansas~

NA

~Colorado~

CDOT does not have any formal guidance for the use of semi-integral abutments, however their use in Colorado is not uncommon. Integral abutments are preferred over semi-integral abutments. Curvature typically would not be a significant factor in the decision of whether to use an integral or semi-integral abutment. The issues with curvature would typically be similar for both integral and semi-integral abutments.

~Delaware~

We are a small state and have only a handful of curved girder bridges to begin with. We are just now getting into designing and constructing semi-integral abutments for straight girder bridges.

~Florida~

Florida does not design semi-integral abutments due to the fact that we do not have de-icing salts.

~Hawaii~

We prefer integral rather than semi-integral, however, we do not exclude the use of these if the design justifies this.

~Idaho~

The girders (primarily prestressed concrete girders) are on chords between the abutments and piers and the concrete deck is placed on the curve. We have not constructed any steel bridges with the girders fabricated with a horizontal curve with the abutments placed radial to the curve.

~Iowa~

With extensive use of integral abutments there is little need for semi-integral abutments.

Iowa has no standard details for semi-integral abutments. Again, there is a concern with movements at bearings.

~Kentucky~

We want the corrosion protection of the concrete diaphragm/backwall over the steel girders.

~Maryland~

We have generally avoided combining horizontally curved superstructures with semi-integral abutments. This is not necessarily due to any specific technical or performance issue(s).

~Michigan~

Curved or large skewed alignments add out of plane forces not considered in developing the integral abutment details.

~Minnesota~

We may in the future but we all has a length limit. Most curved girder bridges use parapet abutments.

~Missouri~

IAB provides lateral support which could be a concern with SIAB unless detailed with support. However, we would prefer IAB unless length or severe curvature would indicate otherwise. We don't have any hard and fast rules on when this would be an issue but it could come up for consideration.

~Nebraska~

No limitations.

~New York State~

Concerns about additional axial forces from earth pressure being introduced into curved girders.

~New Hampshire~

NHDOT has a small number of straight semi-integral bridges but we have not extended the use of integral abutment to the support of curved girders due to unfamiliarity.

~North Dakota~

Our semi-integral bridges have not performed well.

~Ohio~

ODOT chooses to avoid the complex analysis required to resolve the axial loading placed on the curved superstructure. Typical curved girder analysis software applications do not address this loading.

~Pennsylvania~

If an integral abutment cannot be used, PennDOT utilizes a stub abutment or conventional abutment with piles cap and two or more rows of piles. PennDOT does not have details for semi-integral abutments similar to Iowa DOT.

~South Dakota~

Again, very little need for curved structures. If we were to construct a new horizontally curved bridge, it would most likely be with integral abutments. The one horizontally curved bridge with a semi-integral abutment that we do have was a rehab. project where an expansion abutment was made semi-integral.

~South Carolina~

It is difficult to isolate superstructure movement from substructure due to difficulty in predicting direction of longitudinal movement.

~Tennessee~

The occasion to do so has not arisen. There would be no hesitancy to do so, given the right circumstances.

~Texas~

Texas has very limited soil and foundation conditions that are appropriate for semi-integral abutments. We use drilled shaft foundations on a majority of or bridge projects so using semi-integral abutments would be problematic and expensive compared to conventional abutments.

~Vermont~

I am unsure of the actual number but we have been using semi integral abutment end of bridge details for a while in bridges less than or equal to about 100 feet in length. This is the same restriction that we use for straight bridges.

~Virginia~

Not enough information/research in this area.

~Washington State~

1. Semi-integral abutments enable the end expansion joint to be located off the bridge. This prevents water seepage at the ends that causes damage to bearings. 2. Semi-integral abutments allow longitudinal bridge movements that dissipate energy during seismic events and lead to more economical substructure designs.

~Wyoming~

We have not used this type of integral abutment on straight bridges due to good overall performance of integral abutments.

6. *What aspects of the design and performance of horizontally curved, integral or semi-integral abutment, bridges would your agency like to see addressed if the opportunity existed?*

Summary:

For the most part, the participating agencies had varying responses regarding what they would like to see addressed. However, a number of agencies would like to see general guidelines with design examples that explain best design practices for horizontally curved, integral and semi-integral abutment, brides. A number of agencies also show concern for the longitudinal and

radial movement of the structure and of the piles. As with other questions, Washington State is concerned with performance in seismic events.

~Alaska~
None -- Not a common bridge type in Alaska
~Arkansas~
None

~Colorado~
I would like to provide our engineers with some design examples of how to use battered piles and MSE to control the earth pressures & direction of movement on tall and skewed abutments. These could be used if needed for issues related to curvature.

~Delaware~
A comprehensive design guide would be helpful. A report on issues confronted on real-life examples of these types of bridges and how they were addressed would also be helpful.

~Florida~
No needs are required for Florida.

~Hawaii~
Basically general recommendations on limitations on modeling for analysis/design for these types of bridges. Another aspect is curved bridges with skewed abutments with limitations, recommendations, etc.

~Idaho~
Not sure

~Iowa~
Does thermal expansion cause significant movements or stresses not accounted for in normal design procedures? Are there any factors unique to curved integral abutment bridges that should be addressed in design?

~Kentucky~
Stress importance of showing in the design plans, the steel girders condition/geometry before the deck is poured, and when girder webs should be plumb. (Whether before or after deck is poured). Contractors and inspection personnel become concerned when erected steel is out of plumb before deck is poured, and begin questioning the validity of the design plans, and steel fabricator's workmanship, and contractor's erection procedures. The group can sometimes take measures to force steel into an incorrect alignment, without checking with designers.

~Maryland~
How prevalent is this type of design? What has been the experience of owners who have utilized this type of design, specially long-term? What are the best practices in utilizing this type of design, especially any limitations on its use?

~Michigan~
n

~Minnesota~
With semi-integral, is a lug utilized to keep the lateral movements controlled to a normal direction. If not doeas lateral movement cause service issues at the supports.

~Missouri~
We generally pour our concrete diaphragms before we pour the deck. On curved systems, could this be an issue with differential rotation or loading between interior and exterior girders. Differently skewed abutment than intermediate bents; differential rotations; slab cracking. Different pile lateral and vertical stresses. Twisting at the abutment. Wing shear or pavement problems.

~Nebraska~
I would confirm the radial expansion with severe skew and the possibility of uplift affect. I would also confirm the double curvature bending in the pile.

~New York State~
Guidelines on degree of curvature and length that could be utilized without causing distress to curved girders.

~New Hampshire~
NHDOT would like to see information on pile response to the radial loads that a curved structure will generate.

~North Dakota~
None.

~Ohio~
For both integral and semi-integral bridges, a simplified determination of realistic earth pressures exerted on the abutment would be useful.

~Pennsylvania~
PennDOT would like to have the issue of flange bucking due to beam expansion addressed for horizontally curved bridges with integral abutments. Another issue may be the potential variation in cap depth along the abutment length of the integral abutment in regard to twisting and recommendations for maximum overall cap depth and reinforcement detailing.

~South Dakota~
Limiting skew and lengths, as well as degree of curvature

~South Carolina~
Guidelines for predicting direction of longitudinal movement

~Tennessee~

None. The tools in the AASHTO LRFD Bridge Design Specifications already exist.

~Texas~
No opinion, not applicable.

~Vermont~
I am somewhat concerned that bridge with radial integral abutments will exhibit lateral movement due to unbalanced forces resulting from earth pressure.

~Virginia~
How to deal with the forces and displacments/rotations and good detailing parctices.

~Washington State~
Performance in seismic events. Comparison of force transfer to piles/shafts between intergral and semi-integral abutments for temperature and seismic loads.

~Wyoming~
None

7. Is your agency aware of any published or unpublished reports or papers that address the design, monitoring, or performance of horizontally curved, integral or semi-integral abutment, bridges? If so, please provide contact or other information.

Pennsylvania was the only state whose response to this question wasn't in some form of "none."
*Iowa's response came after original summary

~Pennsylvania~
Yes - PennDOT had contracted with Penn State to monitor 4 integral abutment bridges and to develop a design methodology based upon the monitored behavior of the integral abutment bridges. For a copy of the report please contact Beverly Miller at 717-783-4338 bevemiller@state.pa.us. For questions concerning the report, please contact Professor Jeff Laman of Penn State at Jal@engr.psu.edu

~Iowa~
Books by Martin P. Burke and Brian Pritchard on integral abutments have been noted.

8. Is your agency aware of any current or contemplated research regarding horizontally curved, integral or semi-integral abutment, bridges? If so, please provide contact or other information.

Vermont was the only state whose response wasn't in some form of "none."
*Iowa's response came after original summary

~Vermont~
We are monitoring the one curved girder bridge. The monitoring began early last winter so

we have not yet obtained any information. The project Manager for the monitoring project is Chad Allen 802 828 6924. chad.allen@state.vt.us

~Iowa~
Possibly there are a couple of projects in the northeastern US

9. What limitations does your agency place on the design of horizontally curved bridges that do not have integral or semi-integral abutments regarding skew, radius, span length, total length, steel girders, and prestressed girders?

Summary:
For the most part, the participating agencies did not have additional limitations regarding horizontally curved brides without integral or semi-integral bridges. However, the agencies that do have additional limits place a limit on the skew angle and the span length. In general the skew angle is limited to 30-45° and the span length is limited anywhere between 250 ft. to 450 ft.

~Alaska~
No Response

~Arkansas~
None

~Colorado~
CDOT has no formal limitations. CDOT does have published minimum expectations, see Subsection 7.2 of the CDOT Bridge Design Manual.

~Delaware~
We base our designs on a case-by-case basis and do not put any limitations on what can and cannot be used.

~Florida~
N/A

~Hawaii~
We do not have limitations beyond AASHTO specifications and guidelines.

~Idaho~
Beyond the AASHTO LRFD code we have no limitations.

~Iowa~
For prestressed beams the office permits only chorded, curved bridges. Steel girder bridges may use chorded or horizontally curved girders. For chorded bridges the office prefers that pier and abutment skews are the same so that all members for a span are the same length. For all bridges the office prefers that skews not exceed 45 degrees. Horizontal spiral curves are to be

moved off a curved bridge to avoid unwarranted complexity.

~Kentucky~
Follow AASHTO Guide Specification for Horizontally Curved Steel Girder Highway Bridges

~Maryland~
With respect to steel plate or box/tub girders, we have very few specific restrictions on horizontally curved bridges, but rather try to stay within certain guidelines or rules of thumb. In general, we would try to limit the length of continuous units (say, < 1500 ft.) such that fairly conventional joint systems (i.e., finger joints) can be utilized. Excessive skew angles (> 30 to 45 degrees) at end supports are avoided where possible. We try to keep individual span lengths to a reasonable limit (< 250 ft.) to avoid extremely high loads on bearings. We have limited experience with curved prestressed girders, so no such guidelines are established.

~Michigan~
No Response

~Minnesota~
We would utilize our same limitation for integral or semi-integral abutments 30 deg skew 300 ft total length

~Missouri~
The minimum radius is limited by the girder section properties per AASHTO LRFD 6.7.7.

~Nebraska~
Our span limitation is 450 ft on 45 degree skew. No limit with a reason without the severe skew.

~New York State~
No explicit limitations, although we have not used curved prestressed girders.

~New Hampshire~
NHDOT's Bridge Design Manual does not place any limitations on the design of horizontally curved bridges. To date, we have only curved steel girders, not prestressed girders.

~North Dakota~
Skew must be less that 30 deg. Length must be 400' or less.

~Ohio~
No ODOT imposed limitations.

~Pennsylvania~
AASHTO A 4.6.1.2 is followed to determine if the structure is horizontally curved. PennDOT's design manual Part 4 Section 6 and Appendix E contain additional requirements. Design Manual Part 4 is available through PennDOT's web site

248

ftp://ftp.dot.state.pa.us/public/Bureaus/design/PUB15M/DM-4%202007%20Change%20No.%201.pdf.

~South Dakota~
None

~South Carolina~
None

~Tennessee~
No limitations exist. Use of curved bridges on skewed supports are discouraged

~Texas~
Not applicable.

~Vermont~
No Response

~Virginia~
None for steel beams/girders. Not using curved prestressed concrete beams at this time.

 ~Washington State~
Follow AASHTO LRFD guidelines for skew and radius limitations. Steel spans are generally kept below 400 ft. Curved P/S girders have not been constructed yet, although one such bridge is currently under design.

~Wyoming~
Mainly due to the small number of curved bridge designs, we have no limitations other than total length of bridge for the use of integral abutments. Our maximum bridge length having an integral abutment is 380 feet; we try to limit skew to less than 30 with 45 degrees being the maximum.

10. *What AASHTO recommended method(s) does your agency follow for final design of horizontally curved bridges that do not have integral or semi-integral abutments?*

Summary:
The most common method for final design of horizontally curbed brides without integral or semi-integral abutments is the grillage method at 46.2% of the respondents, followed by the FE method at 30.8%, the V load method at 26.9%, and finally M/R method at a mere 7.7%. These percentages do not sum to 100% because 30.8% of the states claim the use of more than one method. It's interesting to discover the V load methods use is so high for final design considering AASHTO recommends its use for only preliminary design.

~Alaska~
V load method
Other (please specify) – For new designs, would used computer methods such as grillage

method verified or checked using the V load method.

~Arkansas~
FE method

~Colorado~
The design method used for curved bridges is as determined appropriate for the situation and is selected by the supervising structure engineer. Over time the V-Load and M/R methods have been generally replaced with finite element grillage and 3-D methods

~Delaware~
FE method

~Florida~
No Response

~Hawaii~
Other (please specify) - We do not have any defined methodology. This is generally left up to the responsible designer.

~Idaho~
Grillage
method
Other (please specify) – MDX software for curved steel design

~Iowa~
Other (please specify) - With only one known exception in the past 10 years, the DOT bridge office has not designed curved bridges. At this point the office does not have software that is usable for curved bridges.

~Kentucky~
Grillage
method
Other (please specify) - MDX, SAP2000 , GT STrudl

~Maryland~
Grillage method

~Michigan~
V load method
Grillage method

~Minnesota~
FE method

~Missouri~
V load method

~Nebraska~

V load method

~New York State~
Grillage method

~New Hampshire~
Grillage method
FE method
Other (please specify) - It has been over a decade since NHDOT designed a curved girder in-house. NH consultants designing curved girders seem to be favoring the Descus software package, which will analyze with either grillage or FE.

~North Dakota~
V load method

~Ohio~
Other (please specify) - ODOT does not list a recommended preference for design methodology of curved bridges.

~Pennsylvania~
FE method
Other (please specify) - Approved FE programs are listed in DM-4 Appendix J;ftp://ftp.dot.state.pa.us/public/Bureaus/design/PUB15M/DM-4%202007%20Change%20No.%201.pdf

~South Dakota~
No Response

~South Carolina~
Grillage method
FE method

~Tennessee~
Grillage method

~Texas~
Grillage method

~Vermont~
M/R method
Grillage method

~Virginia~
Other (please specify) - Using the DESCUS program

~Washington State~

FE method

~Wyoming~
V load method